Strategic Development of Micro-Incremental Forming Process with Size-Effect Based Fracture Modeling for Ultra-Thin Sheets

A Thesis Submitted

In Partial Fulfillment of the Requirements

for the Degree of

Doctor of Philosophy

by

Mainak Pal 2018MEZ0017



DEPARTMENT OF MECHANICAL ENGINEERING INDIAN INSTITUTE OF TECHNOLOGY ROPAR

June 2025

Copyright © "2025" by Indian Institute of Technology Ropar

DEDICATED TO FAMILY AND FRIENDS



DECLARATION

I hereby declare that the work which is being presented in the thesis entitled "Strategic

Development of Micro-Incremental Forming Process with Size-Effect Based

Fracture Modeling for Ultra-Thin Sheets" has been solely authored by me. It presents

the result of my own independent investigation/research conducted during the time

period from January 2019 to January 2025 under the supervision of Prof. Anupam

Agrawal, Professor and Dr. Chandrakant Kumar Nirala, Associate Professor in the

Department of Mechanical Engineering, Indian Institute of Technology Ropar. To the

best of my knowledge, it is an original work, both in terms of research content and

narrative, and has not been submitted or accepted elsewhere, in part or in full, for the

award of any degree, diploma, fellowship, associateship, or similar title of any

university or institution. Further, due credit has been attributed to the relevant state-of-

the-art and collaborations (if any) with appropriate citations and acknowledgments, in

line with established ethical norms and practices. I also declare that any

idea/data/fact/source stated in my thesis has not been fabricated/ falsified/

misrepresented. All the principles of academic honesty and integrity have been

followed. I fully understand that if the thesis is found to be unoriginal, fabricated, or

plagiarized, the Institute reserves the right to withdraw the thesis from its archive and

revoke the associated Degree conferred. Additionally, the Institute also reserves the right

to appraise all concerned sections of society of the matter for their information and

necessary action (if any). If accepted, I hereby consent to my thesis to be available online

in the Institute's Open Access repository, inter-library loan, and the title & abstract to

be made available to outside organizations.

Signature

Name: Mainak Pal

mainek lal

Entry Number: 2018MEZ0017

Date: June, 2025

vii



ACKNOWLEDGMENTS

Firstly, I pay obeisance to The Almighty God, for the blessings, opportunities, and fortitude at every stage of life. There have been numerous helping hands behind the successful completion of my PhD work. First and foremost, I express my sincere gratitude and respect to my thesis supervisor(s) **Prof. Anupam Agrawal**, Professor and **Dr. Chandrakant Kumar Nirala**, Associate Professor, Department of Mechanical Engineering, Indian Institute of Technology Ropar, for their continuous support, patience, and valuable guidance throughout my research journey. Their insightful feedback and encouragement have been invaluable to my research and the completion of this thesis.

I extend my gratefulness to Prof. Sarit Kumar Das, former Director, IIT Ropar and Prof. Rajiv Ahuja, Director, IIT Ropar for their strategic administration and providing access to different facilities and equipment, during my research work at IIT Ropar. I would like to express my great appreciation to Prof. Navin Kumar, HOD (Mechanical Engineering) and Dr. Prabhat Kumar Agnihotri, former HOD for their continuous support throughout my PhD work. I am deeply thankful to the members of my dissertation committee, Dr. Ekta Singla (Chairperson), Prof. Harpreet Singh, Dr. Ravi Kant and Dr. S.C. Martha for their time, effort, and their valuable suggestions during the semester evaluations. Their contributions have significantly improved my work. I want to express my sincere thanks and regards to all the professors for building up my basic knowledge through various course works that I studied during my PhD.

I would like to express my heartiest gratitude to Prof. K. Narasimhan and Prof. MJNV Prasad, Department of Metallurgical Engineering and Materials Science, IIT Bombay for their insightful comments and suggestions during the research discussions which helped me to solve the problems faced during my research work.

I express my special regards to Mr. Varinder Kumar, Senior Technical Assistant, Micromanufacturing Lab., for his valuable guidance, sharing his expertise on the research activities and assistance during the experimentation carried out at IIT Ropar.

I extend my gratitude to my seniors, colleagues and friends in the Advanced Manufacturing Technology Lab. (AMTL): Dr. Harish Kumar Nirala, Dr. Narinder Kumar, Dr. Hreetabh Kishore, Dr. Rakesh Kumar, Dr. Ashutosh Rajput, Mr. Prince Malik, Mr. Amit Kumar, Mr. Arun Kumar, Mr. Neeraj K Prasad, Mr. Devraj Chauhan,

Mr. Suraj Sharma, Mr. Aashish Yadav, Mr. Ayush Srivastava, Ms. Jahnavi Thakur, Ms. Tripty Kumari, Mr. Deep Patel, Mr. Navneet, Mr. Tarun, Mr. Vandit Pandya, Mr. Shubhra K. Nandi, Mr. Peeyush Mahajan for their persistent advice, and valuable assistance during the entire research work. Their camaraderie, collaboration, and support made my PhD experience enjoyable and enriching. I would also like to extend my heartfelt gratitude to my friends, whose support and companionship have been a source of strength throughout my PhD journey. Special thanks to Mr. Gopal Chandra Pal, Dr. Rakesh Kumar Pankaj, Dr. Neeraj Yadav, Dr. Neha Vishnoi, Mr. Raushan Kumar, Mr. Sudhendu Nath Tiwari, Mr. Vivek, Dr. Jay Airao, Mr. Rajesh and Mr. Anand for their encouragement, understanding, and for providing much-needed breaks and laughter.

I sincerely thank all the staff members of the Mechanical Engineering Department, IIT Ropar: Mr. Kaushal Kishor Jha, Mr. Pankaj, Mr. Jagmail Singh, Mr. Ram Kumar, Mr. Sukhwinder Singh, Mr. Hemant, and Mr. Rupinder Singh for helping me out in my research-related work. Further, I am highly indebted to all the staff members of central workshop, IIT Ropar: Mr. Rambir Singh, Mr. Randhir Singh, Mr. Girdhari Lal, Mr. Yograj, Mr. Rajiv Kumar, Mr. Bhupinder, Mr. Jaskaran and Mr. Jaswinder Singh and wish to express my sincere thanks for extending extensive help and support in the experimentation.

I am profoundly grateful to my parents, **Sh. Mahinder Pal** and **Smt. Minati Pal**. Your unwavering support, endless love, and sacrifices have been the foundation of my success. Words cannot express how much your belief in me has meant throughout this journey. Thank you for always being my pillars of strength and for instilling in me the values of perseverance and dedication. I hope to make you proud...!!

Mainak Pal

CERTIFICATE

This is to certify that the thesis entitled "Strategic Development of Micro-Incremental Forming Process with Size-Effect Based Fracture Modeling for Ultra-Thin Sheets" submitted by Mainak Pal (2018MEZ0017) for the award of the degree of Doctor of Philosophy of Indian Institute of Technology Ropar, is a record of bonafide research work carried out under our guidance and supervision. To the best of my knowledge and belief, the work presented in this thesis is original and has not been submitted, either in part or full, for the award of any other degree, diploma, fellowship, associateship, or similar title of any university or institution.

In our opinion, the thesis has reached the standard fulfilling the requirements of the regulations relating to the degree.

Anton Agnal

Prof. Anupam Agrawal

Professor, Department of Mechanical Engineering

Indian Institute of Technology Ropar

Chambralent the winds

Dr. Chandrakant Kumar Nirala

Associate Professor, Department of Mechanical Engineering

Indian Institute of Technology Ropar



LAY SUMMARY

The demand for micro-products made from ultra-thin metal sheets (foils) has grown across several industries due to their unique properties and applications in miniaturized components. Thin foils, typically ranging from a few micrometers to tens of micrometers in thickness, are highly valued for their flexibility, strength, and ability to be precisely employed in micro-manufacturing processes. These foils are used in a variety of industries where miniaturization, precision, and lightweight materials are essential. Micro-forming is a specialized micro-manufacturing process, which can be used to develop small, high-precision parts, which are commonly used in industries like microelectronics, biomedical devices, avionics, and automotive. One of the key challenges is predicting how the material will behave when it is formed, as the properties (like strength and flexibility) of ultra-thin materials can change significantly at microscale. To address these issues, new micro-forming techniques such as micro-deep drawing, micro-extrusion, and micro-stamping have been developed. Microincremental sheet forming (µISF) is a new approach, which eliminates the need for traditional die tools, offering more flexibility, better formability, and improved energy efficiency. In µISF, a tool moves across the surface of the foil to carefully deform it into complex 3D geometrical shapes. The process can produce very precise miniature parts. This work presents the design and development of a micro-forming set-up to study the micro-scale deformation behavior of the CP-Ti-Gr2 foils, focusing on factors like grain size and microstructure. By controlled heat treatment, the grain size of the material were altered, which helped in the improvement of flowability in the material. The study showed that higher annealing temperatures and larger grain sizes increased the ductility of the material, which may lead to higher formability of the micro-parts.

In addition to experimental work, the research work involved numerical simulations in software to model and predict the micro-scale deformation behaviour during the μ ISF process. The simulation also showed that certain toolpath strategies can produce even stress and thickness distribution in the final micro-part. Another critical aspect of microforming is friction, which can cause wear on both the material surface and the forming tools. To improve the process, sustainable lubrication methods was explored. It showed that, using MoS₂ powder instead of liquid lubricant can reduce friction and energy consumption, while improving the surface quality of the formed micro-parts. The study

also investigated the methods to increase the stiffness of the foils, as they tend to bend and distort easily due to their low bending stiffness. Through stacking multiple foils together, the stiffness of the foil was improved with the increase in the forming depth of the micro-parts. The study also explored innovative techniques for creating the precise forming tools required for the μ ISF process. A new technique, Reverse- μ EDM process was used to manufacture micro-forming tools with precise hemispherical shape-end tip having an excellent surface finish. Overall, this work advances the field of micro-forming by addressing challenges related to the material behaviour, tooling, and process optimization, contributing to the development of more efficient and sustainable methods for the fabrication of small high-precision components.

ABSTRACT

Micro-forming is an advanced micro-manufacturing process aimed at producing high-precision, small-scale components made of ultra-thin metallic sheets (foils) for a wide range of applications, such as in microelectronics, biomedical, avionics, and automotive industries. This process involves the deformation of materials with thicknesses in the micrometer range, which presents unique challenges due to the increased sensitivity of the foils to size-effect dependent external forces, such as plastic deformation, anisotropy, springback, and friction. As the thickness of the material decreases, the influence of material properties, surface characteristics, and process parameters becomes more pronounced. The ability to precisely control these variables is crucial for achieving the desired mechanical properties and dimensional accuracy in the final micro-part. The mechanical properties of the material, such as yield strength, ductility, and strain-hardening behavior, can vary significantly with thickness. This makes it difficult to predict the response of foils to external forces and demands more sophisticated modeling and experimentation to ensure successful forming results.

Recent advancements in micro-forming techniques, including micro-deep drawing, micro-extrusion, and micro-stamping, etc. are well established at micro-scale with developed specialized tools and equipment. Micro-incremental sheet forming (µISF) process is a recent development to tackle the issues arising due to size-effect and constraints in the fabrication of required tooling at the micro-scale. It is a die-less process with multifold formability compared to traditional processes, for the production of customized miniature/ micro parts at ultra-precision range with better energy optimization. In µISF, the forming tool navigates through the surface of the foil to precisely deform it to complex symmetric and non-symmetric 3D components as per the prescribed toolpath. In this work, a micro-forming set-up was designed and developed to conduct the µISF experiments. At micro-scale, studying the grain size of the material is crucial to understand the deformation behavior. The intrinsic anisotropy of the foils was minimized through controlled heat treatment, and varying grain sizes, having different microstructures, were generated to investigate their effect on the formability of CP-Ti-Gr2 foils. It was established that higher annealing temperature, increase in grain size and higher step depth assisted in improving the ductility of the foils, leading to enhanced forming depth of the micro-parts. This was explained by a decrease in the material resistance to dislocation motion caused by an increase in the

volume fraction of surface grains (Vs>Vi) at an increasing step depth in the deformation zone (Ar). The microstructural analysis through EBSD also showed similar results with the presence of a higher fraction of LAGBs and larger KAM angle.

This work also involves numerical simulations in ABAQUS®, incorporating the influence of size-effect by coupling it with a suitable toolpath strategy and an appropriate damage mechanics model, to accurately predict the nature of micro-scale deformation in the µISF process. A mixed material model with size-dependent parameters (grain size, thickness, etc.) was considered in the finite element analysis using the theory of surface layer model, to examine the flow stress behavior of the material. The FEA results showed a reasonable agreement with the experimental results to predict the failure of the micro-parts. The FGBIT strategy showed better stress and thickness distribution of the formed micro-part compared to the spiral toolpath.

In micro-forming, friction and wear are critical factors that can significantly impact both the material and tooling. Lubrication plays an essential role in minimizing friction, improving the surface finish, and reducing the occurrence of defects. A sustainable lubrication approach, studying frictional size-effect was also explored through closed and open lubrication pocket models (LPM) theory to improve tribological performance of the formed micro-parts. A significant decrease in the forming load and energy consumption was observed with the environment-friendly MoS₂ powder compared to liquid lubricant.

Some innovative ways of fabricating the forming tool and increasing the stiffness of the foils, for better forming attributes, were explored in this work. The foils are susceptible to bending and distortion under self-weight as they lack stiffness and fail early during forming. The stacking of foils (SOF) approach showed a significant increase in the formability of the target parts, when multiple foils were formed simultaneously to increase the stiffness and plastic deformation of the material. A new approach of Reverse- μ EDM technique was used to fabricate micro-forming tools for the μ ISF process. The study showed that with the correct parameter setting of the discharge energy, a precise stresses free hemispherical-end profile of the tool can be obtained with good surface finish using the Reverse- μ EDM process.

Keywords: μISF, Foils, Thickness-to-grain-size-effect, Heat-treatment, EBSD, Tribology, Stacking of foils, Reverse-μEDM, Numerical simulation, Toolpath.

LIST OF PUBLICATIONS

• Journals:

- Pal, M., Agrawal, A., and Nirala, C. K., 2024, "Enhancing Formability in Micro-Incremental Sheet Forming by a Novel Stacking Method of Ultra-Thin Sheets,"
 Manufacturing Letters, 40, pp. 159–163.
 (https://doi.org/10.1016/j.mfglet.2024.05.002).
- Pal, M., Agrawal, A., and Nirala, C. K., 2024, "An Investigation of the Formability of Ultra-Thin CP-Ti-Gr2 Foils Considering Thickness-to-Grain-Size Effects under Controlled Heat Treatment in μ-ISF," Journal of Manufacturing Processes, 131, pp. 1202-1218. (https://doi.org/10.1016/j.jmapro.2024.09.107).
- 3. **Pal, M.**, Agrawal, A., and Nirala, C. K., "A Size-effect driven Strategy to Improve Tribological Performance in Sustainable Micro-Incremental Forming of Titanium Foils with Solid Lubricants," (Under Review).
- 4. **Pal, M.**, Kumari, T., Agrawal, A., and Nirala, C. K., "Enhancing μ-ISF Prediction Accuracy and Formability by Incorporating Size-effect and Space-filling Fractal Toolpath: Experimental and Numerical Investigation," (**Under Review**).
- 5. Pal, M., Agrawal, A., Nirala, C. K., Prasad, M. J. N. V., and Narasimhan, K., "Insights into the Microstructure and Texture Evolution during Micro-Incremental Sheet Forming of Ultra-thin Titanium Grade 2 Foils," (Under Preparation).
- 6. **Pal, M.**, Kishore, H., Agrawal, A., and Nirala, C. K., "Feasibility Demonstration of Reverse-μEDM Fabricated Hemispherical-End Tool for Micro-Incremental Sheet Forming," (**Under Preparation**).

• Conference Proceedings/ Procedia Journals/ Book Chapters:

1. **Pal, M.**, Kumari, T., Agrawal, A., and Nirala C., K., "Experimental and Numerical Investigation of Micro-incremental Sheet Forming of Ultra-thin CP-Ti-Gr2 Sheets", 7th World Congress on Micro and Nano Manufacturing (WCMNM-2024), Pattaya, Thailand, September 16-19, **2024**. (in Press) (Funded through ANRF International Travel Support (ITS) Scheme).

- 2. **Pal, M.**, Pandya, V., Nirala C., K., and Agrawal, A., "Determining Critical Wall Angle in Micro-Incremental Sheet Forming of SS316L Foils for Formability Assessment", 14th International Conference on Numerical Methods in Industrial Forming (NUMIFORM-2023), AGH UST, Krakow, Poland, June 25-29, **2023**. Lecture Notes in Mechanical Engineering. Springer, Cham. (https://doi.org/10.1007/978-3-031-58006-2 21).
- 3. **Pal, M.**, Agrawal, A. and Nirala C., K., "Influence of Grain-Size on Formability in Micro-Incremental Sheet Forming of Ultra-Thin Titanium Grade 2 Foils", 9th International and 30th All India Manufacturing Technology, Design and Research (AIMTDR-2023) Conference, IIT (BHU) Varanasi, December 8-10, **2023**. (**Book Chapter in Press**).
- 4. Pal, M., Kishore, H., Agrawal A., and Nirala C., K., "Fabrication of Precise Hemispherical End Tool for Micro-Incremental Sheet Forming using ReverseμEDM", 55th CIRP Conference on Manufacturing Systems (CMS-2022), Lugano, Switzerland, June 29 July 1, 2022. Procedia CIRP, 107, 1600-1605. (https://doi.org/10.1016/j.procir.2022.06.001).
- 5. **Pal, M.**, Pandya, V., and Agrawal, A., "Study of Formability Limit Based on Ductile Damage Criteria of Incremental Sheet Forming of Titanium Grade 2 Sheet," Proceedings of the ASME, 16th International Manufacturing Science and Engineering Conference, (MSEC-2021), Cincinnati, Ohio, USA, June 21 25, **2021**. (https://doi.org/10.1115/MSEC2021-64005).
- 6. Mahajan, P., **Pal, M.**, Kumar, R., and Agrawal, A., "Experimental and Simulation Study of Incremental Forming for Titanium Grade 2 Sheet," Proceedings of the ASME 15th International Manufacturing Science and Engineering Conference, (MSEC-2020), Cincinnati, Ohio, USA, June 22 26, **2020**. (https://doi.org/10.1115/MSEC2020-8524).
- Pal, M., Mahajan, P., Athikkai, N., Rai, S., Kishore, H., Kumar, R., and Agrawal, A., "Development of GUI and Comparison of Tool Path Strategies for Incremental Forming of Polycarbonate Sheet," 11th International Conference on Precision, Meso, Micro and Nano Engineering (COPEN-2019), IIT Indore, December 12-14, 2019.

• Publications from Research Work other than Thesis:

1. Kishore, H., Pal, M., Nirala, C. K., and Agrawal, A., 2024, "Thermal Performance Evaluation of Micro Pin-Fin Heat Exchangers: Part I—

- Geometrical Design Parameters Optimization," **International Journal of Precision Engineering and Manufacturing**, 25, pp. 245–254. (https://doi.org/10.1007/s12541-023-00925-1).
- 2. Kishore, H., Pal, M., Nirala, C. K., and Agrawal, A., 2024, "Thermal Performance Evaluation of Micro Pin–Fin Heat Exchangers: Part II—Numerical Simulation and Fabrication Demonstration," International Journal of Precision Engineering and Manufacturing, 25, pp. 255–269. (https://doi.org/10.1007/s12541-023-00926-0).
- 3. **Pal, M.**[†], Mahajan, P. [†], Athikkai, N., and Agrawal, A., "Overcoming Challenges in Forming of Polycarbonate Sheets using Incremental Forming and Enhancing its Industrial Viability via GUI for Toolpath Generation", (**Under Preparation**)

TABLE OF CONTENTS

DECI	LARATION	vii	
ACK	NOWLEDGEMENT	ix	
CERT	ΓIFICATE	xi	
LAY			
ABSTRACT LIST OF PUBLICATIONS		XV	
		xvii	
TABI	TABLE OF CONTENTS		
LIST	LIST OF FIGURES LIST OF TABLES		
LIST			
ABBI	REVIATIONS	xxxiii	
NOTA	ATIONS	XXXV	
CHA	PTER 1: Introduction	1	
1.1	Motivation	1	
1.2	Micro-forming	2	
1.2.1	Introduction to Micro-incremental Sheet Forming (μ-ISF)	4	
1.2.2	Challenges in the μ-ISF Process	5	
1.3	Introduction to ISF	6	
1.3.1	Potential Applications	8	
1.4	Problem Definition	10	
1.5	Organization of the Thesis	11	
СНА	PTER 2: Literature Review	13	
2.1	Introduction	13	
2.2	Development of micro-scale deformation in the µISF process	13	
2.3	Influence of Size-effect	17	
2.4	Tribological aspects in micro-forming	23	
2.5	Formability of micro-parts	26	
2.6	Forming forces	32	

2.7	Forming toolpath	35
2.8	Numerical simulation approach	39
2.9	Research Gaps	42
2.10	Research Objectives	43
СНАР	TER 3: Development of μ-ISF Set-up for Comprehensive	45
	Experimentation on Ultra-Thin Sheets (Foils)	
3.1	Introduction	45
3.2	Work Methodology	46
3.2.1	Development of the μISF set-up	46
3.2.2	Estimation of mechanical anisotropy in the received specimen	49
3.2.3	Tailoring grain size and microstructure of the annealed specimens	51
3.2.4	Preliminary trials and experimental approach	53
3.3	Results	54
3.3.1	Reduction of anisotropy through controlled annealing	54
3.3.2	Correlation between grain size/ microstructure and uniaxial tensile loading	57
3.3.3	Validation of the micro-forming set-up and experiments	60
3.4	Discussion and Analysis	61
3.4.1	Evaluation of formability of the original and heat-treated foils	61
3.4.1.1	Understanding the micro-deformation behavior through surface	63
	and volume grains	
3.4.1.2	Combined effect of grain size and step depth on formability	66
3.4.1.3	Determination of critical t/d ratio for enhanced formability	67
3.4.2	Correlation of grain size and t/d ratio of the foils, with Hall-Petch relation	68
3.4.3	Measurement of the forming forces	70
3.4.4	Microstructure evolution of original and annealed foils	72
3.5	Summary	78
СНАР	PTER 4: Development of Numerical Simulation Model Incorporating	79
	Size-effect	
4.1	Introduction	79
4.2	Work Methodology	80

4.2.1	Size-effect in micro-forming	80
4.2.2	Generation of FGBIT and spiral toolpath	81
4.2.3	Numerical modeling incorporating size-effect	83
4.3	Results and Discussion	88
4.3.1	Forming depth	88
4.3.2	von Mises stress distribution	91
4.3.3	Thickness distribution	92
4.4	Summary	94
СНА	PTER 5: Enhancing Tribological Performance in Micro-incremental	95
	Sheet Forming	
5.1	Introduction	95
5.2	Work Methodology	98
5.2.1	Materials	98
5.2.2	Planetary ball mill: Synthesis of MoS ₂ powder	100
5.2.3	Experimental details	101
5.3	Results and Discussion	103
5.3.1	Tool wear	103
5.3.2	Surface finish and contact pressure	105
5.3.3	Forming depth	108
5.3.4	Grain microstructure	110
5.3.5	Forming forces and deformation energy utilization	111
5.4	Summary	112
СНА	PTER 6: Formability and Precision Improvement in µISF using	115
	Novel Strategies	
6.1	Stacking of Foils (SOF)	115
6.1.1	Introduction	115
6.1.2	Work methodology	116
6.1.2.	1 Development of the SOF set-up	116
6.1.2.	2 Experimental plan	118
6.1.3	Results and Discussion	119
6.1.3.	1 Assessment of formability in SOF	119

6.1.3.2	Comparison of the deformed geometries	120
6.2	Tool precision using Reverse-µEDM	122
6.2.1	Introduction	122
6.2.2	Reverse-µEDM Technology	124
6.2.3	Experimental Approach	124
6.2.4	Results and Discussion	128
6.2.4.1	Material removal rate (MRR) and Tool plate wear analysis	128
6.2.4.2	Surface roughness and dimensional accuracy of the fabricated μISF tool	129
6.2.4.3	Feasibility of the µISF process	131
6.2.5	Summary	132
СНАР	TER 7: Conclusions and Future Directions	135
7.1	Conclusions	135
7.2	Future Directions	137
REFE!	REFERENCES	

LIST OF FIGURES

1.1	(a) Schematic of the μ -ISF process (b) Spiral incremental toolpath	2
1.2	Products developed at micro-scale [4]	3
1.3	Various process parameters used in the μ-ISF process	5
1.4	Few potential applications of the ISF process [30,40–43]	9
2.1	(a) Principle of CNC incremental sheet metal forming by hammering (b) Schematic diagram of the micro-incremental forming system [8]	14
2.2	Categories of size effects during miniaturization [5]	17
2.3	Influence of size effects in micro-forming [59]	18
2.4	Variables that appear with the miniaturization [13]	19
2.5	(a) Grain size effect and (b) Feature size effect [70]	20
2.6	Lubricant pocket theory for the coefficient of friction in micro- forming [87]	24
2.7	Schematic demonstration of the FLD showing principle strain space presenting the FLC and FFL [95]	27
2.8	Measurement of the forming forces in different directions [104]	32
2.9	Conventional type of toolpaths in ISF (a) Spiral (b) Constant Z [112]	36
2.10	Staircase or material ridges formed due to toolpath in ISF [113]	37
2.11	Space-filling fractal toolpath [122]	38
2.12	(a) Flow chart for FEA in ABAQUS® for ISF (b) Meshed sheet with tool	40
3.1	(a) Design and fabrication of μ ISF fixture (b) Complete schematic demonstration of the μ ISF set-up	47
3.2	Development route for μ ISF process (a) Preparation of ultra-thin workpiece (b) Fabrication of micro-forming tool	49
3.3	(a) Uniaxial tensile test dimensions (b) Received specimen cut in	50
	three different directions, viz. RD, DD, and TD	
3.4	Engineering stress-strain curves in RD, DD, and TD for original specimen	50
3.5	(a-e) Optical micrographs: Microstructural analysis of five different	52

	specimens with variation in grain size in RD-ND plane, engineered	
	for studying the formability of the foils at different step depths	
3.6	(a) Incremental spiral toolpath for conical-shaped geometry (b)	54
	Experimental set-up for µISF process on DT-110i multi-axis	
	hybrid-µEDM machine	
3.7	Engineering stress-strain curves in RD, DD, and TD for (a)	55
	Specimen annealed at 650 °C for 60 min (b) Specimen annealed at	
	650 °C for 75 min (c) Specimen annealed at 650 °C for 90 min	
3.8	(a) Schematic view of different cross-sectional planes of the foil	56
	with respect to normal direction (ND) (b) Optical micrographs	
	showing the change in microstructure after annealing along	
	different cross-section planes	
3.9	Uniaxial tensile test results of the test specimens for μ ISF: (a)	57
	Engineering stress-strain curves in the rolling direction (b) Bar	
	graph displaying the average yield strength of the specimen for	
	different microstructural conditions with change in corresponding	
	t/d ratios, (c) Heat treatment of the specimens: Annealing	
	temperature-time profile	
3.10	Surface topography analysis using AFM of different	59
	microstructural conditions (a) MC_1 (b) MC_2 (c) MC_3 (d) MC_4 (e)	
	MC_5	
3.11	Formed components through μISF for trial experiments at different	60
	wall angles (a) 50° (b) 55° (c) 60°	
3.12	Formed CP-Ti Gr2 circular cups at different step depths using μISF	62
3.13	(a) Schematic showing the share of surface and volume grains in	64
	sheet specimen during miniaturization (b) Comparison of surface	
	and volume grains involved in macro-ISF and micro-ISF process	
3.14	(a) Bar graph presenting the forming depth of the components for	66
	different MC with respect to step depth (b) Variation of the t/d ratios	
	corresponding to the average forming depth of all the components	
	in each condition	

3.15	(a) SEM micrograph of the fracture location (b) Failure of the	67
	conical component (c) Successfully formed component with no	
	fracture at 50 µm step depth (MC ₄)	
3.16	Hall-Petch chart displaying the yield stress (σ_y) result of original	69
	and heat-treated Ti foils as a function of grain size $(d^{-1/2})$	
3.17	(a) Real-time monitoring of the axial forces in the μ ISF process (b)	71
	Formed geometry	
3.18	(a) Evolution of forming forces with specimens of different grain	7 1
	size (b) Effect of t/d ratio on the magnitude of the forces, Fz	
3.19	(a) X-ray diffraction (XRD) patterns of the original and annealed Ti	72
	specimens (b) Image quality (IQ) phase map for CP-Ti	
3.20	IPF maps and average grain size of the undeformed original and	73
	annealed specimens (a,c) MC ₁ (b,d) MC ₄	
3.21	IPF maps and average grain size of the deformed original and	74
	annealed specimens (a,c) MC ₁ (b,d) MC ₄	
3.22	IQ maps marked with red and blue color for low and high angle	75
	grains for undeformed specimens (a) MC ₁ (b) MC ₄ , (c,d) (001) and	
	(100) pole figures of the IPF map	
3.23	IQ maps marked with red and blue color for low and high angle	76
	grains for deformed specimens (a) MC_1 (b) MC_4 , (c,d) (001) and	
	(100) pole figures of the IPF map	
3.24	Comparison of LAGBs and HAGBs before and after the	76
	deformation process	
3.25	KAM maps for the (a,c) MC ₁ and (b,d) MC ₄ specimens	77
4.1	Size-effect in micro-scale deformation	81
4.2	Hilbert pattern-based fractal toolpath (order 2-5) [166]	81
4.3	Slicing and fractal geometry infill in each CAD model having	82
	different wall angles at 60°, 75° and 90°	
4.4	(a) Conventional spiral toolpath, and (b) FGBIT for conical-shaped	83
	geometry for µISF	
4.5	Experimental setup for μISF	83

4.6	(a) Engineering stress-strain curve of CP-Ti Gr2 in RD, TD, and	85
	DD (b) Schematic of nucleation, growth, and coalescence of voids	
	[132,167]	
4.7	(a) Representation of the FEA of the deformed conical shape using	86
	FGBIT, and (b) Deformed specimen	
4.8	Comparison between the calculated flow stress curves and	87
	experimental results	
4.9	4.9: Formed conical cups by using FGBIT and spiral toolpath in	88
	μISF (a) 60°, (b) 75°, (c) 90°	
4.10	(a) FEA of the observed fracture in the formed micro-part,	89
	Comparison of average forming depths using (b) spiral toolpath and	
	(c) FGBIT for different wall angles	
4.11	(a) FEA showing the von Mises stresses for (a) Spiral and (b)	91
	FGBIT (c) Path traced to measure the stress variation along the x-	
	direction	
4.12	Comparison of stress distribution using the FGBIT and spiral	92
	toolpath with different wall angles (a) 60° (b) 75° (c) 90°	
4.13	FEA showing the sheet thickness distribution of the formed part	92
4.14	Comparison of thickness distribution with forming depth using the	93
	FGBIT and spiral toolpath with different wall angles (a) 60° (b) 75°	
	(c) 90°	
5.1	Schematic representation of the µISF process	96
5.2	CLP and OLP theory during micro-scale deformation (a) before	97
	deformation (b) deformation using liquid lubricant (Oil) (c)	
	deformation using solid lubricant (dry MoS ₂ powder)	
5.3	(a,b) Microstructure and EDS of the received CP-Ti-Gr2 foil	99
	(c) FESEM micrograph showing the dimension of micro-pores on	
	the foil surface	
5.4	(a,b) FESEM and EDS of the received MoS ₂ powder	100
5.5	(a) Ball mill vial containing the MoS ₂ powder (b) DLS analysis for	101
	MoS ₂ particle size measurement (c) FESEM micrograph showing	
	the reduced particle size of the synthesized MoS ₂ powder	
5.6	(a) Conical curvilinear-shaped profile (b) μ ISF experimental set-up	102

5.7	Microscopic image of the tool tip after µISF with different	103
	lubrication conditions (a) No lubricant (b) Mineral oil (c) MoS ₂	
	powder	
5.8	SEM micrographs of the tool wear (a) Without MoS ₂ powder (b)	104
	With MoS ₂ powder	
5.9	Optical micrographs of the formed internal surface and AFM results	105
	with (a) No lubricant (b) Mineral oil (c) MoS ₂ powder	
5.10	(a) Schematic illustration of lubricant pocket theory (b) SEM	108
	micrograph of the deformed surface with micro-pores	
5.11	(a) Formed micro-part (b) SEM cross-sectional image of the	109
	fracture region (c) Graphical analysis of surface roughness with	
	forming depth and forming angle at fracture	
5.12	Grain microstructure of the deformed foils with (a) No lubricant	111
	(b) Mineral oil (c) MoS ₂ powder	
5.13	(a) Comparison of the measured forces with different lubrication	112
	conditions (b) Energy utilization levels along the z-axis direction	
6.1	(a) Ultra-thin workpiece for μISF process (b) Fabricated SEM	117
	image of micro-forming tool (c) Pictorial demonstration of the μISF	
	fixture for SOF approach	
6.2	(a) Complete schematic representation of the μISF process for	118
	forming multiple foils (b) Experimental view of the SOF approach	
6.3	Formed conical cups in single and multi-foil forming (SOF)	119
6.4	(a) Top foil as a sacrificial sheet with wrinkles (b) SEM micrograph	120
	of the fracture location (c) Bar graph presenting the average failure	
	depth verses number of stacks	
6.5	Comparison of deformed geometries in SOF	121
6.6	(a) Primary discharge and (b) Second order and higher order	124
	discharges in Reverse-µEDM	
6.7	Schematic representation of (a) set up configuration for fabrication	125
	of μ ISF tool using Reverse- μ EDM; (b) on-going Reverse- μ EDM	
	process for µISF tool	
	(c) Experimental set up of Reverse-μEDM process	
6.8	(a) Pre-deformed Titanium tool plate with dimple-shaped	126

	microcavity; SEM image of microcavity (b) before Reverse-	
	μEDM , and (c) after Reverse- μEDM with surface wear	
6.9	Workpiece dimensions	126
6.10	SEM micrographs of the fabricated μISF tool-tip surface finish at	129
	different parametric settings (a) low; (b) moderate; and (c) high	
6.11	SEM micrographs of the fabricated μISF tool machined region at	130
	different parametric settings (a) low; (b) moderate; and (c) high	
6.12	Optical micrograph of the Reverse- μEDM fabricated μISF tool	131
6.13	(a) Incremental spiral toolpath (b) µISF process	132
6.14	Formed conical geometry through µISF	132

LIST OF TABLES

1.1	Various applications of the ISF process	9
2.1	Summary of literature on the development of the μ ISF process	15
2.2	Summary of literature on the influence of size-effect	21
2.3	Summary of literature on the tribological aspects in micro-forming	25
2.4	Summary of literature on the formability in the forming process	30
2.5	Summary of literature on the measurement of forces in the ISF	34
	process	
2.6	Summary of literature on the usage of incremental toolpaths in the	38
	ISF process	
3.1	Uniaxial tensile properties of the specimens at different	58
3.2	microstructural conditions Preliminary trial results of μISF at different wall angles (without	61
	annealing)	
3.3	Experimental results of µISF at different microstructural	63
	conditions	
3.4	Hall-Petch material parameters based on yield stress data	70
4.1	Properties of the CP-Ti Gr2 foil used in the numerical simulation	84
4.2	Flow stress properties used in the numerical simulation	88
5.1	Experimental conditions and input process parameters	102
5.2	Experimental results of the µISF process	108
6.1	Experimental results of the µISF process with SOF	121
6.2	Machining conditions and input process parameters	127
6.3	Machining measured responses	128



ABBREVIATIONS

AFM Atomic Force Microscopy

CAD Computer-Aided Design

CLP Closed Lubricant Pocket

CNC Computerized Numerical Control

COF Coefficient of Friction

CP-Ti-Gr2 Commercially pure-Titanium-Grade 2

EBSD Electron Backscatter Diffraction

FEA Finite Element Analysis

FESEM Field-Emission Scanning Electron Microscopy

FGBIT Fractal Geometry-Based Incremental Toolpath

FLD Forming Limit Diagram

FFC Forming Limit Curve

HAGBs High Angle Grain Boundaries

IPF Inverse Pole Figures

IQ Image Quality

ISF Incremental Sheet Forming

IEG Inter-Electrode Gap

KAM Kernal Average MisorientationLAGBS Low Angle Grain BoundariesLBμM Laser Beam Micro-machining

MC Microstructural Condition

MEMS Micro-electromechanical System

MoS₂ Molybdenum Disulfide
MRR Material Removal Rate

Nd: YAG Neodymium-Doped Yttrium Aluminium Garnet

OLP Open Lubricant Pocket

RD Rolling Directional Plane

R-μEDM Reverse-Micro-Electric Discharge Machining

SEM Scanning Electron Microscopy

SOF Stacking of Foils

TWR Tool Wear Rate

T/D Thickness-to-grain-size

UTS Ultimate Tensile Strength

XRD X-ray Diffraction

μ-EDM Micro-Electric Discharge Machining

μ-ISF Micro-Incremental Sheet Forming

μ-WEDM Micro-Wire-Electro Discharge Machining

NOTATIONS

Area of the deformation zone A_r Macroscopic cross-sectional area of the contact (Total A_o Cross-sectional area of µISF tool-tip \boldsymbol{A} A_{M} Area cross-section covered by the lubrication pockets with MoS₂ powder A_p/A_s Area cross-section covered by the lubrication pockets/ solid contact area Fraction of area covered by oil/ air pockets A_I/A_{air} \boldsymbol{C} Capacitance d Average grain size (diameter) E Strain \mathcal{E}_{pl} Equivalent plastic strain \mathcal{E}_{u} Uniform strain Total Energy utilization in a z-axis direction E_z Feed rate f Axial force in z-direction F_z F_{min} Minimum axial force F_{max} Maximum axial force F_o Forming load Forming load with mineral oil F_1 F_2 Forming load with MoS₂ powder h Forming depth Hall-Petch coefficient K_{v} Locally intensified stress k(E)Contact length ΔL Orientation factor for the single crystal model m Orientation factor related to the slips on deformation M systems for polycrystal n Strain hardening exponent Number of internal grains N_i

Number of surface grains

 N_s

 P_M Pressure transferred to the lubrication pockets filled

with MoS₂ powder

 P_p/P_s Pressure applied to the pores/ solid contact area

 P_L/P_{air} Pressure transferred to the oil/ air pockets

Q Energy stored in the capacitor

 R_a Average surface roughness

s Tool rotation speed

t Thickness of the foil

V Gap voltage

 V_i Volume fraction of the internal grains

 V_s Volume fraction of the surface grains

 V_r Volume of the material removed from the workpiece

 Δz Incremental step depth

 Z_{θ} First location of fracture

 σ Flow stress

 θ or α Forming angle

 θ_f Forming angle at fracture

φ Tool diameter

 σ_{Teng} Average ultimate tensile strength

 σ_v Average yield strength

 σ_o Frictional stress

 σ_N/P_o Normal pressure/ contact pressure

η Size factor

 μ Friction coefficient

 $\tau_R(\mathcal{E})$ Critical shear resolved stress

 $\acute{\boldsymbol{\eta}}$ Stress triaxiality

1.1 Motivation

Manufacturing industries have recently started focusing on developing advanced microfabrication facilities to meet the rising demand for miniaturization and the fast-growing usage of customized micro-products fabricated from ultra-thin sheets (foils), forged billets, rods, etc. Forming these materials into complex metallic components/ structures, or miniature parts, demands extreme accuracy to cater to highly sophisticated applications. However, when the feature size reduces to tens or hundreds of microns, it becomes challenging to fabricate and demands a dedicated approach. One of the approaches is to scale down the traditional equipment and machinery to produce microcomponents/ products. However, manufacturing miniature/micro-products by scaling down the conventional forming techniques for real-world applications is not straightforward, due to the difficulty in scaling down machinery and supporting equipment. Furthermore, macro-scale forming techniques are incapable of incorporating various aspects viz. material size-effects/ microstructure development, tooling design, material non-homogeneity/ anisotropy, and final product handling for post-processing. Micro-forming is an emerging micro-manufacturing process for producing metallic parts of ultra-thin sheets or foils. It is a scaled-down version of the conventional forming processes, where the dimensions of the parts are typically in the range of a few millimetres or microns. Among the micro-forming processes, micro-incremental sheet forming (µ-ISF) is a process that overcomes the limitations of macro-ISF, to enable fabrication of miniature/ micro parts at ultra-precision range with better energy optimization. The schematic representation of the μ -ISF is shown in Fig. 1.1(a). In μ -ISF, the forming tool continuously navigates through the surface of the foil to precisely deform it to any complex symmetric and non-symmetric 3D geometry as per the prescribed toolpath, without using dedicated dies or punches. The process mechanism involves toolpath optimization for complex geometries. It also require precise tool fabrication, reduction in anisotropy of initial foils, proper lubrication etc. Therefore, the μ-ISF process development for forming metallic foils into useful products for various industrial applications is essential.

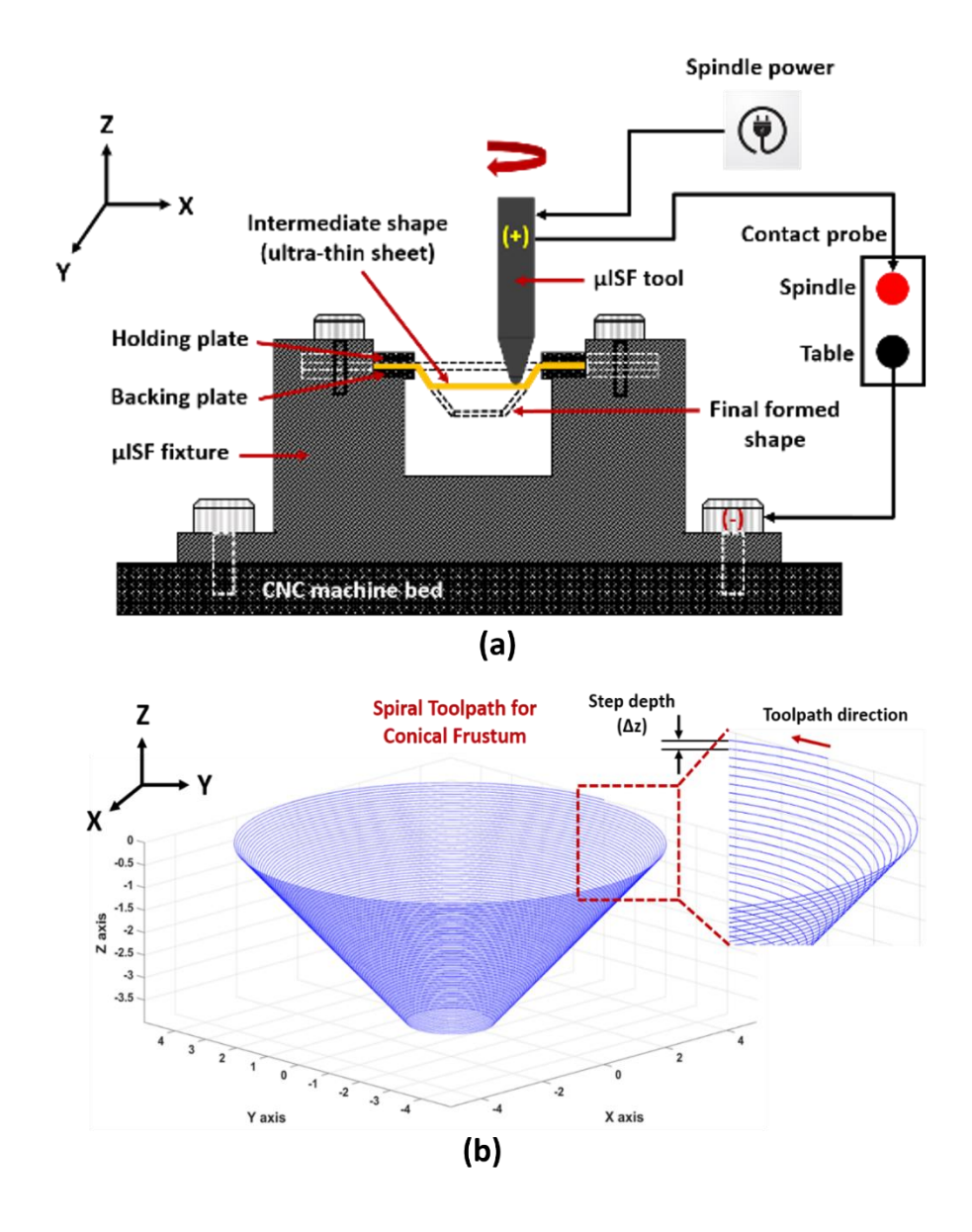


Fig. 1.1: (a) Schematic of the μ-ISF process (b) Spiral incremental toolpath

1.2 Micro-forming

Trend towards miniaturization of the product/ parts and the increasing use of microsystems technology in a rapidly growing field of applications, there is a huge demand for custom micro-parts made of ultra-thin sheets (foils), rods, billets etc. Countries like Japan have taken a leading role in the area of micro-manufacturing including microforming, particularly in applications pertaining to the manufacturing of micro-products and parts for medical and industrial applications. The researchers in the laboratory of mechanical engineering, ministry of trade and industry, Japan, were the first group to propose the micro-factory concept [1]. The concept was to build a desktop miniature-system consisting of several machine tools. The researchers have taken sincere

initiatives in developing specialized knowledge and research skills in the areas of microforming processes [2]. Micro-parts are the parts that are very small and typically have dimensions less than millimeters. These parts must precisely be manufactured to satisfy the precision range of a few microns. Demand for small-sized products has increased significantly due to continued miniaturization in various fields, including medical equipment, communication equipment, micro-electromechanical systems, and microfluidic systems [3]. Micro-forming draws the attention of manufacturers and researchers for fabricating products requiring high precision, low energy consumption and better mechanical properties at lower cost. Micro-forming is used widely in the microfabrication of small and precision parts in various applications such as electronic, optical, bio-medical, aerospace, and computer chips etc. [4]. Figure 1.2 shows various miniaturized products at micro-scale.

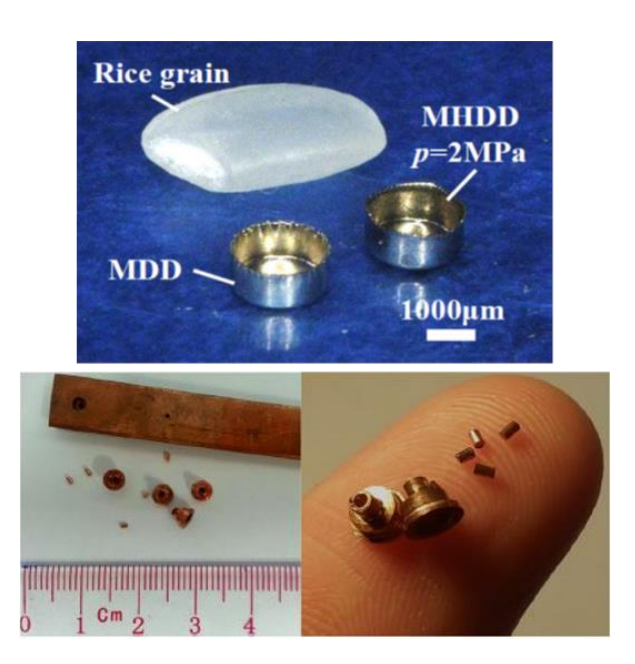


Fig. 1.2: Products developed at micro-scale [4]

Few micro-forming technologies for sheet metal like micro-stamping, micro-deep drawing, etc. are well established at the micro-scale. However, the production of micro-products by scaling down such traditional forming processes is challenging considering the limitations, due to size-effects [5] and its related issues with the auxiliary equipment. The grain size, crystallographic grain orientation and position, grain boundary, microstructure, and surface integrity significantly influence the micro-forming process in the decreasing order of severity. The deformation zone geometry area is such that only a few grains are across the workpiece thickness, and grains crystallographic

orientations exert a significant influence on the plastic responses of the respective materials [6]. These major issues associated with the process leads to reduction in formability, uncertainties in tooling fabrication, imprecision in material handling, inadequate control over the interfacial conditions, etc. [7]. All these problems seem to have their inherency in the plastic strain inhomogeneity caused by the grain anisotropy of the materials, crystallographic structure and texture formation under high plastic strain. Therefore, it is essential to developed to reduce the anisotropy of the materials to restrict the scattering of the process parameters during micro-forming.

1.2.1 Introduction to Micro-incremental sheet forming (μ-ISF)

Micro-incremental sheet forming (µISF) process is a recent development to tackle the issues arising due to size effect and constraints in the fabrication of required tooling at the micro-scale. In brief, it is a scaled-down version of the classical ISF process. The process uses a precise hemispherical-end shaped tool, typically having a radius in the range of 250-500 µm to deform thin metallic sheets/ foils of 50-150 µm thickness into a three-dimensional micro-components. It is a die-less process with multifold formability compared to traditional processes, for the production of customized miniature/ micro parts at ultra-precision range with better energy optimization. It offers higher formability, shape flexibility, high production capability, and better material utilization, compared to other available micro-forming techniques. The forming parameters in µISF also plays an important role in the fabrication of precise microproducts. Few of the dominant parameters are the feed rate, wall angle, spindle speed, type of forming tools (tool diameter and shape) and, incremental step depth etc. The various parameters of the µISF process that influences the deformation mechanism of the parts is shown in Fig. 1.3. The inward arrow marks (in red color) shows the input process parameters and the outward arrows (in yellow color) portrays the output parameters of the µISF process.

The preparation route to develop the μ ISF process is well explained and discussed in detail in Chapter 3. The received foil is first precisely cut to the workpiece dimension required for the μ ISF process. Then it is followed by the fabrication of the forming tool and the designing of the micro-forming fixture. The forming experiments was carried out on a high-precision CNC machine to develop the micro-parts. Several researchers have worked on the development of the μ ISF process. Saotome and Okamoto [8] first

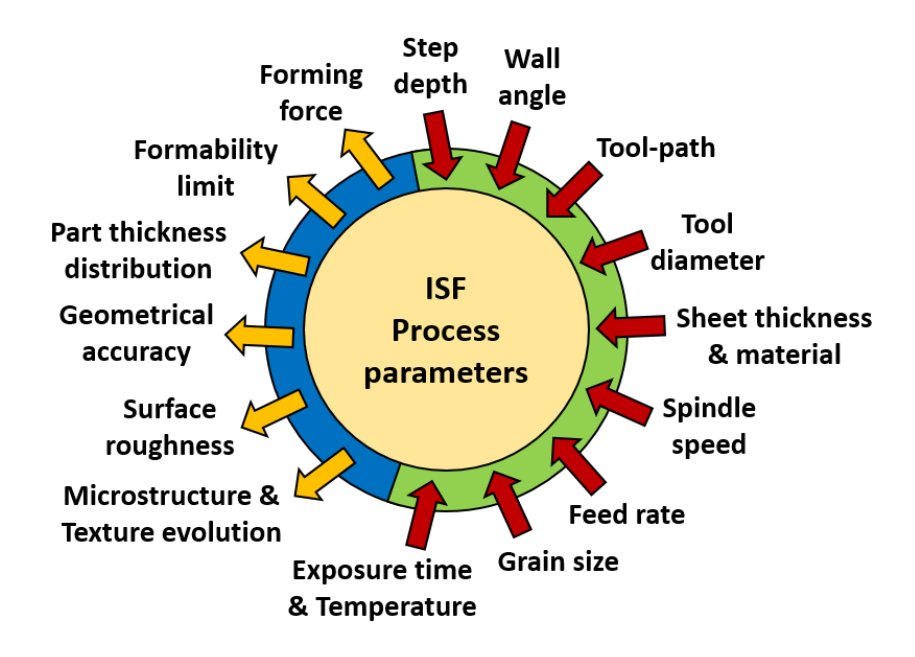


Fig. 1.3: Various process parameters used in the μISF process

suggested an in-situ μISF technique to fabricate a 600 μm long miniature part by repeatedly hammering a thin metallic foil of 10 μm thickness to create tiny incremental deformations. Obikawa et al. [9] developed a numerically controlled milling machine to deform a 12 μm thick foil to produce an array of small dots and pyramids without the use of any backup dies via μISF. They used a hemispherical end tool-tip of radius 500 μm for this process. It was observed that optimum tool rotation speed and step size have significant influence on material formability. Also, the lubrication using water between the tool and foil interface was identified to promote plastic deformation and reduce the forming forces. Bansal et al. [10] produced geometrical profiles of conical and funnel shapes of different wall angles for studying the formability of Al foils. The nature of the forming forces was studied, and a 13 % fluctuation in the cyclic nature of the axial force was recorded when moved from one position to another during forming. Beltran et al. [11] studied the size-effect and its relation with the material formability in the μISF process. A buckling mechanism of failure was discussed, resulting from high friction at the tool-sheet interface and inadequate tension during the clamping of the foil.

1.2.2 Challenges in the μ-ISF process

Although the μ -ISF process has many advantages due to its flexible nature of forming, but it also has few inherent limitations and challenges associated with the process for the large-scale production of the micro-products. The size-effect phenomenon

dominates during the miniaturization of the process which has significant impact on the homogenous deformation of the formed parts due to the scattering of process parameters [12]. Such scattering of the parameters, often leads to non-homogenous deformation due to increase in anisotropy of the material. The major sources of size-effects are pure volume source, surface-to-volume ratio, thickness-to-grain-size (t/d) ratio, surface structure scalability, etc. [5,13]. The issues lie in the reduction in formability, uncertainties in tooling fabrication, imprecision in material handling, inadequate control over the interfacial conditions, etc. The forming tools used for the μ-ISF process are low in bending stiffness, hence a robust fabrication approach is required to make the tools free from residual stresses and inaccuracies. Being a precise fabrication process, the forming time for making the micro-parts is also very high. The forming toolpath plays a vital role in deciding the forming time during the deformation process. The material springback is also a serious concern in this process. Such technologies are required to be developed to reduce the geometrical inaccuracies of the manufactured micro-parts.

1.3 Introduction to ISF

Sheet metal products are widely utilized in several applications ranging from household appliances like kitchen utensils to many high-end applications, such as in automobiles, defence, aerospace, and biomedical industries [14]. In conventional forming processes, sheet metal parts are formed using a press tool which consists of a punch and a matching female die. This requires a specialized process to design and fabricate the tool dies and punches for the forming operation. This increases the cost of the production for customized part fabrication. With recent advancements, new methods of forming sheet metal are now available to create flexible forming facilities, without dies, capable of producing complex-shaped surfaces by applying generic tooling. The goal is to develop die-less forming [15]. Incremental Sheet Forming (ISF) process is a flexible manufacturing process in which the metal sheet is deformed locally to a 3D part. It is flexible because no specialized tool and die is required to deform the sheet metal. The tool used is of hemispherical head-shaped or ball end shaped as it reduces the shear force parallel to the tool. The ISF process is performed on a high-precision multi-axis CNC machine. The toolpath of the geometry can be developed through a Computer-Aided Manufacturing (CAM) software or using programming codes in MATLAB®. Figure 1.1 (b) shows a conventional spiral toolpath strategy used in the forming process. The process is applicable to axisymmetric as well as asymmetric geometrical shapes and the tedious process of manufacturing a dedicated die and tool can be eliminated.

Recent studies on ISF have shown that this mechanism can deform not only sheet metals but also certain thermoplastic materials. These studies demonstrate that this technique is adaptable not just in terms of formability but also in terms of material choices. ISF can be used to create a variety of profiles with a sufficient level of precision, ranging from relatively simple ones like Bezier or splines curves to benchmark shapes like pyramids with square or triangular bases and circular cones. Research on generative sheet metal fabrication techniques, such as deep drawing and ISF, has advanced significantly during the past three decades. The capacity of the spinning process to generate sheets without the use of a die pave way for the ISF process. As a concept, in 1967, a patent filed by Leszak [16] initiated the research in ISF. Leszak, invented an apparatus capable of forming a wide variety of components using single tooling. Mason [17] gave a new vision to the ISF process by his work at the University of Nottingham. Mason in 1978 developed a forming process capable of incrementally forming asymmetrical metal components for rapid prototyping and batch-wise production. In ISF, there is no need for specialized dies to perform the forming process. Absence of dies also minimizes the cost of production. However, the process is comparatively slower than the traditional forming processes like deep-drawing and spinning. Owing to this reason, mass production using ISF process is not an option to industries, but batch production is a very suitable option for ISF.

Jeswiet et al. [15,18] elaborately presented a comprehensive review of the ISF process. Their review article discussed various types of incremental forming processes, equipment and tooling required for this process, and various material process parameters involved in this process. An approach that explains the mechanics of the ISF process was explained by Jackson and Allwood [19]. The ISF mechanics were found to include pure bending, shear parallel to the tool feed, and localized stretching perpendicular to the tool feed. Using membrane analysis, they have thoroughly examined the concepts of creating forming limit diagrams (FLD). Silva et al. [20] also used failure limit diagrams to show the dynamics and formability of the process. Their investigation revealed that during deformation stage, the cracks spread under tensile meridional stress acting under stretching nodes. Experimentations have revealed that localized necking does not precede fracture. Cao et al. [21] presented various advancements and

challenges associated with ISF in their review paper. They discussed doubly curvature surfaces, two-point incremental forming, CAD-based toolpath generation, surface finish and many other challenges required to improve this process. Zhai et al. [22] described various process advancement possibilities associated with ISF, like forming force analysis and its prediction, in their review paper. Further, they also discussed various hybrid ISF strategies, geometric accuracy, sheet thinning, surface finish, and forming efficiency of the process. Behera et al. [23,24] presented a very comprehensive review paper based on the decade long progress of ISF process from 2005 to 2015. This review paper covered various crucial aspects of ISF like various conventional toolpath strategies (spiral and constant z), forming and failure mechanics, simulation of the process, and possible applications.

1.3.1 Potential applications

The ISF process has been recommended by various researchers for customized fabrication or small batch-based productions of metallic parts. Considering the ductility, and malleability of pure Ti and Ti-64 sheets/ foils and their alloys, they have intensive applications in biomedical and aerospace industries, due to their excellent biocompatibility, good corrosion resistance, low density, and high strength [25–27]. The cranial implants [28], dental plates [29], and heel bone implants [30] are the most common ISF applications in the medical sector. The process also has useful applications in the manufacturing of bipolar plates used in fuel cells [31,32]. For MEMS fuel cells, highly conductive thin metallic foils have their application in the design of flow field plates with fine micro-channels [33]. SS foils also find their usage in industrial and space applications [34]. Copper and Brass foils also have their extensive applications in microelectronics industries [35,36]. Aluminum foils are widely used in food, medical and pharmaceutical industries for the packaging and fluid sealing applications [37-39]. A detailed comparative study related to cost effectiveness and batch-size production can be done to understand the profitability of this process over conventional manufacturing processes. Few of the potential applications of the ISF process are shown in Fig. 1.4 and discussed in Table 1.1.



Fig. 1.4: Few potential applications of the ISF process [30,40–43]

Table 1.1: Various applications of the ISF process

Broad area	Product applications
Automotive and aerospace	Automobile head light reflector, exhaust manifolds, motorbike seat and gas tank [44]
	Housings and fairings of aerospace, ship hull structures, Rocket nozzle assembly [45] [46]
	Bus sheet metal body parts Car [47]
	Car tail light bracket [48]
	1/8th scale model of Shinkansen (Bullet Train) [49]
	Stiffening frame for a hydraulic access door of an AIRBUS A320 aircraft [50]
	C-channel fixture designed for aircraft vibration testing [51,52]

	Aultinumenth asia [40]
	Ankle prosthesis [40]
Medical and bio-medical	Cranial implant [51] [52]
	Denture base [53]
	Back seat orthosis [24]
	Bespoke formwork, decorative panels [15]
Architectural	
	Free-form architectural envelopes and
	shapes [54]
Households	Solar cooker/oven [55]
	Dies and molds [56]
Other industrial components	
	Hole Flange [57] [58]

1.4 Problem Definition

The μ ISF process provides a viable micro-manufacturing technique to develop micro-parts made of ultra-thin metallic sheets (foils). In the present work, a micro-forming setup is developed for the fabrication of miniature complex geometrical shapes of ultra-thin sheets. The study incorporates the thickness-to-grain-size-effect, microstructural changes and mitigation of anisotropy in the specimens to achieve homogeneous deformation of the micro-parts with controlled heat-treatment of the specimens. The work also involves finite element simulations, coupling it with an appropriate damage mechanics model considering surface and volume grains effect, to predict the nature of micro-scale deformations during the process. A size-effect driven sustainable lubrication approach is also studied through lubrication pocket models to enhance the surface quality and formability of the micro-parts. It is envisaged that the proposed μ ISF process would face some challenges due to fragility of the foil and difficulty due to lower

formability, bending stiffness, dimensional accuracy and surface finish of the formed micro-components. Hence, few novel attempts in fabricating the forming tool and increasing the stiffness of the foil are explored in this work.

1.5 Organization of the Thesis

The overall work of the thesis is presented in the form of seven chapters as follows:

Chapter 1: This chapter discusses the motivation for the requirement of the micromanufacturing process. It also discusses the introduction and the fabrication route to develop the μ ISF process and the challenges associated with it. The potential applications of the ISF process are also discussed in detail. The chapter concludes by defining the problems taken in this research work and the organization of the thesis.

Chapter 2: This chapter discusses the detailed literature review concerning to the problem definition of the developed process. Further, it addresses the research gaps from the literature survey and various objectives identified for the study.

Chapter 3: This chapter focuses on the development of the µISF process set-up. It involves several trials in finalizing the dimensions of pillars, holding and backing plates, along with the clamping mechanism to ensure uniform blank holding forces during the deformation stage. This also includes comprehensive experimentations on the ultra-thin foils. Mechanical and physical characterization of as-received material is carried out to inspect the extent of material anisotropy. This includes studying the stress-strain relationship, load-displacement response and microstructural changes in different directions w.r.t. the rolling direction. Therefore, the combined effect of the grain size and step depth on the formability of the components is investigated. A relationship between formability and t/d ratio was established and its critical value was obtained.

Chapter 4: This chapter studies the development of a numerical simulation model in ABAQUS® by incorporating the effect of grain size and thickness (size-effect) of the material for the correct prediction of fracture in micro-scale deformation of foils in the µISF process. Based on the behavior of the material at small scale (inhomogeneous continuum), the decrease/ change in the flow stresses can be explained by the surface layer model (based on flow stress, grain size and thickness and other parameters). Furthermore, a comparative study is performed between two different types of incremental toolpaths (FGBIT and spiral) used in the µISF process.

Chapter 5: This chapter discusses a size-effect driven lubrication approach to improve the tribological performance of the micro-parts in the µISF process. The tribological behavior of the surface is highly influenced by the micro-asperities, acting as lubricating pockets, between the tool and workpiece contact regions. Solid lubricants like MoS₂ and Graphite are preferred over oil, grease, etc. as they are recyclable, environment-friendly, and have superior anti-friction properties. A sustainable lubrication approach is presented to counter the size-effect with lesser energy consumption and negligible waste generation.

Chapter 6: This chapter discusses two novel strategies to improve the formability and precision in the µISF process. The study is divided into two parts. The first part investigates the stacking of foils (SOF) approach to enhance the formability of the micro-parts by increasing the stiffness and plastic deformations of the foils. The second part studies a novel method for fabricating precise hemispherical-end shaped tools using the Reverse-µEDM technique for the µISF process.

Chapter 7: This chapter summarizes the key findings of the research work. It provides recommendations for future research, suggesting areas where further investigation could enhance the understanding of the developed µISF process.

2.1 Introduction

This chapter covers various research activities carried out by researchers working in the field of micro-scale deformation/ micro-forming of metallic sheets, rods, billets etc. The history of fabrication of micro-parts is discussed with recent developments in the µISF process. The influence of size-effect causes scattering of process parameters leading to non-homogeneous deformation of the micro-parts. Therefore, it is important to discuss the material size-effects in micro-forming applications. An increase in friction during the material deformation is also a serious issue, which affects the formability and tribological performance of the produced components. The study also covers the impact on the deformation load or the forces developed during the micro-forming process. The geometrical accuracy of the formed parts also depends on the toolpath strategy used in material deformation. Simulating the micro-process through the finite element method is also important to validate with the experimental results. Thus, based on extensive literature, research gaps and research objectives have been identified.

2.2 Development of micro-scale deformation in the µISF process

At the beginning of the 21st century, manufacturing industries in the developed countries were challenged by a set of common issues: aging population, environmental protection, science based manufacturing and manufacturing globalization. Trend towards miniaturization of the product/parts and the increasing use of microsystems technology in a rapidly growing field of applications, such as medical, communication, microelectromechanical, and micro-fluidic systems [3,59], has grown dramatically. In order to create the highest-quality products with the required characteristics and smoother working surfaces, it is necessary to develop novel manufacturing techniques in ultra-precision range. Incremental forming is one of the processes that is suitable for forming custom parts without making any component specific tooling. In the field of micro-manufacturing, which includes micro-forming, Japan has shown leadership, especially in applications related to the production of micro-products and parts for industrial and medical uses [3,60]. In 2001, Saotome and Okamoto [8] first developed a CNC-based micro-forming system to establish a micro-factory for deforming thin

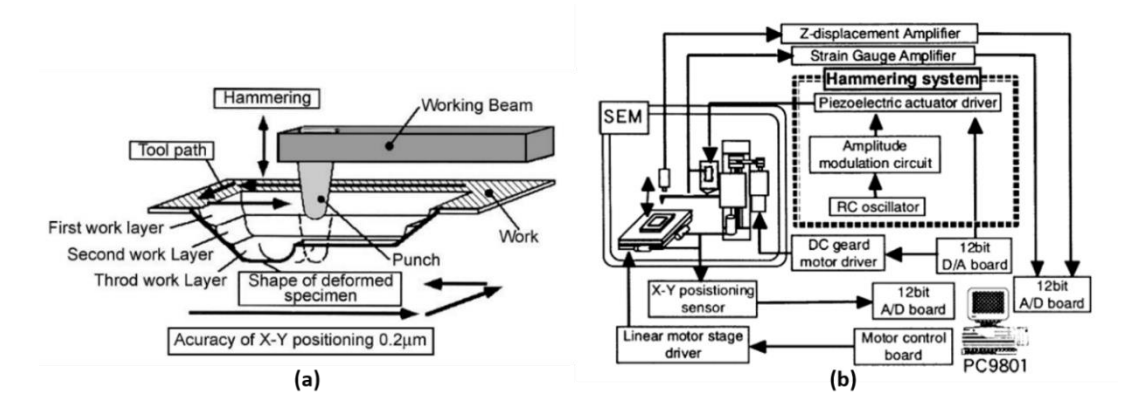


Fig. 2.1: (a) Principle of CNC incremental sheet metal forming by hammering (b) Schematic diagram of the micro-incremental forming system [8]

metallic foils as shown in Fig. 2.1. The authors executed an in-situ µISF experiment to fabricate a 600 μm length miniature components made from 10 μm thick Al foils. Small incremental shell structures were produced through step-by-step hammering of the tip of the hammer on the foil surface to achieve a decent geometrical accuracy of the microparts. Subsequently, Obikawa et al. [9] created a table-top micro-milling machine that uses progressive deformation on thin sheets that are 12 µm thick to create a collection of tiny dots and pyramids. Step size and tool rotation speed were thought to have a significant impact on material formability in µISF. Also, Sekine and Obikawa [61] developed polygonal-shaped complex shell structures on a Al foil of 12 µm thickness using a thin round-tip tool of 100 µm radius. They concluded that the large area of recontact between the forming tool and foil is responsible for pinholes or cracks nucleated on a foil surface. It showed that the forming limit is attributed to the adverse interaction between two adjacent pyramids formed on the surface. Beltran et al. [11] studied the size-effect and its relation with the material formability in the μISF process. A buckling mechanism of failure was discussed, resulting from high friction at the tool-sheet interface and inadequate tension during the clamping of the foil. Bansal et al. [62] created a micro-forming setup and geometrical profiles of conical and funnel shapes with varying wall angles to investigate the formability of Al foils. The cyclic nature of the axial force fluctuated by 13% when it was shifted from one position to another during the forming process, according to research on the nature of the forming forces. In trials involving pyramid-shaped parts, a twisting mechanism of failure was identified as a result of increasing step size and tool deflection in the opposite direction of tool motion. Li et al. [63] developed a novel macro-micro integrated (MMI) µISF process

for fabricating parts with functional surface micro-features. It was found that the MMI forming technique facilitates the uniform thickness distribution of the formed parts and, consequently, improves the surface quality. Mahajan et al. [64] exuted the µISF process on thin foils of SS304 having the thickness of 50, 100, and 200 µm. The foils were initially heat-treated to achieve strain-free microstructure. Through optimized parameters, it was observed that the higher tool diameter and the lower step depth resulted in a lower surface roughness of the micro-parts. Yoganjaneyulu et al. [65] studied the effect of spindle speeds on the formability, microstructure, mechanical properties and fracture behaviour of thin Ti-6Al-4V foils. It was found that the maximum forming limits were achieved at higher spindle speeds due to strengthening of basal texture and weakening of prismatic texture components. Obikawa and Hayashi [66] performed ultrasonic-assisted µISF on three different types of thin metallic foils. An ultrasonic spindle with axial vibration was implemented for improving the shape accuracy of micro-pyramids. In addition, laser heating was used simultaneously, which assisted in increasing the forming limit of the foils. Zheng et al. [67] used a slightly different approach, they used the laser-shock µISF technique to perform the plastic deformation of copper foils for the fabrication of fine micro-channels. The surface quality, micro-hardness and dimensional accuracy of micro-parts were improved through increasing the applied laser power density due to strain hardening effect. Developing a new technique, Shi et al. [68] worked on a water-jet based µISF process to induce the incremental plastic deformations, instead of using a rigid tool to form the sheet metal. However, supporting dies were used to provide proper control to the deformation process. Several types of micro-machined supporting dies were used to produce micro-scale shell parts with designed geometries. A summary of the literature discussed above is presented in Table 2.1.

Table 2.1: Summary of literature on the development of the μISF process

Year	Authors	Key Findings
2001	Saotome and Okamoto [8]	Developed a CNC incremental micro-forming system that created small incremental deformations on thin foils through hammering, and repeated step-by-step cycles to develop various shell-shaped structures.

2009	Obikawa et al. [9]	Suggested that the refinement of forming conditions and usage of smaller forming tools helps to form micro-objects more accurately.
2010	Sekine and Obikawa [61]	Showed that there existed an unconditional and conditional forming limits for forming plural number of particular shape of pyramids on the foil surface.
2013	Beltran et al. [11]	Presented that the buckling mode of failure occurs predominantly in the rolling direction of the foil, due to in-plane forming forces exerted by the tool.
2017	Obikawa and Hayashi [66]	Showed that the ultrasonic vibration improves the forming accuracy of stiff materials or difficult-to-work materials even if the shapes of micro-pyramids are simple.
2019	Bansal et al. [62]	A twisting mode of failure was detected in experiments of pyramid shaped parts due to increase in step size and tool deflection in opposite to tool motion direction.
2019	Shi et al. [68]	Water jet pressure plays an important role in the plastic deformation of the metal foil, and inappropriate combinations of toolpath and water jet pressure leads to buckling failure, which is not found in macro-scale ISF.
2020	Zheng et al. [67]	Laser shock incremental forming can serve as a feasible approach to fabricate metallic micro-channels. The surface quality and dimension accuracy of formed parts can be improved through increasing the applied laser power density.
2023	Li et al. [63]	The MMI-ISF process facilitates the uniform thickness distribution and improves the surface quality of the formed parts in comparison to the conventional ISF.

2023	Mahajan et al. [64]	The tearing mode of failure was observed due to the formation of strain-induced martensite in the deformation of thin foils of SS304. The microstructure and bulk texture analysis relate the orientation and twin fraction with the deformation behavior.
2024	Yoganjaneyulu et al. [65]	The FLD revealed that the speed and vertical step depth increases the limiting major true strain values. Rotational shear stress plays an important role in void coalescence, growth and length wise fracture of the Ti material.

2.3 Influence of Size-effect

The material behaviour changes with miniaturisation, because of the size-effects that occur when the scale is reduced from the conventional size to the micro-scale. With the reduction in size of metallic sheets, size effects gets introduced in the process which greatly influences the micro-forming operation and formability of the metallic sheet specimens used. The primary cause of size effects is the change in material behaviour, than macro-operations. The impacts of friction, grain size, orientation, sample thickness, tool geometry, spring back effects, coarse grain effects, and many other factors are covered in the three categories of size effects: density-based, shape-based, and structure-based as shown in Fig. 2.2 [5].

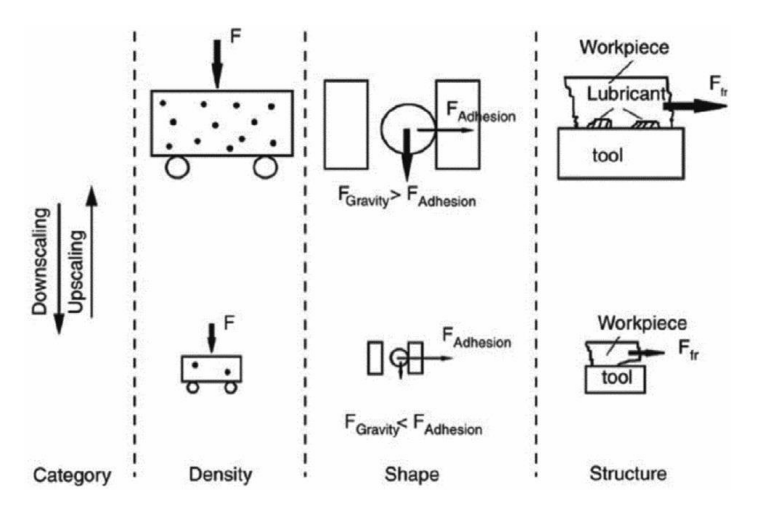


Fig. 2.2: Categories of size effects during miniaturization [5]

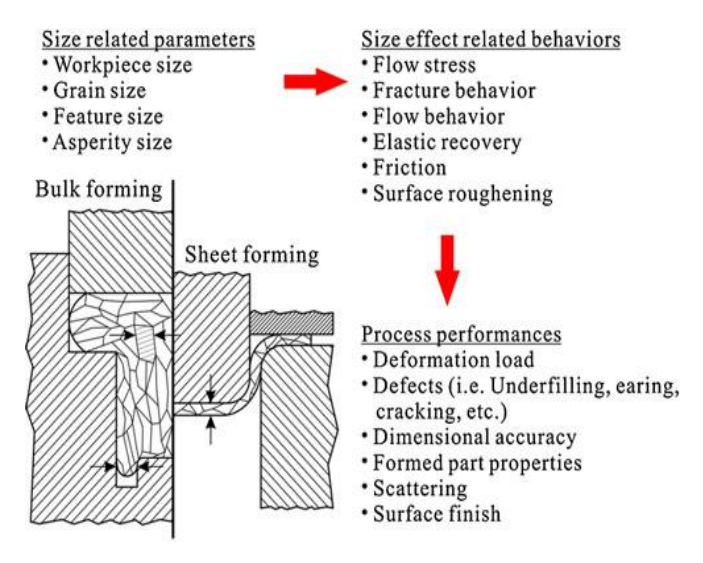


Fig. 2.3: Influence of size effects in micro-forming [59]

The influence of size-effects in micro-forming operations is discussed in a review article as summarized in Fig. 2.3. It discuss the influence of several known size-effects experienced during micro-forming operations, in particular during micro-deep drawing and micro hydro-forming process. Size effects and their categories involved in these processes are described which helps to understand their nature and importance. The problems caused by size-effects in micro-forming considering mechanical behavior, tribology, materials structure, and behavior are also discussed [59,69].

The size-effects are studied by various researchers and study shows that the material flow stress decreases with miniaturization. The surface layer model based on the fact that on small scales, the material cannot be considered as a homogeneous continuum anymore, and the decisive criterion is the ratio of grain size to thickness dimensions. The share of grains representing the surface layer becomes high compared to grains surrounded by other grains for micro-parts. During the plastic deformation process, the grains located at the specimen surface (V_s) and the grains located within the specimen volume (V_i) are expected to behave differently because of the lower forces of constraint in the surface area of the specimen [70]. One consequence of the miniaturization is an increase in the ratio of surface grains to volume grains as discussed in Chapter 3. As a result, the flow of stress is lower as shown in Fig. 2.4, the decreasing flow curves with the increasing of the miniaturization [13]. The same model is adopted when the size effect is studied in sheet metal micro-forming to approximate the maximum force in micro-air bending and micro-punching processes [6,71].

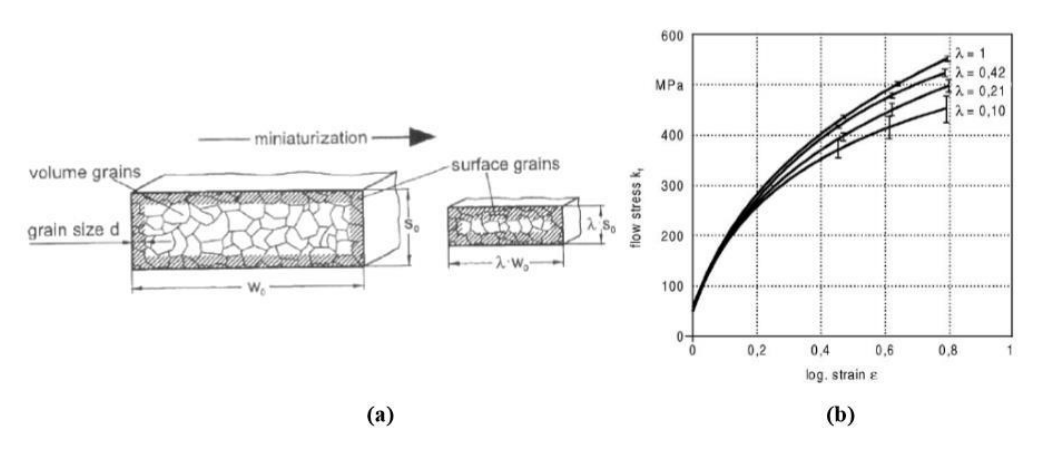


Fig. 2.4: Variables that appear with the miniaturization [13]

In general, there are two different types of size-effects that are widely considered to influence material behaviour. One is geometric size effect, such as the variation of feature and specimen sizes, while the other is the microstructural size of materials, generally represented by grain size. Fig. 2.5 shows these two types of size effects. The grain size effect occurs when the grain size is increased from d' to d while the feature and specimen sizes are kept constant. The feature and specimen size effects; on the other hand, come into existence when the feature and specimen sizes are decreased from D to D' while the grain sizes of materials are kept constant. Currently, both size effects are widely studied in meso and micro-scale forming [70]. For grain size effect, on the one hand, Hall [72] and Armstrong et al. [73] reported that the tensile yield, fracture stress, and the flow stress decrease with the increase of grain size of materials. This fact can be explained by the grain boundary strengthening caused by the pileup of dislocations. The ratio of the total grain boundary surface area to the material volume is decreased with the increase in grain size. This leads to the strengthening effect and flow stress when they decrease the grain boundary. For the feature and specimen size effect, on the other hand, the flow stress of metallic materials with the constant grain size is generally decreased in the size scale of deformation-based manufacturing with the scaling down of specimen dimensions [74].

Some techniques used to reduce the influence of size-effects include cold/hot rolling, heat treatment, effective lubrication, optimization of process parameters, etc. are being carried out in the area of micro-forming. The variation in the number of grains increases the effect of non-homogeneity/ anisotropy in the material leading to an increase in size-effect [75]. This significantly affects the geometrical features of the formed geometry

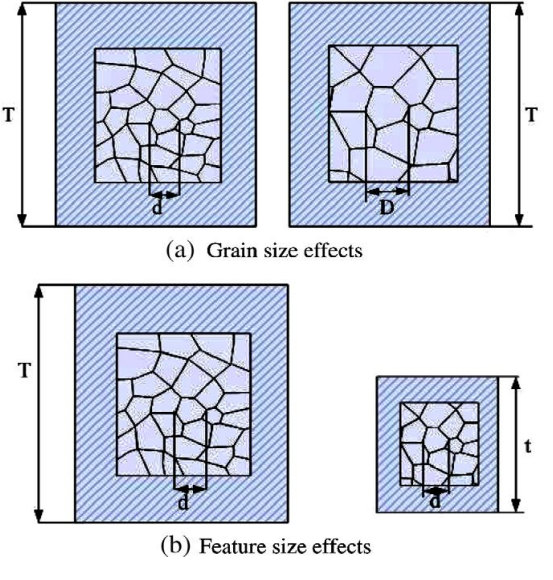


Fig. 2.5: (a) Grain size effect and (b) Feature size effect [70]

and causes changes in the micro-deformation behaviour. Zhu et al. [76] suggested that with controlled heat treatment (annealing), the issue of increase in anisotropy of the material can be minimized/ eliminated. The results were effective in minimizing the influence of the size-effect in the material. Mishra et al. [77] discussed the effect of plastic anisotropy during the sheet forming operations. It was observed that increase in the anisotropy influences the flowability and microstructural texture of the material, which causes high strain localization and premature failure of the geometries. For studying size-effect, range of different t/d ratios can be obtained by varying either the grain size/ sheet thickness or both in the specimen [20]. The physical importance of this parameter is related to the number of grains present through the foil thickness. Chan et al. [78] studied the stress-strain curves of pure copper with various ratios of the specimen size to the grain size of materials. Both the flow stress and fracture strain decrease with the ratio. The annealing temperature is also an important parameter that changes the microstructural behaviour by altering the grain size of the material. The influence of initial grain size on the deformation of thin Cu foils was studied by Hmida et al. [79]. The authors proposed a hardening law in relation to the varying t/d ratios of the foils. It was observed that the ductility, yield, and tensile strength reduced with the decreasing t/d ratio of the specimens. Also, different materials, such as for titanium [80] and Al [81], were further used in the experiments to study the effect of the ratio (t/d), and the same trend of the decrease of flow stress with the ratio was observed. Wang et al. [82] studied the forming characteristics of precise micro-channels made from Cu/Ni

clad foils. The effect of the material grain size and stacking sequence on the formability was investigated in detail. It was observed that higher annealing temperature assisted in increasing the depth of the micro-channels, but resulted in thinner wall thickness and lower surface quality. Chang et al. [83] explained that studying the microstructural changes during deformation is crucial to understand the deformation behaviour. The grain orientation and accumulation of the dislocations in the material greatly affect the formability of the formed components. A summary of the literature discussed on the influence of size-effect is presented in Table 2.2.

Table 2.2: Summary of literature on the influence of size-effect

Year	Authors	Key Findings
1961	Armstrong et al. [73]	Studied the influence of grain size-effects in the microscale deformation of the materials.
2001	Engel and Eckstein [71]	The authors discussed the influence of micro-forming in the industrial production technology. They also studied the various micro-forming process, their progress similarities, problems and general size-effects in micro-scale deformation.
2006	Vollertsen et al. [69]	Reviewed of the state of the art in micro-forming of metals. The occurring problems in miniaturization of forming technologies like micro-bulk forming and micro-sheet metal forming were discussed.
2008	Vollertsen et al. [5]	Discussed the various categories of size-effects. A definition of size-effects and a systematic order for size effects was proposed. The main categories are density, shape and microstructure size effects, which can be subdivided into further subcategories.
2008	Lai et al. [70]	Analyzed the influence of material size-effects and establish a martial model in micro/meso-scale. By combining surface model with theories of single crystal

		and poly-crystal, a mixed material model was proposed. It was found that the flow tress in micro/meso-scale is between single crystal model (lower bound) and poly-crystal model (upper bound).
2008	Lee et al. [84]	Ultimate stress increases with decreasing of t/d ratio while ultimate strain decreases with the decrease of t/d ratio of the specimens.
2009	Vollertsen et al. [13]	Described the changes in flow stress behavior during the miniaturization of the process. A description of size- effects on strength and tribology was discussed with its influence on formability and forming processes.
2012	Chan et al. [78]	Showed that the flow stress has a linear relationship with the ratio of specimen size to grain size (t/d) at a given strain, and the change rate of flow stress with the change of t/d could be considered to be independent of strain.
2013	Hmida et al. [79]	Studied that the yield stress, tensile strength and ductility decrease with the decreasing ratio of specimen size over grain size. The formability for the incrementally formed parts deteriorated as t/d ratio decreases.
2013	Xu et al. [75]	The yield strength of SUS304 stainless foil increases with the decrease of foil thickness and grain size in micro tensile tests.
2013	Fu and Chan [59]	Discussed a review on the state-of-the-art micro- forming technologies to establish several micro- factories. It focused on the size effect-affected deformation behaviors and the mechanisms of the changes of flow stress, flow behavior, fracture

		behavior, elastic recovery, and the surface finish of the
		formed parts.
2014	Musa et al. [74]	Through, uniaxial tensile-testing experiments, it was found that the flow stress of the materials decreased with the decrease of the strip thickness due to size/scale effect.
2015	Gau et al. [81]	They showed that through adjusting annealing conditions such as temperatures, different t/d ratios on the same foil can be obtained with several formability aspects on the micro-channels.
2020	Zhu et al. [76]	Suggested that with controlled heat treatment (annealing), the issue of increase in anisotropy/ non-homogeneity of the material can be minimized/eliminated.
2020	Wang et al. [82]	Examined that the micro channel feature size and surface roughness have significant influence on forming quality of the micro part.

2.4 Tribological aspects in micro-forming

When the forming operation is scaled down from macro dimensions to micro dimensions, friction has a very significant effect on the whole operation due to the micro-scalable surface topography of metal sheet and higher surface to volume ratio of the micro parts. Size effect causes drastic increase in friction in micro-forming applications. Effect of friction explained by Engel [85] showed that there is a decrease in lubrication effect and increase in friction force in micro scale operations due to size-effect. Messner et al. [86] conducted the finite element simulation on conventional upsetting tests to evaluate the friction on cylindrical specimens with dimensions equivalent to micro-forming operations. Considering scaling effect, friction coefficient and flow curves were determined. The frictional behaviour observed can be explained

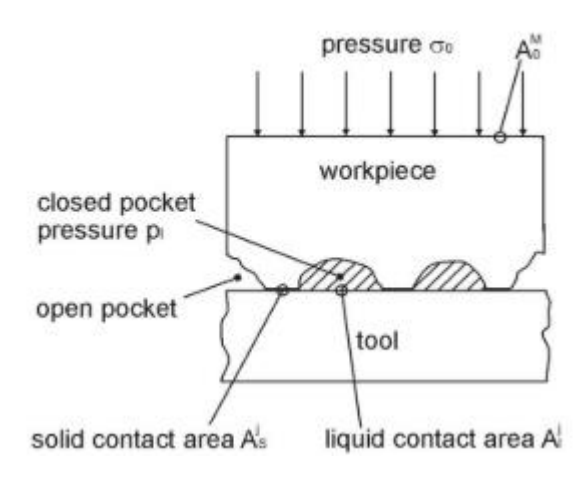


Fig. 2.6: Lubricant pocket theory for the coefficient of friction in micro-forming [87]

by the model of open and closed lubricant pockets (OLP and CLP), also called dynamic and static lubricant pockets, as explained by Vollertsen [87]. When a forming load is applied to a lubricated workpiece surface, the asperities (roughness peaks) start to deform plastically, thus increasing the pressure of the lubricant, which is trapped in the valleys of the peaks. The valleys that do have a connection to the edge of the surface, thus are unable to entrap the lubricants for longer periods. These are called the OLP's. With the increase in normal pressure, the lubricant escapes and is not able to support the forming load. The forming load acts only on the asperities, which result in a higher contact stresses, and more surface flattening, and thus, resulting in higher surface friction. On the contrary, CLP's, do not have a connection to the edge of the surface. The lubricant gets trapped in those pockets and pressurized during forming as show in Fig. 2.6. The developing hydrostatic pressure thus takes a part of the external load, thus reducing the normal pressure with CLP. Geiger et al. [88] conducted extrusion test using different types of lubricants. From the lubrication pocket theories, it was observed that the liquid which was used as lubricant in this process was lost during the micro-extrusion process and a dry solid lubricant was able to provide the necessary lubricating effect. Wang et al. [89] studied the micro-forming process to establish an explicit friction model in micro/mesoscale to calculate the coefficient of friction (COF) considering size effects. With the open-closed pocket assumption and Wanheim/Bay friction law [90], a scaling factor was adopted to describe the size effects on the tribological behaviors in micro-upsetting deformation. Sudarsan and Panda [91] developed serpentine shaped micro-channels through the micro-stamping of thin SS and Al foils. Study showed that the deformation load was significantly influenced by the COF and type of lubricant used. It was found that the application of lubrication resulted in lower forming load and reduced maximum thinning of all the materials. Weidel and Engel [92] studied that during the micro-forming process, few of the micro-pockets or the asperities will be in actual contact with the tool surface. Therefore, the behavior of the asperities during the deformation process is very important for the flattening of the surface and tribological responses. A summary of the literature discussed on the tribological aspects in micro-forming is presented in Table 2.3.

Table 2.3: Summary of literature on the tribological aspects in micro-forming

Year	Authors	Key Findings
1974	Wanheim et al. [90]	A general theory for friction in metal working processes was developed based upon the slip-line theory as a model of analysis in micro-forming operations.
1994	Messner et al. [86]	Proposed a size-dependent FE-simulation applied for studying frictional size-effect in micro-upsetting of cylindrical specimens.
2005	Engel [85]	Studied the tribological conditions between tool and workpiece in micro-forming operations. The author suggested that conventionally used friction laws cannot explain the general tribological surface topography in micro-forming.
2008	Geiger et al. [88]	A free bending concept was established for the investigation of size effects in micro foil forming that relates the study of spring-back and bending moment.
2009	Weidel and Engel [92]	To study the micro-tribological behavior, modelled the asperities as representation of pyramids with a base area of 120 μ m×120 μ m and a height of 32 μ m. Flattened with a high-resolution experimental setup

		which enables in-situ observation of the contact area in micro-forming.
2011	Vollertsen et al. [87]	Studied the influence of speed and the punch diameter in micro-deep drawing, taking the micro-tribology into account, which takes place at the contact of individual asperities. Temperature dependent viscosity of the lubricant was examined to study the frictional size-effect.
2014	Wang et al. [89]	Based on the Wanheim/Bay friction law and open- closed pocket assumption, the scaling factor and liquid pressure are considered in the calculation of COF. A new friction model was developed including scaling factor, fraction of real contact area, and liquid pressure.
2022	Sudarsan and Panda [91]	Studied the effect of lubrication on the formability of serpentine shaped micro-channels in terms of peak load, maximum thinning and thickness distribution along the channel wall.

2.5 Formability of micro-parts

Formability is a measure of maximum deformation possible in a sheet without failure. It has been reported that ISF exhibits higher formability than conventional forming processes like the spinning or deep drawing process [46]. Due to high elastic modulus and high yield strength of the sheet metal parts, the metallic parts have the advantage to deform efficiently with good stiffness and an excellent strength-to-weight ratio. However, for a given process and deformation geometry, the forming limits vary from material to material. The primary concern is whether the desired deformation can be accomplished without failure of the workpiece. Formability is presented by a Forming limit diagram (FLD). FLD is also refereed as principle strain space Keeler-Goodwin diagram, given by Keeler [93] for the tension-tension strain space and then further elaborated by Goodwin [94] for the tension-compression strain space in the left quadrant. This diagram is broadly used to characterize the limit to which the metal sheet

can be plastically deformed deprived of necking or fracture. The ISF process enhances the formability limit of the material significantly compared to other traditional metal forming process. The forming limit curve (FLC) is calculated by determining the inplane major and minor strains along the pre-defined path of localized necking, followed by interpolation of the measured strains. This leads to form a bell shaped curvature by considering of the strain value of the necking region [95]. The forming limit by fracture in the principle strain domain, proposed by Atkins [96] in 1996, combined the concept of FFL line with the critical decrease in the thickness of the metal sheet and failure data subjected to stress triaxiality ratio. The stress triaxiality is expressed as the fraction of the average stress to the von Mises stress, on which the ductile damage mechanism works with voids growth principle [97]. Ductile fracture model was productively explored by Wu et al. [98] to evaluate the fracture formability limit during the incremental forming process. The model used plastic work principle and the assumption of the isotropic hardening theory.

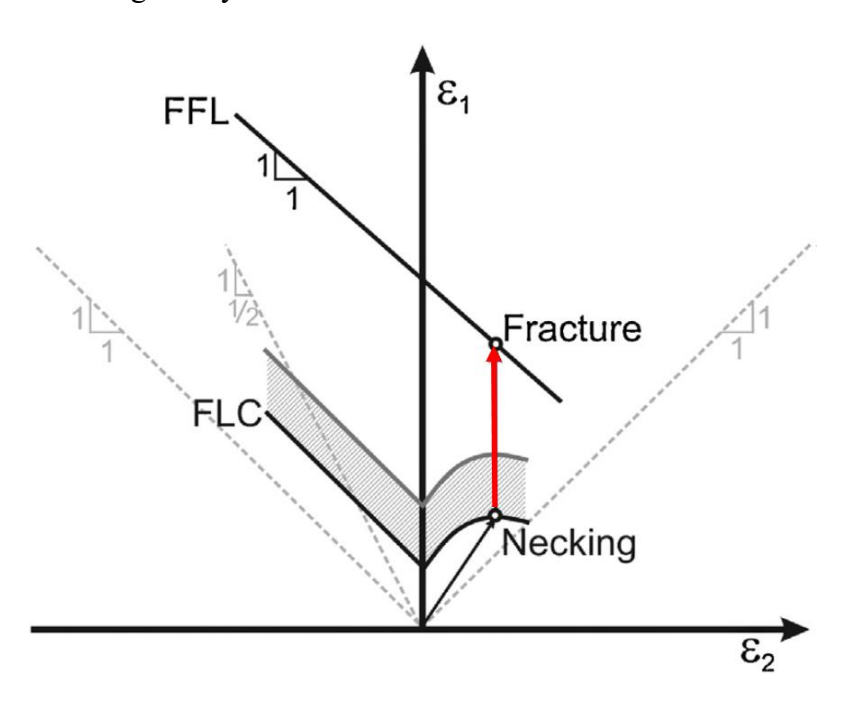


Fig. 2.7: Schematic demonstration of the FLD showing principle strain space presenting the FLC and FFL [95]

Fig. 2.7 presents the illustration of the principle strain space for the FLC and FFL lines. Beginning of the necking region, shift from the FLC to the FFL line is described by the sharp turn of the strain space moving in the upright direction to fracture because of the plastic instability and excessive necking. In general, typical sheet forming tests normally

combine the bending with the in-plane loading of the work piece surface for conventional sheet formability tests. Though, it is difficult to directly obtain FFL from strain measurements from the circular grid analysis study in conventional forming because of the in-homogeneous plastic deformation [95]. In ISF process, it is helpful to study both the FLD and FFL of the sheet metal formed truncated conical or pyramidal shaped components with different wall angles due to the process capability to obtain linear stretching of in-plane strain routes from the start of necking until failure with less localized bending of the sheet metal [99]. The experimental technique utilized for obtaining the FLC involves electrochemical etching or laser ablation of the sheet and the generation of circular grid over the sheet's region to be formed. By measuring the major and minor diameter of the ellipses, the true major and minor strains are calculated using the following equations 2.1 and 2.2 [20]. Where, a and b are the major and minor axes of the ellipse after deformation, and R is the radius of the circular grid.

$$E1 (Major strain) = \ln(a/2R)$$
 (2.1)

$$E2 (Minor strain) = \ln(b/2R)$$
 (2.2)

In ISF, different forming parameters such as feed rate, step depth, tool diameter and tool rotation have significant impact on the formability of the material. Several researchers examined the effects of various parameter on the formability of the different component shapes [46]. Isik et al. [95] used the fundamental concept of plastic flow associated with damage mechanics to suggest a new experimental technique to determine the forming limit by fracture in ISF. The results helped in the revision of plasticity concepts of critical sheet thickness reduction and distortion in metal forming field. Nirala and Agrawal [100] presented a sheet thickness prediction model to estimate the thickness of the sheet before conducting the experiments. The calculated model for determining the sheet thickness was also developed to validate it with the experimental results. The authors also investigated the fracture forming limit for two different circular and elliptical shaped geometry. Sheet fracture was observed for both the profiles. The fracture points were witnessed above the FFL line. Shim and Park [101] performed the ISF experiments to determine the forming limit curve for different types of shapes i.e. triangle, square, pentagon, hexagon, octagon, circle and square with round corners. Various strain paths were applied to the sheet by imposing different tool paths and the major and minor strains of deformed grids around cracks were measured. It was found

that the formability of the sheet shows a distinct dependence on the strain path and appears as a straight line in the FLD.

In micro-scale deformation, Sudarsan et al. [102] studied the FLD of a 200 µm thick SS304 foil using a sub-size limiting dome height (LDH) test to deform rectangular specimens of different widths. It was observed that there was marginal change in limiting strains due to the change of punch diameter from 30 mm to 50 mm. At higher forming speeds, decrease in the limiting strains were observed due to higher strain rate sensitivity of the ultra-thin SS304 foils. Zhu et al. [76] performed a series of μ-LDH tests to investigate the temperature effect on the formability of the as-received CP Ti Gr2 foils. Four FLCs for room temperature, 100 °C, 200 °C, and 300 °C were created. They suggested that forming the foils by using high-velocity impact process at the elevated temperature can increase the formability and have more uniform thickness distribution of the micro-parts. Mashalkar et al. [103] studied the empirical (analytical), numerical, and experimental approach to calculate the FLCs for 90 µm brass foil. Gau et al. [81] conducted a series of experiments on the annealed and as-received aluminum 1100 foils of 50 µm and 75 µm to investigate the influence of size effects on the formability of the micro-channels. It was concluded that the Al foil with lower t/d ratio (annealed at a higher temperature) has the better formability (larger channel depth) regardless of the deformation modes. Hmida et al. [79] showed that the formability of the copper foils has significant impact on the grain sizes of the specimens. It showed that the formability in the µISF process decreased with the decrease in the t/d ratio of the foils. Wang et al. [104] examined the deformation and forming behaviors of pure nickel thin sheets of 100 µm. The formability of microchannel was evaluated from the aspects of thickness thinning and surface roughening of the formed parts. Yoganjaneyulu et al. [65] studied the influence of tool rotational speed on the formability of ultra-thin Ti-6Al-4V alloy foils in the μISF process. It was found that the maximum forming limits were achieved at higher spindle speeds due to strengthening of basal texture and weakening of prismatic texture components. FLC showed that an increase in spindle speed can delay the onset of local plastic deformation, thereby higher limiting strain can be achieved at higher speeds. A summary of the literature discussed on the formability in the forming process is presented in Table 2.4.

Table 2.4: Summary of literature on the formability in the forming process

Year	Authors	Key Findings
1965	Keeler [93]	FLD have been empirically constructed to describe the strain states, or combinations of major (\mathcal{E}_1) and minor (\mathcal{E}_2) principal strains, at which a highly localized zone of thinning or necking becomes visible in the surface of sheet metal.
1968	Goodwin [94]	Proposed a Keeler-Goodwin forming limit curve for the tension-compression strain space for different materials.
1996	Atkins [96]	Combined the FFL curve with FLC to provide the information of ductile fracture criteria for large-deformation finite-element calculations.
2001	Shim and Park [101]	Showed that the formability of the sheet displays a distinct dependence on the strain path and appears as a straight line in FLD.
2008	Silva et al. [20]	The overall formability in ISF process was explained through combining the study of stress and strain for small localized deformation.
2012	Lou et al. [99]	Proposed a new ductile damage criterion taking the consideration of void nucleation, void growth and stress triaxiality to construct a fracture FLD curve for dual phase steels.
2013	Hmida et al. [79]	Studied the influence grain size-effect on the formability of the thin copper foils.
2014	Isik et al. [95]	Used of the theory of plasticity to proportional strain loading paths, under plane stress conditions, to analyze

		the FFL line and to introduce the shear fracture during forming.
2018	Nirala and Agrawal [100]	Predicted forming limit for two wall profiles, viz., circular and elliptical wall. A methodology was presented to predict and calculate sheet thinning during ISF.
2019	Mashalkar et al. [103]	Proposed an analytical approach to study the FLC for ultra-thin brass foil.
2019	Sudarsan et al. [102]	Presented the effect of circular grid size, stretching direction punch size and deformation speed on limiting strains to develop the FLD in micro-LDH test.
2020	Wang et al. [104]	Studied the formability of pure Nickel thin sheets with various grain sizes and t/d ratios. A new constitutive model based on Hollomon's equation was established to predict both the flow stress and fracture strain.
2020	Zhu et al. [76]	Performed μ -LDH test of 75 μ m annealed Ti foils with variation in punch speeds to determine the FLD. Annealed foils obtained better formability with uniform thickness distribution.
2021	Wu et al. [98]	Ductile fracture criterion considering the scope of stress triaxiality was employed for studying the FFL curve.
2024	Yoganjaneyulu et al. [65]	Presented the influence of tool rotational speed on the formability of ultra-thin Ti-6Al-4V foils in the μ ISF process.

2.6 Forming forces

For safe design and utilization of all machine tools during the forming processes, it is crucial to estimate the maximum forming force requirement during the deformation of the material. Furthermore, the quality of produced components and material failure are also dependent on the forming forces. During the deformation process, the sheet experiences increase in strain hardening due to movement of dislocations in the material. This leads to increase in the magnitude of stresses during the stretching of the sheets. The forming forces generated in the material adapts to reach the equilibrium position with uniform thinning of the material, which helps to achieve the desired dimensional profile of the deformed shape. Incremental forming is studied by various researchers to analyse the influence of process parameters on forming forces. Petek et al. [105] used a piezoelectric principle-based dynamometer to measure the forming forces. The forming force increased with an increase in the wall angle of the geometry and the tool diameter. The amplifier used during the force measurement amplifies the electrical signals generated during the deformation process and in-situ data is recorded with computerbased software using the dynamometer. The forming forces were recorded in three principal directions with respect to the dynamometer measurement axis i.e. F_x and F_y (circumferential directions) and F_z (axial direction) as shown in Fig. 2.8.

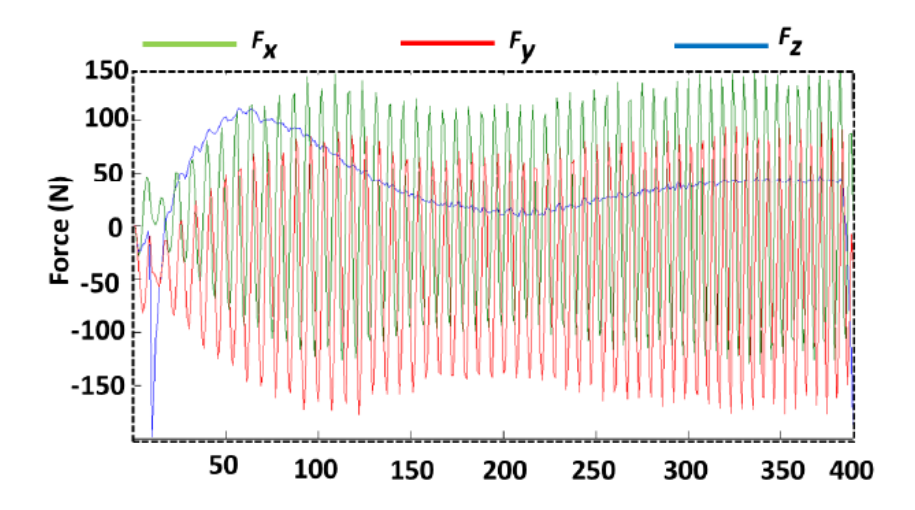


Fig. 2.8: Measurement of the forming forces in different directions [105]

The initial increase in force trend could be caused by the bending mechanism. As the deformation process progresses, the contact area between the sheet and the tool increases and starts stretching of the sheet surface. The sheet stretching would result in

increased forming forces due to strain hardening of the sheet. The in-plane forces (Fx and Fy) tend to increase with increase in the wall angle, this happens because the stretching of the sheet increases which requires high strain rate [19]. Santiago et al. [106] found that the maximum axial force value increases with an increase in tool diameter and incremental step depth. This is because of the increased contact area between the tool and the workpiece and more material deformation per step. Based on the above two parameters, Aerens et al. [107] developed an empirical relation to estimate the forming force for components with uniform wall angle. The approximate formula to estimate axial force was recommended based on the regression studies carried out on different types of materials.

A few failure models have been developed in the literature by understanding the forming force behavior [108]. Although the value of the forming forces in circumferential directions tends to be small compared to the force in the axial direction, the trend of the forming forces in circumferential directions might be used as a potential indicator for preventing material failure [109]. Chang et al. [110] developed an analytical model and conducted an experimental validation of forming force during the ISF process. The developed model can predict the forming force for single-point ISF, multi-point ISF, and incremental hole flanging process. Further, the model is developed by calculating the contact area of the forming tool with the sheet and performing membrane analysis of the developed contact stress. Bansal et al. [62] studied the cyclic nature of the axial force in µISF. The forces fluctuated by around 13% when it was shifted from one position to another during the forming process of micro-parts. This fluctuation was contributed by planar anisotropy of AL 5052-H19 material. Beltran [11] measured the forming forces to study as an indication to start of bukling mode of fracture during deformation of thin SS foils. The failure of the micro-parts were characterized by the sudden drop in Z forces before actual failure.

Hmida et al. [79] carried out the microstructural size-effect study based on the grain size of the copper foil. It was found out that the increase in grain size decreases the tensile strength, yield strength and, ductility of the sheet with the decrease in the measured forming forces. Similarly, Srivastava and Tandon [111] studied the grain size dependency on the nature of the forming forces in the ISF process. It was observed that the increase in grain size results in decrease in the peak value of forming force. A

summary of the literature discussed on the measurement of forming forces is presented in Table 2.5.

Table 2.5: Summary of literature on the measurement of forces in the ISF process

Year	Authors	Key Findings
2005	Jeswiet et al. [112]	They had used a specially designed cantilever type of sensor with strain gauge Wheatstone bridges. This design's <i>in-situ</i> calibration was done by applying bending and axial loads at the appropriate bridge direction and results were recorded and verified.
2006	Ambrogio et al. [108]	They studied the sheet's failure (AA 1050-O) during ISF based on the trend of forming forces. Further, the bending of the sheet to be formed is the most relevant mechanism until the maximum force was achieved.
2009	Petek et al. [105]	With the increase of a wall angle and tool diameter causes larger forces and deformations. Rotation tool does not have any influence on the force and deformation size but has a strong influence on the quality of the surface.
2010	Aerens et al. [107]	Based on an analytical force analysis of the process and results of FEM simulations, a formula to compute the radial component (Fr) of the force was introduced.
2011	Santiago et al. [106]	Forming force is an important indicator that can be monitored on-line and utilized for real time process control.
2013	Beltran [11]	The drop in the forming forces can be studied as a signal indicator to the start of necking or failure of the formed parts during the deformation stage.

2013	Hmida et al. [79]	The forming forces show an excellent correlation with the results of tensile tests. The decrease in the level of the forming forces with respect to the grain size was demonstrated and it was consistent with the Hall–Petch effect.
2014	Li et al. [109]	Studied the trend of the forming forces and had found that due to strain hardening of the sheet the forming forces tend to increase up to a point and after that due to thinning of the sheet the magnitude of these forces tend to decrease.
2015	Srivastava and Tandon [111]	An empirical model was proposed which establishes the mathematical relationship between the forming force and forming depth, with change in the grain size of the specimen in ISF.
2019	Bansal et al. [62]	Showed that the nature of forming forces in incremental forming of both macro-scale and micro-scale parts were similar. However, the fluctuation in axial force is much higher in micro-scale parts compared to that obtained in macro-scale parts.
2019	Chang et al. [110]	Developed an analytical model and conducted an experimental validation of forming force during ISF process.

2.7 Forming toolpath

ISF is a highly flexible process and the formed geometry depends on the forming toolpath. When the sheet is being deformed, the sheet material starts to deform along the direction of the toolpath. The sheet stretches in the negative z-direction movement of the tool to attain the final geometrical shape. When the toolpath is represented through various increments to subdivide the deformation into incremental steps, such toolpath is known as an incremental forming toolpath. Incremental toolpath generation is a vital step in ISF for the fabrication, and numerical prediction of the desired geometrical

shape. To explain the deformation mechanism and have a better understanding of the process, two different type of conventional toolpaths (constant z and spiral) are shown in Fig. 2.9. The forming tool travels a defined path in the x-y plane, which is dependent on the required geometry. Then, the increment of the tool is provided in the negative-Z direction, which is generally called as step depth/ down (Δz) (Fig. 2.9). The quality of the formed part depends on the toolpath strategy adopted and forming tool-sheet interaction [14]. At present, many existing CAM (Computer Aided Manufacturing) software are commercially available to generate an incremental toolpath for ISF processes like Siemens NX 8.0®, CATIA® and Delcam PowerMILL 10® etc. However, such commercial toolpaths do not provide much flexibility to the generated incremental toolpath.

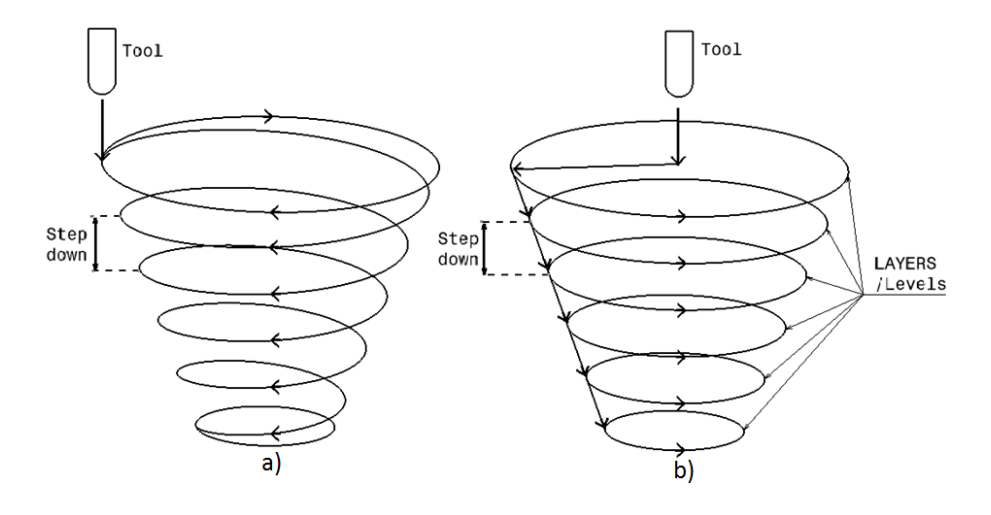


Fig. 2.9: Conventional type of toolpaths in ISF (a) Spiral (b) Constant Z [113]

In ISF, the deformation is governed by the single point contact between the sheet and the forming tool. The surface finish of the formed components depends on the material ridges or staircase (Fig. 2.10) formed due to the incremental nature of these toolpaths [114]. Smaller increments or step depth results in the improved surface finish but forming time increases due to such toolpath implementation. The surface finish of the produced component may differ while maintaining the same incremental depth. The dependent variables could be the generated components complexity or the changing wall angle. In the literature, spiral toolpaths have been used to enhance the surface finish of produced components [115]. Malhotra et al. [116] created an incremental tool path strategy based on the theory of volumetric error and constant scallop height of the formed component. Li et al. [117] conducted an experimental and numerical study based

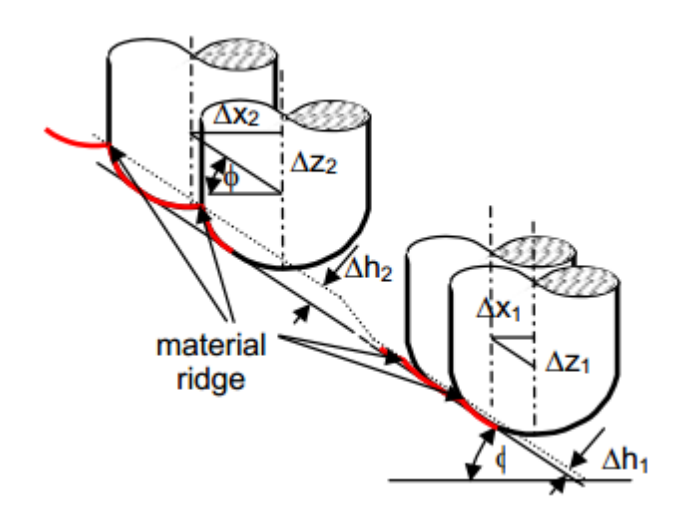


Fig. 2.10: Staircase or material ridges formed due to toolpath in ISF [114]

on three different types of incremental toolpaths. The position of the sheet and its minimum thickness zone were found to be related. Their analysis confirmed that the incremental step depth determines the position of the minimum thickness zone, whereas the tool diameter mostly determines the minimum thickness. Blaga et al. [118] used the constant z and spiral incremental toolpaths to understand the optimal forming strategy. The optimal forming strategy had been verified in terms of homogeneity of the strain distribution, thickness distribution, minimal force distribution, and geometrical accuracy. Lu et al. [115] developed a novel incremental toolpath approach based on feature detection algorithm and generation of equipotential lines. The results suggest that the new tool path stretches the sheet in a different way and results in good thickness distribution, geometric accuracy and surface quality. Lingam et al. [119] established a toolpath compensation algorithm to enhance the geometrical accuracy of the formed parts. Force equilibrium method along with thickness calculation methodology was developed for various types of geometries i.e. free forms, multiple feature geometries etc.

The spiral toolpath engages with the sheet continuously, therefore the toolpath do not leaves any marks on the formed surface and promotes uniform thickness distribution of the sheet metal. Singh et al. [120] performed the experimental and numerical investigations on structural thinning of deformed geometries. Study showed that continues spiral toolpath provided slightly more uniform thickness compared to stepped contour toolpath. Boudhaouia et al. [121] performed an experimental and numerical study for a spiral toolpath strategy while forming a conical geometry. Forming forces

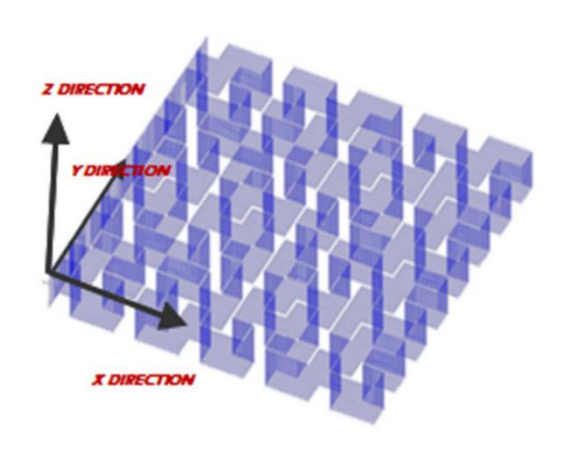


Fig. 2.11: Space-filling fractal toolpath [122]

and geometrical accuracy had been analyzed and found to be in good agreement with the FE analysis. Recently, Nirala and Agrawal [122] used a space-filling fractal toolpath (Fig. 2.11) to compare with the geometries formed with spiral and constant z toolpaths. Better formability, stress, and thickness distribution have been observed by adopting the proposed toolpath strategy. A summary of the literature discussed on the usage of incremental toolpaths is presented in Table 2.6.

Table 2.6: Summary of literature on the usage of incremental toolpaths in the ISF process

Year	Authors	Key Findings	
1994	Matsubara [123]	Unilateral incremental toolpath has been used for the first time in ISF.	
2007	Ambrogio et al.	Investigations on multistage ISF and presented its benefits over the single stage ISF.	
2010	Malhotra et al. [116]	Proposed a 3D incremental tool path strategy based on volumetric error and constant scallop height of the formed component.	
2013	Lu et al. [115]	Developed a novel incremental toolpath approach based on feature detection algorithm and generation of equipotential lines	

2013	Blaga et al. [118]	Studied the constant z and spiral incremental toolpaths, and increment location for constant z toolpath has been shifted by 90° to understand the optimal forming strategy.
2016	Lingam et al. [119]	Established a toolpath compensation algorithm and extended their work by implementing the developed toolpath compensation strategy into variety of components like free forms and multiple feature geometries.
2016	Singh et al. [120]	Showed that the spiral toolpath provided slightly more uniform thickness compared to the contour toolpath.
2018	Li et al. [117]	Expanded the work on ultrasonic assisted ISF and studied the material flow characteristics of the sheet during deformation.
2018	Boudhaouia et al. [121]	For the experimental and FE analysis, spiral toolpath strategy was used to form a conical geometry to support the results for lower forces and geometrical accuracy.
2018	Nirala and Agrawal [122]	Proposed a space-filling fractal curved toolpath to improve the formability and thickness distribution of the formed parts.

2.8 Numerical simulation approach

Numerical simulation using finite element analysis (FEA) provides a good prediction of various output parameters, without actually conducting extensive experiments. The FEA is a computational tool used to predict the deformations, forming forces, stresses and strains throughout any material structure (sheet or foil) [125]. Elastic-plastic material models are required to define the properties of the sheet. Material stiffness matrix can be written explicitly for the isotropic elasto-plastic model for the deformation analysis of the ISF process. The isotropic elastic plasticity theory (ABAQUS® user manual) has been used while performing initial dynamic explicit simulations of ISF [126]. This is

one of the simplest model used for the calculations of plasticity-related problems in ABAQUS®. Other FE software are also available such as LS Dyna®, Altair HyperWorks®, Hypermesh® suite etc. to perform the numerical analysis of the ISF process.

The accuracy of ABAQUS® results depends on the quality of technical data available as input to the FEA model. Parameters like Young's Modulus (E), poisson's ratio (v), material density (δ), strain hardening exponent (n), friction coefficient (μ) and material constant need to be accurately known for any sheet metal forming simulation. Meshing affects the accuracy of results and computational time. Generally, adaptive meshing is preferred to optimize computational time with accuracy. Adaptive meshing avoids the mesh element distortion, hour-glass effect of the elements and element entanglement. This may further reduce computational time and improve FEA predictions. Equilibrium equations are the basis of FEA, and calculations are made to determine if these partial differential equations will converge. Both implicit and explicit integration strategies are used to solve these problems. The implicit scheme is unconditionally stable as it requires several iterations to converge to the equilibrium. In contrast, the explicit scheme starts by computing the equilibrium condition at the beginning of the time step (Henrard et al.) [127,128]. A flow chart work methodology has been explained graphically in Fig. 2.12(a) to carry out the finite element analysis of the ISF process and Fig. 2.12(b) shows the meshed sheet and the analytically rigid forming tool.

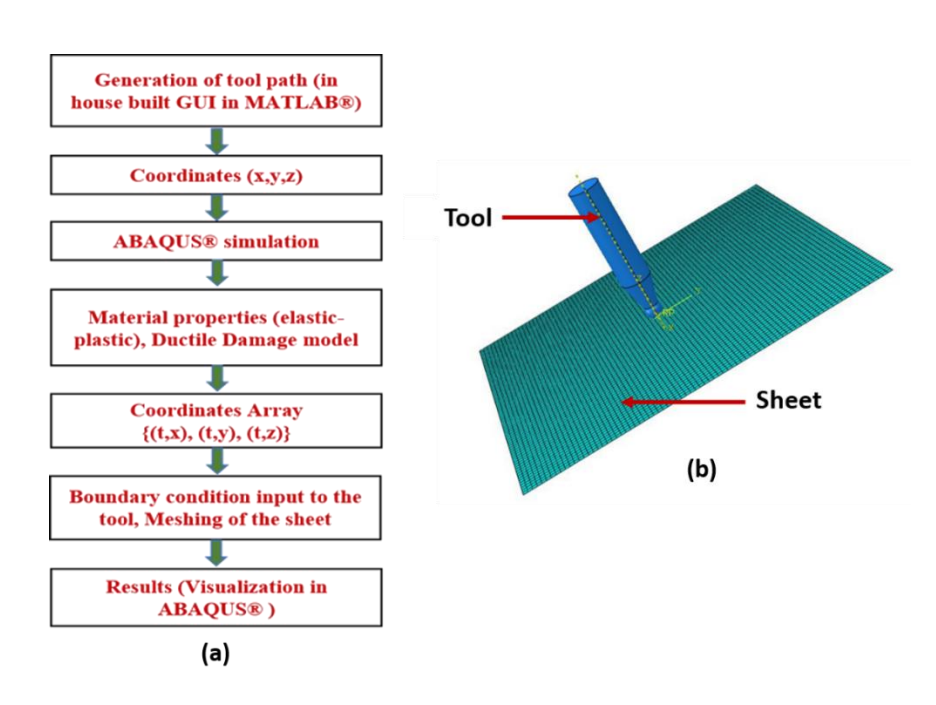


Fig. 2.12: (a) Flow chart for FEA in ABAQUS® for ISF (b) Meshed sheet with tool

Kim et al. [125] discussed the importance of FEM based simulations to predict the actual nature of the deformation process. The proposed method used the thickness strain distribution as a main parameter to study the forming limit of the developed geometrical shapes. Bambach et al. [129] used a new method to quantitatively evaluate the FE calculations on ISF. Simpson's rule was used for the section integration of the shell elements. The optical deformation measurement system (ARAMIS) was used to record the displacement and strain fields during the forming stage. The data sets obtained from measurements were mapped into the FEM software to make a reasonable comparison with the experimental results. Nirala et al. [130] performed the numerical and experimental analysis of stepped features through multi-stage ISF process. Both the results showed a practical agreement to each other. Boudhaouia et al. [121] used the spiral toolpath strategy to form a conical geometry and studied the experimental and FE analysis to predict the evolution of the forming forces and geometrical profile of the component.

Continuum damage mechanics represents a class of methods for modelling the effect of material damage within the framework of continuum mechanics. The characteristic features are that the effect of damage within a material is averaged over a volume and represented by a continuous variable that is related to the density of the defects within the material. The models require material parameters derived from experiments to characterize a particular material, and the quality of these parameters directly influences the accuracy of the numerical results. Though the micro-mechanics material degradation due to nucleation and coalescence of voids, cavities, and micro-cracks, the damage variable D reflects the average degradation of material at the macro (continuum) scale. Present prediction methods use this theory to develop the theory of fracture mechanics and use it effectively to predict practical failure scenarios [131]. FEA software like ABAQUS® is equipped with various inbuilt material models like ductile damage and Johnson-Cook plasticity models. These failure models are an extension of the failure criterion proposed by Hancock and Mackenzie [132]. However, GTN [133] and Lemaitre [134] failure models are also developed to predict failure through numerical models in ISF.

A more simplified failure criteria, ductile damage fracture model predicts the onset of failure based on growth, nucleation and voids coalescence. The equivalent plastic strain at which the failure of the material occurs, depends on the stresses developed during simulation. Hence this damage model uses the assumption that the equivalent plastic

strain (\mathcal{E}_{pl}) at the onset of the failure, is the function of stress triaxiality ($\acute{\eta}$) and equivalent plastic strain rate ($\acute{\epsilon}_{pl}$) [126]. A size-effect based ductile failure model was developed by Firouzjaei et al. [135] to predict the initiation of fracture during micro-deformation of the SS foils. There was a fair amount of agreement between the experimental and numerical data and the suggested model. Lower fracture strains were observed with the increase in grain size, which was consistent with the fracture mechanism transforming from tensile to shear mode. Ran et al. [136] proposed a fracture energy based damage model for studying the size-effect related to material micro-plastic deformation. The implemented model showed good agreement with both the experimental and numerical simulation results. Later, Xu et al. [137] utilized the extended GTN based coupled damage model to study the meso/micro deformations of thin copper foils by incorporating the size-effect related constitutive equations. Both experimental and numerical investigations were studied to evaluate the forming limit of the material.

2.9 Research Gaps

From the literature review, it has been observed that there are few micro-forming processes available to meet the growing requirements of micro-products made from ultra-thin sheets. Micro-incremental sheet forming (µISF) process is a technique which can overcome the limitations of forming high-aspect ratio thin metallic products and increase the industrial acceptability to develop several micro-factories to sustain several industrial applications. However, these foils come with inherent anisotropy due to its cold-rolled deformation. Further, the micro-scale deformation characteristics and microstructural evolution of thin foils is not explored in detail. Another challenge that has not been thoroughly addressed is the numerical modelling of the µISF process, owing to the limits of continuum-based models in predicting fracture at micro-scale deformation. The incremental toolpath and its variants have been limited to the toolsheet interaction at the wall region. Hence it is desired to observe the benefits of using a toolpath which deforms the base region as well. In µISF, the size of the surface asperities is comparable to both the thickness of the sheet and tool diameter. The consequence of this size-effect is increased friction, adversely affecting the tribological properties, and making it difficult to achieve a decent surface finish of the micro-parts. The foils are susceptible to bending and distortion under self-weight as they lack stiffness and fail early during forming. Some inaccuracies also lies in the fabrication of micro-forming tools used in this process. Therefore, some novel strategies are required to be developed to tackle the issue of lower formability of the parts and precision in tool fabrication in the μ ISF process.

2.10 Research Objectives

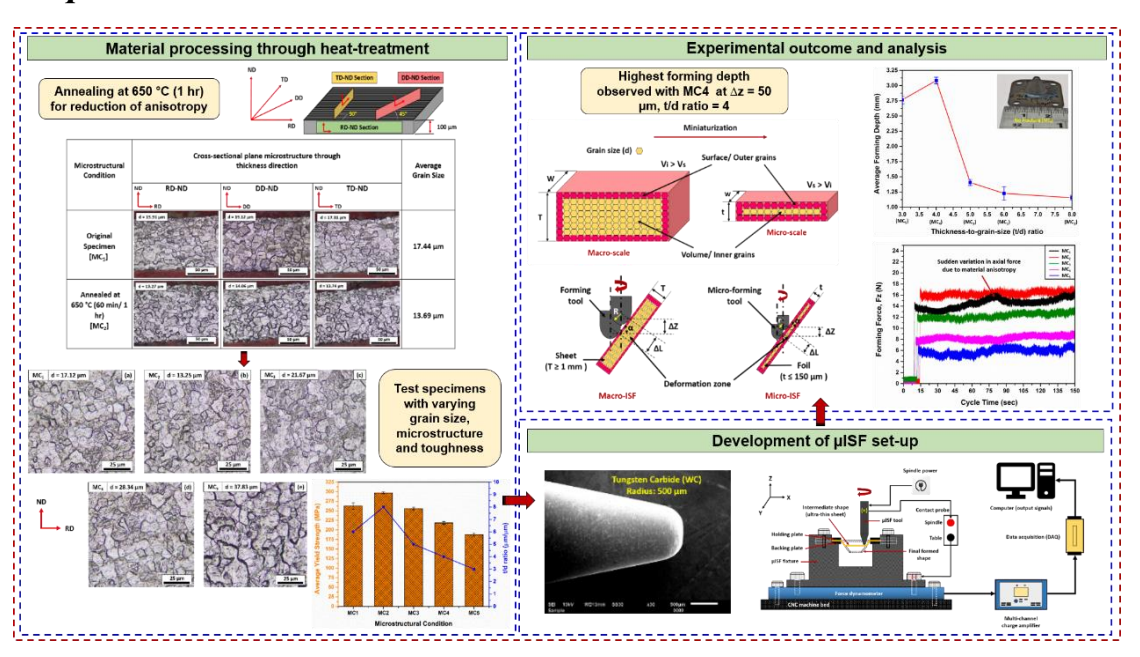
The objectives of the present work are as follows:

- 1. Design and development of a micro-incremental sheet forming (μISF) set-up for comprehensive experimentation on ultra-thin sheets.
- 2. Development of a numerical simulation model by incorporating size-effect, for accurate failure prediction in the μ ISF process.
- 3. Enhancement of tribological performance of the micro-parts during µISF.
- 4. Formability and precision improvement in µISF through novel strategies:
 - (a) Stacking of foils
 - (b) Tool precision using Reverse-µEDM process.

Chapter 3

Development of μ-ISF Set-up for Comprehensive Experimentation on Ultra-Thin Sheets (Foils)

Graphical Abstract¹



3.1 Introduction

The production of micro-products by scaling down such traditional forming processes is challenging considering the limitations, due to size-effects [5] in micro-forming operations. Major issues associated with the process are reduction in formability, uncertainties in tooling fabrication, imprecision in material handling, inadequate control over the interfacial conditions, discrepancies in micro-forming fixture, etc. [138]. Mishra et al. [139] discussed the effect of plastic anisotropy during the sheet forming operations. It was observed that increase in the anisotropy influences the flowability and microstructural texture of the material, which causes high strain localization and premature failure of the geometries. In a recent study, Zhu et al. [140] suggested that with controlled heat treatment (annealing), the issue of increase in anisotropy of the material can be minimized/ eliminated. The results were effective in minimizing the

¹Pal, M., Agrawal, A., and Nirala, C. K., 2024, "An Investigation of the Formability of Ultra-Thin CP-Ti-Gr2 Foils Considering Thickness-to-Grain-Size Effects under Controlled Heat Treatment in μ-ISF," **Journal of Manufacturing Processes**, 131, pp. 1202-1218. (https://doi.org/10.1016/j.jmapro.2024.09.107).

influence of the size-effect in the material. Material like Titanium (α -Ti) is hard to deform at room temperature due to its hexagonal close-packed (HCP) structure with less active deformation slip planes. Therefore, heat treatment above the recrystallization temperature can help in enhancing the movement of dislocations in the material [141]. Commercially pure Titanium Grade 2 (CP-Ti-Gr2) has received special attention from several research communities because of its lightweight, high-quality corrosion resistance, high specific strength, low density, and biocompatible nature [142]. It is widely used for defence, aerospace, marine, automobile, orthodontic and orthopedic applications [41]. To meet the demand for products made of Ti, many research groups are trying to investigate the mechanism of plastic deformation of CP-Ti Gr2 foils [76,143].

In this chapter, a micro-forming fixture set-up is designed and developed to carry out the µISF experiments. The anisotropy and grain-size-effect (t/d ratio) plays a crucial role in achieving a higher deformation of foils. The variation in the number of grains along thickness increases the effect of non-homogeneity/ anisotropy in the material [144]. This significantly affects the geometrical features of the formed geometry and causes changes in the micro-deformation behavior due to size-effects. A comprehensive investigation is done to reduce the anisotropy of the received cold-rolled foil by performing controlled annealing in an inert gas environment. The work also attempts to improve the formability of ultra-thin CP-Ti-Gr2 foils by varying the grain sizes through targeted heat treatment. The impact of annealing temperature, step depth, and t/d ratio are studied by establishing stress-strain behavior, forming force measurement, and forming limit estimation of the foils. The obtained results show a strong influence on the initial grain size of the material, which is consistent with the Hall-Petch relation. The combined selection criteria of t/d ratio and step depth could be used to optimize the design parameters of the µISF process. The microstructural analysis through EBSD results showed a good correlation with the obtained forming depth results.

3.2 Work Methodology

3.2.1 Development of the µISF set-up

For the investigation of formability of the foils in μ ISF, an experimental setup was designed and developed. Thin foils are easily susceptible to slacking/ bending due to their low bending stiffness and self-weight. Any loose contact or alterations may affect

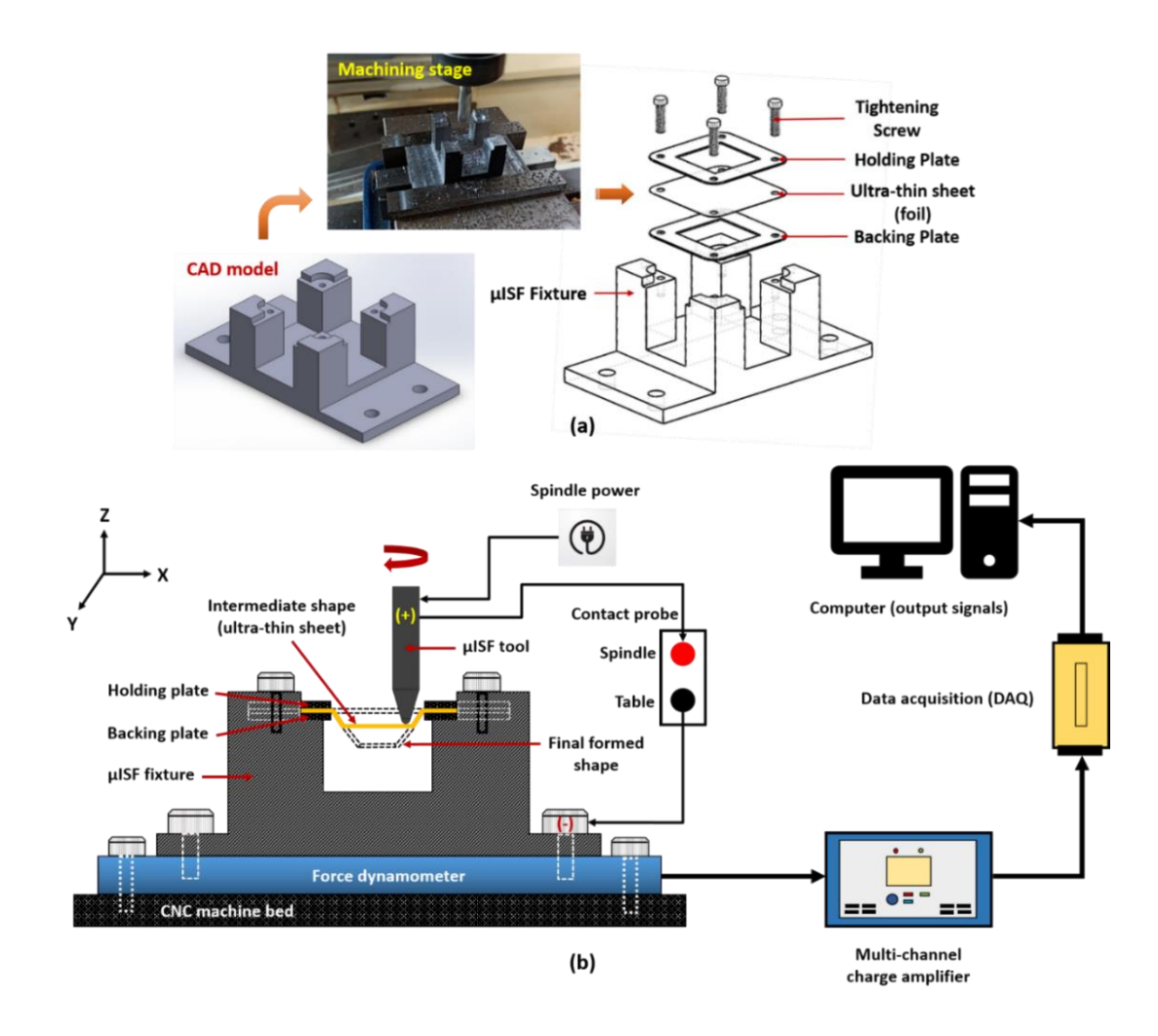


Fig. 3.1: (a) Design and fabrication of μ ISF fixture (b) Complete schematic demonstration of the μ ISF set-up

the dimensional accuracy of the formed part and prevent it from further deformation. This can be avoided with an effective design of the micro-forming fixture. Bansal et al. [62] suggested to use rubber pads between the holding plate and the foil to induce higher tension, in order to eliminate the initial slacking of the foils. However, it was not recommended in all the forming experiments, because adhesion between the rubber pad and the foil surface was observed, making it difficult to remove after the experiments. This gave rise to unnecessary distortions/ damage in the final formed geometry. As a result, the rubber pad was not used in the experiment for better surface flatness of the foils. Figure 3.1(a) shows the design and fabrication process of the µISF fixture. The dimensions of the fixture structure, a two-bracket assembly of holding and backing plates, along with the clamping mechanism were designed in SolidWorks®. A working area of 15 mm x 15 mm was made at the center of the plates to carry out the forming operation. These plates provide stability and support to the workpiece and prevent it

from moving excessively or deforming undesirably during the forming operation. It also ensures uniform pressure distribution between the adjacent surfaces of the foil and the plates to provide the necessary tension, and avoid initial bending of the foils. As a result, the usage of the rubber pads can be eliminated. To ensure the flatness of the foil and bracket on the XY plane, the top and bottom faces of the two constraint plates were carefully polished to remove the surface asperities. It helped in retaining the flatness and symmetry between the faces of the foil and the two plates while positioning the assembly on the fixture. The final designed schematic illustration of the μ ISF set-up is shown in Fig. 3.1(b).

The steps involved in the preparation of the workpiece are explained in Fig. 3.2(a). First, the CP-Ti-Gr2 foil (purity of 99.8 %) in the form of cold-rolled sheets was cut using a nano-sec pulsed class IV Nd:YAG fiber laser, into a precise rectangular workpiece of dimension 30 mm x 25 mm for the µISF experiment as shown in Fig. 3.2a(i,ii, iv). The scanning electron microscope (SEM) and energy dispersive spectroscopy (EDS) images confirm the thickness and purity of the workpiece specimen. A Dino-lite edge digital microscope (AM4515 series) was used to inspect the edge quality of the workpiece after LBµM (Fig. 3.2a(iii)). Usually, the tool is of hemispherical ended shape. For deforming softer sheets like Al, SS, etc., tool steel, or HSS are used as the tool material. However, to deform hard-to-form material like Ti (HCP at room temperature), a relatively harder material is required. For CP-Ti-Gr2 foil, Tungsten Carbide (WC) was selected as the tool material, which reduces the wear of the tool-tip during the µISF process. A circular rod of 3 mm diameter of WC (80.32% W, 10.07% Co, 8.18% C) shown in Fig. 3.2b(i) was used for making the tool for the µISF process. The tool was manufactured in-house by the μ -turning process, using a PCD insert at a speed of 500 rpm with a low depth of cut of 10 µm (Fig. 3.2b(ii, iii)). SEM (Jeol Ltd., JSM-6610LV) image in Fig. 3.2b(iv) illustrates the circular profile of the fabricated hemispherical-end tool of radius 500 µm. Another process used for fabricating the forming tool is the Reverse-µEDM process. Reverse-µEDM is a proven technique, that is used for making miniature electrodes [145], which was recently explored by Pal et al. [146] for the fabrication of a precise forming tool for μ ISF. This is explained in detail in Chapter 6.

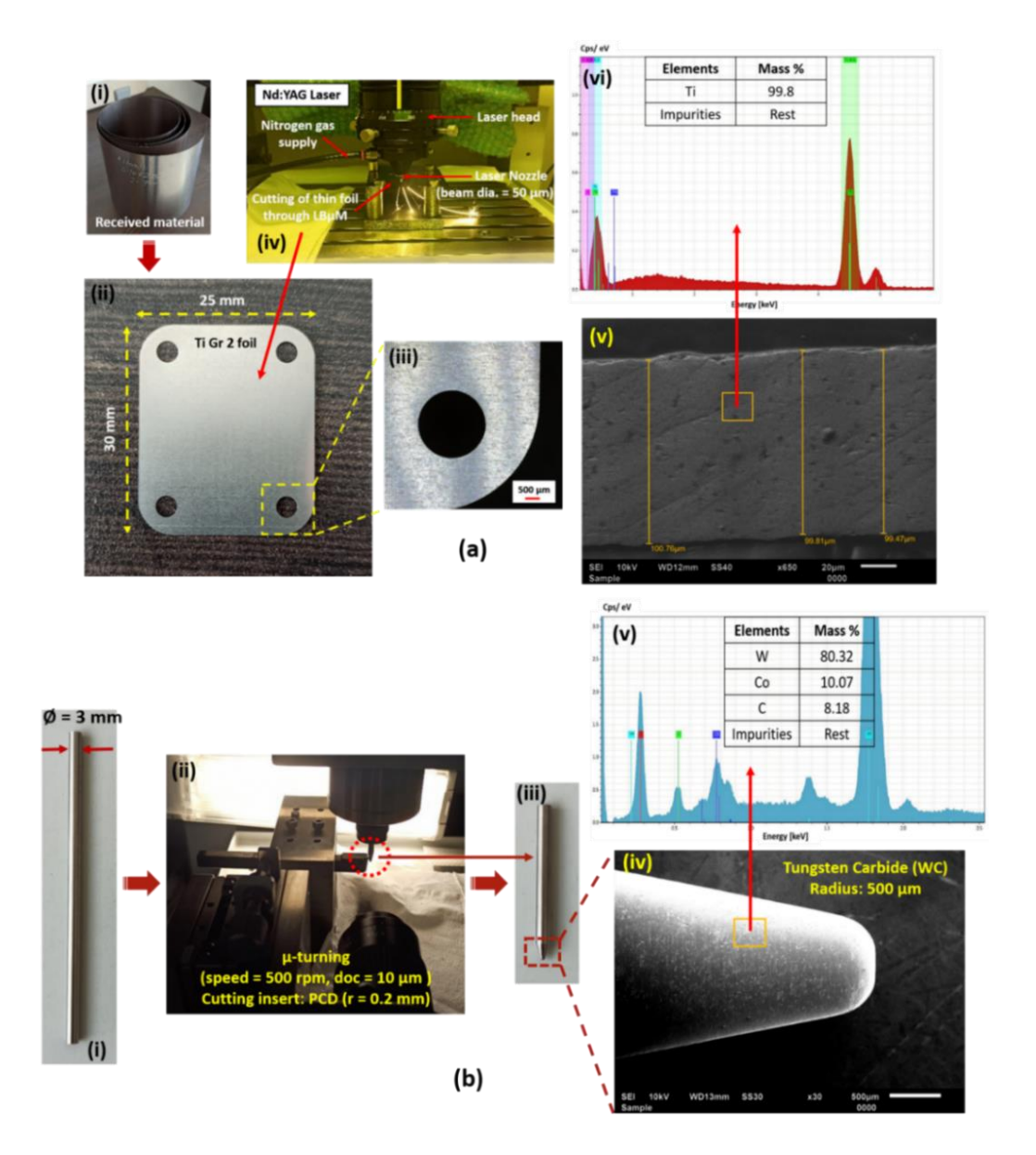


Fig. 3.2: Development route for μISF process (a) Preparation of ultra-thin workpiece (b) Fabrication of micro-forming tool

3.2.2 Estimation of mechanical anisotropy in the received specimen

Non-homogeneous nature of materials in micro-scale causes scattering of process parameters, which significantly impacts the formability and flow stress of the process [147]. The phenomenon responsible for such behaviour is labelled as "size-effect" [69]. To inspect the anisotropic properties of the received material, uniaxial tensile tests were performed. The tensile specimens were precisely cut from a 100 μ m thickness CP-Ti-Gr2 foil by using the micro-wire-electro discharge machining (μ WEDM) process at a feed rate of 0.1 mm/min as per the ASTM E-345 standard for tension testing of metallic foils. The μ WEDM process, being a non-contact type, ensures no burrs or residual

stresses induced onto the workpiece. The geometrical dimension of the tensile specimen is shown in Fig. 3.3(a). The gauge length was taken as 15 mm and the width of the gauge was 4.2 mm. In order to avoid any undesirable or premature failure during testing, the thickness direction of the specimens was precisely polished. The test specimens were prepared in three different directions viz., Rolling direction (0°, RD), Diagonal direction (45°, DD), and Transverse direction (90°, TD) as presented in Fig. 3.3(b). Three samples from each direction were considered to validate the repeatability of the test results. The uniaxial tensile test was carried out on Tinius Olsen H50KS universal testing machine (UTM), at a uniform strain rate of 0.00833 s⁻¹.

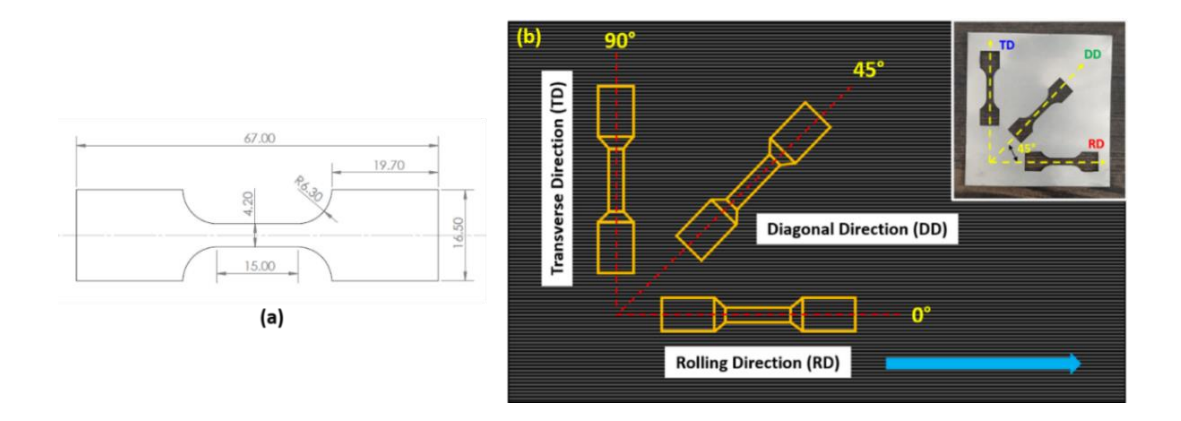


Fig. 3.3: (a) Uniaxial tensile test dimensions (b) Received specimen cut in three different directions, viz. RD, DD, and TD

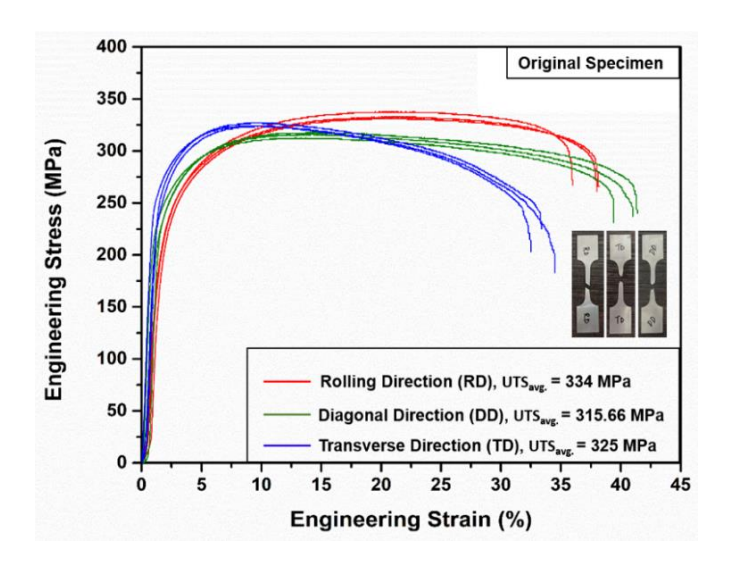


Fig. 3.4: Engineering stress-strain curves in RD, DD, and TD for original specimen

Engineering stress-strain curve of the original (as received, without annealing) foil is shown in Fig. 3.4. It shows the variation in the magnitude of the ultimate tensile strength (UTS_{avg.}) of the specimen in RD, DD, and TD as 334 MPa, 315.66 MPa and 325 MPa, respectively. The obtained results clearly show the presence of mechanical anisotropy in the received foil due to scattering of the tensile parameters, measured in all three directions. This confirms that the flow stress is highly influenced by the anisotropy of the material, which is inherently present in the cold-rolled foils. Such changes in the properties affect the micro-deformation behaviour of micro-parts. As a result of the non-uniform distribution of the flow stress and yield surface, the designing procedure for the μ ISF process becomes difficult.

3.2.3 Tailoring grain size and microstructure of the annealed specimens

When a specimen size is miniaturized, a departure from the material's polycrystalline to single-crystal behaviour is most likely to occur [70], owing to the reduction in the number of grains in the deformation zone (across the thickness of the foil). To investigate the size-effect phenomenon in the micro-scale deformation, range of different t/d ratios can be obtained by varying either the grain size/ sheet thickness or both in the specimen [148]. The physical importance of this parameter is related to the number of grains present through the foil thickness. During the scaling down of a particular dimension, the ratio gets changed and leads to size effect [13]. In general, the microstructure of a polycrystalline miniaturized material contains fewer grains in the deformation zone. When the number of grains across the foil thickness decreases, increase in the size-effect may occur in the material. Therefore, for designing the µISF process, it is necessary to select appropriate forming parameters considering the thickness and grain size of the foil.

The annealing temperature is an important parameter which changes the microstructural behaviour by altering the grain size of the material. In the present work, the grain sizes were varied in the test specimens to achieve different t/d ratios while keeping the thickness of the foil unchanged. Accordingly, five unlike microstructural conditions (MC) were produced to study the micro-deformation behaviour with size effect in the μISF process. The microstructure of the original and that of the annealed specimen (650 °C, 1 hr) were designated as MC₁ and MC₂ respectively. To generate a wide range of grain sizes, the MC₂ specimen was further heat-treated for 2 hours and furnace cooled at a rate of 5 °C/ min. in a closed argon environment at temperatures of 300 °C, 400 °C,

and 500 °C respectively. The temperature range of annealing was set to achieve a target grain size, without increasing the influence of size-effect in the material. The grain size of the specimen was developed such that the t/d ratio doesn't approaches unity. When the grain size and sheet thickness are of the same order of magnitude, deformation behaviour may be highly uncertain due to the presence of only one layer of grains across the sheet thickness. It will also lead to very high anisotropy in the sheet material. Such temperature variation resulted in three new microstructures which are referred to as MC₃, MC₄, and MC₅.

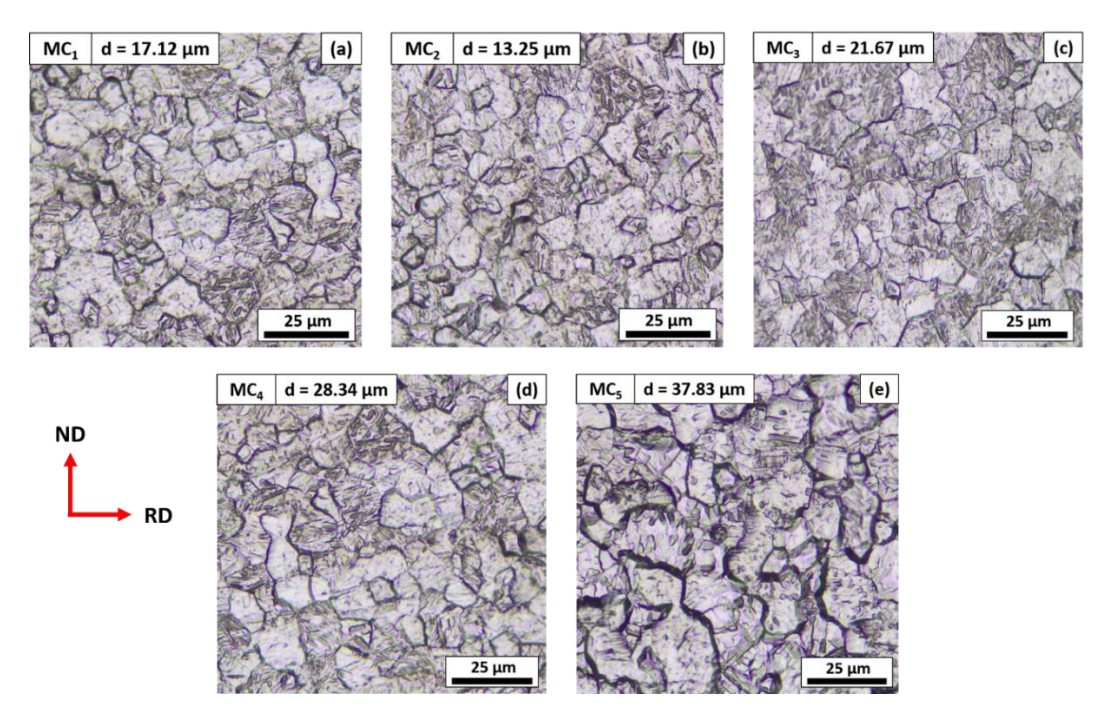


Fig. 3.5: (a-e) Optical micrographs: Microstructural analysis of five different specimens with variation in grain size in RD-ND plane, engineered for studying the formability of the foils at different step depths

To capture the microstructure, the cross-sectional planes (RD-ND) of the specimens were first embedded on a flat epoxy resin platform and sequentially polished using the SiC-coated emery paper of different grit sizes. The surface was further polished with a colloidal alumina solution and diamond paste (abrasive size of 0.25 μm) to eliminate the surface asperities. Later, it was cleaned and swab-etched with the Kroll's reagent to reveal the grain boundaries. Figure 3.5(a-e) shows the optical images of the microstructural surfaces of five different specimens with variation in the average grain size (d), measured along the RD-ND plane. The grain sizes were determined using the ASTM E112 linear-intercept method from the micrographs acquired with a Leica DM4-

M optical microscope from five arbitrary positions for each sample. Figure 3.5(a, b) exhibits the measured grain diameter of the original and annealed specimens with average sizes of 17.12 μm and 13.25 μm. The second stage of annealing (Fig. 3.5(c, d and e)) initiated uniform growth in the grain size of the specimens. Average grain sizes of 21.67 μm, 28.34 μm, and 37.83 μm were observed for the MC₃, MC₄, and MC₅ specimens. It can be observed that the grain size increases with the rise in the annealing temperature. The effect of the thickness and average grain size of the foil is quantified by calculating the t/d ratio of the specimens. These results are used to study the correlation of varying grain sizes with the mechanical properties of the annealed foils through uniaxial tensile test.

3.2.4 Preliminary trials and experimental approach

Initially micro-forming preliminary trials were conducted to verify the repeatability and feasibility of the developed µISF set-up. First, the assembly of the workpiece blank (CP-Ti Gr2 foil) and two plates were precisely clamped on the μISF fixture and tightened with the bolts. The manufactured micro-forming tool of radius 500 µm was then attached to the collet of the machine spindle. The µISF toolpath was generated through an in-house developed graphical user interface (GUI) in MATLAB® App Designer utility (R2021a release). Spiral based incremental toolpath was selected to form a benchmark geometry such as a conical component which is shown in Fig. 3.6(a). A target depth of the geometrical part was set in regard to the angle of forming. This was carried out to assess the formability of the part for any specific depth with the variation in forming parameters. To set a target depth for all the experiments, the opening radius (R_1) of the cone was taken as 5 mm and the bottom radius (R_2) was equal to two times the radius of the tool (rtool). The parts were formed at three different forming angles of 50°, 55°, and 60° on a numerically controlled high-precision multi-axis hybrid-μEDM machine (Mikrotools Ltd., DT-110i). The machine provides a position accuracy of ± 1 $\mu m/100$ mm on a linear scale resolution of 0.1 μm , precisely in all three axial directions. The complete experimental setup for performing the µISF is shown in Fig. 3.6(b). The tool was given a rotational speed of 500 rpm and incremental step depth (Δz) of 30 μ m during the forming process. Tests were repeated four times for each wall angle and the average value of the forming depth was considered. After the successful validation of the feasibility test, final micro-forming experiments were performed with the annealed foils.

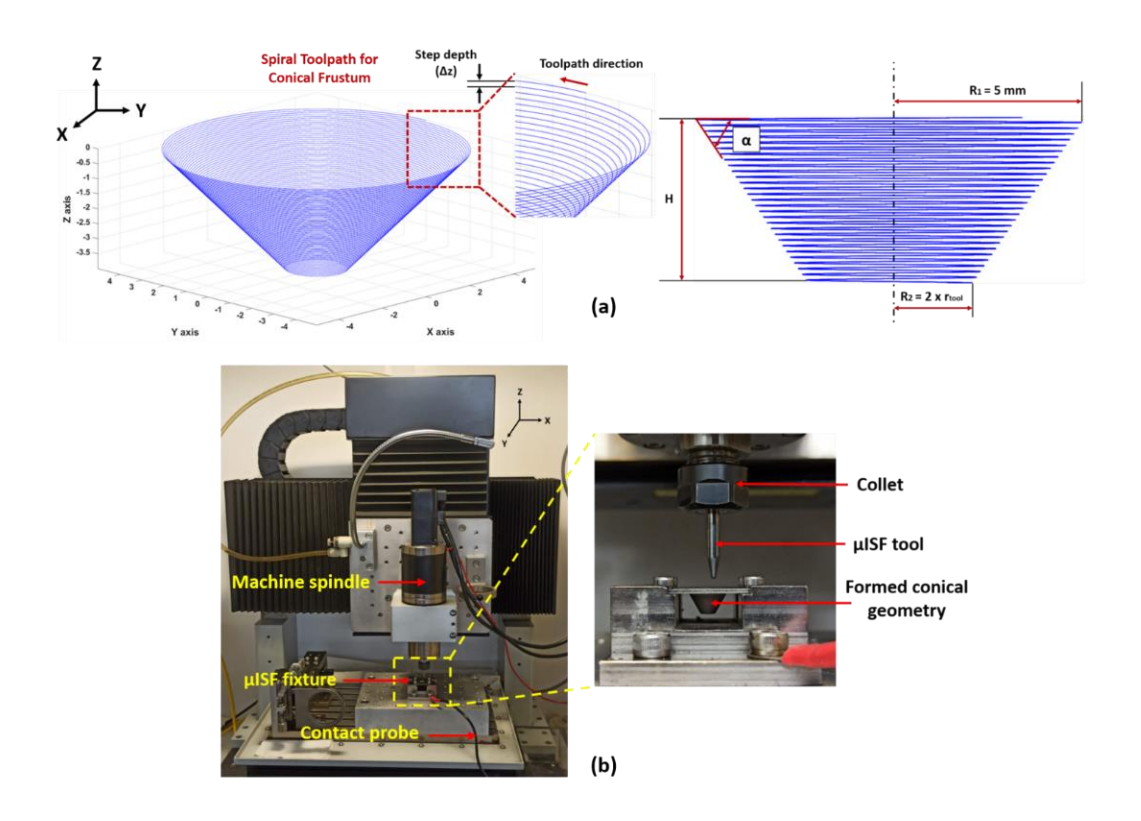


Fig. 3.6: (a) Incremental spiral toolpath for conical-shaped geometry (b) Experimental set-up for μISF process on DT-110i multi-axis hybrid-μEDM machine

3.3 Results

3.3.1 Reduction of anisotropy through controlled annealing

In micro-scale forming, anisotropy present in the material influences the deformation mechanism of the process. Due to size-effect, there is a high chance of scattering of material properties because of the lesser number of grains in the deformation zone, leading to anisotropy in thin foils. The grain crystallographic orientations and boundary sliding may also induce anisotropy in the material properties, due to the variations in the applied direction of the deformation load. An increase in the process scatter results in high surface degradation and leads to non-optimal control in the quality of the microformed components. Such phenomenological shifts and abnormalities in material behaviour decrease the forming efficiency of the process. [149]. The difference in the mechanical properties in Fig. 3.4 clearly shows the presence of anisotropy in the received material. Therefore, it is necessary to reduce the effect of non-homogeneity in the material. To minimize the scattering of properties in different directions, controlled argon gas-induced annealing of the original foils was performed in a closed tube furnace

(Carbolite Gero make), above the recrystallization temperature at 650 °C for different time periods i.e. 60 min., 75 min., and 90 min. respectively. It was observed that by carrying out the annealing of the specimen for 60 min at a constant rate of 5 °C/ min., anisotropy in the specimen was considerably reduced compared to the other holding time. The least scatter in the average UTS was seen with a value around $\sim 340 \pm 0.41$ MPa in all three directions as presented in Fig. 3.7(a). The tensile strength of the specimens was slightly increased on average, compared to the original specimen (324 \pm 7.41 MPa), with decreased ductility (Fig. 3.4). Whereas, increasing the holding time of the furnace heating for, i.e. 75 min. and 90 min. resulted in more scattering of the properties in the material. From Fig. 3.7(b, c), it was witnessed that the UTS_{avg.} of the specimens were randomly distributed in different directions. For 75 min. holding time, the highest UTS_{avg.} of 352 MPa was observed for RD, and lowest of 339.66 MPa in DD. Similarly, for the 90 min., the range of the UTS_{avg.} lies from 341.33 MPa to 373.66 MPa in DD and RD. While the overall scatter for both the holding time were 345 ± 5.22 MPa and 354 ± 13.73 MPa respectively. It was important to note that with higher annealing time, the rolled Ti foils exhibited higher flow stress but smaller fracture strains.

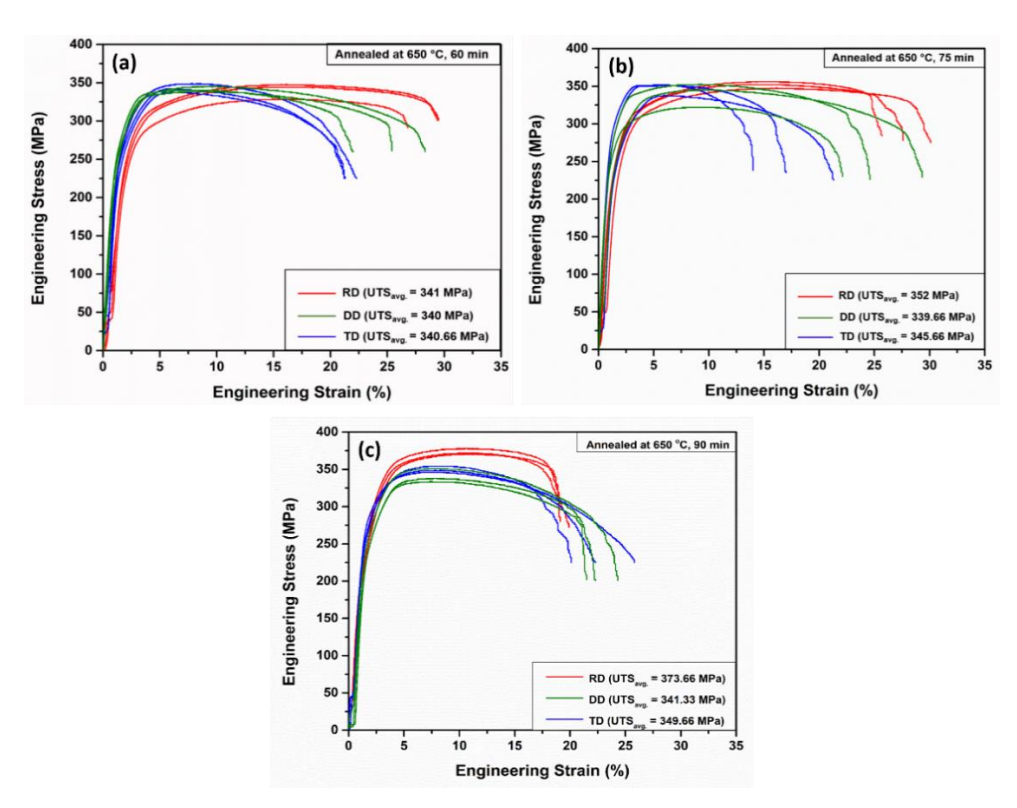


Fig. 3.7: Engineering stress-strain curves in RD, DD, and TD for (a) Specimen annealed at 650 °C for 60 min (b) Specimen annealed at 650 °C for 75 min (c) Specimen annealed at 650 °C for 90 min

To analyse the decrease in anisotropy of the foil in the case of annealed specimen, MC₂ (650 °C, 60 min), the size of the grains across different cross-sectional planes were measured in the thickness direction (RD-ND, DD-ND, and TD-ND) and were compared with the originally received foil (MC₁) as illustrated through schematic in Fig. 3.8(a). In the original specimen, initial grain sizes of 15.91 μ m, 19.12 μ m, and 17.31 μ m were observed in different planes with an average size of 17.44 μ m. The grains along the DD-ND plane were more elongated compared to other measured planes. After the heat treatment, new stress-free equiaxed grains were formed, which were homogenously distributed in all three directions. The same was confirmed through the grain size measurement, and it came out with an average grain size of 13.69 μ m throughout the foil thickness. The microstructures of the foil through cross-sectional planes thickness are presented in Fig. 3.8(b). The uniform distribution of homogenous grain sizes can be observed (13.27 μ m, 14.06 μ m, and 13.74 μ m). It helped in minimizing the influence of size-effect in the material, by increasing the number of grains across the foil thickness.

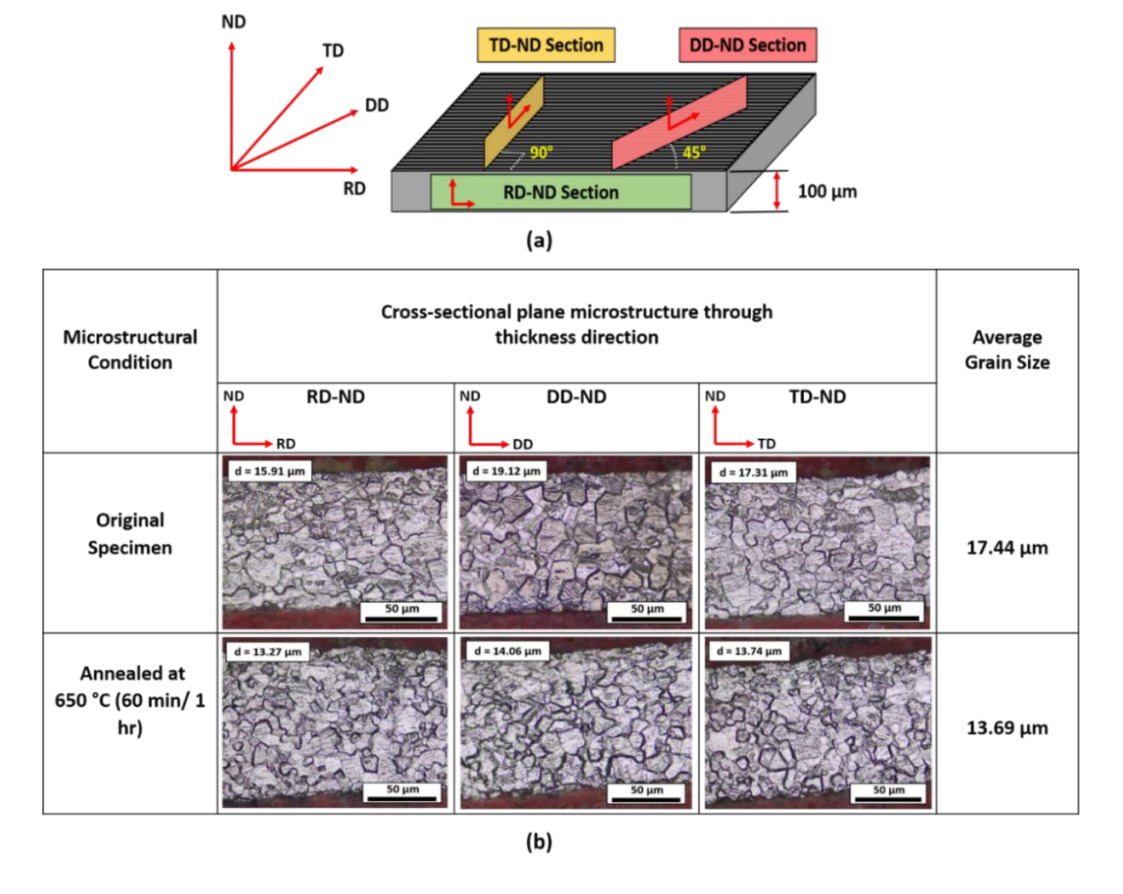


Fig. 3.8: (a) Schematic view of different cross-sectional planes of the foil with respect to normal direction (ND) (b) Optical micrographs showing the change in microstructure after annealing along different cross-section planes

3.3.2 Correlation between grain size/microstructure and uniaxial tensile loading

To study the effect of changing grain size, uniaxial tensile tests were performed for all five microstructural specimens with respect to the rolling directional plane (RD) of the foil. Three specimens for each sample were utilized to ensure the homogeneity and repeatability of the tensile tests. The selected temperature range was found to be suitable for producing favourable grain sizes as per the design considerations for µISF process. The optical micrographs of five foils with different grain sizes are discussed in Fig. 3.5(a-e). Corresponding, engineering stress-strain curves are plotted to compare the mechanical properties of the heat-treated and original foils (Fig. 3.9(a)). The results show that the tensile responses were completely different for each combination. Annealing above the recrystallization temperature, the strength of the MC₂ specimen was marginally increased, and the formation of equiaxed smaller grains led to the increase in the flow stress of the material.

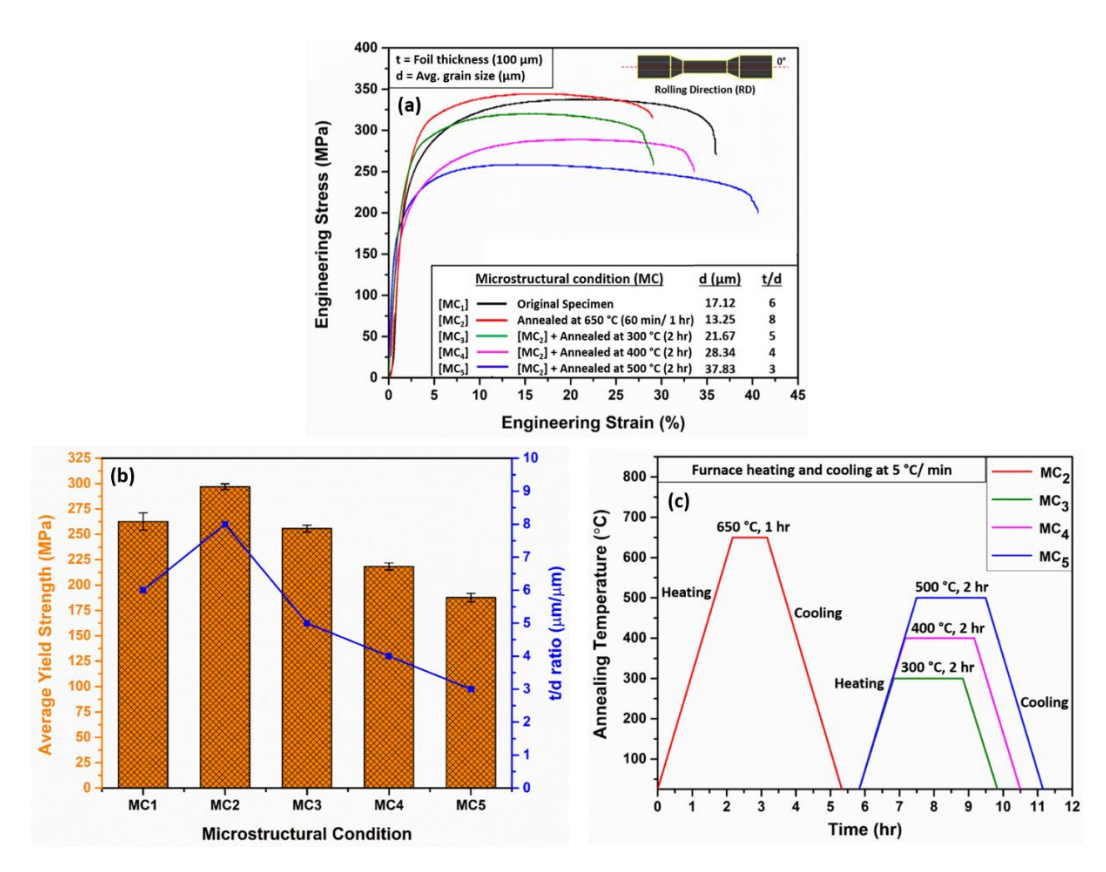


Fig. 3.9: Uniaxial tensile test results of the test specimens for μISF: (a) Engineering stress-strain curves in the rolling direction (b) Bar graph displaying the average yield strength of the specimen for different microstructural conditions with change in corresponding t/d ratios, (c) Heat treatment of the specimens: Annealing temperature-time profile

This can be explained by the Hall-Petch effect [72,150], which articulates that the material with a smaller grain size shows higher strength, compared to the material with a higher grain size. However, on further heat treatment of the samples (MC₃, MC₄, and MC₅), the yield strength (σ_y) of the foil decreases with an increase in ductility (Fig. 3.9(a, b)) due to the thermal softening of the material [151]. This results in the growth of grain and grain boundaries with the rise in the annealing temperature. A similar trend was also observed by Jing et al. [143] while examining the size effect in the microforming of the CP-Ti Gr2 foils. The uniaxial tensile properties and grain sizes of different MC specimens are presented in Table 3.1.

Table 3.1: Uniaxial tensile properties of the specimens at different microstructural conditions

MC	Avg. Grain Size, d (μm)	t/d ratio (µm/µm)	Avg. Yield Strength , σ_Y (MPa)	Avg. Ultimate Tensile Strength , σTeng (MPa)	Total Elongation (%)	Uniform Strain, Eu (%)	Strain Harde ning Expone nt, n
MC ₁	17.12	6	262.66	338.33	35.84	20.85	0.18
MC ₂	13.25	8	297.0	345.66	28.91	14.32	0.17
MC ₃	21.67	5	255.66	319	29.33	17.21	0.19
MC ₄	28.34	4	218.33	288.33	33.67	23.56	0.24
MC ₅	37.83	3	187.66	259	40.76	12.73	0.27

An increase in the yield strength (297 MPa) and t/d ratio (8) of the MC₂ specimen was observed with the reduction in the average grain size from 17.12 μm to 13.25 μm. This corresponds to an increased number of grains through the foil thickness and minimization the anisotropy after the annealing process. Previous studies have shown that if the number of grains across the foil thickness is increased, the influence of the size effect can be reduced [12]. The scatter of the yield strength was least in the case of the MC₂ specimen and was highest for the initial MC₁ specimen. After the heat treatment of MC₂, a minor increase in the scatter was witnessed in the MC₃ and MC₄ specimens. In MC₅, the increase in the scatter of the yield strength was marginally high compared to the MC₃ and MC₄ (Fig. 3.9(b)). It was due to the presence of lesser grains/ large grain

size in the cross-sectional thickness of the specimen which may have induced size effect related deviations during testing. Figure 3.9(c) shows the heating and cooling slopes of the temperature-time profile of the heat-treated samples.

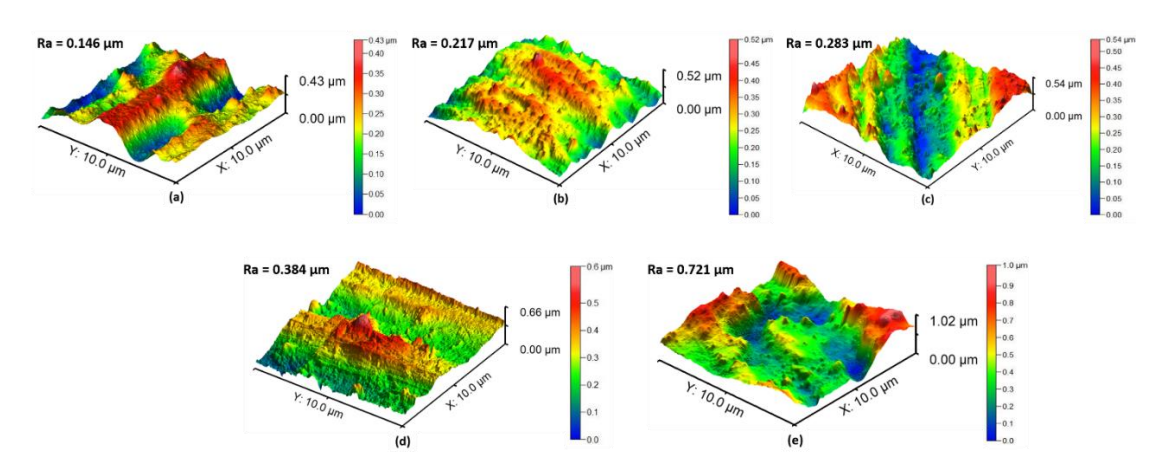


Fig. 3.10: Surface topography analysis using AFM of different microstructural conditions (a) MC₁ (b) MC₂ (c) MC₃ (d) MC₄ (e) MC₅

Low number of grains weakens the deformation coordination between the individual grains. Therefore, with the increase in the grain size, the surface becomes rougher after heat treatment [152]. The results of the atomic force microscopy (AFM, Bruker Multimode 8-HR) illustrate the 3D surface topography of different MC specimens in Fig. 3.10. To ensure the repeatability of the roughness measurement, five different scanning areas were selected on the surface of each specimen, with an area dimension of $100~\mu m^2$ and scan rate of 1 hertz to determine the average surface roughness (Ra) values. The surface quality of the specimens tends to decrease by increasing the temperature of the heat treatment process. A slight increase in the Ra was observed for MC₂ (0.217 μ m) compared to MC₁. On further annealing, the roughness peaks gradually increased to 0.384 μ m for MC₄. It was observed that the quality of the surface degraded on heating the specimen at 500 °C (MC₅) for 2 hrs. This led to the formation of few irregular-sized grains within the cross-sectional thickness (Fig. 3.5(e)). It shows that a higher temperature of annealing might cause more degradation of the surface and render it useless for micro-forming operations.

3.3.3 Validation of the micro-forming set-up and experiments

The results of the developed conical cups in the preliminary tests of µISF are shown in Fig. 3.11. It can be observed that the geometry formed with the wall angle (α) of 50° and 55° successfully achieved the target depth of 4.776 mm and 5.712 mm respectively, without the failure of the component. However, when the angle of forming was increased to 60°, early fracture of the component occurred at an average failure depth of 1.317 mm. A digital height gauge (Mitutoyo made) was used to measure the forming depth of the formed micro-components. Five different measuring regions from the bottom of the formed part were selected to record the average forming depths. The results of the trials with the corresponding forming depths in three different cases are shown in Table 3.2. Typically in ISF, an increase in the value of α causes a reduction in the forming depth, thus decreasing the formability of the parts [15]. To scrutinize the relationship of α with the forming depth in μ ISF, it was essential to form the parts beyond the target depth limit in the first two cases. It was noticed that the failure occurred in both cases, but eventually, the failure depth was reduced from 7.264 mm to 6.657 mm when α was changed from 50° to 55°. These initial results successfully portrays the feasibility of the micro-scale deformation in the µISF process.

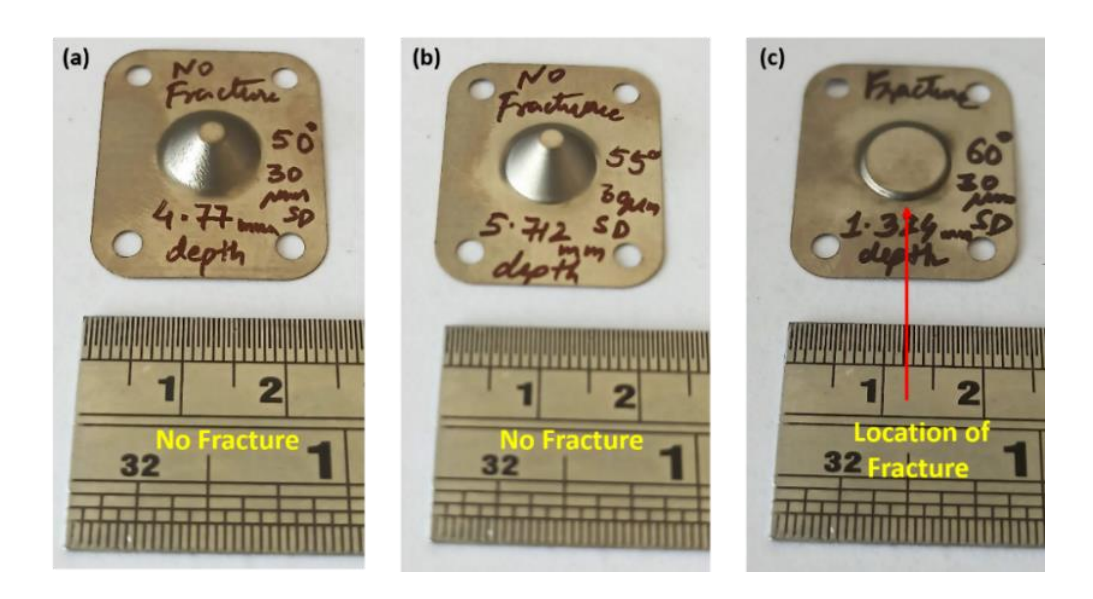


Fig. 3.11: Formed components through μISF for trial experiments at different wall angles (a) 50° (b) 55° (c) 60°

Table 3.2: Preliminary trial results of µISF at different wall angles (without annealing)

Case	Wall Angle (α)	Target Depth (mm)	Failure Occurred (Yes/ No)	Average formed depth (mm)
1	50°	4.776	No	4.776
2	55°	5.712	No	5.712
3	60°	6.928	Yes	1.317

Based on these results, final experiments were carried out with the heat-treated foils. The original workpiece specimen (MC₁) and with other four different grain sizes (d) were incrementally deformed to obtain several conical-shaped geometries using three different Δz (10 μ m, 30 μ m, and 50 μ m) at an uniform wall angle (α) of 60°. The tool was given a constant displacement velocity (feed rate) of 15 mm/min and rotation of 500 rpm. Normal lubricating oil was used at the tool/foil interface during forming to reduce the frictional effects. The experimental results of the formed parts with different MC and step depths are displayed in Fig. 3.12. In this work, step depth and the annealing temperature were considered as the experimental process parameters. At the initial stage of the deformation process, notable variations in the formability of the parts were observed due to the effect of the material grain size and step depth of forming.

3.4 Discussion and analysis

3.4.1 Evaluation of formability of the original and heat-treated foils

The formability in both the original and heat-treated foils was evaluated and the results of the micro-forming experiments are presented in Fig. 3.12. It was observed, that the parts formed with smaller grain sizes (MC₂) showed early cracks and reduction in formability, unlike the parts with larger grain sizes. However, a significant increase in failure depth and good geometrical accuracy of the component was observed in the specimens (MC₃, MC₄, and MC₅) after the second round of annealing as shown in Table 3.3. The geometrical accuracy of MC₄ (annealed at 400 °C) was observed to be the best of all the five categories. A slight decrease in the formability was observed in the MC₅ specimen. Though, by following the repetitions of the μISF experiments, it was understood that the deformation behaviour was noticeably affected by the range of step depth used during the experiment. Generally, in ISF an increase in the magnitude of step

Microstructural	Incremental step depth (ΔΖ)			
Condition	10 μm	30 μm	50 μm	
MC ₁	fracture MC+ 60° 10 0.733 MM mm	Fracture MC-1 30 Mm 1.356 Mm	Fracture 60 50 1.649 mm	
MC ₂	10 0.724 mm	Fraction 60° 30 1.171 Mm	1.547 MM	
MC ₃	M. 22 6 10, 73 4 0 0.7320		Sommer of the second	
MC ₄	Transfer of the second	Men Stades	No special section of the section of	
MC ₅	Hers 360° 10 pm 0.678 pm	Nes 60 3 has	Fretwo Co 50 pm 6.35 8 mm	

Fig. 3.12: Formed CP-Ti Gr2 circular cups at different step depths using µISF

depth results in a decrease in the forming depth at which the failure of the part takes place [15]. The combined effect of the grain size and step depth on the formability of the component is still unexplored in µISF. This deformation behaviour at the microscale is due to the influence of size-effect, and can be explained through the surface layer model [70].

Table 3.3: Experimental results of µISF at different microstructural conditions

Designation of the Specimen	Microstructural Condition (MC)	Average Failure Depth (mm)		
			Step Depth (\(\Delta \mathbf{Z}\))	
		10 μm	30 μm	50 μm
MC_1	Original Specimen	0.731	1.336	1.616
MC ₂	Annealed at 650 °C (60 min/ 1 hr)	0.722	1.195	1.548
MC ₃	MC ₂ + Annealed at 300 °C (2 hr)	0.742	1.445	2.034
MC4	MC2+Annealed at 400 °C (2 hr)	0.761	1.560	6.928 mm (No Fracture, Achieved target depth)
MC ₅	MC ₂ + Annealed at 500 °C (2 hr)	0.665	1.358	6.276

3.4.1.1 Understanding the micro-deformation behaviour through surface and volume grains

During the miniaturization of the specimen, the volume fraction of the surface grains (V_s) increases and surpasses the volume fraction of the internal grains (V_i) [70]. The share of V_s and V_i in the bulk and micro-range specimens is schematically demonstrated in Fig. 13.3(a). The surface grains are located close to the free surface of the specimen compared to the grains at the inside, which are bounded by distinct grain boundaries. Figure 13.3(b) illustrates the distribution of the surface and internal grains in the deformation zone during the macro-ISF and micro-ISF process. With the decrease in the specimen size, the number of grains in the deformation zone reduces, and approaches to single-crystal behaviour with lower flow stresses [153]. The flow stress (σ) of the material at the micro-scale can be expressed by Eqs. (3.1) and (3.2):

$$\sigma = \frac{N_s \sigma_s + N_i \sigma_i}{N} \qquad (N = N_s + N_i)$$
 (3.1)

$$\sigma = (\eta)\sigma_s + (1 - \eta)\sigma_i$$
 $(N_s = \eta N)$ $1 \ge \eta \ge 0$ (3.2)

$$A_r = \Delta l \times (t/T) \tag{3.3}$$

Here, N_s and N_i are the number of surface grains and inner grains, N is total number of grains, σ_s and σ_i are the flow stress of the surface grains and inner grains and η refers to the size-dependent parameter for size-effect. Here, the deformation zone is defined as the area $(A_r = \text{contact length } (\Delta l) \text{ x thickness } (t/T))$ along the foil thickness during two successive tool-sheet interactions as shown schematically in Fig. 13.3(b) and in Eq. 3.3.

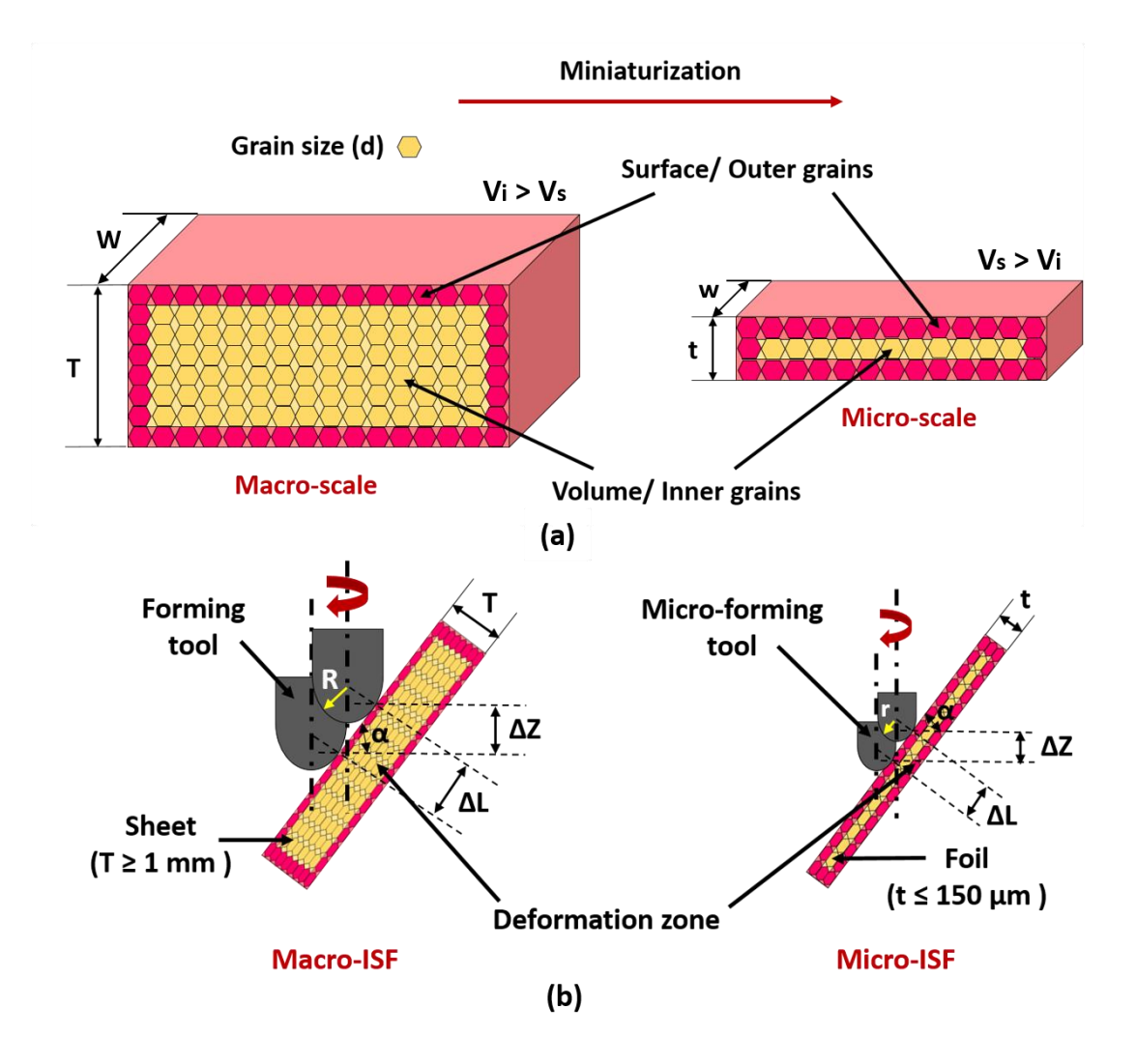


Fig. 13.3: (a) Schematic showing the share of surface and volume grains in sheet specimen during miniaturization (b) Comparison of surface and volume grains involved in macro-ISF and micro-ISF process

The magnitude of the contact length depends on the step depth of deformation. On increasing the value of the step depth, Δl increases with the increase in the share of internal and surface grains. In a bulk material, the volume of internal grains are higher than the surface grains across the thickness of the material. Therefore, in macro-ISF process, on each pass of the tool or during the tool-sheet interaction, a higher share of internal grains are involved during deformation than the surface grains along the thickness, T as shown in Fig. 13.3(b). The internal grains offer more resistance and hardening against the deformation, and require higher forming forces for the deformation of the material. While the free surface is easy to deform and results in lower flow stresses, due to less restriction in the movement of dislocations [70]. This restriction in the flow of the material with higher Δz increases during macro-ISF process, which results in early fracture and lower forming depth due to the presence of several internal grains.

Whereas, in micro-ISF process, the participation of surface grains are higher in number compared to the internal grains in thin foils (t) (Fig. 13.3(b)). Thus, increasing the value of step depth in µISF, a higher fraction of surface grains will undergo plastic deformation during forming. These grains experience low restrictions owing to the absence of dislocation barriers at the free surface. As a result, a higher value of step depth helps in achieving better flowability of the material in µISF. The results of the average failure depths obtained with different MC and t/d ratios presented a good agreement with the changing Δz and are shown in Table 3.3. It can be seen that the parts formed with Δz of 50 µm has the highest forming depth in all the cases. It is attributed to the increase in volume fraction of the surface grains (V_s) with respect to increase in the value of step depth. The geometries formed with step depth of 10 µm has the lowest forming depths, due to less domination of the surface grains over internal grains. Also at lower step depth, the tool marks are closer to each other, which may have induced high fictional effects leading to excessive thinning and fracture of the foil surface. However, a moderate and higher forming depth was observed with step depth of 30 μm. For each MC, a similar trend in the formability was observed when Δz was increased from 10 μ m to 50 μ m.

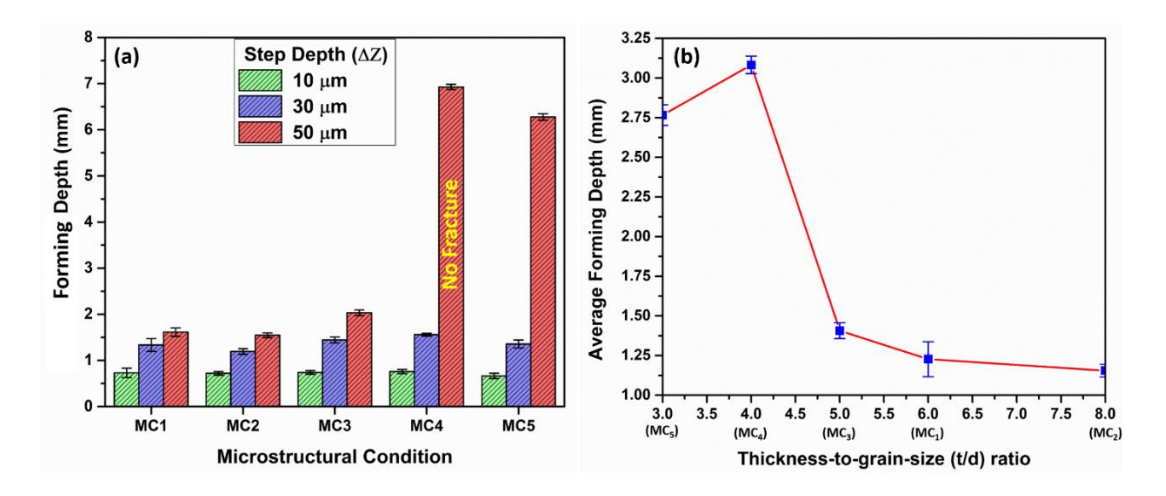


Fig. 3.14: (a) Bar graph presenting the forming depth of the components for different MC with respect to step depth (b) Variation of the t/d ratios corresponding to the average forming depth of all the components in each condition

3.4.1.2 Combined effect of grain size and step depth on formability

Overall, the combined effect of initial grain size and varying step depths on the formability of the micro-parts can be explained through Fig. 3.14(a, b). A slight decrease in the forming depth was observed for the MC₂ specimen after controlled heat-treatment of the original foil (MC₁) for all the step depths. However, the formability increased with the increase in the step depth from 10 µm to 50 µm. The scattering of the properties (standard deviation) was also reduced after annealing. The SEM image in Fig. 3.15(a) shows an enlarged view of the fracture location on the cracked wall surface of the MC₂ component. The premature failure of the component, shown in Fig. 3.15(b) resulted due to the high strain localization at the grain boundaries, leading to more thinning at the deformed regions. The well-defined and strengthened grain boundaries (small grain size) create hindrance to the source of dislocation movements in the material, resulting in lower ductility [154].

The MC₃ and MC₄ specimens showed a good improvement in the forming depths due to the growth of grain size in the material. For MC₄, the result is quite interesting, as the formed part accomplished the target depth of 6.928 mm at step depth of 50 µm without any fracture of the foil (Fig. 3.15(c)). The obtained geometries of the formed conical cups were precise and free of defects and cracks. The experiments were repeated three times to confirm the formability results. Despite of having a better ductility than the MC₄ specimen, the formability of the parts decreased for the MC₅ specimen. This may

have arisen due to size-effect and surface abnormalities in the MC₅ specimens (Fig. 3.10(e)). However, a decent forming height of 6.276 mm was witnessed with the increase in step depth.

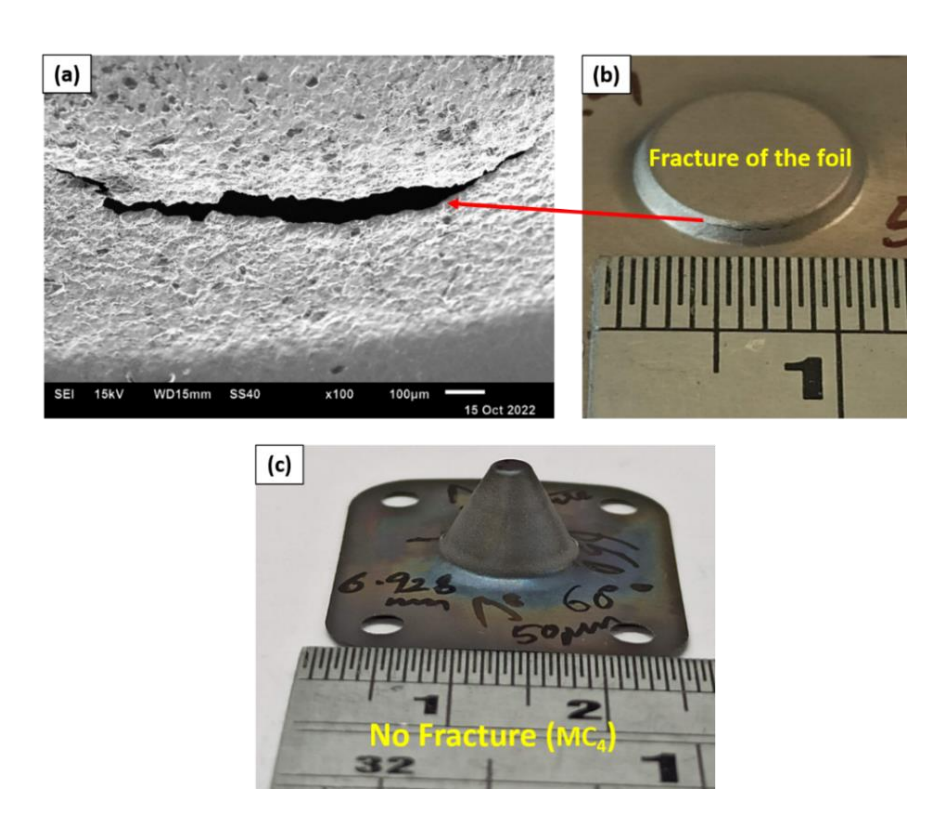


Fig. 3.15: (a) SEM micrograph of the fracture location (b) Failure of the conical component (c) Successfully formed component with no fracture at 50 μm step depth (MC₄)

3.4.1.3 Determination of critical t/d ratio for enhanced formability

The surface layer model explains that the grains which are near to the foil's surface are less constrained, and are expected to deform more than the grains present in the interior region of the foil [155]. Chan and Fu [78] documented that the micro-plastic behaviour of thin foils is strongly correlated to the t/d ratio of the material. When the t/d ratio is very low, the dislocations of the grains are more susceptible to free-surface annihilation, leading to strain localization of local grains with a reduction in both strength and ductility [156]. Hence, it is necessary to obtain an optimum range of t/d ratios for designing the μ ISF process. It was observed that the t/d ratio of the developed microstructures has a significant impact on the obtained average forming depths of the components, shown in Fig. 3.14 (b). Figure 3.9(b) demonstrates the change in the flow stress and ductility behaviour of the specimens due to the variation in the t/d ratios. The

flow stress of the recrystallized foil (MC₂) substantially increased at a t/d ratio from 6 to 8, because of smaller equiaxed grains. However, there was a gradual decrease in the strength of the specimens, when the t/d ratio fell below 8. It was seen that the decrease in the t/d ratio of the foil is attributed to the increase in the forming depth of the microparts upto a critical limit of 4.

Interestingly, a critical value of the t/d ratio was obtained at which the highest average forming depths were observed (Fig. 3.14 (b)). Similar results were obtained when the step depths were changed from 10 μ m to 50 μ m. For t/d ratios less than 4, the forming depth starts decreasing, this implies that at a certain t/d ratio of the foil, the formability of the foil is optimum. Hence, the combination of foil properties (t/d ratio) and process parameters (step depth) during the μ ISF process could be tailored and optimized based on this criteria.

3.4.2 Correlation of grain-size and t/d ratio of the foils, with Hall-Petch relation

Hall-Petch relation demonstrates the dependence of yield strength on the grain size of the material. In the present work, the yield stress (σ_y) values of various specimens are plotted as a function of the inverse square root of the measured grain size ($d^{-1/2}$, $\mu m^{-1/2}$). From Fig. 3.16, it can be seen that the yield stress values of all specimens lie closer to the fitting line and follow a trend similar to Lederich et al. [157]. The material constants (σ_o , K_y) of the Hall-Petch equation (3.4) were determined by fitting with a linear correlation between σ_y and $d^{-1/2}$ [72,73,150].

$$\sigma_{y} = \sigma_{o} + K_{y} d^{-1/2} \tag{3.4}$$

Here, σ_o is the frictional stress and K_y is the Hall-Petch coefficient (slope). In this equation, σ_o describes the stress for dislocation glide within an isolated region of the grain and K_y reflects the magnitude of hardening or required local intensified stress to propagate yielding across the grain boundaries.

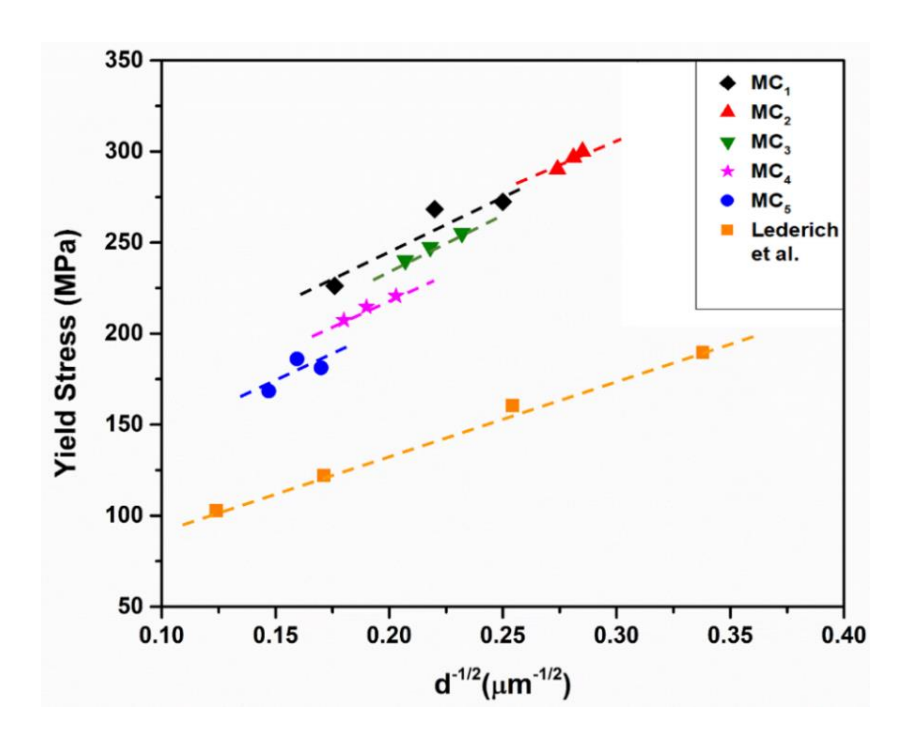


Fig. 3.16: Hall-Petch chart displaying the yield stress (σ_y) result of original and heat-treated Ti foils as a function of grain size ($d^{-1/2}$)

Both the original and annealed specimens exhibited homogenous values of the slope, K_y in the range of ~ 405 - 445 MPa μ m^{1/2} and were slightly higher than that stated in the literature [157,158]. The slope decreases with the increase in the grain size (lower t/d ratio). Higher K_y was witnessed for the MC₂ specimen due to strengthening of the grain boundaries with finer grains, which resists the dislocation slip during deformation. A decrease in K_y was observed from ~ 436 MPa μ m^{1/2} to 405 MPa μ m^{1/2} when the annealing temperature was increased from 300 °C to 500 °C (MC₃, MC₄, and MC₅), similar to that observed by Stanford et al. [159].

The σ_o values were higher in the original (~181 MPa) and annealed specimens (~147 - 205 MPa) compared to the literature [157] (~85 MPa) presented in Table 3.4. This could have resulted due to the heterogeneity in grain size distribution, developed strains, and manifestation of residual stresses, which are inherently present in the cold-rolled foils [160]. Using these results, grain size strengthening effects can be estimated to investigate the microstructure design and deformation mechanics of various materials [161].

Table 3.4: Hall-Petch material parameters based on yield stress data

Microstructural Condition	Friction Stress, σ ₀ (MPa)	Hall-Petch Coefficient, K _y (MPa μm ^{1/2})
MC ₁	181	424
MC_2	205	445
MC ₃	174	436
MC ₄	163	411
MC ₅	147	405
Lederich et al. (1978)	85	400

3.4.3 Measurement of the forming forces

The real-time monitoring of the forming forces during the μ ISF process was done using a KISTLER® force dynamometer. The schematic illustration of the μ ISF fixture mounted on a force acquisition device is shown in Fig. 3.1(b). A funnel-shaped conical geometry was formed and the force in the negative z-direction (axial in nature, F_z) was measured. The forces were recorded for all five conditions of the foils with different grain sizes, formed with step depths of 10 μ m, 30 μ m, and 50 μ m. It was observed that real-time monitoring of force data can be effective in determining the onset of failure due to abrupt drops in the forming forces. As it is difficult to observe the fracture of the component with the naked eye or through the cracking sound of the foil. The force monitoring results show the first location of fracture (Z_0) during the deformation of CP-Ti Gr2 foil in Fig. 3.17.

Sudden decrease in the magnitude of the axial force implies that a crack has initiated in the material, and further movement of the tool on the fracture region opens up the crack further, causing a severe dip in the force values. The forces are further bisected into two different forming zones at micro-scale [62]. The first zone is due to the pure bending when the tool touches the foil surface. A deviation in the geometrical compliance was observed at the start of the bending zone. It is the zone where the F_z reaches its highest value (F_{max}) as illustrated in Fig. 3.17(a). In the second, work hardening zone, a significant reduction in the force was observed when the wall region of the component was formed (Fig. 3.17(b)). In this zone, the thinning and softening of the material takes place that provides a good forming stability, to achieve a constant deformation load

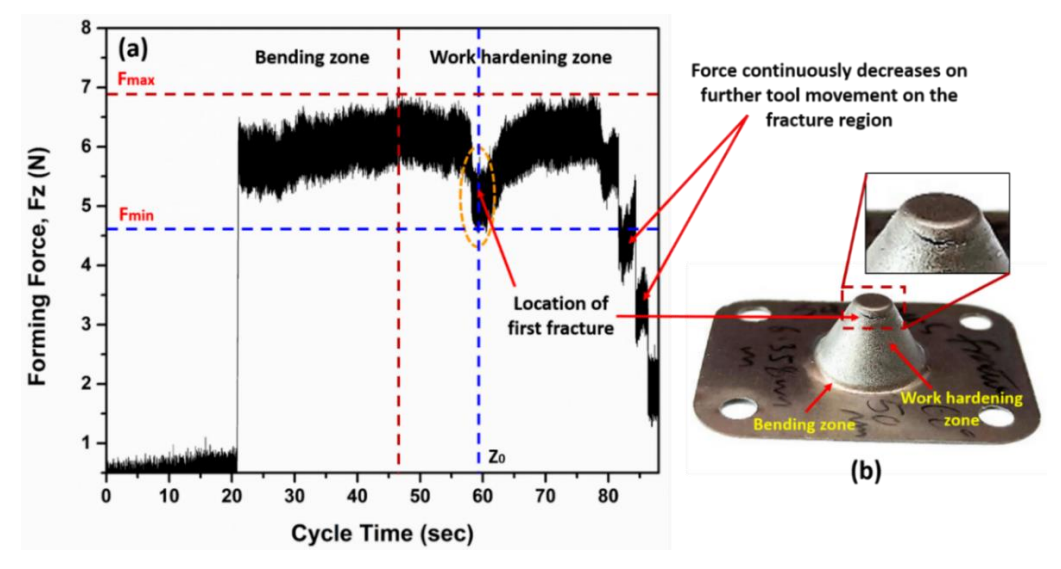


Fig. 3.17: (a) Real-time monitoring of the axial forces in the μ ISF process (b) Formed geometry

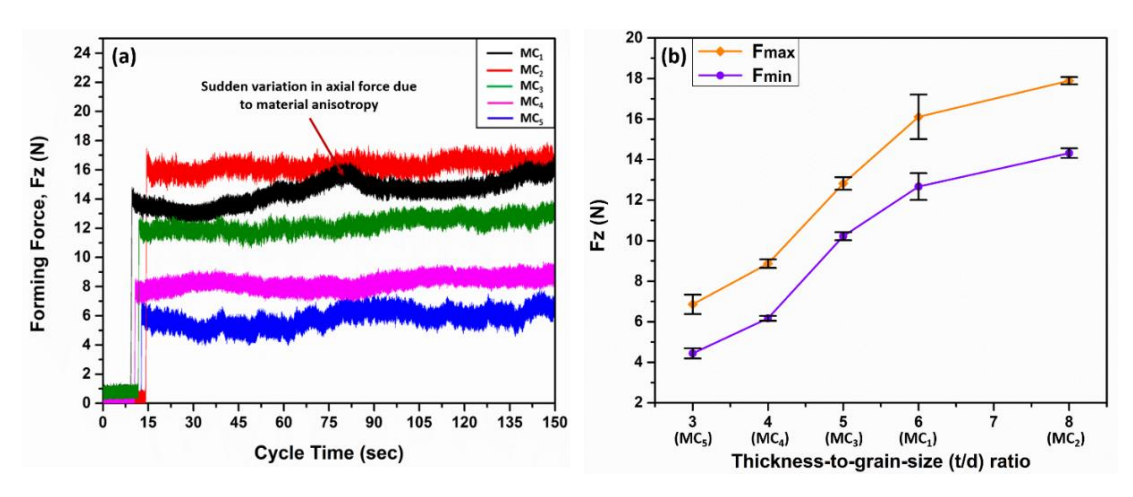


Fig. 3.18: (a) Evolution of forming forces with specimens of different grain size (b) Effect of t/d ratio on the magnitude of the forces, F_z

before decreasing to F_{min}, once the failure of the part takes place.

To understand the influence of grain size-effect on the forming forces, a comparative analysis of F_z was performed, for the original and heat-treated foils as shown in Fig. 3.18(a). The average value of F_z for all three step depths was used for the analysis. The MC₁ specimen shows larger cyclic variations (less stability) in the forces, while lower cyclic variations (more stability) were observed for MC₂. This variation could be due to the inherent anisotropic properties in MC₁, whereas the specimen in MC₂ has lower anisotropy due to annealing. Stability in the forces was observed for MC₃ and MC₄, after attaining a few millimetres of depth in the work hardening zone with the least deviation

in case of MC₄. However, the force deviations were slightly on the higher side for MC₅, due to an increase in the surface asperities and loss of equilibrium between the material thinning and work hardening [79]. Decrease in the F_{max} and F_{min} were observed with the decrease in the t/d ratio of the specimens, with the highest value at a t/d ratio of 8 for MC₂ (17.89 N) and the lowest at t/d ratio of 3 for MC₅ (6.86 N) (Fig. 3.18(b)). This is in correlation with the yield strength values (Fig. 3.9(b)), which decrease with an increase in the grain size, following the Hall-Petch relation. Lower forming forces also correspond to higher formability of the components, which can be useful to design the process at micro-scale (Fig. 3.14(b)).

3.4.4 Microstructure evolution of original and annealed foils

The microstructural and texture analysis of the original, annealed and deformed foil was performed using the electron backscatter diffraction (EBSD) and X-ray diffraction (XRD) techniques. Small samples of dimension $10 \text{ mm} \times 10 \text{ mm}$ were cut from different directions with respect to RD for the microstructural study. The XRD analysis was carried out on a Rigaku Ultima-III diffractometer using Cu-k α radiation with a wavelength of 1.5406 A $^{\circ}$. From the X-ray 2-theta measurements and Rietveld analysis,

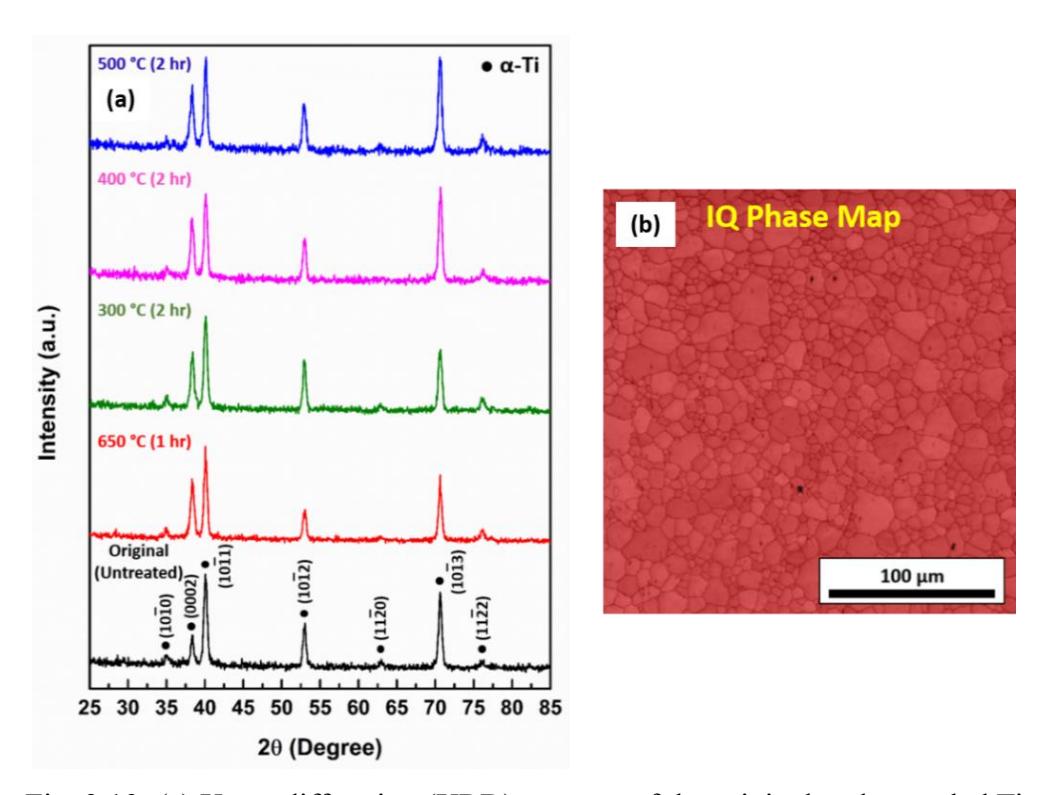


Fig. 3.19: (a) X-ray diffraction (XRD) patterns of the original and annealed Ti specimens (b) Image quality (IQ) phase map for CP-Ti

it was found out that no phase transformation occurred during the heat-treatment of the Ti foil as the annealing temperature was increased. Figure 3.19(a) shows the XRD peak results of the original and annealed specimens as also observed by other researchers [162]. However, there was an increase in the basal plane intensity (I_{0002}) after the heat-treatment of the specimen compared to the original foil. This indicates that more number of crystallographic basal slip planes were activated and oriented in a particular direction, mostly preferably $\{11\overline{20}\}$.

The initial and post-deformed microstructures of the foils were studied using a FEI QuantaTM SEM (Joel JSM-IT800) equipped with an EDAX Aztec-Crystal EBSD detector from Oxford Instruments. The EBSD scans were carried out on the specimen surfaces with the electron beam parallel to the rolling direction of the foil. For optimal statistical reliability and accurate analysis, the EBSD scans covering more than 300 grains were acquired for every condition with a step size of 0.2 μm. A typical cleanup processing was performed on the EBSD raw data with a minimum confidence index (CI) of 0.1. The EBSD data was used for plotting the inverse pole figures (IPF) and image quality (IQ) maps of undeformed and deformed samples. The IQ map in Fig. 3.19(b) shows the presence of single alpha phase (red color) of the original Ti foil.

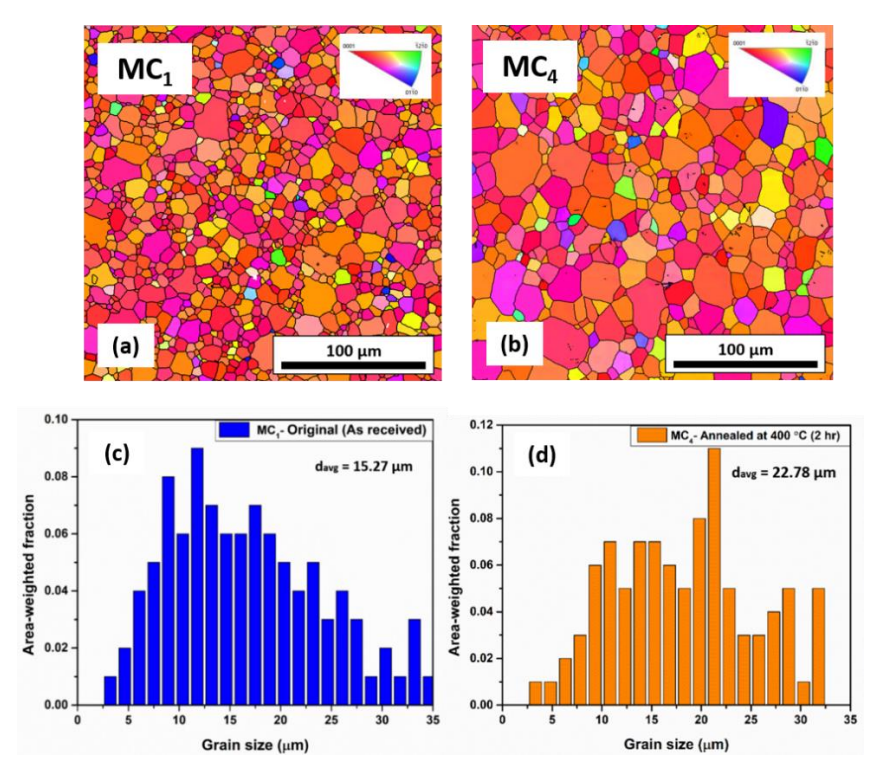


Fig. 3.20: IPF maps and average grain size of the undeformed original and annealed specimens (a,c) MC₁ (b,d) MC₄

The sample surface preparation for the EBSD analysis was carried out by polishing with progressively finer water-based diamond suspensions (size of 0.5 μ m). Finally, electropolishing was carried out using an electrolyte solution comprising of 80 % methanol and 20 % perchloric acid (STRUERS®) at 23 V, 1.97 A for 12 s. The polishing time was optimized based on several trial runs. The EBSD IPF maps obtained by analyzing the EBSD diffraction patterns for all the samples (undeformed (MC₁) and deformed (MC₄) conditions) are shown in the Fig. 3.20 and Fig. 3.21 respectively. These two specimens were taken for the analysis to study the evolution of microstructure after the deformation with 50 μ m step depth. The equivalent circular diameter method was used to determine the average grain size of the foils in RD-TD. The initial grain size of the undeformed specimens for MC₁ and MC₄ were 15.27 μ m and 22.78 μ m. After the deformation, a reduction in the grain size was observed to 5.88 μ m and 4.11 μ m respectively.

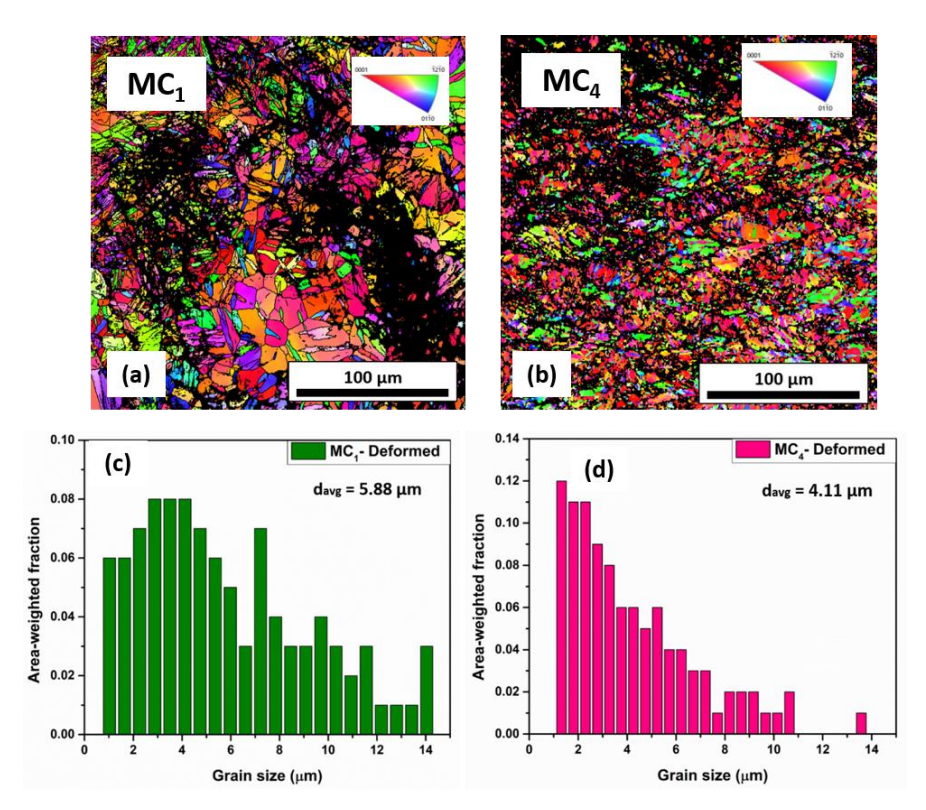


Fig. 3.21: IPF maps and average grain size of the deformed original and annealed specimens (a,c) MC₁ (b,d) MC₄

This shows a significant grain refinement in the deformed specimens with the bigger grains getting dissociated to smaller sub-grains. A significant amount of deformation twins were also observed on the deformed surface for both the specimens. The twinning is common in α -Ti materials when subjected to severe deformation at higher step depth.

These twins occur due to the limited availability of active slip systems in the material with HCP structure [65]. Figures 3.22(a,b) and 3.23(a,b) shows the IQ maps marked with low angle (2–15°) and high angle (>15°) grain boundaries in red and blue color, respectively. The grains which have the misorientation angle between 2–15° are called low angle grain boundaries (LAGBs) and the misorientation angle greater than 15° are known as high angle grain boundaries (HAGBs).

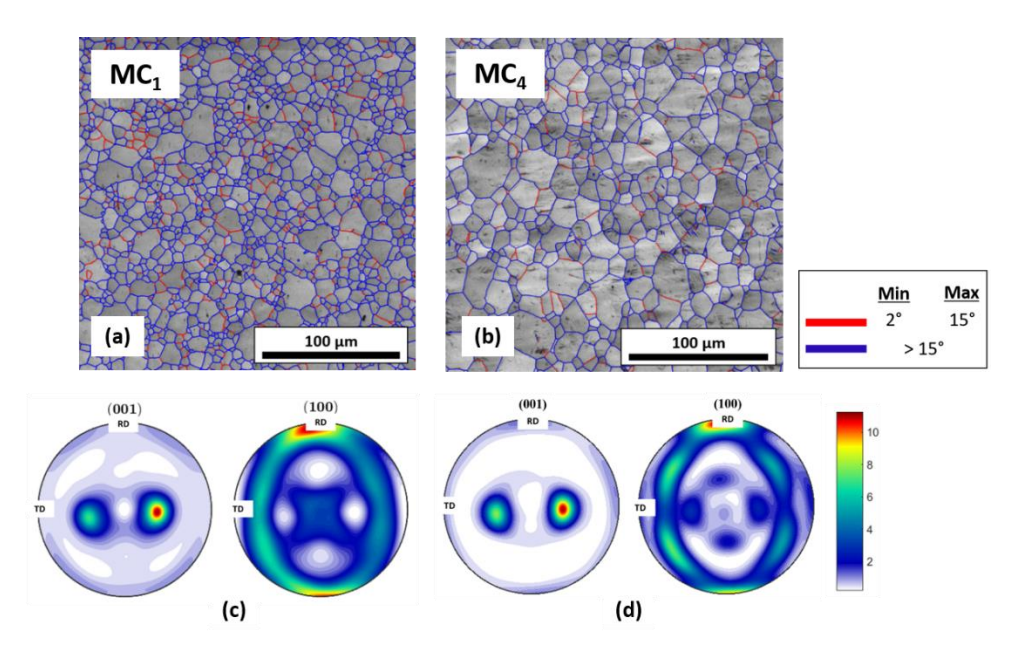


Fig. 3.22: IQ maps marked with red and blue color for low and high angle grains for undeformed specimens (a) MC₁ (b) MC₄, (c,d) (001) and (100) pole figures of the IPF map

It can be seen from Figs. 3.22(a,b) and 3.23(a,b) that the fraction of HAGBs are more compared to the LAGBs. For the initial MC₁ specimen, the fraction for the LAGBs and HAGBs are 18.3 % and 81.7 %. Whereas, for the MC₄ specimen, the fraction for the LAGBs and HAGBs are 12.4 % and 87.6 %. This shows that the increase in the grain size of the annealed MC₄ has higher amount of HAGBs and have different crystallographic grain orientation in the specimen. After the deformation process, a significant change in the area fraction of the LAGBs and HAGBs were observed. For the deformed MC₁ specimen, the fraction for the LAGBs increases to 51.4 % and HAGBs decreases to 48.6 % and for deformed MC₄ specimen, the fraction for the LAGBs increases to 67.2 % and HAGBs decreases to 32.8 %. This change in the misorientation angles can be observed in Fig. 3.24. As the foil starts to deform in μISF, the stretching, bending and shearing of the material contributes to the deformation of the crystals and sub grains. Grain fragmentation can be observed within the grains and

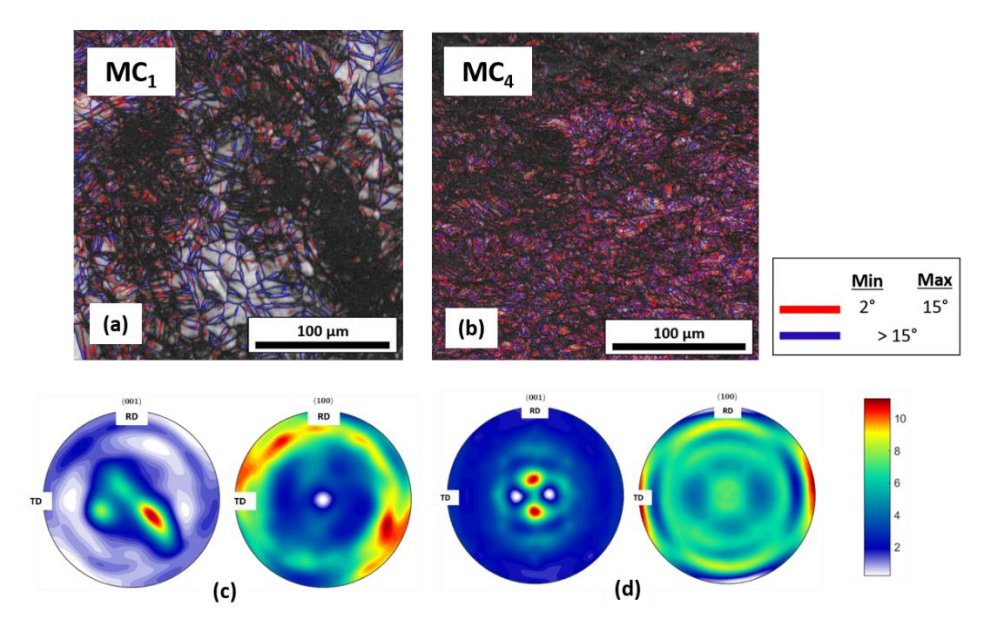


Fig. 3.23: IQ maps marked with red and blue color for low and high angle grains for deformed specimens (a) MC₁ (b) MC₄, (c,d) (001) and (100) pole figures of the IPF map

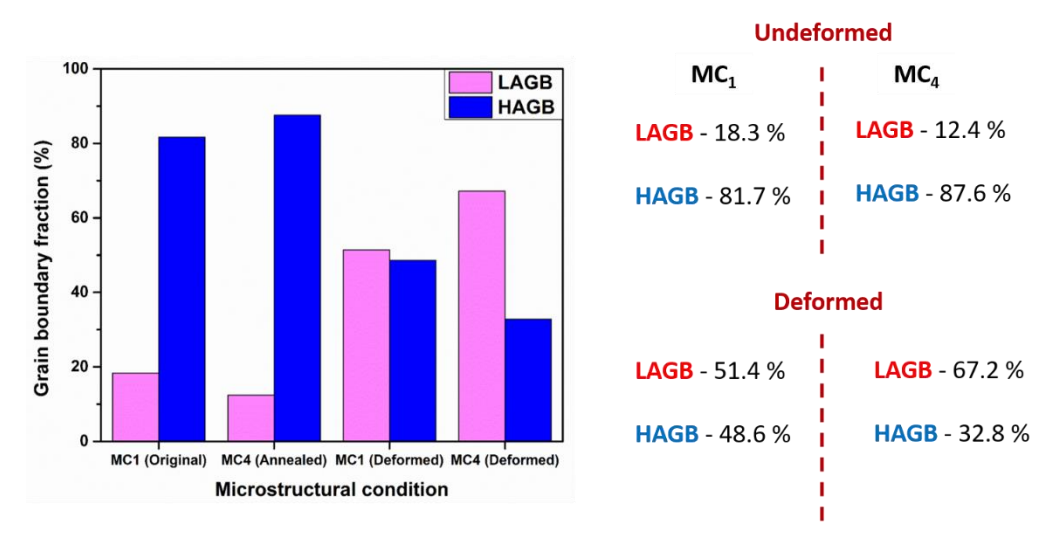


Fig. 3.24: Comparison of LAGBs and HAGBs before and after the deformation process

sub-divisions of the grains, as seen by dense unindexed region (black in color) in EBSD analysis of the deformed part. The higher fraction of LAGBs in MC₄ after deformation can be due to higher dislocation density of the grains post heat-treatment. The mobility of the dislocations might have increased with less restrictions of the grains at the grain boundaries, leading to higher plastic deformation and strained grains. The orientation of a few selected grains is shown with the help of pole figures for the basal (001) and prismatic (100) planes, simulated in MATLAB® from the bulk-XRD analysis is shown

in Figs. 3.22(c,d) and 3.23(c,d) respectively. The pole figures of the MC₁ and MC₄ specimens in Fig. 3.22(c,d) and shows the <0001> fiber texture TD split as observed by Wang and Huang [163] for the HCP materials. However, the texture was completely changed and disappears, with the rise in the intensity after the deformation process. This is caused by the change in grain misorientation and crystal rotations, causing microstructural instability in the specimen.

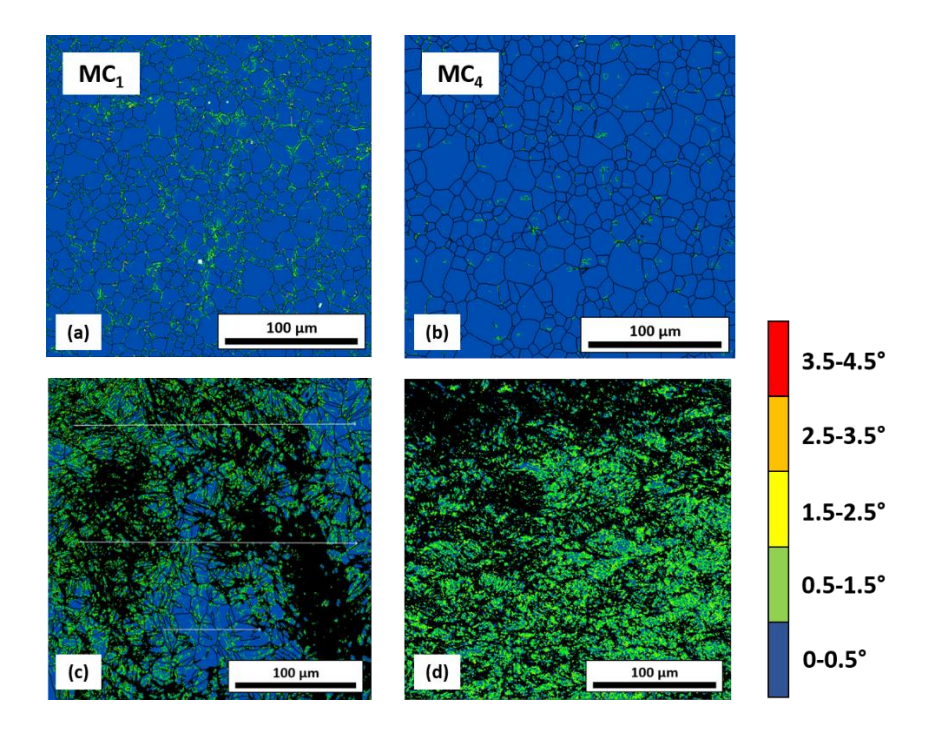


Fig. 3.25: KAM maps for the (a,c) MC₁ and (b,d) MC₄ specimens

The EBSD results of the Kernal average misorientation (KAM) maps is shown in Fig. 3.25. The KAM angle is an indication of local plastic strain in the grains and the higher values of KAM angle suggest the presence of strained grains and greater concentration of geometrically necessary dislocations [12]. The KAM maps shows that the intensity of the dislocation density increased post-deformation with the increase in the fraction of strain localized grains. The increase in mean KAM angle for MC₁ was from 0.67° to 1.21° and for MC₄, it was from 0.48° to 1.68°. There was an increase in the percentage of strained grains after the micro-forming process for MC₄ compared to MC₁ specimen. These results are in correlation with the increased fraction observed with LAGBs, which lead to more plastic deformation of the formed parts. Higher forming depth was observed for MC₄ (6.928 mm) and lower depth for MC₁ (1.616 mm) as shown in Fig.

3.14(a). Therefore, the results of the KAM maps shows that the increase in strained grains may have led to higher material deformation of MC₄ specimen at similar operating process parameters.

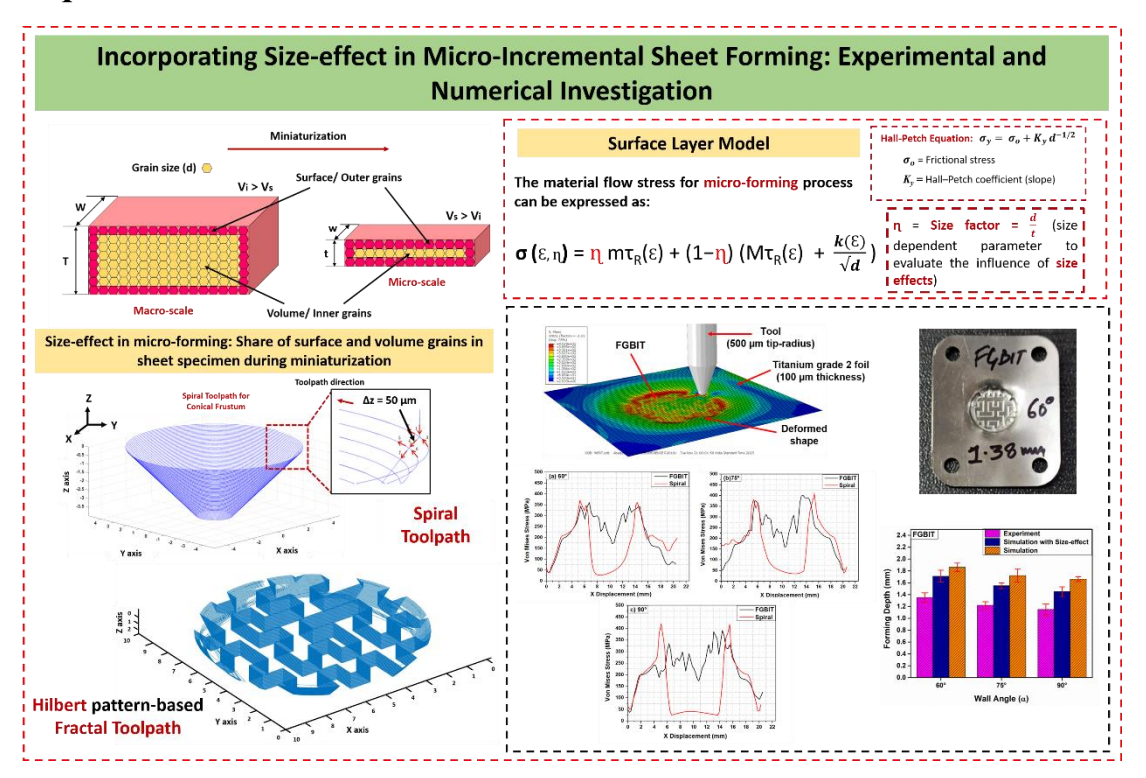
3.5 Summary

This chapter highlights the design and development of the micro-forming fixture for carrying out the micro-scale plastic deformation of ultra-thin sheets (foils). These foils are vulnerable to easy distortion or bending due to their low stiffness and thickness in the micron range. A robust investigation was carried out to design the fixture with the holding and backing plates to counter the relative movement between the foil and the plates during deformation. The forming tool was built in-house using the micro-turning process. Controlled heat treatment was performed to generate a wide spectrum of grain sizes. The effect of different microstructures/ grain sizes on the formability of CP-Ti-Gr2 foils were studied. Tests were performed to investigate the combined effect of grain sizes and incremental step depth on the formability and forming forces in the µISF process. The annealing temperature of 400 °C (MC₄) was most conducive in enhancing the formability of the geometrical parts, upto a critical t/d value of 4. It was found that the magnitude of the forming forces decreased with the reduction in the t/d ratio of the specimens. The measured forming forces were in excellent correlation with the uniaxial tensile tests data, with respect to the grain size correlated through the Hall-Petch relation. The results showed good repeatability in the accuracy of the developed shapes and their ability to achieve higher forming limits with reasonable aspect-ratio of the micro-parts. The microstructural analysis through EBSD showed that the presence of higher fraction of LAGBs and larger KAM angle in the material after deformation led to higher forming depths of the micro-parts.

Chapter 4

Development of Numerical Simulation Model Incorporating Size-effect

Graphical Abstract²



4.1 Introduction

Due to miniaturization, size-effect causes scattering of process parameters, which significantly impacts the formability and flow stress of the material. To study the size-effect at micro-scale, Lin et al. [164] explored the deformations physics through micro-mechanics based modelling of different materials for thin foils. The influence of material grain size, microstructure and fracture strains were studied to predict the nature of micro-scale deformation. Fu and Chan [78] explored the grain size-effect and fracture behaviour of thin Cu foils by varying the sheet thickness and grain size of the specimen. It was found that the magnitude of flow stress, fracture strain, and the number of micro-

²Pal, M., Kumari, T., Agrawal, A., and Nirala, C. K., "Enhancing μ-ISF Prediction Accuracy and Formability by Incorporating Size-effect and Space-filling Fractal Toolpath: Experimental and Numerical Investigation," (Under Review)

voids in the fracture region reduced with the decrease in the t/d ratio of the specimens [165].

In this chapter, a size-effect based numerical model is developed for the µISF process. The effect of the thickness and grain size of the material is considered for accurately simulating the micro-scale deformation of thin sheets in µISF. FGBIT and spiral toolpaths have been used for carrying out the simulation. The simulation have been performed using the ABAQUS® platform. The accuracy of ABAQUS® results depends on the quality of technical data available as input to the FEA model. FEA is a computational tool used to predict the deformations, forming forces, stresses, and strains throughout any material structure (sheet or foil). The flow stress behavior of thin foils considering the grain size-effect has been considered in the updated numerical simulation based on the theory of the surface layer model. Through this model, the influence of size-effect in the micro-forming process can be analyzed.

4.2 Work Methodology

4.2.1 Size-effect in micro-forming

The flow stress of the specimens is greatly affected by the non-homogeneous nature of materials in micro-scale, causing the scattering of process parameters and properties of the process. Such behavioral changes in the properties occurs due to the phenomenon of size-effect, when miniaturization of the specimens takes place. The material behaves differently when there is a departure from the material's polycrystalline to single-crystal deformation behavior [69]. The variation in the number or size of grains and their orientation increases the non-homogeneity/ anisotropy in the material [144]. This significantly affects the geometrical features of the formed geometry and causes changes in the deformation behavior at the micro-scale. The occurrence of the size effect in the micro-forming process can be analyzed through the surface layer model [70,166] based on the study of surface grains (V_s) and internal grains (V_i) stresses as shown in Fig. 4.1. The flow stress (σ) of the material at the micro-scale can be expressed by Eq. 4.1.

$$\sigma = \frac{N_S \sigma_S + N_i \sigma_i}{N} \qquad (N = N_S + N_i) \tag{4.1}$$

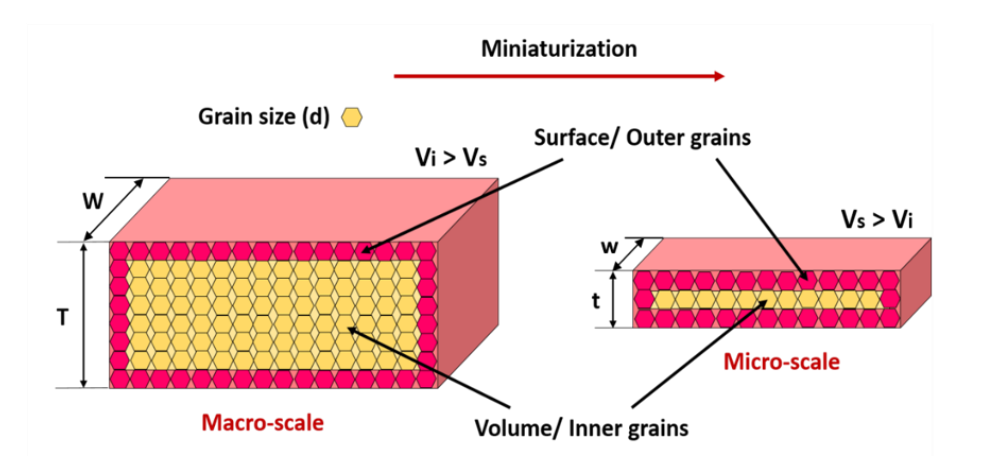


Fig. 4.1: Size-effect in micro-scale deformation

4.2.2 Generation of FGBIT and spiral toolpath

Space-filling curves were first introduced by G. Peano in 1890 [101]. The mathematical space-filling curves known as fractals have drawn a lot of attention from various researchers because of their distinctive representation [99]. Earlier studies have shown the use of fractal toolpaths in rapid prototyping and FDM processes [59], as well as in machining operations [60,61]. The concept of fractal geometry serves as the basis for the generation of the fractal toolpaths [105]. Figure 4.2 shows the fractal toolpaths based on the Hilbert pattern [62].

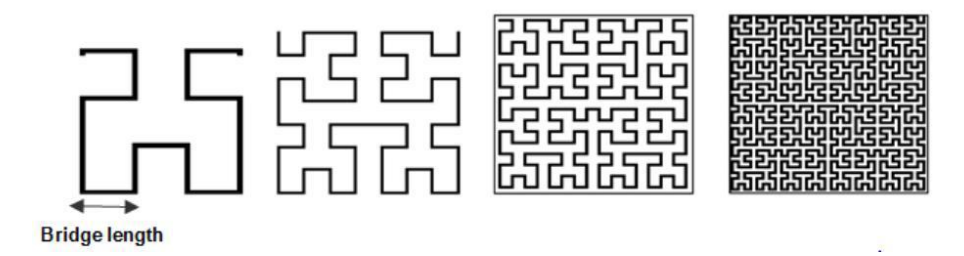


Fig. 4.2: Hilbert pattern-based fractal toolpath (order 2-5) [167]

In this work, a fourth order Hilbert pattern-based fractal toolpath has been employed to form conical-shaped geometrical micro-parts. The toolpath code was developed in MATLAB®. Unit sub-intervals were added to extend order one curve into higher-order curves. The order of the curve is decided by the required geometrical dimensions of the cup, while the bridge gap/ length is governed by the diameter of the forming tool [62]. Forming vertical walls is a challenging task in the μ ISF process. This fractal toolpath helps in overcoming the limitation of forming higher wall angle micro-products. The

maximum forming depth achieved without any fracture in the conventional i.e. spiral toolpaths and FGBIT has been used as a metric for formability assessment in this study.

A graphical user interface (GUI) developed using MATLAB® App Designer (R2021a release) was used for the generation of a spiral toolpath for different wall angles, i.e., 60°, 75°, and 90°. GUI offers a user-friendly interaction, employing basic graphical elements and enabling users to achieve desired outcomes with minimal variable inputs. For FGBIT, a unique approach, involving specific steps to ensure the accuracy of the toolpath generation was used. Firstly, CAD model of the conical geometry was prepared using SolidWorks® for different wall angles. Secondly, the saved CAD models were subsequently converted to the .STL format and then imported into a slicer software (PrusaSlicer) as shown in Fig. 4.3. The slicing procedure gradually involves adjusting the parameters such as layer height, infill density, infill angle, etc. for utilizing the fractal pattern for the part filling, resulting in the generation of the fractal toolpath. To crosscheck the precision and the line-formation of the generated toolpath, third step consists of conducting toolpath verification using MATLAB®. The toolpath codes were imported for analysis, enabling the extraction and visualization of the toolpath coordinates. The final toolpath for the spiral and FGBIT used for the micro-forming experiment is shown in Fig. 4.4 and the experimental setup for µISF is presented in Fig. 4.5.

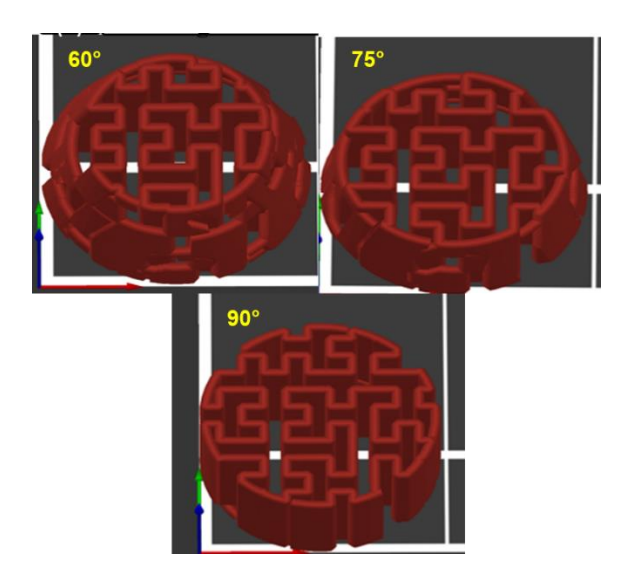


Fig. 4.3: Slicing and fractal geometry infill in each CAD model having different wall angles at 60°, 75° and 90°

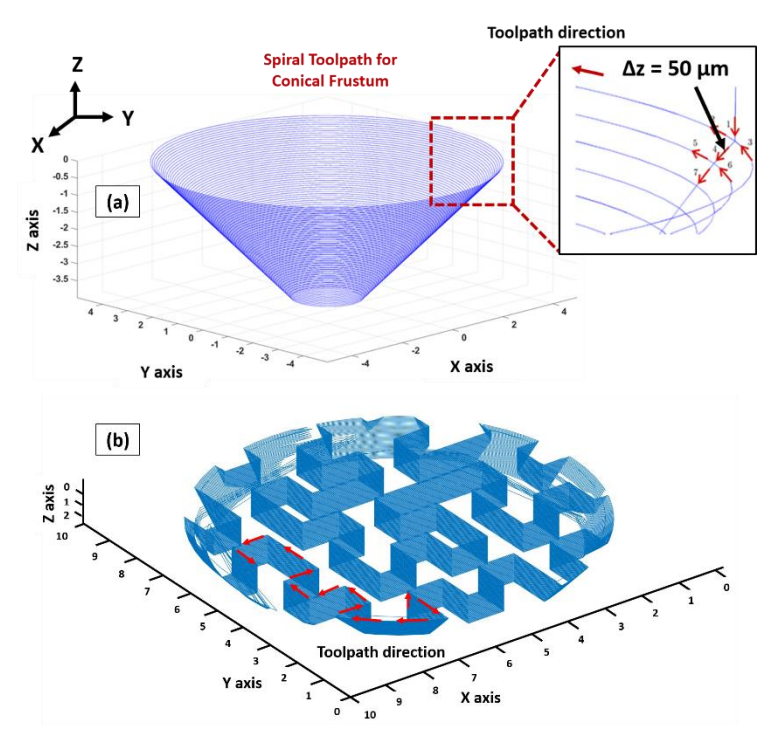


Fig. 4.4: (a) Conventional spiral toolpath, and (b) FGBIT for conical-shaped geometry for μISF

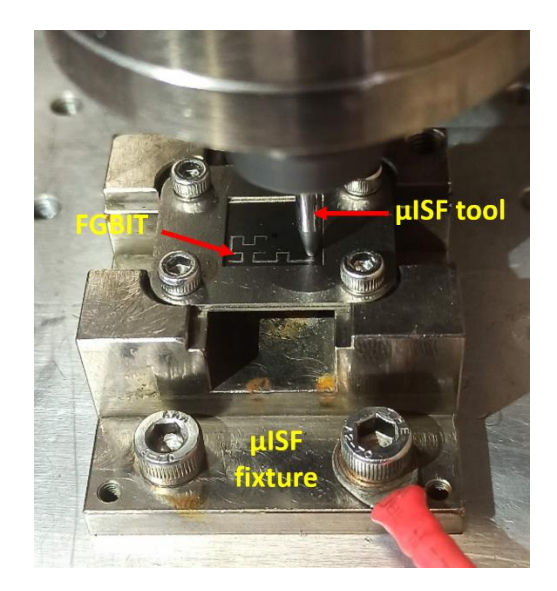


Fig. 4.5: Experimental setup for μISF

4.2.3 Numerical modeling incorporating size-effect

A 3D elastic-plastic isotropic hardening model based on the von Mises yielding criterion was used for the numerical simulation in ABAQUS®/ Explicit suite. The tool was considered as analytic rigid body and the CP-Ti Gr2 foil was taken as deformable. For meshing, S4R shell elements (0.25 mm mesh size) were chosen with five integration

points for their high precision and efficient CPU processing. The computational time for simulations ranged from approximately 24 to 28 hours before fracture. The CPU was configured with a clock speed of 2.20 GHz and RAM of 128GB. Master-slave contact algorithm was used for the tool/ foil surface interactions with a friction coefficient (μ) of 0.33 [142], as per Coulomb's friction law (4.2), where Fn and Ft are the normal and tangential friction force components.

$$Ft = \mu Fn \tag{4.2}$$

To determine the mechanical characteristics of the foil, a series of uniaxial tensile tests were conducted in three different directions (RD, TD, and DD) as shown in Fig. 4.6(a). As discussed in Chapter 3, the initial tensile results showed that the material was high in anisotropy in different testing directions. Therefore, the results from all three directions were utilized and averaged results were used for the numerical simulation analysis in ABAQUS® as presented in Table 4.1. The test was conducted in accordance with the ASTM E-345 standard. The step time and the step distance for the amplitude of the toolpath in x, y, and z coordinates can be calculated based on the equations (4.3) and (4.4).

Step time
$$(t) = \frac{Step \ distance}{Velocity \ of \ the \ tool}$$
 (4.3)

Step distance (d) =
$$[(x_2 - x_1)^2 + (y_2 - y_1)^2 + (z_2 - z_1)^2]^{1/2}$$
 (4.4)

Table 4.1: Properties of the CP-Ti Gr2 foil used in the numerical simulation

Mechanical properties	Magnitude	
Density	4.51 gm/cm ³	
Poisson's ratio	0.33	
Average ultimate tensile	340 MPa	
strength (UTS)		
Average yield strength	262 MPa	
Modulus of elasticity	120 GPa	
Uniform strain	20.85 %	
Strain hardening exponent	0.18	

A ductile damage fracture-based void growth model (VGM) was used to simulate the μ ISF process. If the damage reaches a particular threshold, this model predicts the initial fracture of the material. Material fragmentation during plastic deformation leads to the production of voids and nucleation, which in turn causes fracture in the material as a result of various plastic strains as shown in Fig. 4.6(b). The material is assumed to be homogenous and isotropic in the FEA model. Here, the model assumes that the equivalent plastic strain, ϵ_{pl} (4.5) at which the failure of the material occurs, is the function of stress triaxiality, $\dot{\eta}$ (4.6), and equivalent plastic strain rate ($\dot{\epsilon}_{pl}$) [126]. The $\dot{\eta}$ value incorporated for the μ ISF simulation was calculated from initial uniaxial tensile FEA runs. The FEA of the formed geometry using the FGBIT strategy and experimental specimen are shown in Fig. 4.7(a,b).

$$\mathcal{E}_{pl} = \phi \left(\dot{\eta}, \dot{\epsilon} pl \right) \tag{4.5}$$

$$\dot{\eta} = \frac{\text{Hydrostatic stress (p)}}{\text{von Mises stress (q)}}$$
(4.6)

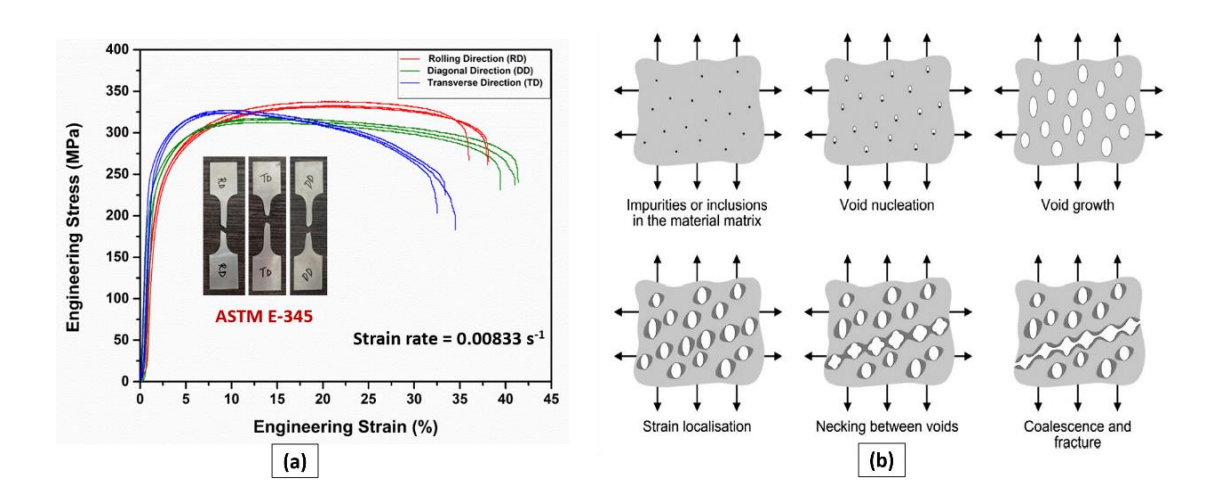


Fig. 4.6: (a) Engineering stress-strain curve of CP-Ti Gr2 in RD, TD, and DD (b) Schematic of nucleation, growth, and coalescence of voids [97,133]

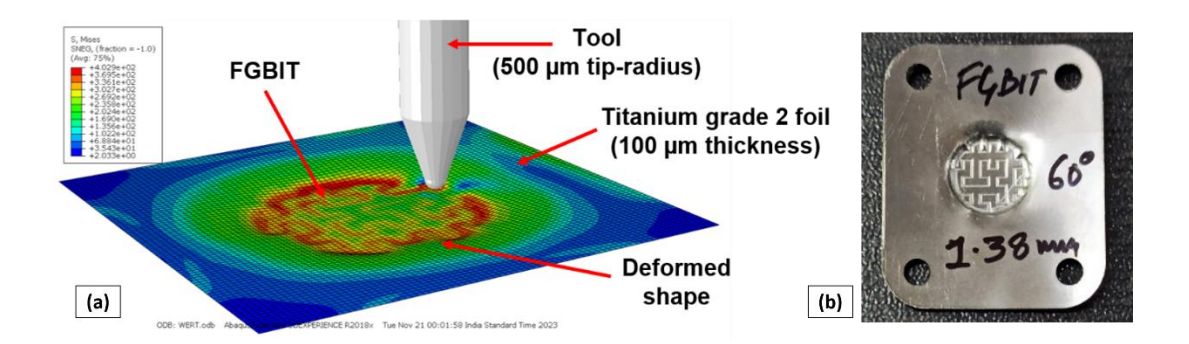


Fig. 4.7: (a) Representation of the FEA of the deformed conical shape using FGBIT, and (b) Deformed specimen

Material size effects are very important problems in micro-forming process design. Size-effect significantly affects the geometrical features of the formed geometry and causes changes in the micro-deformation behavior of the micro-parts, resulting in scattering of the properties. Based on the behavior of the material at a small scale (inhomogeneous continuum), the decrease/ change in the flow stresses can be explained by the surface layer model [70,155] (based on flow stress, grain size and thickness) as discussed in Eq. 4.1. Through Eq. 4.1, we can express the flow stress for micro/meso-forming process in this form (Eq. 4.7), taking the consideration of single crystal and polycrystal models [72,168]. With Ns = η N, Eq. 4.7 can be expressed by using η , which can be used as a size dependent parameter to evaluate the influence of size effects as shown in Eq. 4.8. The size-effect parameter, η is termed as size factor, which is further simplified as the ratio of grain diameter (d) to the thickness (t) of the sheet ($\eta = d/t$) [70].

$$\sigma(\mathbf{E}) = \frac{N_{s}m\tau_{R}(\mathbf{E}) + N_{i}(M\tau_{R}(\mathbf{E}) + \frac{\mathbf{k}(\mathbf{E})}{\sqrt{\mathbf{d}}})}{N}$$
(4.7)

$$\sigma(\mathcal{E}, \eta) = \eta \operatorname{mt}_{\mathcal{R}}(\mathcal{E}) + (1-\eta) \left(\operatorname{Mt}_{\mathcal{R}}(\mathcal{E}) + \frac{k(\mathcal{E})}{\sqrt{d}} \right) \qquad (N_{\mathcal{S}} = \eta N) \qquad 1 \ge \eta \ge 0$$
 (4.8)

$$\tau_{R}(\mathcal{E}) = \tau_{o} + k_{s} \mathcal{E}^{n} \quad (\sigma \circ (\mathcal{E}) = M \tau_{R})$$
(4.9)

Where, $\tau_R(E)$ in Eq. 4.9 is the critical shear resolved stress according to crystal plastic theory and Schmid law [168]. The value of σ o(E) obtained from Hall–Petch analysis is also related with the critical resolved shear stress as M τ_R . M is the orientation factor

related to the slips on deformation systems for polycrystal and m is the orientation factor for the single crystal model ($m \ge 2$). k(E) is the locally intensified stress needed to propagate general yield across the polycrystalline grain boundaries [7]. The value of the size factor η may vary with different specimen grain diameters and thicknesses. Here, the material used in the experiments is CP-Ti Gr2 and the grain size is 17.12 μ m (received material), having a thickness of 100 μ m with t/d ratio of 6 respectively.

Generally, the flow stress curves can be identified with an exponential law. LSM (least square method) was used to calculate the undetermined coefficients in the model. The flow stress curves for various values of the size factor were plotted for the plastic region as shown in Fig. 4.8. For the required material parameter $\eta=0.17$, the flow stress graph was observed considering the microstructural aspects of the material used in the experiment. The experimental flow stress also showed a good agreement with the modeled results. Therefore, the results of the mixed material model based on this surface layer model, considering size-effect was used for the FE analysis in ABAQUS® for the correct prediction of fracture of the specimens in the micro-scale domain of the μ ISF process. The properties of the flow stress used in the numerical simulation is shown in Table 4.2.

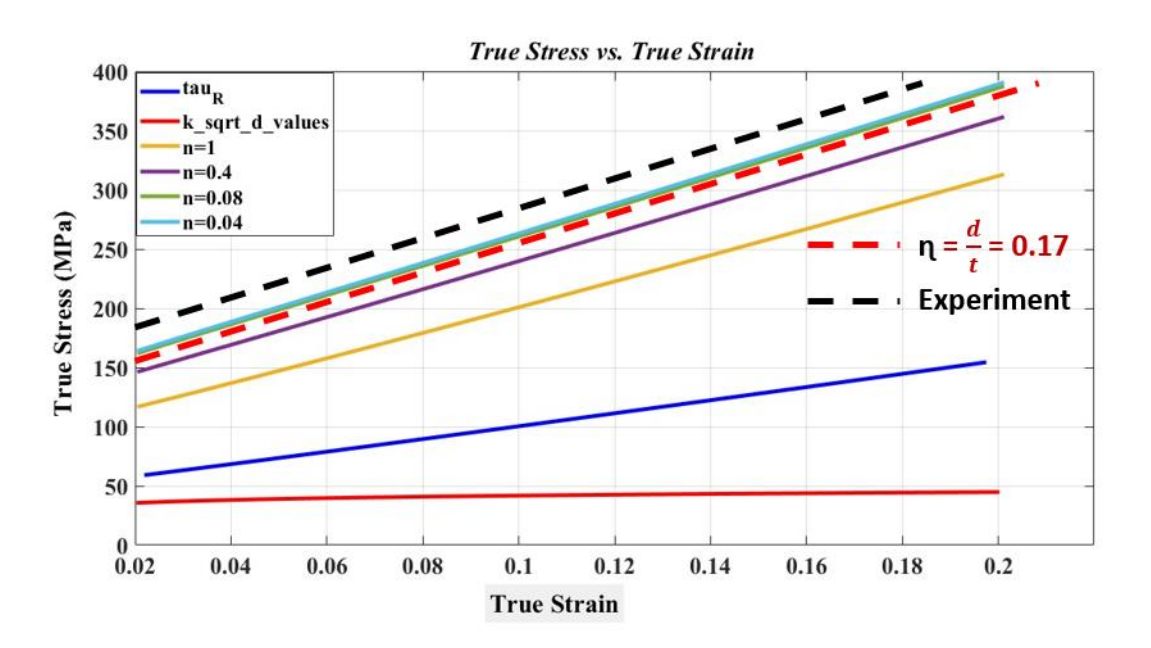


Fig. 4.8: Comparison between the calculated flow stress curves and experimental results

Table 4.2: Flow stress properties used in the numerical simulation

Flow stress properties	Magnitude		
<i>k</i> (ε)	424 MPa μm ^{1/2}		
M	2.5		
m	2		
d	17.12 μm		
t	100 μm		
η	0.17		
$ au_{ m o}$	55 MPa [169]		
ks	250 MPa [169]		
n	0.7		



Fig. 4.9: Formed conical cups by using FGBIT and spiral toolpath in μ ISF (a) 60°, (b) 75°, (c) 90°

4.3 Results and Discussion

4.3.1 Forming Depth

The experiments were performed on a multi-purpose hybrid- μ EDM machine (Mikrotools Pte Ltd., DT-110i). Three different forming angles (α) of 60°, 75°, and 90° were selected to generate conical micro-parts with FGBIT and spiral toolpaths. The geometries were formed at a constant step depth (Δz) of 50 μ m and the tool was given

a clockwise rotation of 500 rpm and feed rate of 10 mm/min. The setup for performing the μ ISF is shown in Fig. 4.5. The results of the micro-forming tests with varying wall angles and toolpaths are presented in Fig. 4.9. Although the failure occurred for all the cases, it was observed that the micro-parts formed with FGBIT achieved higher forming depths than the components formed with the spiral toolpath. In spiral toolpath, the tool does not cover the bottom section of the component as shown in Fig. 4.9, and has a smooth surface finish at this untouched part of the geometry. However, in FGBIT strategy, the toolpath covers the whole part of the geometry, which helps in minimizing the pillow effect and increases the forming depth. This trend was similar with all the formed parts with the change in forming angles. However, with the increase in α , the formability starts to decrease. Highest average forming depths were observed with α of 60° and the lowest for 90° , for both the toolpath strategies.

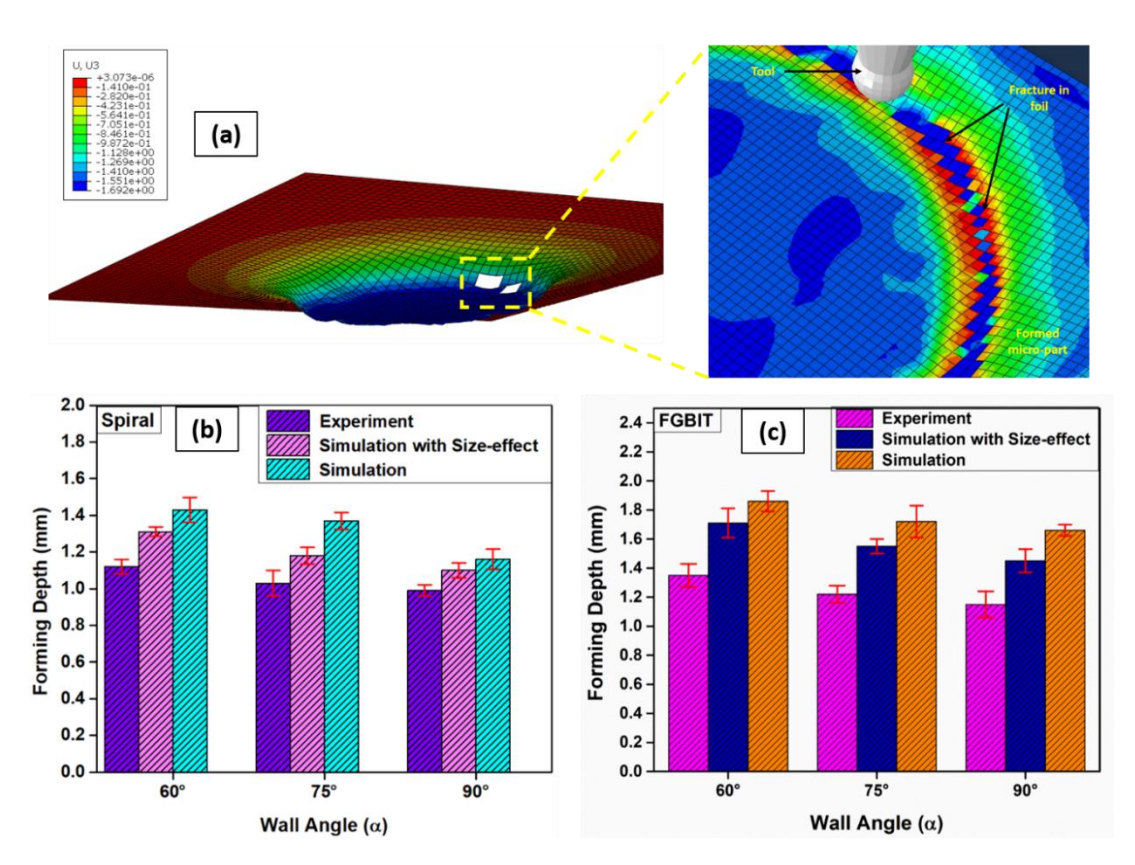


Fig. 4.10: (a) FEA of the observed fracture in the formed micro-part, Comparison of average forming depths using (b) spiral toolpath and (c) FGBIT for different wall angles

It was interesting to note from the experiments and simulations that by using FGBIT toolpath failure of the sheet could be avoided by few more increments, which is quite significant for such extreme forming conditions. In μ ISF, forming high vertical angles

like 90° is very challenging, and generates high residual stresses in the component. This results in premature failure due to excessive thinning of the foil as per sine-law [15] as shown in the FEA results in Fig. 4.10(a). In this regard, the FGBIT strategy provides a better route to form high wall angle geometries due to delay in the localized fracture of the micro-parts. This toolpath helps in increasing the formability of the geometries by increasing the number of increments during the plastic deformation. The numerical simulation results in ABAQUS® also show a promising agreement with the experimental results as presented in Fig. 4.10(b,c) for both the toolpaths. A significant increase of about 19.5-34.1 % was observed in the forming depths of the parts using the FGBIT strategy.

However, considering the size-effect into account in the numerical simulations helped in achieving more accurate prediction of fracture of the formed parts. The forming depths predicted using the size-effect incorporated numerical model was more close to the experimental results observed for both the toolpaths at all wall angles. A significant decrease in error of 12-15 % was observed between the simulation and experimental results after incorporating the size-effect in the model. Further, the foils are assumed to be isotropic in simulations, however, in actual practice, the foils are anisotropic in nature. Fine mesh will give better results, though the computation cost in terms of simulation time increases in that case. The simulations can be improved by implementing the anisotropic yield criteria like Hill's yield criteria into the simulations which will require the development of an explicit integration scheme in conjunction with subroutines like UMAT/VUMAT for material modelling with size-effect [170,171].

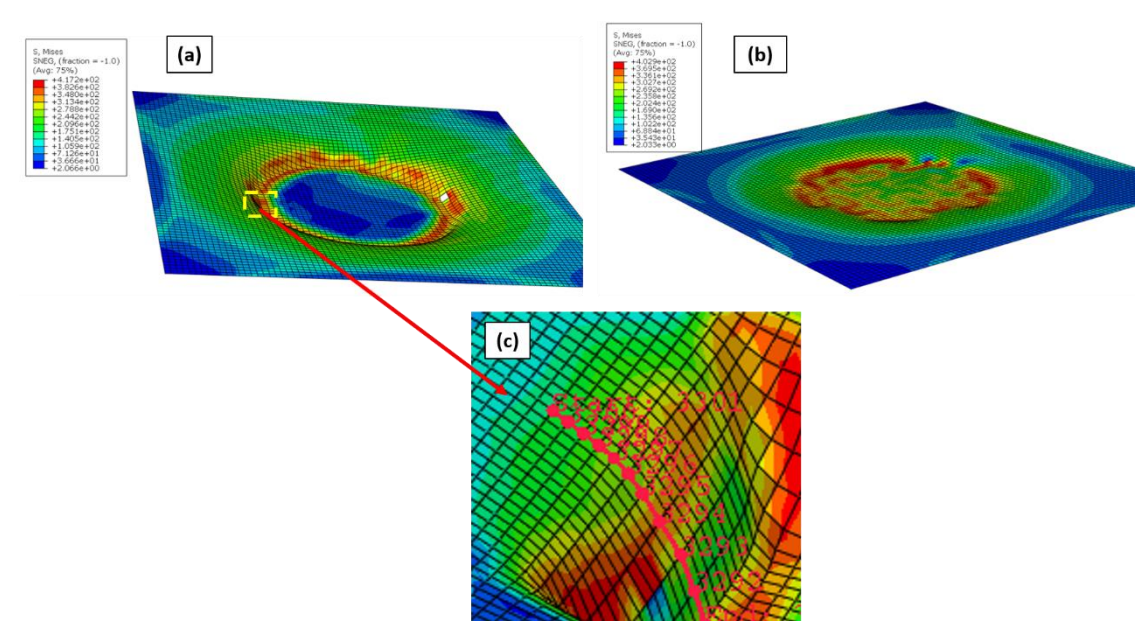


Fig. 4.11: (a) FEA showing the von Mises stresses for (a) Spiral and (b) FGBIT (c) Path traced to measure the stress variation along the x-direction

4.3.2 von Mises stress distribution

The size-effect incorporated numerical simulations were performed to study the von Mises stresses developed during the µISF process. The stresses distribution were measured with the x-displacement direction for all formed geometries for FGBIT and traditional spiral toolpath as shown in Fig. 4.11. It was found that the von Mises stresses are lower in magnitude and more uniformly distributed in FGBIT than the spiral toolpath for varying wall angles of the formed geometry. In FGBIT, the deformation stresses are distributed over the entire profile of the formed part. Whereas, in a spiral toolpath, there is no interaction of forming tool with the sheet face at the flat base regions. This results in the localization of deformation in the wall regions only. FGBIT basically helps in eliminating the rigid body translation of the foil surface [167]. Due to such deformation nature with FGBIT, the effective stress requirement for plastic deformation is low with less strain hardening of the components. The results clearly show better effective stress distribution in the case of FGBIT when compared with traditional toolpath as shown in Fig. 4.12(a,b,c). Though the nature of the deformation remains the same in both cases, however, this uniform stress distribution in FGBIT also helps in increasing the formability of the micro-cups.

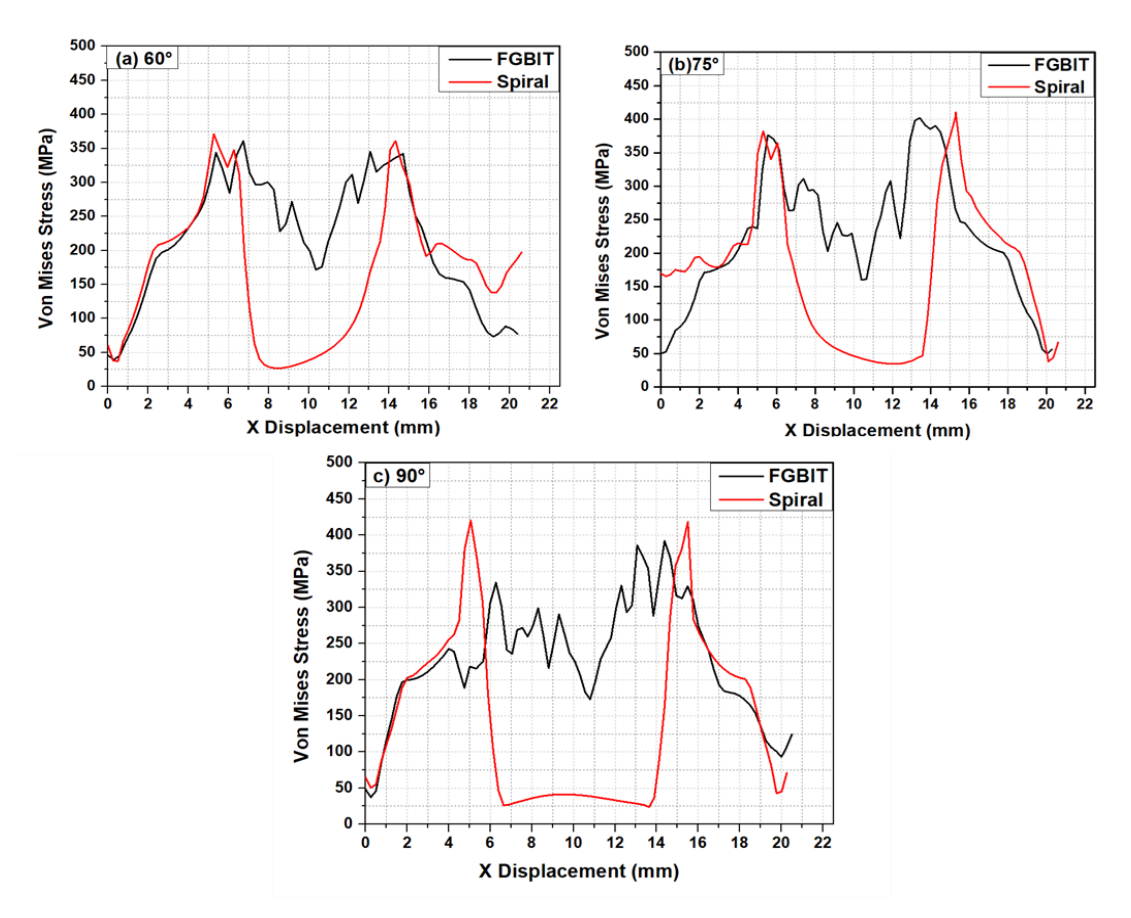


Fig. 4.12: Comparison of stress distribution using the FGBIT and spiral toolpath with different wall angles (a) 60° (b) 75° (c) 90°

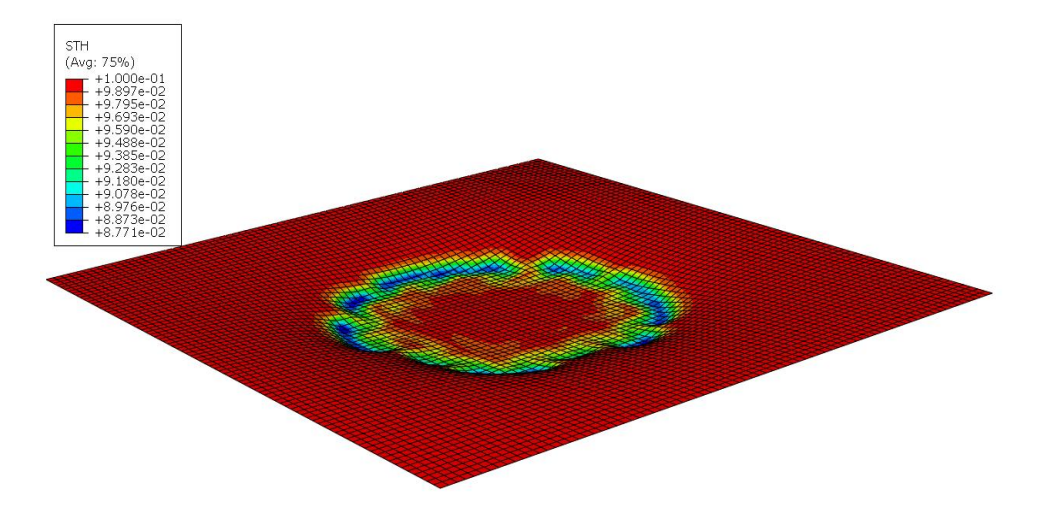


Fig. 4.13: FEA showing the sheet thickness distribution of the formed part

4.3.3 Thickness distribution

The thickness measurement location for simulated FGBIT and spiral toolpath are the same as shown in Fig. 4.11(c) and the simulated sheet thickness distribution of the

formed part is shown in Fig. 4.13. The FEA results for the FGBIT and spiral strategy show comparatively less difference in the rate of foil thinning at the location of fracture of the component. This result is attributed to the change in forming wall angles from 60° to 75° during the deformation stage (Fig. 4.14(a,b)). This deformation behavior is very much dependent on the tool sheet interaction. When the wall angle is shifted to 90°, a significant increase in the thinning rate of the foil was observed for FGBIT due to more increments in tool movement over the whole region of the deformed shape as seen in Fig. 4.14(c). Therefore, the thickness reduction rate is more uniform for FGBIT compared to the conventional spiral toolpath. This also helped in increasing the forming depth of the micro-parts, especially at higher wall angles as already discussed in Fig. 4.10. More uniform thickness distribution can be achieved by reducing the bridge length of FGBIT by increasing the order of FGBIT. However, that will further increase the forming time, which is already a limitation of this toolpath for effective application.

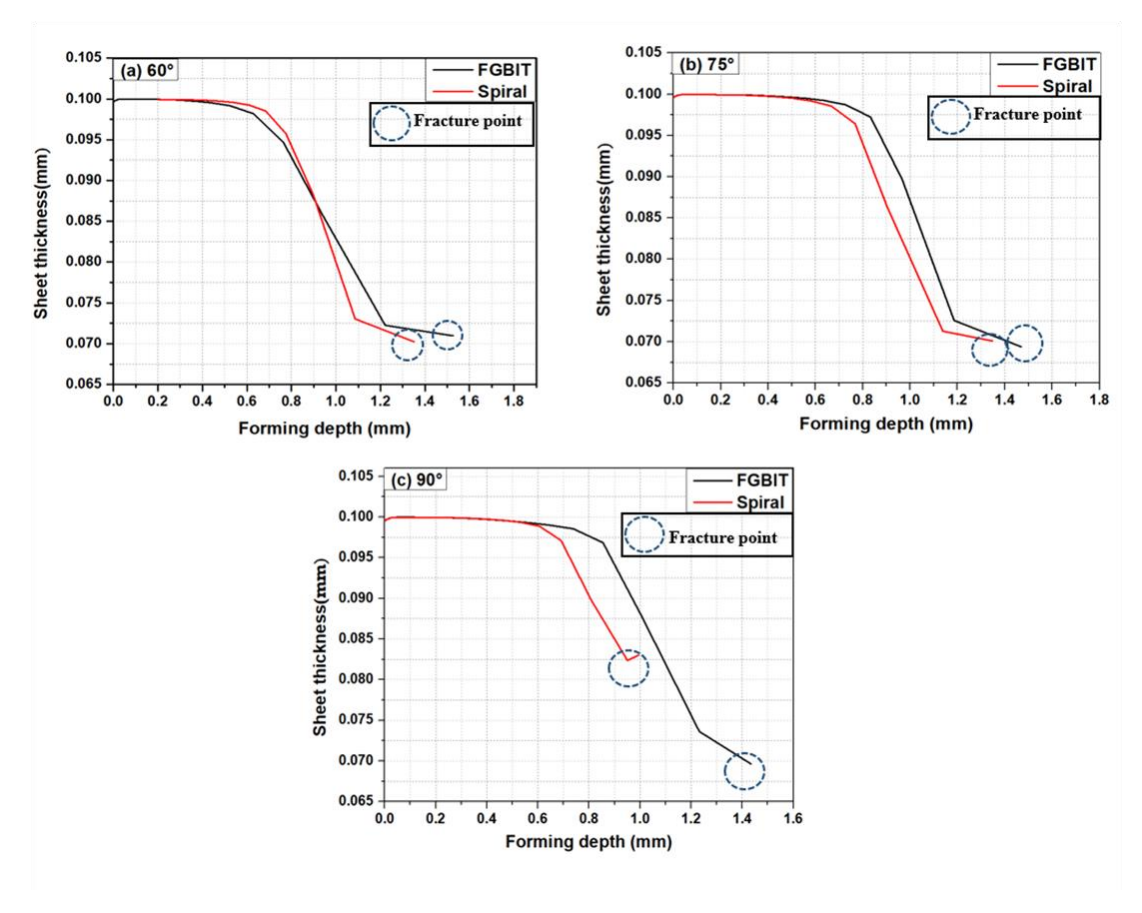


Fig. 4.14: Comparison of thickness distribution with forming depth using the FGBIT and spiral toolpath with different wall angles (a) 60° (b) 75° (c) 90°

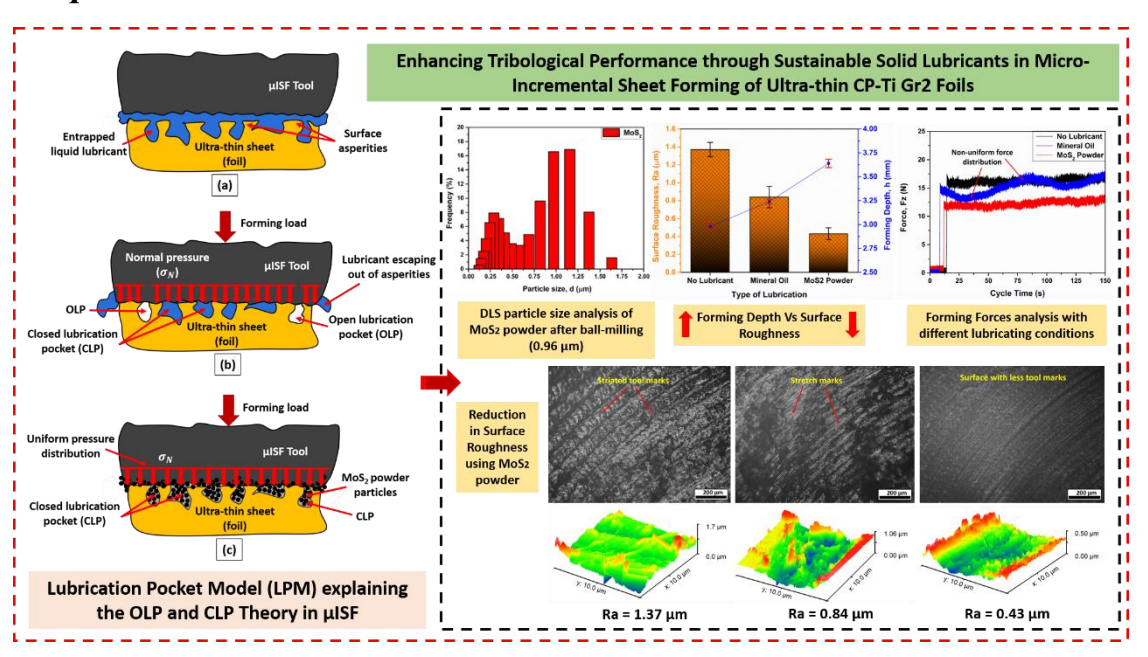
4.4 Summary

Material behavior is significantly different in the micro-forming process with the decrease in dimensions. In this chapter, a numerical model is developed by incorporating the phenomenon of size-effects in the micro-scale deformation of the µISF process. Using the theory of surface layer model, a mixed material model, containing the sizedependent parameters (grain size, thickness etc.) is proposed and used in the FE analysis to study the flow stress behavior of the material. The developed FEA model was successful in predicting the deformation behavior at micro-scale by accurately predicting the flow stress behavior and failure of the micro-parts as compared to the experimental results. A significant decrease in error by 12-15 % of forming depth was observed between the simulation and experimental results after incorporating the sizeeffect in the material model in ABAQUS®. The formability of CP-Ti Gr2 foil is evaluated and compared by forming the conical cups with two different toolpaths. Conventional spiral and FGBIT is an attempt to improve the formability, stress, and thickness distribution of the micro-parts, which are major limitations in the µISF process. The von Mises stresses were found to be lower in magnitude and more uniformly distributed in FGBIT than the spiral toolpath. From the numerical and experimental investigations, it was observed that FGBIT provides better formability for all varying wall angles. Through FGBIT, the fabrication of vertical-shaped parts can be targeted in µISF. Addressing the limitations of uniform stress and geometrical thickness distribution, FGBIT demonstrates superior formability, making it most suitable for the customized production of miniature parts made of ultra-thin foils.

Chapter 5

Enhancing Tribological Performance in Micro-incremental Sheet Forming

Graphical Abstract³



5.1 Introduction

In metal-forming operations, adopting sustainable manufacturing and optimum practices can help minimize the energy requirement during the deformation process [172]. For the fabrication of products made of ultra-thin Titanium foils, micro-forming can be a suitable and economical process for small-scale productions. The schematic representation of the µISF process is shown in Fig. 5.1. The aesthetic appearance of a product is significantly affected by the surface roughness of the geometry, which also impacts the performance and duty life [173]. Lubricants are widely employed in industrial and mechanical systems to reduce the friction and wear rate of the moving parts. Therefore, choosing a suitable lubricant can be useful in metal-forming operations [174,175], which can withstand high-temperature deformation, improve surface roughness, and do not pose any hazardous effect on the environment [176].

³Pal, M., Agrawal, A., and Nirala, C. K., "A Size-effect driven Strategy to Improve Tribological Performance in Sustainable Micro-Incremental Forming of Titanium Foils with Solid Lubricants," (Under Review)

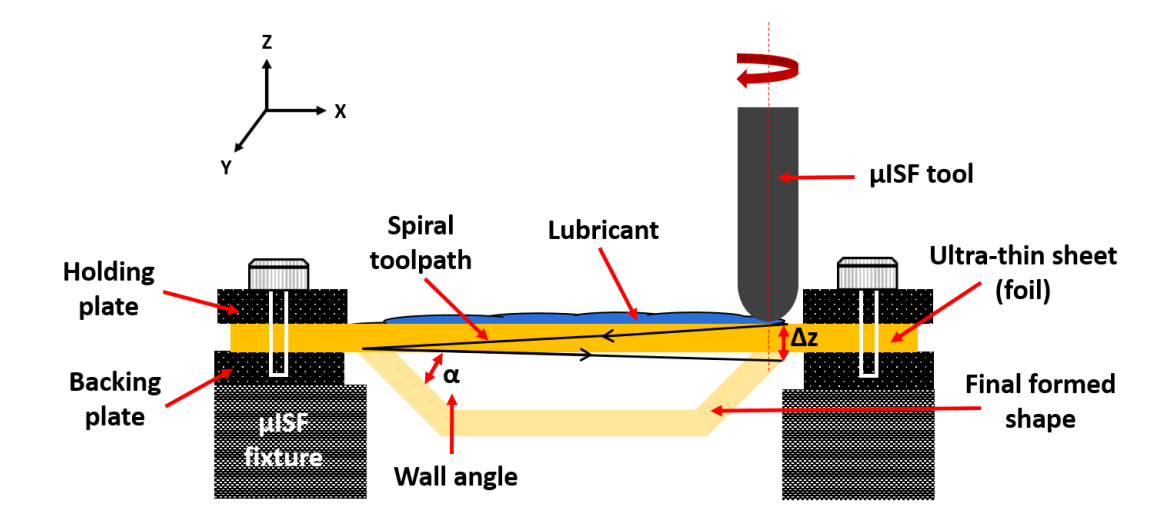


Fig. 5.1: Schematic representation of the μ ISF process

With miniaturization, the tribological conditions between the tool and the workpiece change drastically due to the size-effect, leading to higher friction and poor surface finish [90]. The frictional size-effect was studied by Vollertsen [5] and Geiger et al. [6] in sheet metal operations. Due to the high surface-to-volume ratio of the micro-parts, friction significantly affects the surface topography of the formed components. Therefore, a suitable lubrication can be effective in reducing the surface friction and enhancing the surface quality in micro-forming applications. The transfer of the load/ force on the sheet surface during the forming process was discussed by Engel [85]. The research focused on studying the individual contacts of the surface asperities of the contact region through the closed and open lubrication pocket (CLP and OLP) models, as illustrated in Fig. 5.2. The pocket theories describe how different types of lubricants can become trapped in the asperities of the tool-sheet interface and improve the surface properties [177]. The schematic demonstration in Fig. 5.2 explains the initial and final material deformation stages in the µISF process using liquid and solid lubricants.

Liquid lubricants like oils and grease are used in several applications in food processing, machinery, and textile industries. However, the usage of these lubricants may cause health and environmental related problems, when used for longer periods [178,179]. For sheet-forming operations, viscous liquid lubricants may not get retained inside the small asperities when the deformation load is applied for larger cycles. In such cases, sustainable solid lubricants like Molybdenum disulfide (MoS₂), Graphite, etc. can provide better anti-wear and load-bearing capacity than liquid lubricants to generate parts with good surface finish. MoS₂ is used as a dry lubricant and does not require a

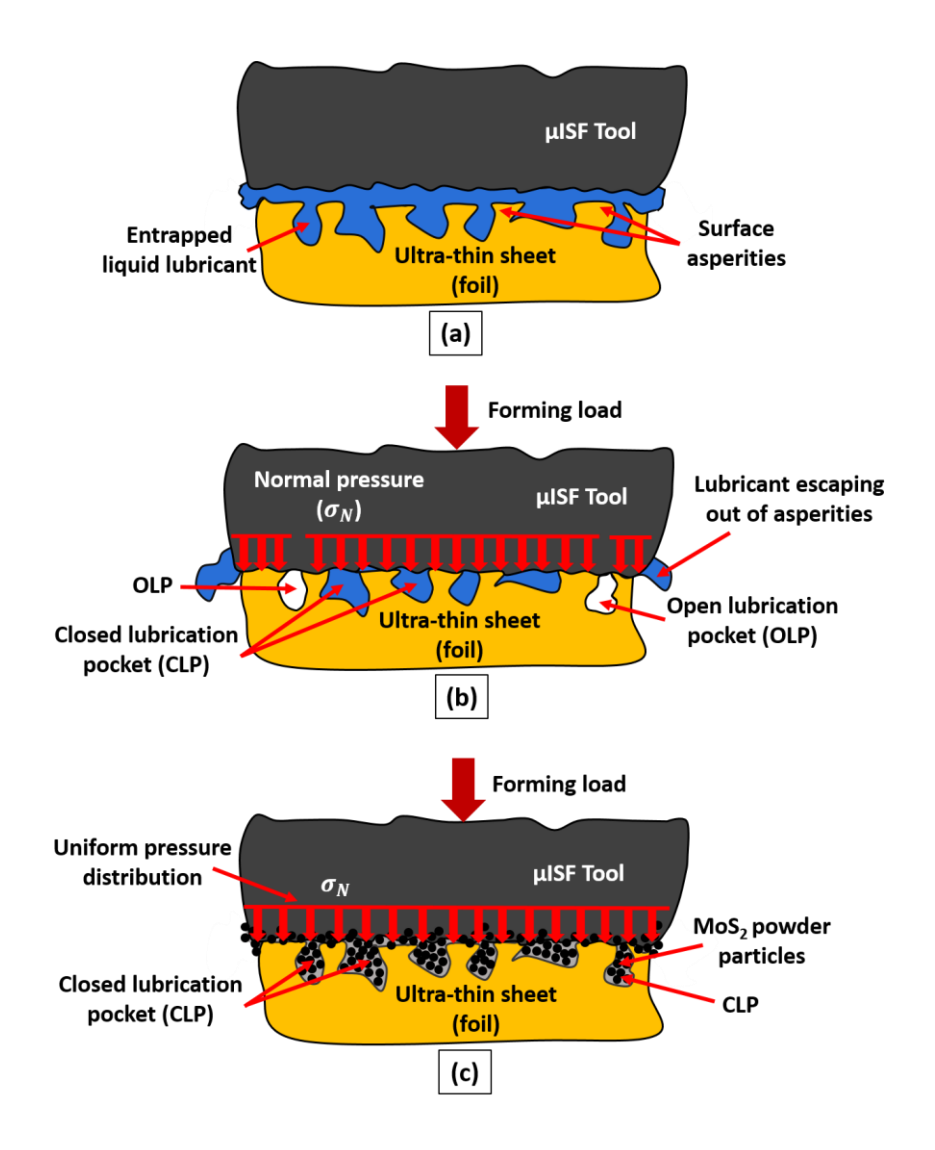


Fig. 5.2: CLP and OLP theory during micro-scale deformation (a) before deformation (b) deformation using liquid lubricant (Oil) (c) deformation using solid lubricant (dry MoS₂ powder)

humid environment for surface lubrication. It also has a remarkable ability to perform in high-temperature and vacuum conditions, which makes it an attractive lubricant for space/ aircraft applications [180,181]. Fan et al. [182] used MoS₂ powder as a self-lubricating coating material for the hot ISF of the Ti-6Al-4V sheet. The results showed improved surface quality and retention of the coated material without oxidation of the Ti-6Al-4V. In another study, Zhang et al. [183] carried out warm ISF of AZ31 alloy with organic binders and MoS₂ powder-coated surfaces as lubricants, which displayed improved lubrication effects at elevated temperatures. Hussain et al. [184] also suggested that a surface-coated lubrication method can enhance the surface finish and formability of the Titanium sheet in the ISF process. Jawale et al. [185] studied the changes in microstructural behavior using different types of surface lubricants during

the deformation of Copper sheets. The surface roughness values were measured at the top and bottom regions of the formed geometries to correlate with the forming depth.

It is observed that limited studies are available on the surface lubrication of ultra-thin foils in micro-forming operations. Thus, the present work investigates the effect of solid and liquid lubricants on the surface quality of the formed micro-parts. A novel approach is suggested to study the frictional size-effect through closed and open lubrication pocket models (LPM) in the μISF process. The model theory correlates the particle size of the synthesized MoS₂ powder with the size of micro-tribological pockets and contacts of the surface asperities. The MoS₂ particles can remain embedded in the micro-pores of the surface for a longer duration and provide a continuous source of lubrication with less contact pressure during the micro-forming process. The presented investigation establishes MoS₂ as an effective lubricant than mineral oil in the μISF process to improve the surface finish of the micro-parts with minimum energy utilization.

5.2 Work methodology

This section discusses the materials, auxiliary equipment, and synthesizing techniques required for the µISF process. It also presents the experimental details and process parameters used in the micro-forming of CP-Ti-Gr2 foils.

5.2.1 Materials

Ultra-thin commercially pure Titanium Grade 2 (CP-Ti-Gr2) foils of 100 μm thickness were used to perform the μISF experiments. Titanium and its alloys are widely used for aerospace, defence, automobile, and biomedical applications due to its lightweight, high specific strength, and biocompatible nature [142,186]. To investigate the lubrication effect of the received cold-rolled CP-Ti-Gr2 foil, a metallurgical examination was performed to study the grain microstructure and surface properties. Several pieces of 10 mm x 10 mm dimension were cut from the foil, according to the rolling and transverse directional (RD-TD) plane. The cut-out specimens were hot-mounted on a flat epoxy resin platform and consecutively polished using SiC-coated emery papers of different grit sizes (coarser to fine). Later, the surface was cleaned with ethanol and further polished on a velvet cloth with a 40 μm colloidal alumina solution. To reveal the grain boundaries, the surface was swab-etched for 15 seconds with a Kroll's reagent (3 ml HF, 6 ml HNO₃, and 92 ml distilled water). A clear image of the grain microstructure of

the specimen can be observed in Fig. 5.3(a), which was captured through an optical microscope (Leica DM4-M). Five different regions of the surface were scanned to measure the grain size of the obtained microstructure. An average grain size (d) of 24.65 \pm 0.39 μm was observed using the ASTM E112 linear-intercept method. Energy dispersive spectroscopy (EDS) was also employed to confirm the chemical composition of the received foil. The elemental map of the detected constituents is shown in Fig. 5.3(b). A field emission scanning electron microscopy (FESEM- Jeol, JSM-7610FPlus) was carried out to study the surface characteristics of the received foil. The FESEM microscopic images shown in Fig. 5.3(c) display a cluster of micro-pockets or pores present on the foil surface. Several areas were scanned to calculate the average size of the micro-pores. The magnified view at 200x shows the region covered by the micropores, having an average dimension of approximately $19.57 \pm 1.16~\mu m$, which is of less size compared to the grain microstructure size. For the lubrication purpose, mineral oil and MoS2 powder were used during the μ ISF experiments.

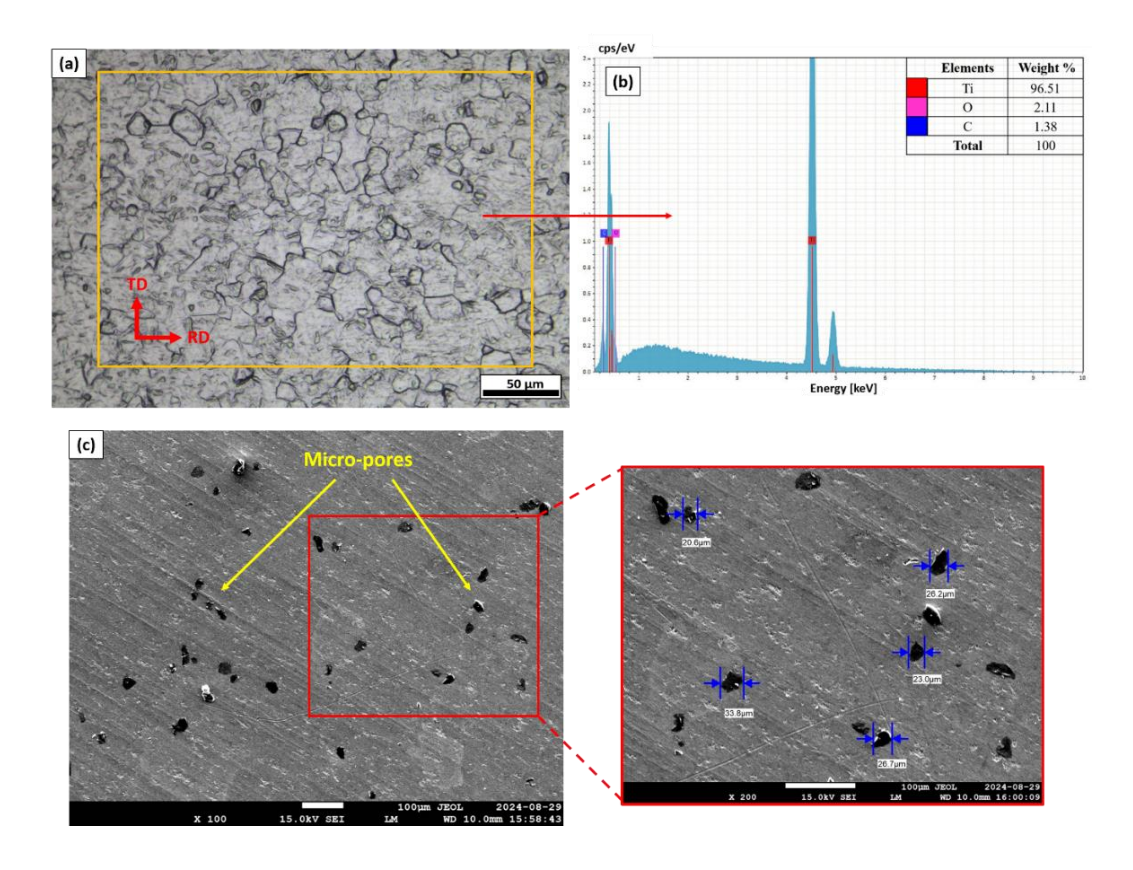


Fig. 5.3: (a,b) Microstructure and EDS of the received CP-Ti-Gr2 foil (c) FESEM micrograph showing the dimension of micro-pores on the foil surface

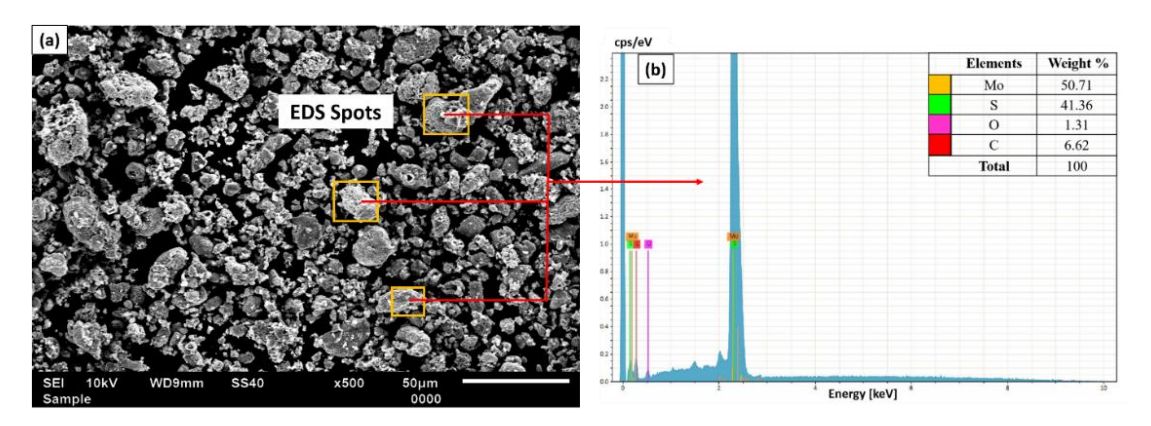


Fig. 5.4: (a,b) FESEM and EDS of the received MoS₂ powder

5.2.2 Planetary ball mill: Synthesis of MoS₂ powder

Liquid and solid lubricants were used for lubrication purposes during the µISF experiments. MoS₂ powder as a solid lubricant was selected for the surface lubrication. The characterization of particle size and elemental composition of the received MoS₂ powder was carried out through FESEM and EDS. The metallurgical results of the analysis are presented in Fig. 5.4(a,b)). It was observed that the average particle size of the initially received MoS₂ powder was comparatively similar i.e. $18.78 \pm 0.24 \mu m$ in comparison with the size of the micro-pockets (19.57 \pm 1.16 μ m) observed on the foil surface, containing the asperities with an average surface roughness of 1.07 µm. Therefore, for effective lubrication of the contact surface and uniform pressure distribution during deformation, the powder particles must stay entrapped between the asperities and micro-pockets of the surface for longer durations as illustrated in Fig 5.2. To counter the escaping out of the MoS₂ particles during the μISF process, the size of the powder particles was significantly reduced, homogenized, and synthesized using the ball-milling process. A planetary ball-mill (FRITSCH Pulverisette-7) was used to perform the dry ball-milling at a speed of 250 RPM in two tungsten carbide (WC) vials containing 5 mm WC balls as shown in Fig. 5.5(a). The weight-to-powder ratio of the balls was kept constant at 10:1. The ball-milling time was optimized by experimenting for 5 time periods (5 hr, 10 hr, 15 hr, 20 hr, and 25 hr). The required size of the MoS₂ particles was achieved after 20 hrs of ball-miling. For longer durations, say 25 hrs and above, agglomeration of the powder particles was observed, and so it was discarded for further ball-mill. The grain size of the synthesized MoS₂ powder was measured through a particle size analyzer (Microtrac, Nanotrac Flex), which works on the principle of dynamic light scattering (DLS) method. The DLS bar graph in Fig. 5.5(b) displays the

spectrum of the particle size obtained from the analysis. A 94.88 % reduction in the average particle size of 0.96 ± 0.05 µm was observed for the synthesized MoS₂ powder. The particle size can be confirmed through the FESEM micro-graphs taken after the ball-milling process as presented in Fig. 5.5(c). It can be seen that the MoS₂ particle sizes are very small compared to the size of the micro-asperities.

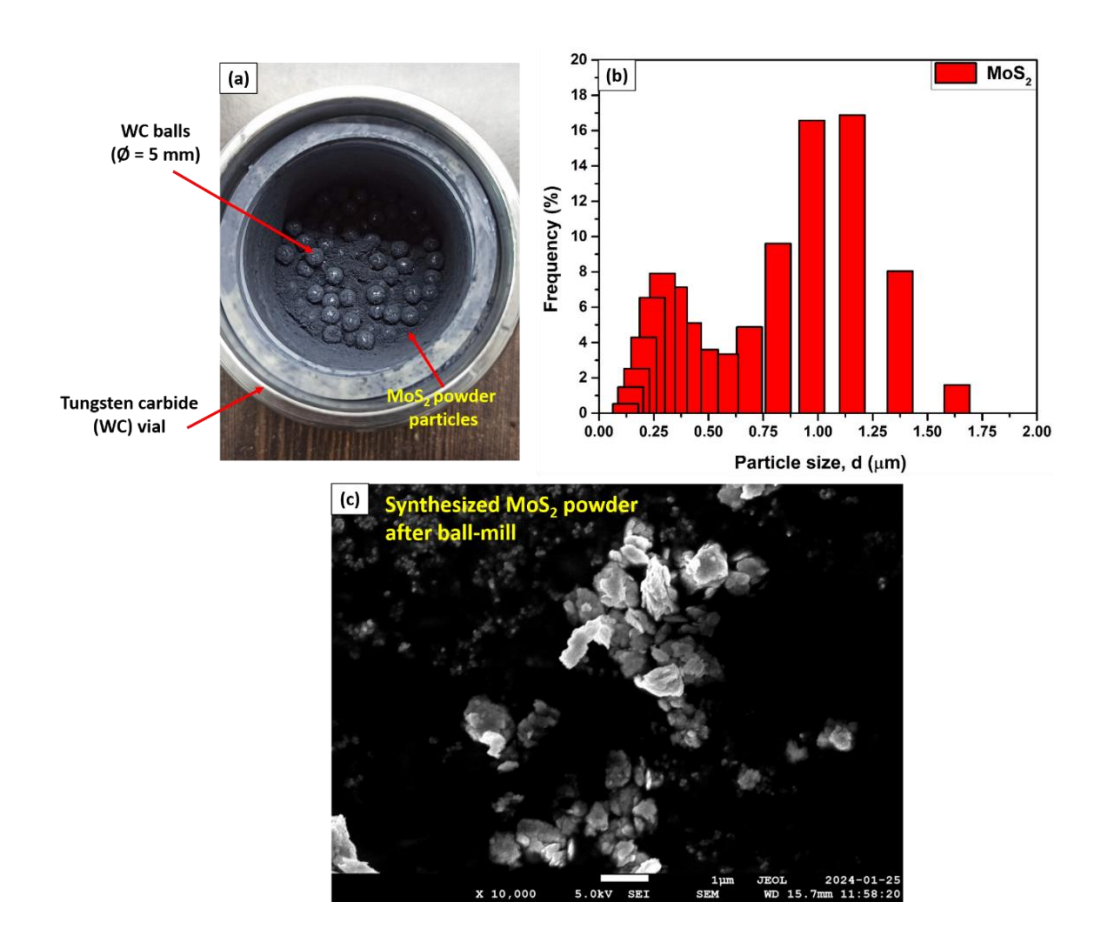


Fig. 5.5: (a) Ball mill vial containing the MoS₂ powder (b) DLS analysis for MoS₂ particle size measurement (c) FESEM micrograph showing the reduced particle size of the synthesized MoS₂ powder

5.2.3 Experimental details

The µISF experiments were executed on a numerically controlled high-precision multi-axis hybrid-µEDM machine (Mikrotools Ltd., DT-110i). A spiral based toolpath was used to form a conical curvilinear-shaped micro-part as shown in Fig. 5.6(a). The experimental set-up of the µISF process is illustrated in Fig. 5.6(b). Mineral oil and MoS₂ powder were the two types of lubricants used during the µISF experiments. The process parameters were selected and optimized based on the experimental results

obtained through initial trials. Therefore, all the geometries were formed with a step depth of 50 μ m (Δz) having a variable wall angle ($\theta = 25^{\circ}$ -80°). The tool was given a constant feed (f) of 50 mm/min and a clockwise rotational speed (s) of 500 RPM [187]. The full details of the experimental plan and process parameters are discussed in Table 5.1.

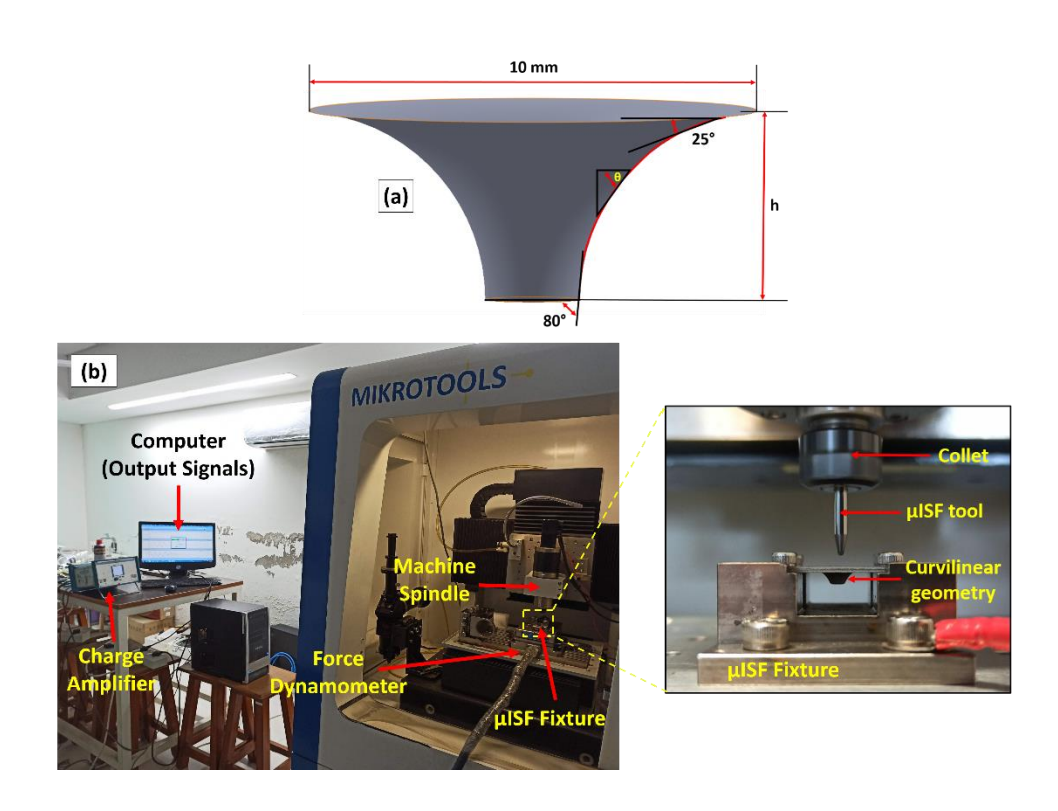


Fig. 5.6: (a) Conical curvilinear-shaped profile (b) µISF experimental set-up

Table 5.1: Experimental conditions and input process parameters

μISF Process parameters	Values		
Foil material, thickness (t)	CP-Ti-Gr2, 100 μm		
Tool material, diameter (φ)	Tungsten carbide (WC), 1 mm		
Step depth (Δz)	50 μm		
Wall angle (θ)	25°- 80°		
Rotational speed (s)	500 RPM		
Feed rate (f)	50 mm/min		
Toolpath	Spiral		
Lubrication conditions (LC)	No lubricant, Mineral oil, MoS ₂		
	powder		

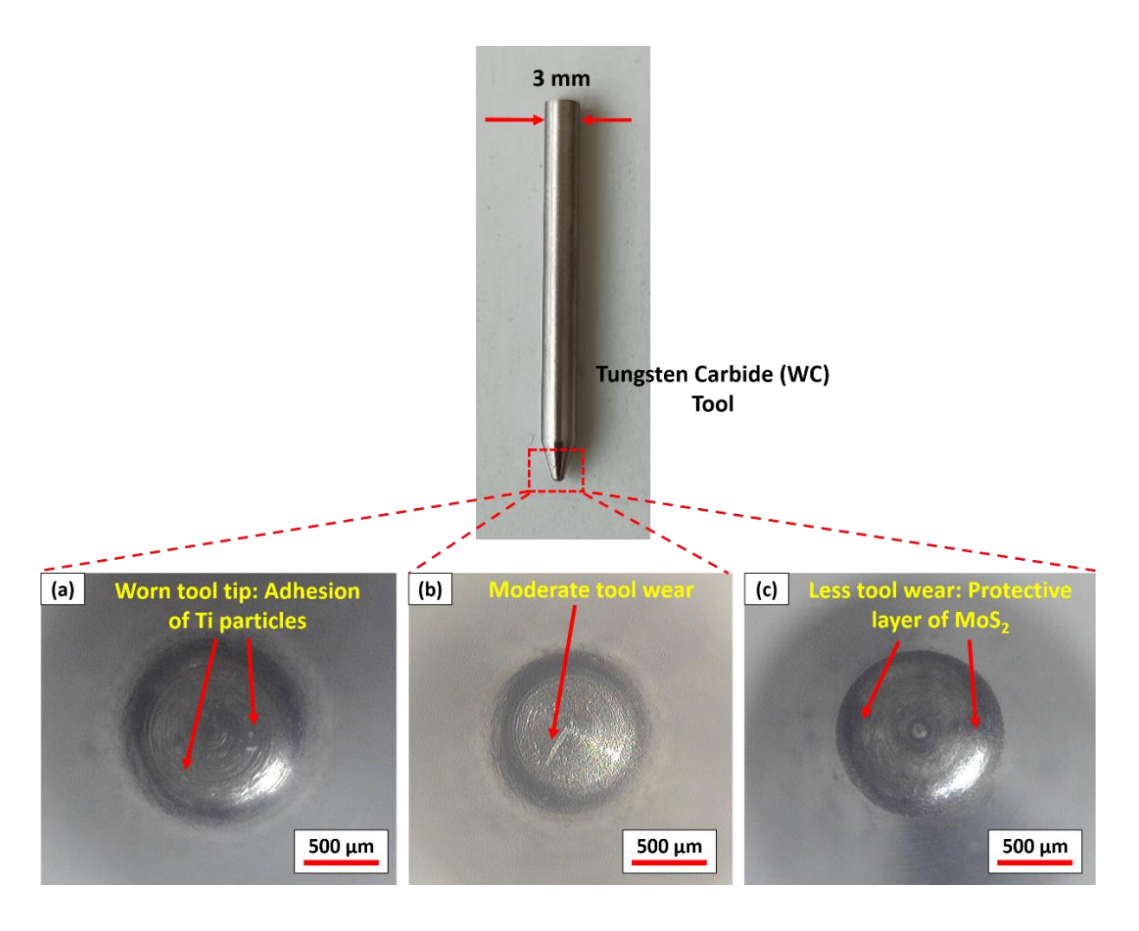


Fig. 5.7: Microscopic image of the tool tip after μISF with different lubrication conditions (a) No lubricant (b) Mineral oil (c) MoS₂ powder

5.3 Results and discussion

This section presents the comparison of tool wear and a discussion regarding the surface quality of the formed micro-parts with different lubrication conditions. It also discusses the effect of lubrication on the formability, grain microstructure and evolution of forming forces during the μ ISF experiments.

5.3.1 Tool wear

The wear of the tool is much more noticeable in classical and macro-scale forming operations. However, in the μ ISF process, the tool usually requires good rigidity and hardness of the tool-tip to reduce the surface friction and distortion of the formed micro-part. To examine the surface profile of the tool, discretely different tools were used for the experiments for different lubricating conditions. The magnified microscopic image of the tool-tips are shown in Fig. 5.7, taken just after the experiments. A clear indication and difference in the surface quality of the tool can be observed when the lubrication

conditions are altered. In the absence of lubrication, a worn-out tool tip can be seen with small particles of Titanium adhered to the tool surface as shown in Fig. 5.7(a). This designates that significant chipping of the workpiece has occurred due to the lack of lubrication and an increase in friction at the tool-foil interface, resulting in the deterioration of the formed surface. The problem of adhesion of the workpiece material can be minimized by using necessary lubrication during the forming process. In the second case, the foil was formed using mineral oil as a lubricating agent. The lubrication was provided to fill out the micro-pores or asperities present on the foil surface and maintain a reasonable contact pressure between the tool and the foil surface. However, moderate tool wear was observed compared to the first case with a decrease in the frictional effect (Fig. 5.7(b)). No surface chips were observed during the experiment. The SEM micrograph of the tool is shown in Fig. 5.8(a), and the wear of the tool can be observed on the surface for the first two cases. Interestingly, when the synthesized MoS₂ powder was used as surface lubrication, a protection layer or covering of the powder particles was seen on the surface of the tool tip, which is shown in Fig. 5.7(c). The presence of MoS₂ particles prevents the excessive wear-out of the tool by providing a lubricating layer that reduces the direct contact between asperities on the surfaces. The powder particles help provide a low-friction between the sliding surfaces and reduce the affinity of the surfaces to adhere to each other. This results in less deterioration of the tool surface and withstands a proper lubricating effect during the entire experiment. A clear micro-graph of the MoS₂ lubricated tool-tip is shown in the SEM image in Fig. 5.8(b), where the protective layer/ coating of the MoS₂ powder can be observed with less wear of the tool surface captured after the µISF experiments.

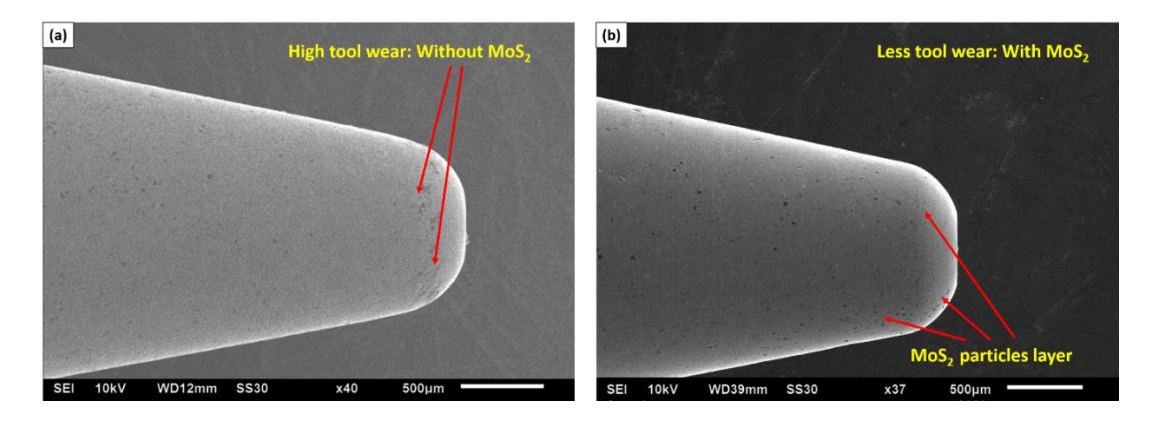


Fig. 5.8: SEM micrographs of the tool wear (a) Without MoS₂ powder (b) With MoS₂ powder

5.3.2 Surface finish and contact pressure

The surface quality of the formed product is primarily important in the fabrication of miniaturized parts. The characterization of the deformed surface was carried out through an optical microscope and the surface roughness (R_a) was measured by using an Atomic force microscopy (AFM, Bruker Multimode 8-HR) process. The process uses a small cantilever (length = $125 \mu m$, width = $40 \mu m$, stiffness = 40 N/m) with a sharp tip at its end to measure the roughness of the surface. The scanner with tip moves and scans, along the x, y, and z directions, with high precision to calculate the Ra value. Five scanning areas of 100 µm² were selected for each specimen to determine the average Ra. The surface analyses was carried out in the RD-TD plane of the specimen (deformation region), measured in both directions as shown in Fig. 5.9. The initial experiments were performed without the use of lubricants. With no lubrication pockets available between the asperities of the surface, results in the formation of striated tool marks on the internal region of the formed geometry. These marks can be observed in Fig. 5.9(a), which led to a high R_a value of 1.37 µm. The tool marks were prominent and an indicator of the material and tool adhesion, which caused high friction and roughness of the surface. Subsequently, to reduce the effect of friction and surface roughness, the geometries were formed with mineral oil and synthesized MoS₂ powder.

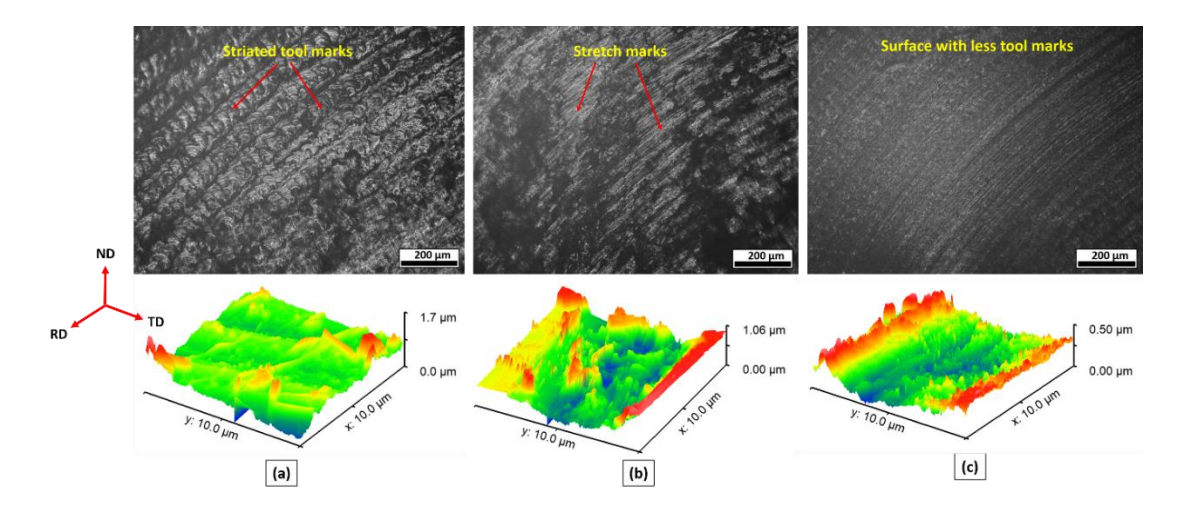


Fig. 5.9: Optical micrographs of the formed internal surface and AFM results with (a) No lubricant (b) Mineral oil (c) MoS₂ powder

The entrapment of the lubricants between the pores of the surface is necessary to minimize the coefficient of friction and surface roughness [6]. Considering the frictional size-effect in micro-scale deformation, liquid lubricants such as oils, and grease follow

the principle of open lubrication theory [85]. According to this theory, oils are most likely to form an OLP with the micro-asperities located on the edges of the surface. At the edges of the contact, the asperities/ pores are unable to avoid the escape out of the lubricants when a deformation load is applied on the sheet. On the other hand, the inner part of the contact forms a CLP and has the lubricant entrapped between the surface pores and the tool surface [4,87]. The phenomenon is very well explained through a schematic representation in Fig. 5.2(b). The theoretical distribution of the applied forming load (F_o) by the tool is described by Eqn. 5.1, where P_p and P_s are the pressure applied to the pores and the solid contact areas. A_o is the macroscopic cross-sectional area of the contact (5.2), where A_p is the area cross-section covered by the lubrication pockets and A_s is the sum of the solid or real contact area (Fig. 5.10(a)) [87].

$$F_o = P_o A_o = P_p A_p + P_s A_s$$
 $(A_s > A_p)$ (5.1)

$$A_o = A_p + A_s \tag{5.2}$$

$$P_p A_p = P_L A_L + P_{air} A_{air}$$
 (5.3)

$$F_1 = P_L A_L + P_{air} A_{air} + P_s A_s$$
 (5.4)

For homogeneous deformation of the surface, the distribution of the normal pressure/ contact pressure (σ_N/P_o) must be uniform to keep the lubrication mechanism intact. In the case of lubricant, such as mineral oil entrapped in the pocket asperities, some fraction of F_o will be transferred by the pressure of the oil (P_L), and the force share is given by P_L A_L. The other part share will be borne by the force exerted by the air (P_{air} A_{air}) due to the formation of both OLP and CLP contacts at the intersection region (5.3) and P_s A_s remains constant. The CLP's are formed by the entrapment of the oil in the surface asperities, whereas the OLP's are formed by the entrapment of the air molecules at the surface edges due to the outflow of the oil. Therefore, the total forming load gets changed to F₁ due to the uneven distribution of the contact pressure between the surface asperities of the foil (5.4). From the FESEM image in Fig. 5.3(c), it can be observed that the area fraction of solid contact is more than the fraction of pores $(A_s > A_p)$. As the deformation steps increase, more liquid (oil) from the pores will escape out due to this uneven contact pressure. This will lead to an increase in the number of open-pocket formations and the area fraction covered by the air (Aair). In such instances, the pressure born by the oil layer (P_L) will increase the overall contact pressure (decrease in A_L) and forming load (F₁), resulting in non-homogeneous deformation with an increase in

friction and surface roughness of the formed part. The quality of the surface obtained with the mineral oil is shown in Fig. 5.9(b). However, it has relatively less stretch and tool marks and improvement in the roughness, Ra of 0.84 μ m compared to the previous case (no lubrication).

$$F_2 = P_M A_M + P_s A_s (5.5)$$

Whereas, in a dry solid lubricant, MoS₂ particles follow an ultra-low friction regime and have low shear strength between the sliding layers of the contact surface [180]. The MoS₂ powder was reused for all the experiments to reduce material wastage and the cost of the fabrication process. The LPM theory states that the powder particles do not form an OLP's at the contact region of the surface. The particles can remain embedded in the micro-pores of the surface for a longer duration and provide a continuous source of lubrication. This leads to the formation of CLP's in the entire region of the deformation load with no escape out of the particles from the edges (Fig. 5.2(c)) [85]. Therefore, the forming load (F₂) distribution can be represented as the combination of pressure transferred to powder particles and solid surface $(P_M A_M + P_s A_s)$, where A_M is the crosssection covered by the lubrication pockets with MoS₂ powder (5.5). The smaller size of the MoS₂ powder particles (0.96 \pm 0.05 μ m) was effective in staying entrapped within the asperities and grain boundaries of the surface. The deformed surface containing the micro-pores filled with MoS₂ powder is shown in Fig. 5.10(b). With the formation of a lubricant-sealed environment with CLP, a low uniform contact pressure of the forming load is maintained over the entire contact surface during the forming process. The homogeneous deformation load bear by the powder particles and solid surface results in the flattening of the surface (less tool marks) and enhances the surface quality of the part as observed in Fig. 5.9(c). It was remarkable to observe that the roughness values were drastically reduced to 0.43 µm, which is lower than what was recorded while using liquid lubrication (oil). Table 5.2 shows the experimental results of the µISF process.

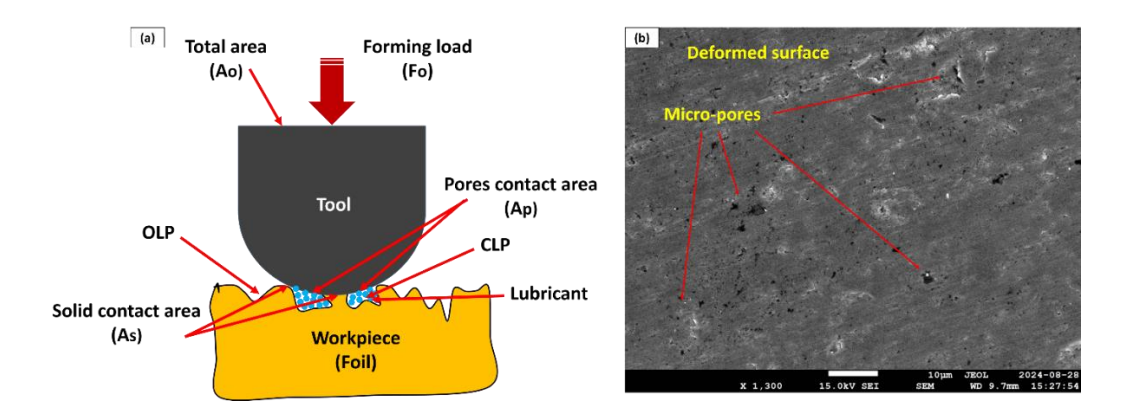


Fig. 5.10: (a) Schematic illustration of lubricant pocket theory (b) SEM micrograph of the deformed surface with micro-pores

Table 5.2: Experimental results of the μISF process

Lubrication	Lubricant	Average	Average	Maximum	Average
conditions	type	surface	forming	forming	grain size,
(LC)		roughness,	depth,	force,	d (µm)
		R _a (µm)	h (mm)	$F_z(N)$	
LC ₁	No lubricant	1.37	2.98	18.42	4.69 ± 0.25
LC_2	Mineral oil	0.84	3.27	17.98	5.98 ± 0.36
LC ₃	MoS_2	0.43	3.64	12.87	9.82 ± 1.14
	powder				

5.3.3 Forming depth

The effect of different lubricants on the tribological performance was investigated in terms of the formability of the formed micro-product. The formed component is shown in Fig. 5.11(a). The test was repeated thrice for each case to minimize the experimental uncertainty. With no lubrication, the obtained internal surface was rough and deteriorated with several micro-cracks. It was attributed to an increase in the frictional effects leading to surface deterioration and significant tool wear. This had a direct impact on the forming capability of the surface to undergo plastic deformation. The geometry with a lower average forming depth (h) of 2.98 mm was obtained due to the premature

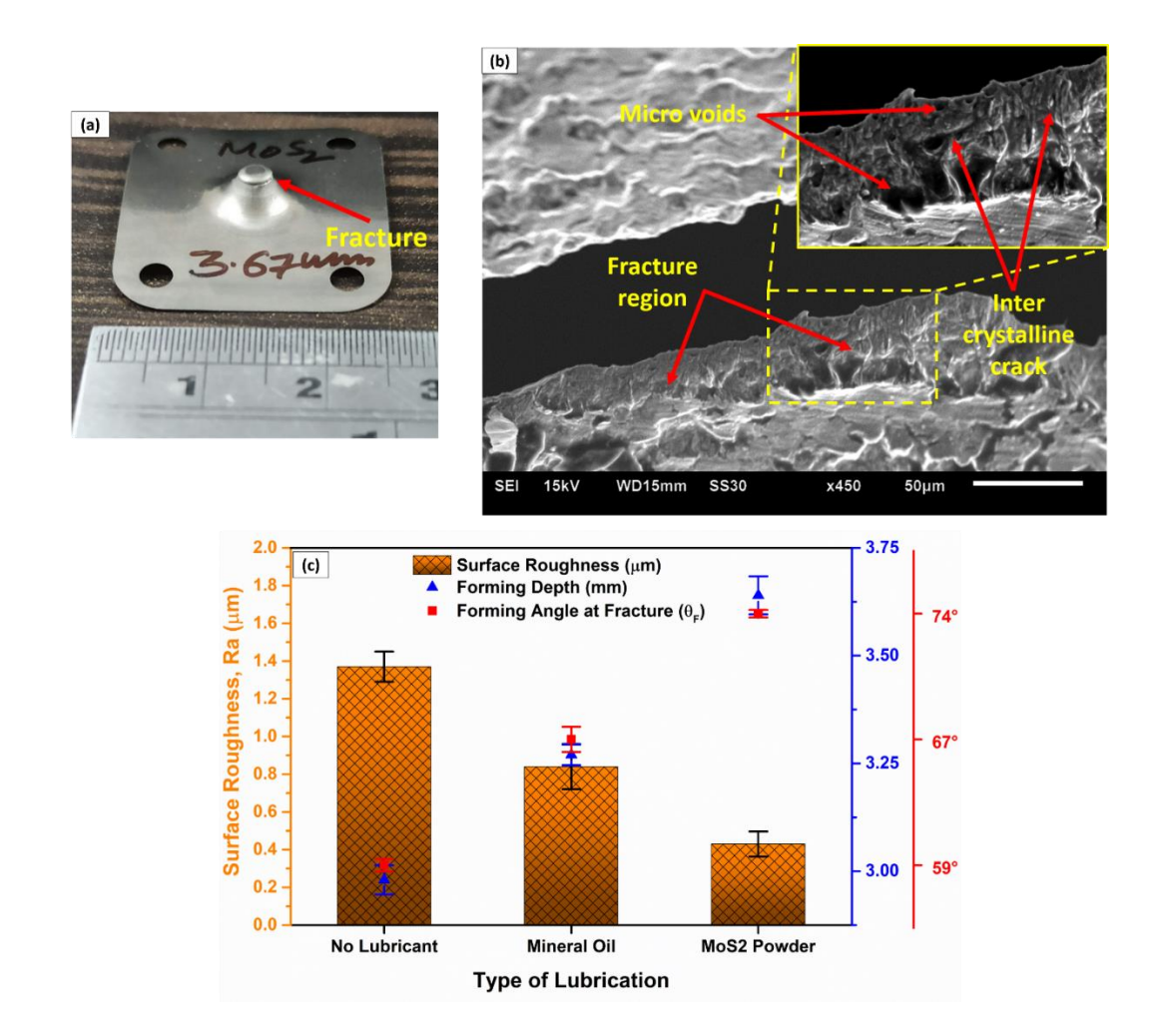


Fig. 5.11: (a) Formed micro-part (b) SEM cross-sectional image of the fracture region (c) Graphical analysis of surface roughness with forming depth and forming angle at fracture

fracture of the foil at the lower portion of the part ($\theta_f = 59^\circ$). The SEM image in Fig. 5.11(b) shows the cross-sectional view of the fracture region of the formed part. Several micro-voids can be observed with inter-crystalline cracks in the region, which led to the failure of the component. A slight improvement in the surface roughness was observed with the use of mineral oil filling the lubrication pockets. The enhancement of the surface quality delayed the formation of early cracks and increased the formability of the parts upto the height of 3.27 mm. The fracture of the part was observed at a forming angle of 67°. In contrast to the liquid lubricant, the MoS₂ powder showed better formability due to uniform pressure distribution and quality of the surface. The fracture of the part was observed at a higher average depth of 3.64 mm with an increase in forming angle (θ_f) of 74°. The tool wear rate was also improved with no chipping of the material surface. The graphical analysis of the surface roughness with the forming depth

and forming angle at fracture is shown in Fig. 5.11(c). A 22.14 % increase in the forming depth was witnessed with a 68.61 % decrease in the surface roughness when formed with the synthesized MoS₂ powder. It shows that the quality of the surface has a significant influence on the deformation ability of the material.

5.3.4 Grain microstructure

For the microstructural analysis, small samples were cut through the wire-µEDM process from the bottom portion of the deformed micro-parts. The internal region of the part that experienced the maximum deformation (near the crack region) was selected to measure the grain size of the deformed surface as observed in Fig. 5.12(a). The deformed surface was carefully polished and etched to capture the microstructure of the surface. Figure 5.12(b,c,d) shows the optical micro-graphs of the deformed surface, formed with different mediums of lubrication. It was observed that the grain sizes of the deformed foils were significantly reduced compared to the grain size of the received foil $(24.65 \pm 0.39 \,\mu\text{m})$. Several micro-cracks can be seen on the deformed region when no lubricant was used (pre-mature failure of the part), drastically reducing the average grain size to $4.69 \pm 0.25 \,\mu m$ as shown in Fig. 5.12(b). However, when the foils were formed with mineral oil and MoS₂ powder, patches of elongated grains were observed with the average grain size increased from $5.98 \pm 0.36 \,\mu m$ to $9.82 \pm 1.14 \,\mu m$ as presented in Fig. 5.12(c,d). This indicates a significant grain refinement of the foil after the forming process. The formation of new grain boundaries and the dissociation of grains into subgrains may have resulted from larger strains at the deformation zone. The elongated subgrains with the lubricants also correspond to an increase in the strain values of the deformed surface, which aided the increase in the achieved forming depth of the microparts as displayed in Table 5.2.

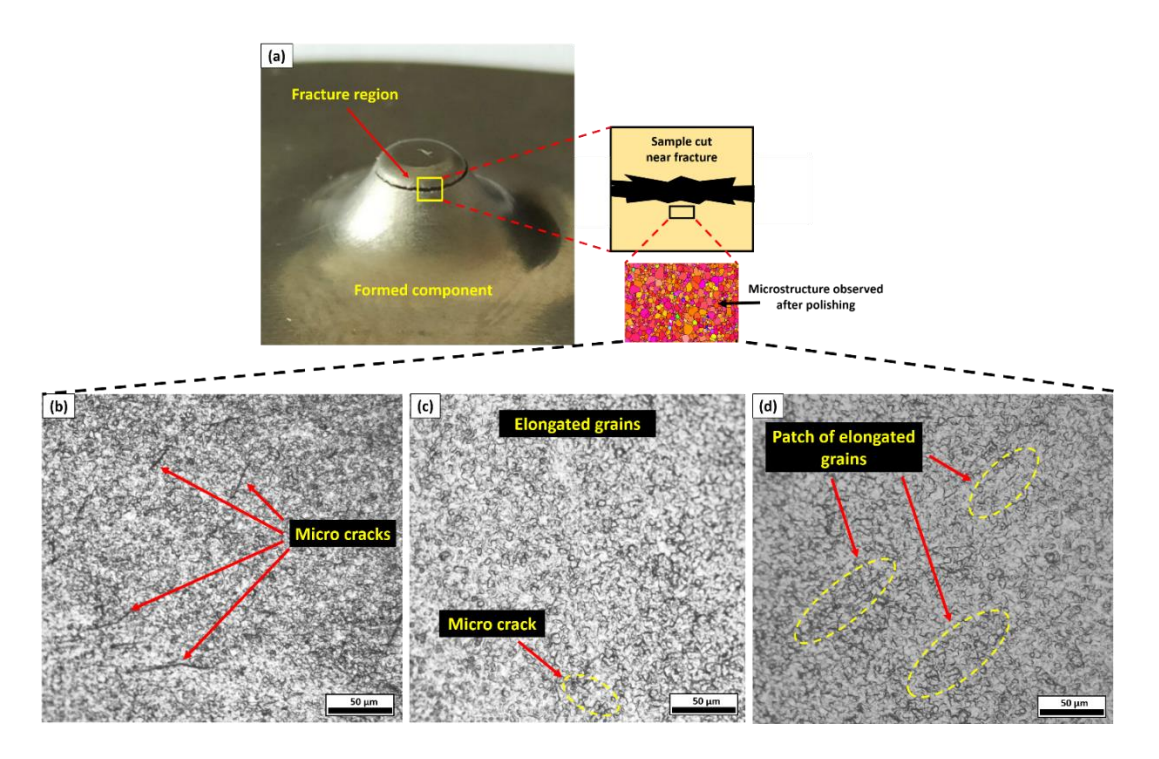


Fig. 5.12: Grain microstructure of the deformed foils with (a) No lubricant (b) Mineral oil (c) MoS₂ powder

5.3.5 Forming forces and deformation energy utilization

The proposed approach focuses on the reduction of process energy consumption by decreasing the amount of force/load requirement in the µISF process. For this purpose, a KISTLER® force dynamometer was used to monitor the evolution of the forming forces during the experiments. The forces were measured and recorded in a negative zdirection (F_z) of the applied load when the target micro-parts were formed with different lubricants as shown in Fig. 5.6(b). The forces along the x-axis and y-axis directions were neglected due to their low magnitude (~ 1-2 N). Since the forming parameters were kept constant for all experiments (spindle rpm, tool dia., etc.), the low torque generated at the contact surface was also ignored for the energy requirement. The results of the forming forces are presented in Fig. 5.13(a) and Table 5.2. A higher magnitude of the forces (Fz = 18.42 N) was observed when the foil was formed without the lubricant. From the force determination, the energy required for the µISF process can be obtained. Neglecting the energy components in the x-axis and y-axis directions, the energy (E_z) can be calculated by using the force value (F_z) and entity of the z-direction displacement [172]. An energy consumption of 54.89 mJ was observed in the first case as presented in Fig. 5.13(b). The results were attributed to an increase in friction force due to the lack of lubrication at the contact region of the tool-foil interface. The adherence of the material on the tool

surface and chip formation also might have induced a higher deformation load leading to larger energy utilization.

However, when the mineral oil was used as a lubricant, a slight decrease in the maximum magnitude of force was seen as 17.98 N. The formation of OLP's and CLP's by the oil with the surface asperities reduces the friction by bearing a part of the forming load applied by the tool. While, a non-uniform force distribution was observed due to changes in the magnitude of the forming loads and pressure of the lubrication pockets, resulting in cyclic instability during the forming process as depicted in Fig. 5.13(a). The energy requirement was also increased to 58.79 mJ due to the higher forces and forming depth. A substantial reduction of 30.13 % in the force value (F_z = 12.87 N) was observed when fine particles of MoS₂ powder were used in the lubrication process. The closed pockets developed by the powder particles with the entire asperities of the contact region helped in maintaining a uniform and lower friction/ deformation load (fluctuations) of the forming tool. This led to a low energy consumption of 46.84 mJ (14.65 % reduction) with the deformation load. The force results are in correlation with the obtained surface roughness and energy requirements in the fabrication of the micro-parts in the µISF process.

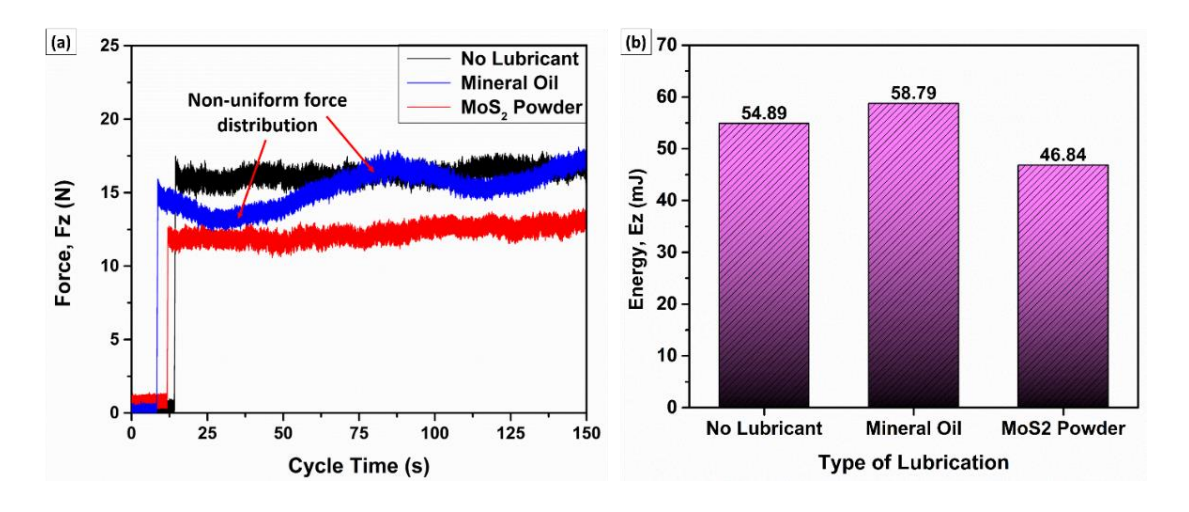


Fig. 5.13: (a) Comparison of the measured forces with different lubrication conditions (b) Energy utilization levels along the z-axis direction

5.4 Summary

The presented research highlights the use of environment-friendly MoS₂ powder as a potential lubricant to enhance the tribological performance of the fabricated micro-parts

with a reduction in energy consumption and waste generation. The smaller particle size formed a good correlation with the size of the micro-asperities/ pores (19.57 \pm 1.16 μm) present on the surface to achieve the necessary lubrication during the forming process. The MoS2 powder forms a protective layer on the tool surface and provides a low-friction regime between the sliding surfaces. It decreases the affinity of the surfaces to adhere to each other and reduces the wearing-out of the tool during the forming stage. A novel approach is suggested to study the frictional size-effect through closed and open lubrication pocket models (LPM) in the μISF process. Using MoS2 powder, the distribution of the forming load (F_{o}) of the tool was well-supported by the formation of CLP's over the entire tool-sheet interaction region leading to a 68.61 % reduction in the surface roughness (R_{a} = 0.43 μm) and a 22.14 % increase in the forming depth (h = 3.64 mm) with a 14.65 % reduction in the energy consumption (E_{z} = 46.84 mJ) during deformation.

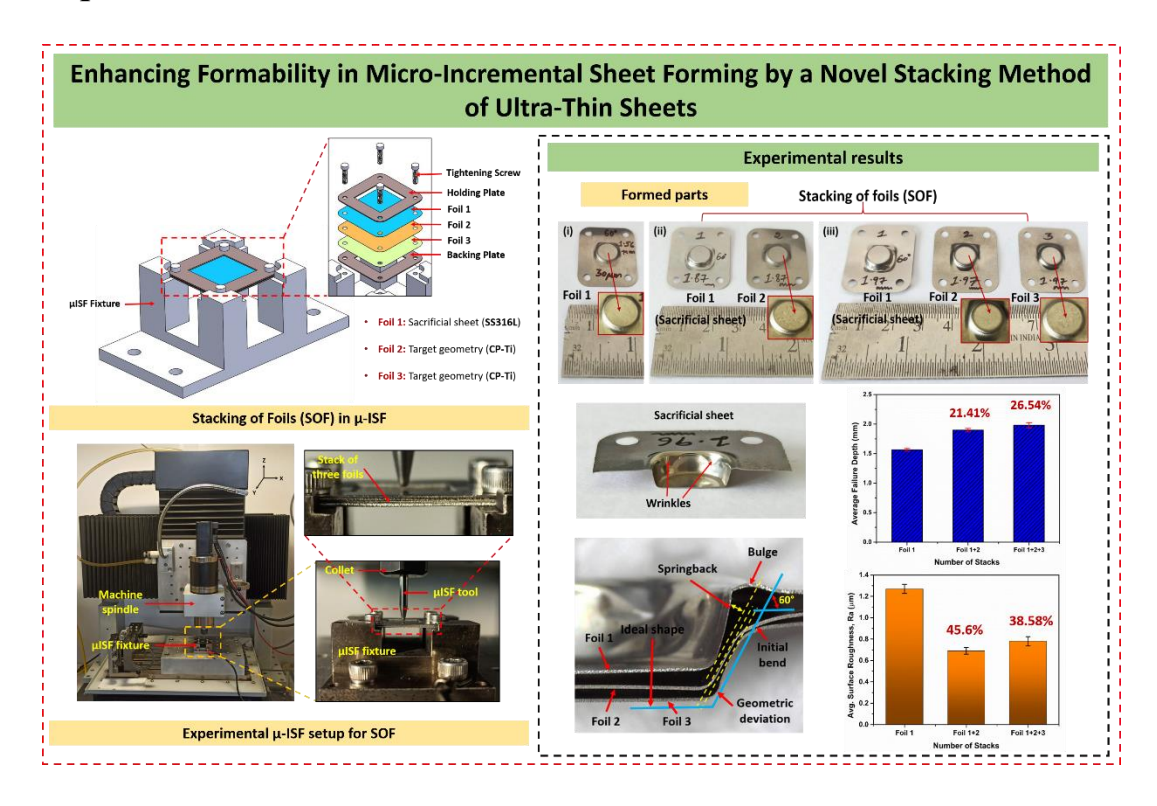
Chapter 6

Formability and Precision Improvement in µISF using Novel Strategies

This chapter studies novel strategies to improve the precision and formability in the μ ISF process. The study is divided into two parts. The first part (section 6.1) investigates the stacking of foils (SOF) approach to enhance the formability of the micro-parts by increasing the stiffness and plastic deformations of the foils. The second part (section 6.2) studies a novel method to fabricate precise hemispherical-end shaped tools using the Reverse- μ EDM technique for the μ ISF process.

6.1 Stacking of Foils (SOF)

Graphical Abstract⁴



6.1.1 Introduction

In the μ ISF process, foils are greatly affected by the high degree of relative motion between the tool and foil surface. This causes slackening of the foil at the initial stage

⁴Pal, M., Agrawal, A., and Nirala, C. K., 2024, "Enhancing Formability in Micro-Incremental Sheet Forming by a Novel Stacking Method of Ultra-Thin Sheets," Manufacturing Letters, 40, pp. 159–163. (https://doi.org/10.1016/j.mfglet.2024.05.002)

of the deformation, and affects its formability. To tackle this issue, researchers are working on the development of a forming fixture with a protruded feature to apply extra tension in order to eliminate the early bending of thin foils [62]. Another concern with these foils is that they have very low bending stiffness and are susceptible to get damaged during the fixturing and material handling stage [71]. At macro-scale, it has been suggested to use a dummy sheet to improve the formability and surface quality of the targeted components [188]. In another study, a three-sheet ISF is reported to enhance the forming efficiency of the process by targeting the low formable sheet between the upper and lower auxiliary sheets [189]. Based on the limited works on stacking of sheets at macro-scale, it appears that stacking multiple foils between the holding and backing plates of the fixture would be a constructive approach to improve the stiffness of the foils and may lead to enhanced formability. Thus, in this chapter, a novel multi-sheet stacking based µISF process is developed to tackle the challenges imposed by the lack of stiffness of thin foils, and enhance the formability of commercially pure Titanium Grade 2 (CP-Ti-Gr2) foils through SOF method. It is suggested that combining two or three foils together increases the overall stiffness, and leads to a change in deformation behaviour, which is more like the one at the macro-scale, with a lesser size-effect that pre-dominates at the micro-scale.

6.1.2 Work methodology

This section discusses the procedure for the development of the SOF experimental setup and auxiliary equipments required for the μ ISF process. It also presents the experimental plan and process parameters of the SOF method to carry out the μ ISF on CP-Ti-Gr2 foils.

6.1.2.1 Development of the SOF set-up

CP-Ti-Gr2 is extensively used for aerospace, automobile, defence, and orthopedic applications because of its light-weight, high specific strength, excellent corrosion resistance, and biocompatible nature [142]. Thus CP-Ti-Gr2 foil was selected for carrying out the μISF experiments. To investigate the formability of 100 μm thickness CP-Ti Gr2 foils, a micro-forming fixture was designed and developed to carry out the μISF experiment as discussed in Chapter 3. The received foil was cut into a 30 mm x 25 mm rectangular workpiece, using a path-guided Nd:YAG fiber laser through the laser beam micro-machining (LBμM) technique with less burrs on the workpiece edges. The

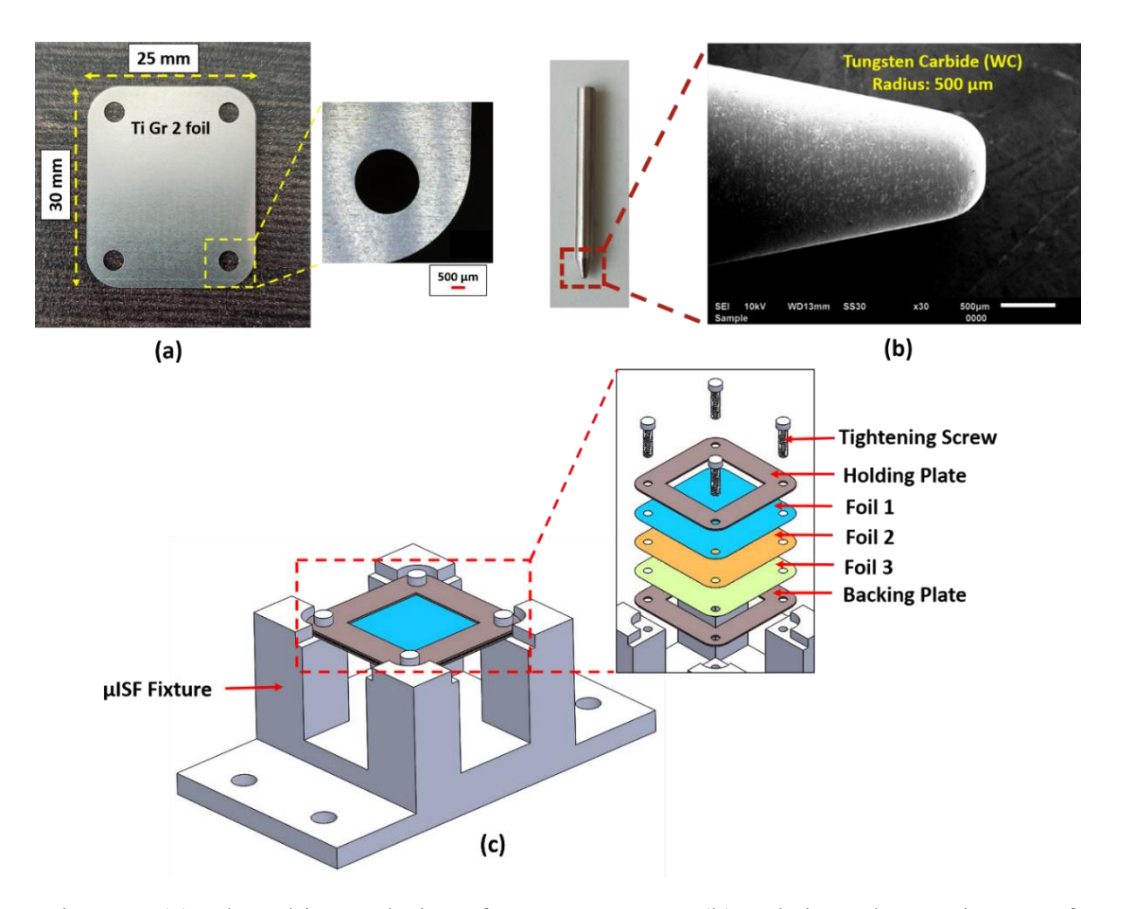


Fig. 6.1: (a) Ultra-thin workpiece for μISF process (b) Fabricated SEM image of micro-forming tool (c) Pictorial demonstration of the μISF fixture for SOF approach

magnified view of the cut section and edge quality of the workpiece is shown in Fig. 6.1(a). The forming tool for the μISF was fabricated in-house using the μ-turning process. Usually for deforming softer sheets of Al, SS, tool steel, or HSS are used as the tool material. However, to deform hard-to-form material like Ti (HCP at room temperature), a relatively harder material is required. Hence, Tungsten Carbide (WC) was selected as tool material, which reduces the wear of the tool-tip during the μISF process. A hemispherical-end shaped tool of radius 500 μm was prepared using a WC circular rod of 3 mm diameter (Fig. 6.1(b)). Thin foils are less stiff and thus more prone to damage due to difficulties in fixturing and material handling. To overcome this problem, a dedicated μISF fixture was fabricated to ease out the fixturing process and constraint the relative motion by forming multiple foils simultaneously. This approach helps in increasing the stiffness and minimizes unwanted distortion of the foils at the preliminary stage of the process. In SOF, using a different material as a top foil can be effective in increasing the formability of the micro-parts. The designed pictorial representation of the SOF based μISF fixture is shown in Fig. 6.1(c).

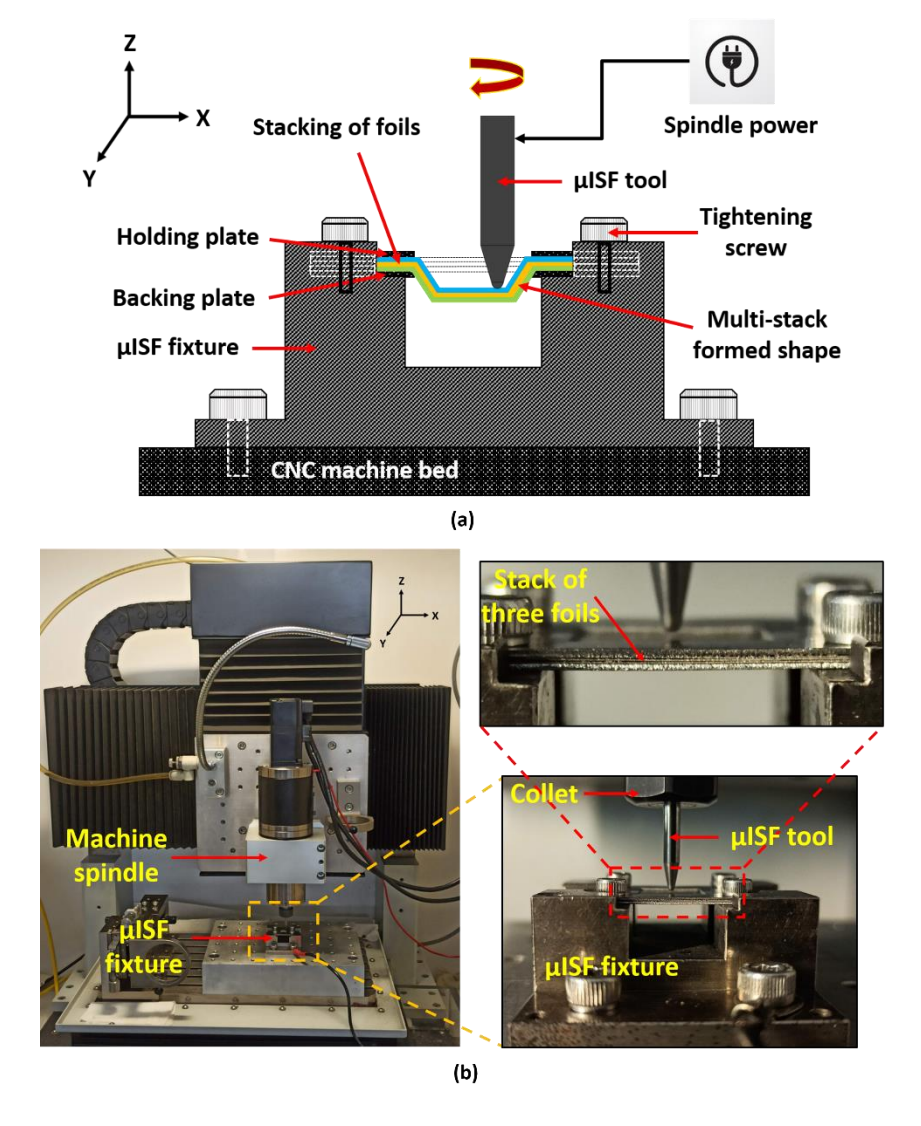


Fig. 6.2: (a) Complete schematic representation of the μISF process for forming multiple foils (b) Experimental view of the SOF approach

6.1.2.2 Experimental plan

The SOF method is an effective approach to overcome the limitation of low formability in micro-scale deformation process. Figure 6.2(a) shows the complete schematic demonstration of the μ ISF process for SOF. A spiral based toolpath was selected to form a conical shaped benchmark geometry. The toolpath was generated through an in-house developed graphical user interface (GUI) in MATLAB® (R2022a release). The forming parameters were optimized based on the repeatability and dimensional accuracy of the formed micro-parts obtained during the trial experiments. Accordingly, all the geometries were formed at a uniform wall angle of 60° (α) and an incremental step depth of 50 μ m (Δz). The tool was given a constant feed of 25 mm/min and clockwise rotation of 500 rpm. To start with, a single CP-Ti Gr2 foil (Foil 1) was formed first using the

usual micro-forming method on a high-precision multi-axis hybrid- μ EDM machine (Mikrotools Ltd., DT-110i). Subsequently, to compare and study the effect of increasing stiffness on the formability of the foils, SOF method was initially carried out to plastically deform two (Foil 1+2) and three (Foil 1+2+3) foils together. A slightly softer material, SS316L of 100 μ m thickness was chosen as the top foil in this process. It helps in providing a cushion to the target Ti foils for better formability of the micro-parts. The experimental view of the μ ISF process is shown in Fig. 6.2(b).

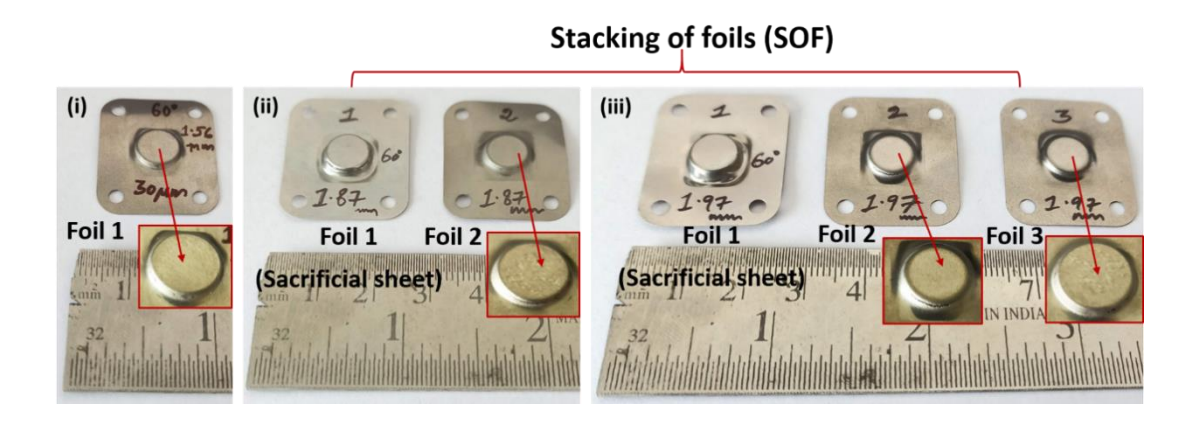


Fig. 6.3: Formed conical cups in single and multi-foil forming (SOF)

6.1.3 Results and discussion

This section presents results on assessment of formability and deformed geometry of foils during the μ ISF experimentation.

6.1.3.1 Assessment of formability in SOF

To improve the stiffness and formability of the foils in µISF, a SOF strategy was implemented for forming multiple foils. A nominal average failure depth of 1.564 mm was observed, when a single CP-Ti Gr2 foil was formed. Later, SOF was carried out using two and three foils together as shown in Fig. 6.3. For the top foil, SS316L material was used in the experiment, which helps in minimizing the tool-tip wear during the forming process. Being a softer material, the top foil has higher ductility (Foil 1), and undergoes more plastic deformation than the Ti foils. This leads to better material distribution/ stretching of the Ti foils (Foil 2 and Foil 3) by inducing extra compressive stresses, resulting in better formability of the micro-parts compared to the single foil forming (non-stacked). However, some wrinkles were observed on the formed surface of the top foil (wall region), which makes it unfit for the analysis and perhaps be discarded after forming the target geometry (Fig. 6.4(a)). Therefore, it acted like a

sacrificial sheet, and assisted in increasing the forming depth of foil 2 and foil 3. As a result, the sacrificial sheet helps in eliminating the direct contact of the tool-tip with the formed shape, resulting in better surface finish and higher forming depth, by delaying the fracture of the targeted parts. The SEM image in Fig. 6.4(b) shows the magnified image with localized fractured region of the formed component. A significant increase of 21.41 % and 26.54 % in the formability was observed in SOF with an average failure depths of 1.897 mm (Foil 1+2) and 1.979 mm (Foil 1+2+3) as illustrated graphically in Fig. 6.4(c). With the increase in stacking number of foils, larger strains in Foil 2 and Foil 3 assisted in increasing the flowability of the material leading to higher forming depths. The experimental results of the µISF process is presented in Table 6.1.

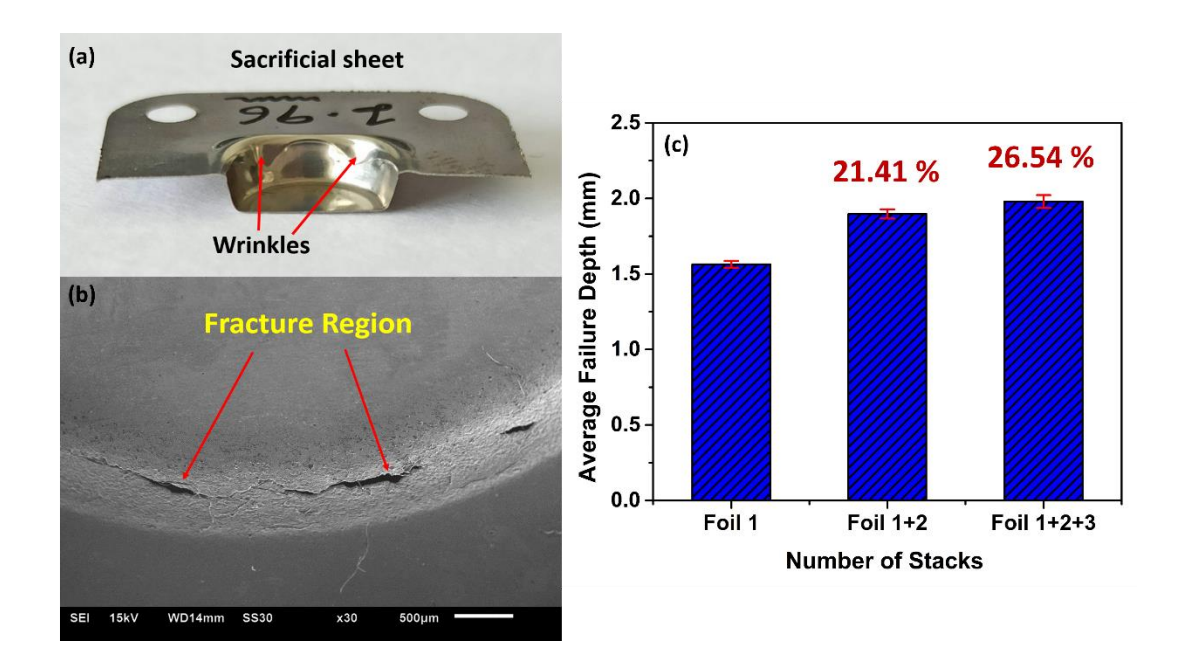


Fig. 6.4: (a) Top foil as a sacrificial sheet with wrinkles (b) SEM micrograph of the fracture location (c) Bar graph presenting the average failure depth verses number of stacks

6.1.3.2 Comparison of the deformed geometries

The cross-sectional profile of the deformed geometries produced through SOF is shown in Fig. 6.5. In the top formed geometry (sacrificial sheet), a significant deviation in the geometrical shape was observed compared to the required geometry (ideal conical shape). The sacrificial sheet is more prone to damage and distortion (wrinkles) due to

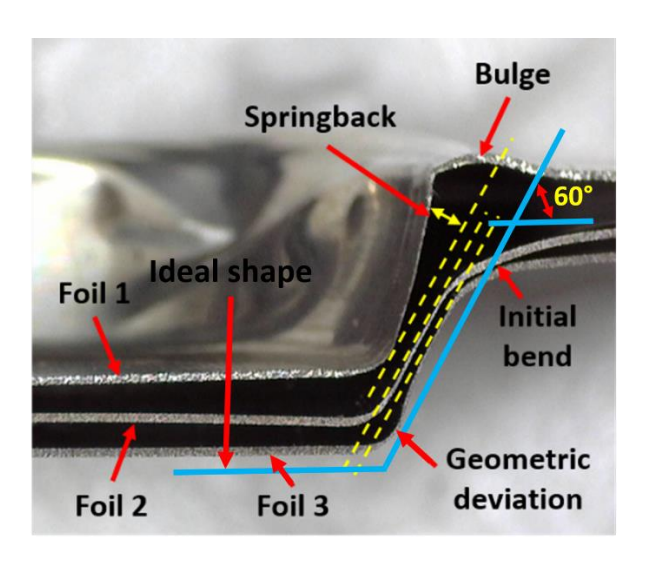


Fig. 6.5: Comparison of deformed geometries in SOF

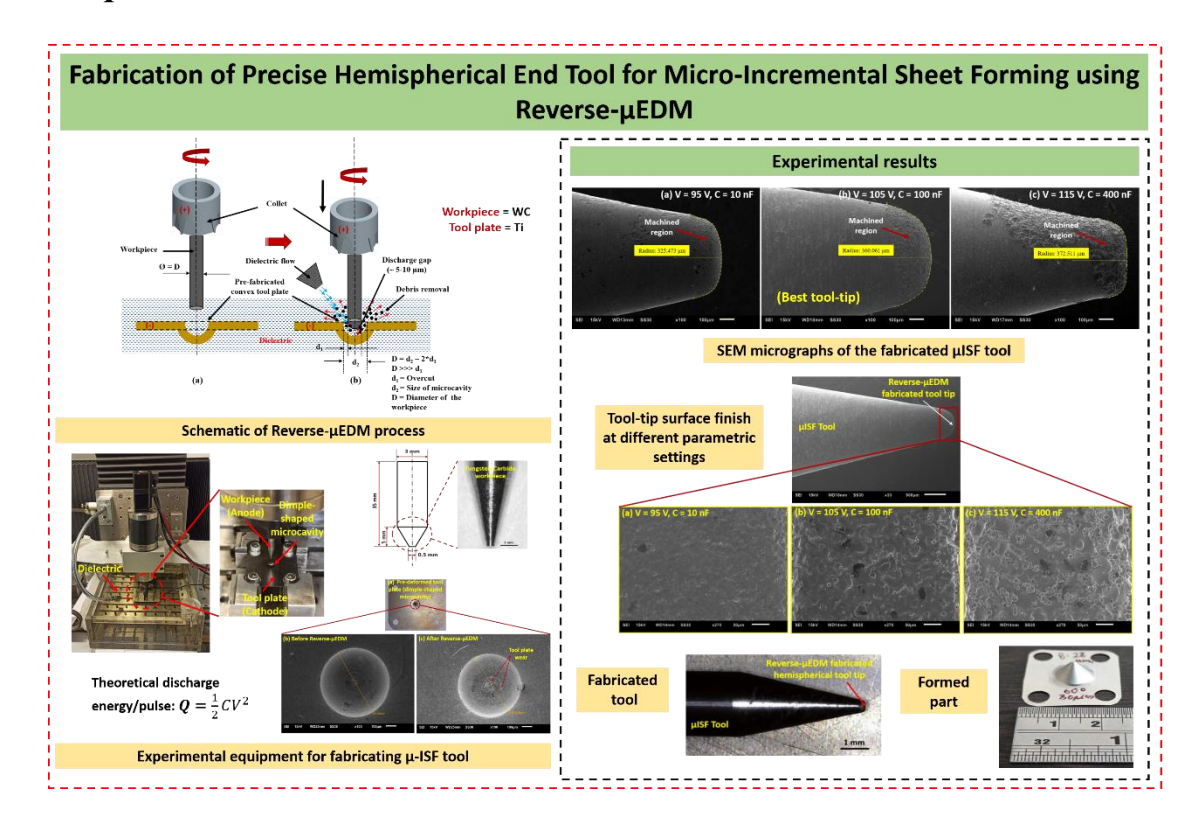
direct contact of the tool on the foil surface compared to the CP-Ti Gr2 (target) foils. A bulge formation can be seen at the initial bending region of Foil 1, which usually takes place during the first interaction of the tool. The elastic recovery was also dominant and led to substantial springback in the deformed shape in Foil 1, as observed in Fig. 6.5. However, in Foil 2 and Foil 3, the target parts experienced a moderate springback effect in the deformed geometry. Thus the SOF approach seems to have a positive impact on dimensional accuracy of the micro-parts as the number of foils increases.

Table 6.1: Experimental results of the μISF process with SOF

	Failure depth (mm)				
Type of geometry	Foil 1	Foil 1+2	Foil 1+2+3		
	1.563	1.875	1.962		
Conical shape	1.588	1.892	1.997		
	1.541	1.924	1.978		
Average depth	1.564	1.897	1.979		
(mm)					

6.2 Tool precision using Reverse-μEDM

Graphical Abstract⁵



6.2.1 Introduction

In μ ISF, flexible foils of thickness typically less than 150 μ m are plastically deformed to complex geometrical shapes. It is done using a ball point-like hemispherical end tool with a diameter of less than 1 mm steering along a numerically controlled pre-defined toolpath. To carry out the process in such microscales, designing and fabricating a precise forming tool is challenging, especially if the tool is made up of hard materials, viz. tungsten carbide. Therefore, development of micro-metallic objects require a robust tool making approach to endure tough working circumstances in order to increase the life of the tool and miniaturized parts. The tool must have a rigid bending stiffness and smooth hemispherical tip surface for accurate work flow. There are a few micro-machining techniques such as micro-turning, micro-grinding and micro-EDG which are capable of making micro-forming tools. However, dimensional control and surface profile remain poor while using those processes. Also, there remain the chances of a

_

⁵**Pal, M.**, Kishore, H., Agrawal A., and Nirala C., K., "Fabrication of Precise Hemispherical End Tool for Micro-Incremental Sheet Forming using Reverse-μEDM", 55th CIRP Conference on Manufacturing Systems (CMS-2022), Lugano, Switzerland, June 29 – July 1, **2022**. **Procedia CIRP**, 107, 1600-1605. (https://doi.org/10.1016/j.procir.2022.06.001)

high magnitude of residual stresses. A recently explored non-conventional micromachining process, called Reverse micro electro discharge machining (RµEDM), has proven its capability of producing single or arrayed, complex protrusions in a high aspect ratio and dimensional accuracy. The Reverse-µEDM process generally consists of a cylindrical workpiece and an axisymmetrically aligned tool plate having specific features according to the final product [11]. Nirala and Saha [12] explored the Reverse-µEDM method to produce micro-rods of height 946 µm with 30 µm tip diameter successfully. The researchers demonstrated the process configuration by reversing the polarity associated with µEDM drilling. Kishore et al. [13,14] numerically studied the average surface roughness of the micro pins-fins (MPFs) fabricated through Reverse-µEDM technology. Later the authors also proposed a hybrid technology by combining the methods of Reverse-µEDM and LASER based micro-machining for the development of arrayed shaped MPFs [15]. Considering the study on surface quality, dimensional accuracy and aspect ratios, Singh et al. [194] also successfully manufactured fine microrods via Reverse-µEDM process.

Roy et al. [195,196] investigated and discussed the process ability to generate 3D convex shaped hemispherical micro feature with a conventionally drilled blind micro hole on a tool substrate (cathode) using Reverse- μ EDM process. Results indicated that secondary and higher order discharges from the edges and corners of the blind hole assisted the removal of debris, which lead to the generation of micro features on the anode. As a result, Reverse- μ EDM thus provides an effective route to explore its benefits to develop high precision hemispherical tool-tips for μ ISF.

The literature survey suggests that there is very few attempts for the fabrication of high quality µISF tools. In this chapter, a feasibility test is demonstrated for the development of micro-forming tool used for the µISF process through Reverse-µEDM technology. The use of this non-contact based machining technology for manufacturing µISF tools provides a novel approach for its fabrication. Reverse-µEDM process is highly acknowledged for its thermal management based applications in avionics, microfluidics, biomedical and microelectronics industries for the production of micro components [14,15]. A parametric study has been performed with three different input settings at low, moderate and high set of parameters to characterize and compare the dimensional profile of the fabricated tool.

6.2.2 Reverse-µEDM technology

Reverse-µEDM process can be defined as the modified version of the conventional straight polarity micro electro-discharge machining (µEDM). This process is widely used for the fabrication of high aspect ratio single and multiple 3D microfeatures/protrusions of different cross-sections, simply by swapping the polarity used in the µEDM process [12,19]. In Reverse-µEDM, the material deletion takes place owing to the numerous repetitive electric discharges from different sites of the workpiece surface (anode) surrounded by the die-electric medium. Fig. 6.6 shows the different types of discharges that occur during the material removal process in Reverse-µEDM. The difference in the nature of discharge depends on whether the debris particles are present or not between the walls of the anode/cathode which directly affects the interelectrode gap (IEG) [13]. Fig. 6.6(a) explains the occurrence of primary discharges, which takes place due to the absence of debris particles in the dielectric. The IEG reduces when debris accumulate and get stick on to the walls of the electrode, which results into secondary order or higher order discharges as shown in Fig. 6.6(b). Besides, the secondary/higher order discharges influences the rate at which the material gets removed from the workpiece surface and affects the dimensional accuracy and surface profile of the micro-features.

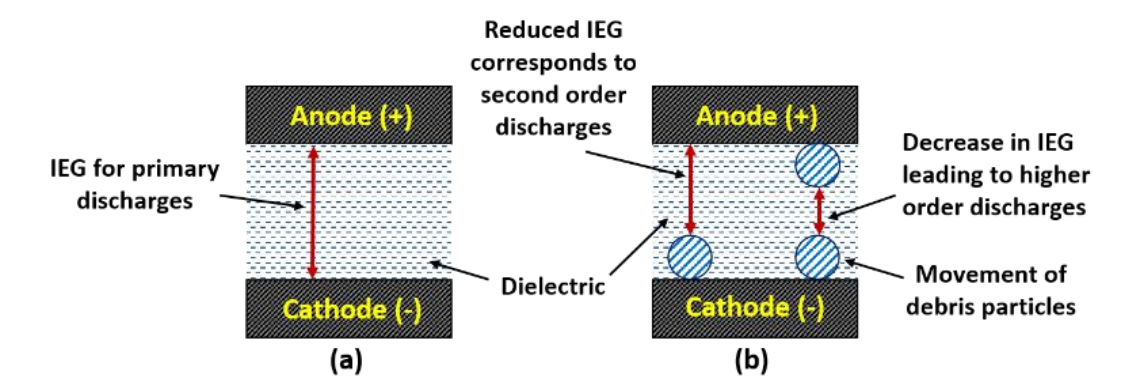


Fig. 6.6: (a) Primary discharge and (b) Second order and higher order discharges in Reverse-μEDM

6.2.3 Experimental approach

For the fabrication of micro-forming tools using Reverse- μ EDM technology, a set up configuration of tool plate and workpiece was established to carry out all the experiments on a numerically controlled RC circuit based multi-axis hybrid- μ EDM

machine (make and model: Mikrotools Pte Ltd., DT110i). The machine head travels with a precise position accuracy of $\pm 1~\mu m$ on a linear optical scale of $0.1 \mu m$ resolution in three different axial directions. The RC circuit type configuration of this machine provides an additional advantage of removing the material with a single discharge in Reverse- μ EDM process for achieving better geometry and surface quality. Conferring

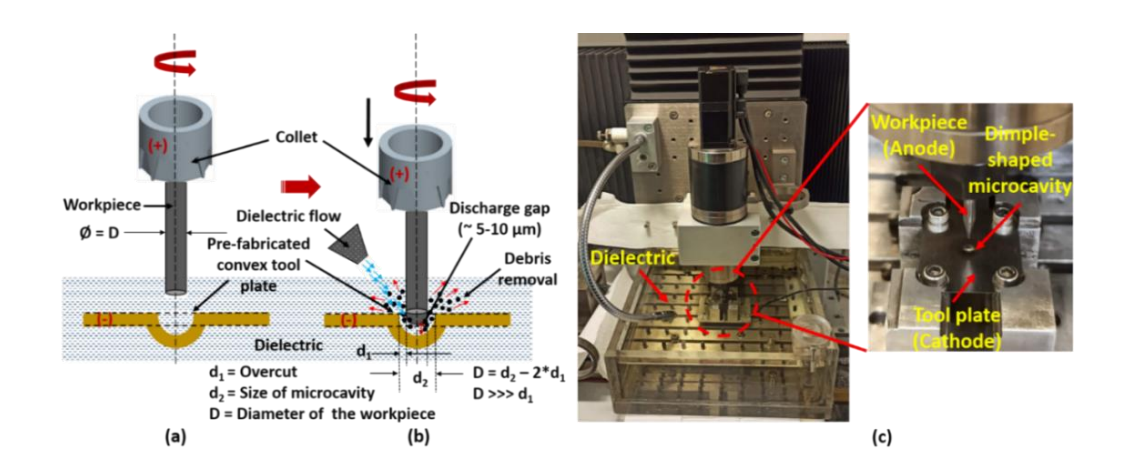


Fig. 6.7: Schematic representation of (a) set up configuration for fabrication of μISF tool using Reverse-μEDM; (b) on-going Reverse-μEDM process for μISF tool

(c) Experimental set up of Reverse-µEDM process

to the dis-charging and charging time of the capacitor, high pulse frequency can be attained with a lower amplitude of current discharges. Based on this, theoretical discharge energy/pulse can be calculated via Eq. 6.1 [12].

$$Q = \frac{1}{2}CV^2 \tag{6.1}$$

Here, Q represents the energy stored in the capacitor, C denotes the user specified value of capacitance for discharging, and V denotes the user specified gap voltage or open-circuit voltage. The developed set for the fabrication of the micro-forming tool using Reverse- μ EDM process is illustrated in Fig. 6.7. Figure 6.7(a) presents the schematic view of the initial set up configuration required for the development of micro-forming tool using Reverse- μ EDM technique, whereas Fig. 6.7(b) shows the on-going fabrication process. The pictorial view of the workpiece-toolplate constituted experimental set up for making μ ISF tool is displayed in Fig. 6.7(c). To carry out the experiment, first step was to produce a dimple-shaped microcavity on the surface of a tool plate, which acted as a cathode during Reverse- μ EDM. A thin sheet of 200 μ m

thickness commercially pure Titanium (grade 2) was used as a tool plate material having cross-sectional area of 25 mm x 30 mm as presented in Fig. 6.8(a).

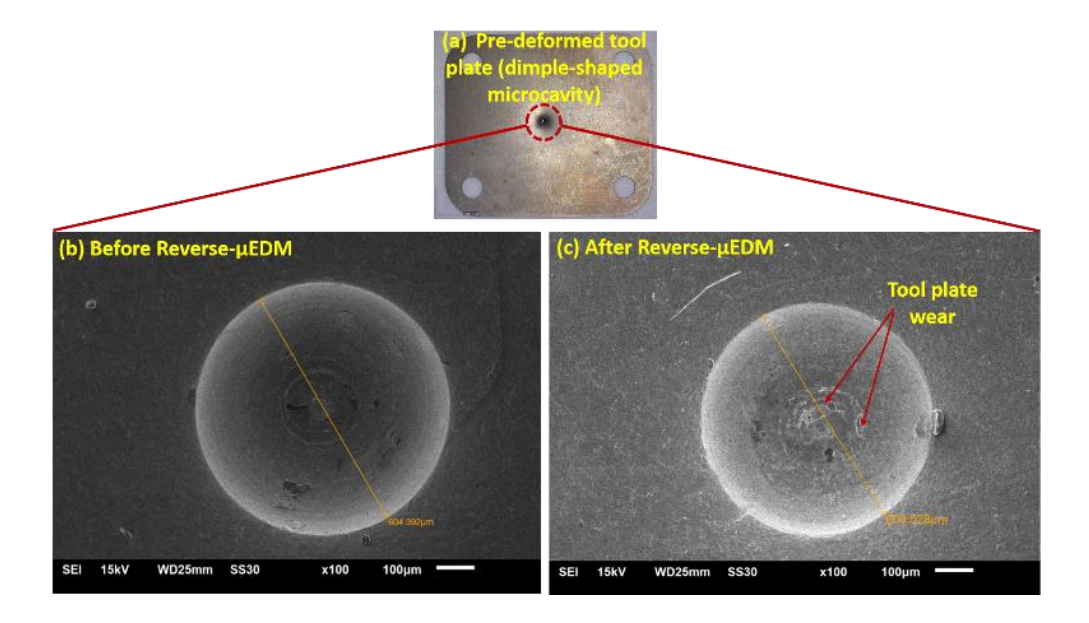


Fig. 6.8: (a) Pre-deformed Titanium tool plate with dimple-shaped microcavity; SEM image of microcavity (b) before Reverse-μEDM, and (c) after Reverse-μEDM with surface wear

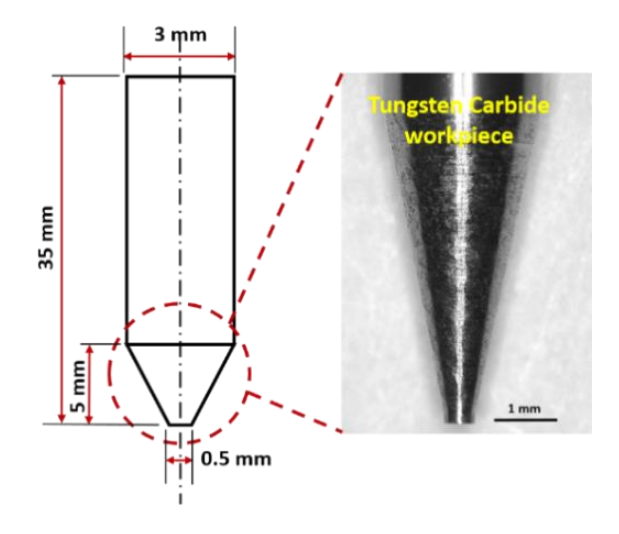


Fig. 6.9: Workpiece dimensions

A microcavity of approx. $600 \, \mu m$ diameter and $300 \, \mu m$ depth was generated by precisely deforming the tool plate positioned on a rigid fixture using a firm hand tool, having similar dimensions as of the formed dimple. A cylindrical shape Tungsten carbide (68% W, 8% Co, 18% C) rod of 3 mm diameter was taken as a workpiece material (anode) for all the experiments. The dimensions of the workpiece used in the experiment is depicted

in Fig. 6.9. During the experiment, 100 rpm rotation was given to the workpiece, which was axis-symmetrically aligned with the pre-deformed microcavity of the tool plate, rigidly fixed on the fixture (Fig. 6.7(c)). Both the electrodes (cathode and anode) were placed inside the dielectric tank filled with continuous flow of dielectric oil (hydrocarbon-based) for the smooth removal of the debris particles. The workpiece was machined with a constant downward feed rate of $20 \, \mu \text{m/min}$.

Table 6.2: Machining conditions and input process parameters

Reverse-µEDM process parameters	Values		
Machine set up	RC type		
Workpiece (Anode)	Tungsten Carbide		
Tool plate (Cathode)	Titanium (Grade 2)		
Dielectric	Hydrocarbon Oil		
Electrode feed rate	20 μm/min		
Capacitance (C) range	10-400 nF		
Voltage (V) range	95-115 V		
Parametric Combinations	Capacitance (nF)	Voltage (V)	
Low (Set 1) Moderate (Set 2) High (Set 3)	10 100 400	95 105 115	

Based on different values of the capacitance (C) and discharge voltage (V), three different input parametric combinations of the discharge energy: (i) low (Set 1) (ii) moderate (Set 2), and (iii) high (Set 3) were studied to examine the theoretical machining capability of the multi-axis machine using Reverse-µEDM. Respective

values of input parameters and machining conditions are presented in Table 6.2. The developed micro-forming tools were then physically characterized and compared for MRR, tool wear, surface roughness, and dimensional accuracy.

6.2.4 Results and discussion

6.2.4.1 Material removal rate (MRR) and Tool plate wear analysis

The MRR is one of the major responses in Reverse- μ EDM, owing to the lower discharge gaps, workpiece material and dimensions during the machining process. MRR of the μ ISF tool can be estimated using the Eqs. 6.2 and 6.3 [19].

$$MRR = \frac{Vr}{T} = \frac{[V - v]}{T} \tag{6.2}$$

$$v = Ah \tag{6.3}$$

Here, V_r is the volume of the material removed from the workpiece, T is the total machining time, V represents the volume of the original workpiece before Reverse- μ EDM, v denotes the volume of the workpiece after the machining process, A is the cross-sectional area of μ ISF tool-tip, and h is the height of the machined tool-tip.

Table 6.3: Machining measured responses

Parametric Combinations	Machining time approx. (mins.)	MRR (mm³/min)	Tool plate wear rate (mm³/min)	Avg. surface roughness, Ra (µm)
Low (Set 1)	52	0.019	0.011	0.92
Moderate (Set 2)	46	0.053	0.034	1.27
High (Set 3)	32	0.137	0.063	1.54

Table 6.3 presents the measured responses of MRR of the workpiece and tool plate wear rate during the Reverse-µEDM process at different parametric settings. Higher values of the MRR and tool plate wear rate in set 3, justified the process of material removal that the discharges happened at a higher rate due to high parametric combinations of C and V, which increased the theoretical discharge energy of the process as compared to

set 1 and set 2 arrangements. Fig. 6.8(b,c) shows the SEM micrographs of the tool plate before and after Reverse-µEDM. Tool plate wear can be easily observed after the machining. Due to the concave shape of the pre-deformed microcavity, the flushing of the debris from the walls of the electrodes becomes difficult. Hence, a high parametric combination of capacitance and gap voltage provides a possible route to avoid the accumulation of debris at the corners and edges of the microcavity. The research carried out by Roy et al. [17] also suggested the same motive for the generation of convex shape micro-features using a blind hole. In addition, uniform rotation of the workpiece during machining also offers a uniform erosion of the material equally from every portion of the workpiece. Therefore, these high order discharges are quite favorable for the generation of hemispherical shape like micro-features on the workpiece surface. However, high parameter settings results in poor surface quality of the machined surface, which limits the productivity of the micro-forming tool.

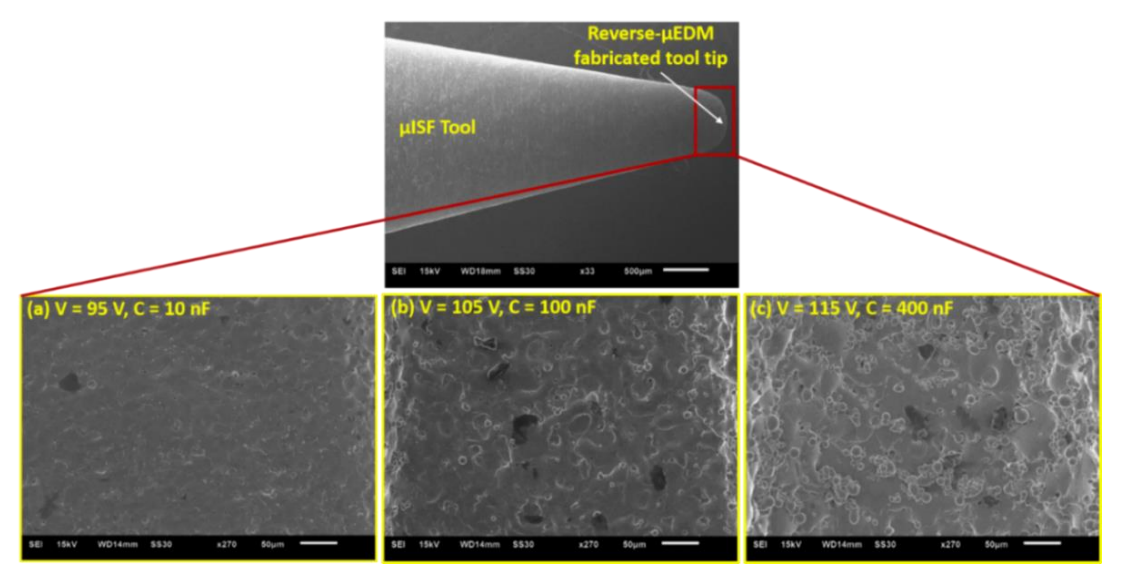


Fig. 6.10: SEM micrographs of the fabricated μISF tool-tip surface finish at different parametric settings (a) low; (b) moderate; and (c) high

6.2.4.2 Surface roughness and dimensional accuracy of the fabricated µISF tool

The surface quality and dimensional accuracy of the hemispherical end tip of a microforming tool plays an important part in the μ ISF process. In μ ISF, the tool-tip navigates along the surface of the metallic thin foils to deform the thin sheet into small geometrical shapes. Thus, the geometrical accuracy of the final formed component largely depends upon the surface quality of the tool surface. Fig. 6.10 shows the SEM (Jeol Ltd., JSM-6610LV) images of the fabricated μ ISF tool surface quality at different parameter

settings. It was evident from the images that the tip surface obtained with lower (Set 1) parametric combination (Fig. 6.10(a)) produced better quality surface using ReverseµEDM. This implies that higher value of discharge energy generates comparatively large size craters due to large value of capacitance and voltage, which increases the surface roughness (Ra) of the tool-tip surface as shown in Fig. 6.10(b,c). The tool diameter was expected to be equal to the diameter of the pre-fabricated dimple on the Reverse-µEDM tool-plate in an ideal case. As a result of the inherent stochastic nature of tool wear and over-cut in the Reverse-µEDM process, there had been variations in the curvature of the fabricated tool-tip. These variations were observed through a visible inspection of the SEM images of the tool-tip. A careful analysis of the SEM images shows a clear arc of the fabricated tool-tip with the imaginary circles drawn in every case to estimate the radius of the developed tool as shown in Fig. 6.11.

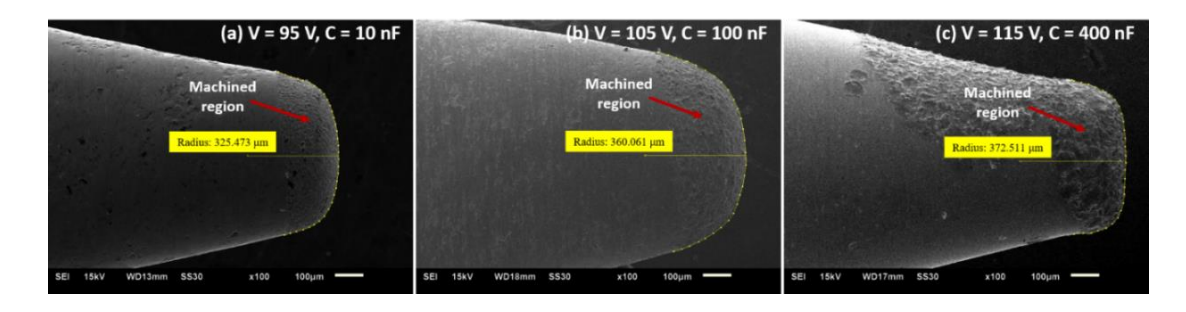


Fig. 6.11: SEM micrographs of the fabricated μISF tool machined region at different parametric settings (a) low; (b) moderate; and (c) high

The finest hemispherical profile of the tool-tip was observed for the moderate (Fig. 6.11(b)) set of parameters with a radius of 360.061 μ m. Whereas, the tool produced with high parameter settings exhibited poor dimensional accuracy and surface quality (Fig. 6.11(c)). For evaluating the surface roughness, several measurements were recorded from the tool-tip surface at different regions using a Surfcom 130A profiler (span length = 5 mm, scanning speed = 0.3 mm/s, cut off = 0.25 mm, waviness filter type = Gaussian profile, ISO'84). From these readings, the average surface roughness (Ra) of the machined region was calculated as presented in Table 6.3. The Ra values of the machined surface increased from lower to higher energy segment in the range of 0.92 μ m to 1.54 μ m.



Fig. 6.12: Optical micrograph of the Reverse-μEDM fabricated μISF tool

6.2.4.3 Feasibility test for µISF process

This section demonstrates the feasibility test of the µISF process using the fabricated micro-forming tool through Reverse-µEDM. In µISF, thin metallic foils are plastically deformed by precise movement of the tool over the foil surface, uniquely programmed to follow a specified toolpath. For the feasibility test of the developed µISF tool, the fabricated tool with best surface quality (Set 1) was chosen to carry out the µISF process. Fig. 6.12 represents the optical micrograph (Leica DM4 M optical microscope) of the μISF tool developed through Reverse-μEDM. A 100 μm thin SS316L foil was clamped on the micro-forming fixture, specifically programmed to follow a spiral incremental toolpath as shown in Fig. 6.13(a,b). The thin foil was incrementally deformed by small step by step deformations in negative z direction at a constant step depth of 30 µm with a wall angle of 60°. The tool was given a rotation of 500 rpm and feed rate of 500 μm/min. during the experiment. The final formed conical geometry is presented in Fig. 6.14. It was observed that the part was formed up to a height of 8.28 mm, without any fracture of the foil surface. Since, the core content of the work is focused on the fabrication feasibility, further investigation is certainly required to examine the effect of tool surface quality on the geometrical shapes formed through µISF.

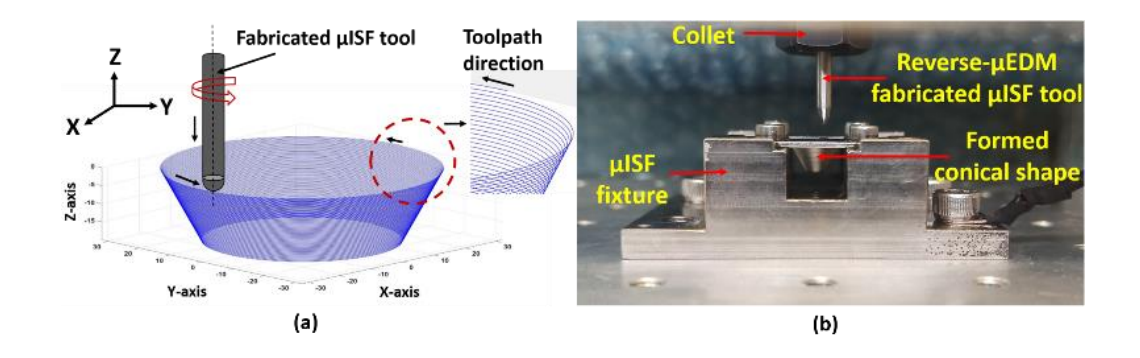


Fig. 6.13: (a) Incremental spiral toolpath (b) µISF process



Fig. 6.14: Formed conical geometry through µISF

6.2.5 Summary

The first part of this chapter presents a novel die-less SOF approach for enhancing the stiffness and formability of ultra-thin CP-Ti Gr2 foils. In SOF, the top foil (SS316L) can be used as a sacrificial sheet to increase the productivity of the process. A remarkable increase of about 21-27 % in the formability of the micro-parts were observed with SOF. Highest average failure depth of 1.979 mm was observed, when three foils were formed together (Foil 1+2+3). Precise parts can be formed in SOF with less geometrical deviation and springback. The main motive of the present investigation was to develop this novel idea of stacking of foils at micro-scale. Further studies can be done to examine the surface finish, dimensional accuracy, thickness distribution and optimization of number of stacked foils, for maximizing the stiffness and formability in the μISF process.

The second part demonstrates a novel approach of manufacturing micro-forming tools for the μ ISF process using the Reverse- μ EDM technology. Three parametric combinations of capacitance and voltage of discharge energy has been performed to examine their effect on the fabricated tool geometry and surface quality. The tool fabricated with lower (Set 1) discharge energy exhibited low values of surface roughness (0.92 μ m) of the tool-tip. Set 2 (moderate) arrangements have been successful to develop the finest hemispherical profile of the tool (V = 105 V, C = 100 nF). While the highest setting lacks in both dimensional accuracy and surface quality. Higher input energy increased the MRR and tool plate wear rate of the process, leading to secondary and high order discharges, which assisted the flow of debris removal for producing hemispherical tool-tips. It can be summarized from the experimental results that on increasing the discharge energy, the machining time is reduced at the cost of surface roughness and dimensional accuracy. Feasibility test of μ ISF process indicates that the proposed method for generating micro-forming tools have been successful in forming small thin metallic components/ parts.

7.1 Conclusions

This chapter discusses the inferences drawn from the research work carried out towards the strategic development of the micro-incremental sheet forming (µISF) process. A summary is also presented at the end of each chapter. This chapter presents a comprehensive overview of the research work and will provide an insight into the overall study. The key contributions lie in the development of the micro-forming set-up and comprehensive experiments to study the formability of the foils with controlled heat-treatment. Incorporating the influence of size-effects in the numerical simulation is also an important part to ensure accurate prediction of the micro-scale deformation. Also, the selection of the correct toolpath is a crucial factor in improving the formability and dimensional accuracy of the micro-parts. Size-effects cause a drastic increase in friction in micro-forming applications. Thus a sustainable lubrication approach is studied with a reduction in energy consumption and waste generation. Novel strategies like SOF and Reverse-µEDM technique can be useful in enhancing the formability and precision in the µISF process. Further, few possible future directions are also presented in this chapter. The following major conclusions are drawn:

- Micro-forming experimental set-up has been designed and fabricated to conduct the μISF experiments. The holding and backing plates helped in countering the relative movement between the foil and the plates. These plates provided uniform distribution of pressure between the adjacent surfaces of the foil and the plates to provide the necessary tension during forming, and avoid the initial bending of the foils. The preliminary experiments were successful to deform the foils into several conical-shaped micro-parts using an in-house built microforming tool.
- Controlled heat treatment was performed to generate a wide spectrum of grain sizes of the foil. Annealing at 650 °C for 60 min (1 hr) was effective in minimizing the anisotropy of the foils with relatively less scattering of the mechanical and metallurgical properties. Homogenous stress-free equiaxed

- grains ($d_{avg.}$ = 13.69 μ m) were observed in three different cross-sectional planes measured in the thickness direction (RD-ND, DD-ND, and TD-ND). The yield and tensile strength of the specimens decreased with the decreasing t/d ratio.
- The formability of the parts increased with increase in grain size (d) of the specimen, upto a critical t/d value of 4. The annealing temperature of 400 °C (MC₄) was most conducive in enhancing the formability of the geometrical parts. With the increase in step depth (Δz = 50 μm) in μISF, an increase in the forming depth was observed. This was attributed to an increase in the volume fraction of surface grains (V_s>V_i) in the deformation zone (A_r), leading to less resistance to the motion of dislocations in the material. The combined selection criteria of t/d ratio and step depth could be used to design the μISF process parameters to achieve optimized results.
- The microstructural analysis through EBSD showed the presence of a higher fraction of LAGBs (67.2 %) and a larger percentage of KAM angle (1.68°) or strained grains after deformation in the material, which led to higher forming depths of the micro-parts.
- Using the surface layer theory at micro-scale, a numerical simulation model was
 developed by incorporating size-effects to accurately predict the micro-scale
 deformation behavior and fracture of the micro-parts during the μISF process. A
 decrease in error of 12-15 % was observed between the simulation and
 experimental results after incorporating the size-effects in the FEA model.
- In comparison to spiral toolpath, FGBIT improves the formability, stress, and thickness distribution of the micro-parts, which is a major limitations of the μISF process. Through FGBIT, the fabrication of vertical-shaped miniature parts made of ultra-thin foils can be targeted in μISF.
- A novel approach is suggested to study the frictional size-effect through closed and open lubrication pocket models (LPM). The distribution of the forming load (F_o) of the tool was well-supported by the formation of CLP's over the entire tool-sheet interaction region. Successful penetration and entrapment of the powder particles between the surface asperities facilitate a uniform contact pressure (σ_N/P_o) leading to a 68.61 % reduction in the surface roughness (R_a = 0.43 μ m) of the formed product compared to other lubrication conditions.

- Environment-friendly MoS₂ powder served as a potential lubricant to enhance the tribological performance of the fabricated micro-parts. It forms a protective layer on the tool surface and provides a low-friction regime between the sliding surfaces to avoid wearing-out of the tool.
- The formation of new grain boundaries and the dissociation of grains into elongated sub-grains (larger strain values) lead to a 22.14 % increase in the forming depth (h = 3.64 mm) of the micro-parts. Considering the environmental impact, the deformation energy requirement was less to form a curvilinear conical part with the MoS₂ powder. A significant 30.13 % decrease in the forming forces (F_z = 12.87 N) and a 14.65 % reduction in energy consumption (E_z = 46.84 mJ) were observed.
- The stacking of foils 'SOF' approach was used for enhancing the stiffness and formability of ultra-thin CP-Ti Gr2 foils. An increase in the average failure depth of 1.897 mm and 1.979 mm were observed, when two and three foils were formed simultaneously compared to forming single foil (1.564 mm). The sacrificial sheet used as top foil (SS316L) helped in eliminating the direct contact of the tool-tip with the formed shape, resulting in better surface finish of the target geometry (38-45 % reduction in Ra). Precise micro-parts were formed with SOF with less geometrical deviation and springback.
- A novel approach of Reverse-μEDM technique was used to fabricate microforming tools for the μISF process. Three parametric combinations of capacitance and voltage of discharge energy was used to examine their effect on the fabricated tool geometry and surface quality. Set 2, moderate (V = 105 V, C = 100 nF) arrangement was successful to develop the finest hemispherical-end profile of the tool with relatively good surface finish, having a Ra value of 1.27 μm. The proposed method for generating micro-forming tools was successful in the micro-scale deformation of thin metallic parts.

7.2 Future Directions

The future possibilities of the present work are listed below:

For the formability assessment, different type of materials such as Copper,
 Nitinol, Stainless steel, etc. and their alloys can be explored to target applications

- oriented micro-parts (MEMS, micro-channels, etc.) to increase the process acceptability in the industries.
- Crystal-plasticity based finite element modelling (FEM), visco-plastic selfconsistent (VPSC) and molecular dynamics (MD) simulations can be performed
 using the constitutive laws to understand the mechanism of grain orientation,
 rotation, dislocation density change, microstructure and texture evolution during
 the deformation process at the micro and nano scales.
- Different size-effect driven friction models can be developed to study the microtribological interactions of the forming tool with the foil surface. An empirical relationship between the micro-pores and lubricant particle size can be established to predict the nature of the stresses distribution during the microscale deformation.
- Some fractal-based incremental toolpath strategies are available like Peano curve, Gosper curve, fractal toolpath with rounded corners, and fractal toolpath with chamfer pattern etc. Future research work can be focused on applying such toolpaths to more complicated geometries in the µISF process.
- The SOF method can be optimized for the number of foils that can be stacked together to increase the productivity of the process. Furthermore, different type of foil material can be used at different levels of the stack for maximizing the stiffness and formability of the targeted micro-parts.
- Warm or Heat-assisted µISF set-up can be developed to increase the formability
 of the materials that are hard to form at room temperature. This will enhance the
 movement of dislocations in the material, leading to higher forming depths and
 uniform thickness distribution of the micro-parts.

- [1] Qin Y, Brockett A, Ma Y, Razali A, Zhao J, Harrison C, et al. Micromanufacturing: Research, technology outcomes and development issues. International Journal of Advanced Manufacturing Technology 2010;47:821–37. https://doi.org/10.1007/s00170-009-2411-2.
- [2] Mishima N, Tanikawa T, Ashida K, Maekawa H. DETC2002 / D FM -34 164. Proceedings of DETC'02 ASME 2002 Design Engineering Technical Conferences and Computer and Information in Engineering Conference 2002;DFM-34164.
- [3] Qin Y. Micro-forming and miniature manufacturing systems development needs and perspectives. Journal of Materials Processing Technology 2006;177:8–18. https://doi.org/10.1016/j.jmatprotec.2006.03.212.
- [4] Pradeep Raja C, Ramesh T. Influence of size effects and its key issues during microforming and its associated processes A review. Engineering Science and Technology, an International Journal 2021;24:556–70. https://doi.org/10.1016/j.jestch.2020.08.007.
- [5] Vollertsen F. Categories of size effects. Production Engineering 2008;2:377–83. https://doi.org/10.1007/s11740-008-0127-z.
- [6] Geiger M, Kleiner M, Eckstein R, Tiesler N, Engel U. Microforming. CIRP Annals Manufacturing Technology 2001;50:445–62. https://doi.org/10.1016/S0007-8506(07)62991-6.
- [7] Pal M, Agrawal A, Nirala CK. An Investigation of the Formability of Ultra-Thin CP-Ti-Gr2 Foils Considering Thickness-to-Grain-Size Effects under Controlled Heat Treatment in μ-ISF. Journal of Manufacturing Processes 2024;131:1202–18. https://doi.org/10.1016/j.jmapro.2024.09.107.
- [8] Saotome Y, Okamoto T. An in-situ incremental microforming system for three-dimensional shell structures of foil materials. Journal of Materials Processing Technology 2001;113:636–40. https://doi.org/10.1016/S0924-0136(01)00651-3.
- [9] Obikawa T, Satou S, Hakutani T. Dieless incremental micro-forming of miniature shell objects of aluminum foils. International Journal of Machine Tools and Manufacture 2009;49:906–15. https://doi.org/10.1016/j.ijmachtools.2009.07.001.
- [10] Bansal A, Lingam R, Yadav SK, Venkata Reddy N. Prediction of forming forces in single point incremental forming. Journal of Manufacturing Processes 2017;28:486–93. https://doi.org/10.1016/j.jmapro.2017.04.016.

- [11] Beltran M, Malhotra R, Nelson AJ, Bhattacharya A, Reddy N V., Cao J. Experimental Study of Failure Modes and Scaling Effects in Micro-Incremental Forming. Journal of Micro and Nano-Manufacturing 2013;1:1–15. https://doi.org/10.1115/1.4025098.
- [12] Dhal A, Panigrahi SK, Shunmugam MS. Achieving excellent microformability in aluminum by engineering a unique ultrafine- grained microstructure. Scientific Reports 2017. https://doi.org/10.1038/s41598-019-46957-4.
- [13] Vollertsen F, Biermann D, Hansen HN, Jawahir IS, Kuzman K. Size effects in manufacturing of metallic components. CIRP Annals Manufacturing Technology 2009;58:566–87. https://doi.org/10.1016/j.cirp.2009.09.002.
- [14] Duflou JR, Habraken AM, Cao J, Malhotra R, Bambach M, Adams D, et al. Single point incremental forming: state-of-the-art and prospects. International Journal of Material Forming 2018;11:743–73. https://doi.org/10.1007/s12289-017-1387-y.
- [15] Jeswiet J, Micari F, Hirt G, Bramley A, Duflou J, Allwood J. Asymmetric single point incremental forming of sheet metal. CIRP Annals Manufacturing Technology 2005;54:88–114. https://doi.org/10.1016/s0007-8506(07)60021-3.
- [16] Leszak E. Apparatus and Process for Incremental Dieless Forming. United States Patent Office 1967:1964–6.
- [17] Mason B. Mason, B., "Sheet Metal Forming for Small Batches," B.Sc Thesis, University of Nottingham, 1978. n.d.
- [18] Jeswiet J. Asymmetric incremental sheet forming. Advanced Materials Research 2005;6–8:35–58. https://doi.org/10.4028/www.scientific.net/amr.6-8.35.
- [19] Jackson K, Allwood J. The mechanics of incremental sheet forming. Journal of Materials Processing Technology 2009;9:1158–74. https://doi.org/10.1016/j.jmatprotec.2008.03.025.
- [20] Silva MB, Skjoedt M, Atkins AG, Bay N, Martins PAF. The Journal of Strain Analysis for Engineering Design 2008. https://doi.org/10.1243/03093247JSA340.
- [21] Cao J, Banu M. Opportunities and challenges in metal forming for lightweighting: Review and future work. Journal of Manufacturing Science and Engineering, Transactions of the ASME 2020;142:1–24. https://doi.org/10.1115/1.4047732.
- [22] Zhai W, Li Y, Cheng Z, Sun L, Li F, Li J. Investigation on the forming force and surface quality during ultrasonic-assisted incremental sheet forming process. International Journal of Advanced Manufacturing Technology 2020;106:2703—

- 19. https://doi.org/10.1007/s00170-019-04870-0.
- [23] Behera AK, Verbert J, Lauwers B, Duflou JR. Computer-Aided Design Tool path compensation strategies for single point incremental sheet forming using multivariate adaptive regression splines. Computer-Aided Design 2013;45:575–90. https://doi.org/10.1016/j.cad.2012.10.045.
- [24] Behera AK, Lauwers B, Duflou JR. Computers in Industry Tool path generation framework for accurate manufacture of complex 3D sheet metal parts using single point incremental forming 2014;65:563–84.
- [25] Otsu M, Taniguchi H, Takashima K. Micro-incremental forming of Ti and Au foils by indentation method. Key Engineering Materials 2007;345-346 II:1101–4. https://doi.org/10.4028/0-87849-440-5.1101.
- [26] Araújo R, Teixeira P, Montanari L, Reis A, Silva MB, Martins PAF. Single point incremental forming of a facial implant 2014. https://doi.org/10.1177/0309364613502071.
- [27] Beal JD, Boyer R, Sanders D, Company TB. Forming of Titanium and Titanium Alloys 2006;14:656–69. https://doi.org/10.1361/asmhba0005146.
- [28] Lu B, Ou H, Shi SQ, Long H, Chen J. Titanium based cranial reconstruction using incremental sheet forming 2016:361–70. https://doi.org/10.1007/s12289-014-1205-8.
- [29] Eriksen RS, Arentoft M, Paldan N, Holstein J V. Micro forming of titanium. International Journal of Material Forming 2009;2:601–4. https://doi.org/10.1007/s12289-009-0482-0.
- [30] Ambrogio G, Sgambitterra E, De Napoli L, Gagliardi F, Fragomeni G, Piccininni A, et al. Performances Analysis of Titanium Prostheses Manufactured by Superplastic Forming and Incremental Forming. Procedia Engineering, vol. 183, 2017, p. 168–73. https://doi.org/10.1016/j.proeng.2017.04.057.
- [31] Peng L, Liu D, Hu P, Lai X, Ni J. Fabrication of metallic bipolar plates for proton exchange membrane fuel cell by flexible forming process-numerical simulations and experiments. Journal of Fuel Cell Science and Technology 2010;7:0310091–9. https://doi.org/10.1115/1.3207870.
- [32] Reuther F, Dix M, Kräusel V, Psyk V, Porstmann S. Model validation of hollow embossing rolling for bipolar plate forming. International Journal of Material Forming 2024;17:1–18. https://doi.org/10.1007/s12289-023-01804-w.
- [33] Sudarsan C, Sajun Prasad K, Hazra S, Panda SK. Forming of serpentine microchannels on SS304 and AA1050 ultra-thin metallic sheets using stamping technology. Journal of Manufacturing Processes 2020;56:1099–113.

- https://doi.org/10.1016/j.jmapro.2020.05.013.
- [34] Reddy IN, Reddy VR, Sridhara N, Basavaraja S, Venkatanarayana M, Rao VS, et al. Development of SiO2 based thin film on metal foils for space application. Ceramics International 2013;39:8493–8. https://doi.org/10.1016/j.ceramint.2013.02.082.
- [35] Yu Q, Liu X, Tang D. Extreme extensibility of copper foil under compound forming conditions. Scientific Reports 2013;3:1–6. https://doi.org/10.1038/srep03556.
- [36] Moorhouse CJ, Villarreal FJ, Baker HJ, Hall DR. Laser drilling of copper foils for electronics applications. IEEE Transactions on Components and Packaging Technologies 2007;30:254–63. https://doi.org/10.1109/TCAPT.2007.897960.
- [37] Lamberti M, Escher F. Aluminium foil as a food packaging material in comparison with other materials. Food Reviews International 2007;23:407–33. https://doi.org/10.1080/87559120701593830.
- [38] Dordevic D, Buchtova H, Jancikova S, Macharackova B, Jarosova M, Vitez T, et al. Aluminum contamination of food during culinary preparation: Case study with aluminum foil and consumers' preferences. Food Science and Nutrition 2019;7:3349–60. https://doi.org/10.1002/fsn3.1204.
- [39] Heilig ML. United States Patent Office, METALLCFLUD SEAL can mass produce these metallic wafers in great quantity, Howard W. Avery, Schenectady, N.Y., assignor to Gen especially from foil ranging in thickness from .005' to eral Electric Company, a corporation of New. ACM SIGGRAPH Computer Graphics 1994;28:131–4. https://doi.org/10.1145/178951.178972.
- [40] Ambrogio G, Napoli L De, Filice L, Gagliardi F, Muzzupappa M. Application of Incremental Forming process for high customised medical product manufacturing. Journal of Materials Processing Technology 2005;163:156–62. https://doi.org/10.1016/j.jmatprotec.2005.02.148.
- [41] Niu L, Wang S, Chen C, Qian SF, Liu R, Li H, et al. Mechanical behavior and deformation mechanism of commercial pure titanium foils. Materials Science and Engineering A 2017;707:435–42. https://doi.org/10.1016/j.msea.2017.09.080.
- [42] Leyens C, Peters M. Titanium and Titanium Alloys, Fundamental and Applications, Wiley. 2003. https://doi.org/10.1007/978-3-319-69743-7 7.
- [43] Kalaichelvi V, Karthikeyan R, Santana A, Afonso P, Zanin A, Wernke R. ScienceDirect ScienceDirect Modelling, Simulation and Control of Incremental Sheet Metal Forming Process using CNC Machine Tool Modelling, Simulation and Control of Incremental Sheet Metal Ketul Bhattathiri Process using CNC Machine Ketul Patel a, V. Procedia Manufacturing 2018;26:95–106.

- https://doi.org/10.1016/j.promfg.2018.07.012.
- [44] Hagan E, Jeswiet J. Analysis of surface roughness for parts formed by computer numerical controlled incremental forming. Proceedings of the Institution of Mechanical Engineers, Part B: Journal of Engineering Manufacture 2004;218:1307–12. https://doi.org/10.1243/0954405042323559.
- [45] Allwood JM, King GPF, Duflou J. A structured search for applications of the incremental sheet-forming process by product segmentation. Proceedings of the Institution of Mechanical Engineers, Part B: Journal of Engineering Manufacture 2005;219:239–44. https://doi.org/10.1243/095440505X8145.
- [46] Jeswiet J, Young D. Forming limit diagrams for single-point incremental forming of aluminium sheet. Proceedings of the Institution of Mechanical Engineers, Part B: Journal of Engineering Manufacture 2005;219:359–64. https://doi.org/10.1243/095440505X32210.
- [47] Liu G. The application of single point incremental forming technology of sheet metal in bus prototyping. Advanced Materials Research 2011;338:46–55. https://doi.org/10.4028/www.scientific.net/AMR.338.46.
- [48] Li J, Shen J, Wang B. A multipass incremental sheet forming strategy of a car taillight bracket. International Journal of Advanced Manufacturing Technology 2013;69:2229–36. https://doi.org/10.1007/s00170-013-5179-3.
- [49] Lora FA, Boff U, Yurgel CC, Folle L, Schaeffer L. Validation of the computer simulation process applied to the incremental forming process for the evaluation of strain paths. Key Engineering Materials 2013;554–557:2453–61. https://doi.org/10.4028/www.scientific.net/KEM.554-557.2453.
- [50] Hirt, G., Bambach, M., Bleck, W., Prahl, U., and Stollenwerk J. The development of incremental sheet forming from flexible forming to fully integrated production of sheet metal parts, Lecture Notes in Production Engineering Advances in Production Technology. 2015.
- [51] Gupta P, Szekeres A, Jeswiet J. Design and development of an aerospace component with single-point incremental forming. International Journal of Advanced Manufacturing Technology 2019;103:3683–702. https://doi.org/10.1007/s00170-019-03622-4.
- [52] Gupta P, Szekeres A, Jeswiet J. Manufacture of an aerospace component with hybrid incremental forming methodology. International Journal of Material Forming 2021;14:293–308. https://doi.org/10.1007/s12289-020-01601-9.
- [53] Mladomir Milutinovića, Robert Lenđela Michal Potranb, Dragiša Vilotića, Plavka Skakuna MP. APPLICATION OF SINGLE POINT INCREMENTAL FORMING FOR MANUFACTURING OF DENTURE BASE. Journal for

- Technology of Plasticity 2014;39:16–23.
- [54] Asghar J, Lingam R, Shibin E, Reddy N V. Tool path design for enhancement of accuracy in single-point incremental forming. Proceedings of the Institution of Mechanical Engineers, Part B: Journal of Engineering Manufacture 2014;228:1027–35. https://doi.org/10.1177/0954405413512812.
- [55] Jack Jeswiet;, Duflou J, Szekeres A. Custom Manufacture of a Solar Cooker.pdf. vol. Advanced M. 2005.
- [56] Allwood JM, Shouler DR, Tekkaya AE. The increased forming limits of incremental sheet forming processes 2007;344:621–8. https://doi.org/10.4028/www.scientific.net/KEM.344.621.
- [57] Cristino VAM, Silva MB, Wong PK, Tam LM, Martins PAF. Hole-flanging of metals and polymers produced by single point incremental forming. International Journal of Materials and Product Technology 2015;50:37–48. https://doi.org/10.1504/IJMPT.2015.066865.
- [58] Bambach M, Voswinckel H, Hirt G. A new process design for performing hole-flanging operations by incremental sheet forming. Procedia Engineering 2014;81:2305–10. https://doi.org/10.1016/j.proeng.2014.10.325.
- [59] Fu MW, Chan WL. A review on the state-of-the-art microforming technologies. International Journal of Advanced Manufacturing Technology 2013;67:2411–37. https://doi.org/10.1007/s00170-012-4661-7.
- [60] Saotome Y, Yasuda K, Kaga H. Microdeep drawability of very thin sheet steels. Journal of Materials Processing Technology 2001;113:641–7. https://doi.org/10.1016/S0924-0136(01)00626-4.
- [61] Sekine T, Obikawa T. Single point micro incremental forming of miniature shell structures. Journal of Advanced Mechanical Design, Systems and Manufacturing 2010;4:543–57. https://doi.org/10.1299/jamdsm.4.543.
- [62] Bansal A, Jiang B, Ni J. Die-less fabrication of miniaturized parts through single point incremental micro-forming. Journal of Manufacturing Processes 2019;43:20–5. https://doi.org/10.1016/j.jmapro.2019.03.046.
- [63] Li Y, Zhao G, An D, Chen J, Zhao G. A novel macro-micro integrated incremental sheet forming process for fabricating parts with functional surface microfeatures. Journal of Materials Processing Technology 2023;320:118130. https://doi.org/10.1016/j.jmatprotec.2023.118130.
- [64] Mahajan P, Patil J, Mishra S. Micro incremental forming of thin SS304 foils and its microstructural study. IOP Conference Series: Materials Science and Engineering 2023;1284:012045. https://doi.org/10.1088/1757-

- 899x/1284/1/012045.
- [65] Vigneshwaran YG, Abdullah SSS. Influence of spindle speeds on the formability , microstructure , mechanical properties and fracture behaviour of Ti 6Al 4V alloy foils during single point micro incremental forming (SPMIF) process. International Journal of Material Forming 2024. https://doi.org/10.1007/s12289-024-01851-x.
- [66] Obikawa T, Hayashi M. Ultrasonic-assisted incremental microforming of thin shell pyramids of metallic foil. Micromachines 2017;8. https://doi.org/10.3390/mi8050142.
- [67] Zheng C, Pan C, Tian Z, Zhao X, Zhao G, Ji Z, et al. Laser shock induced incremental forming of pure copper foil and its deformation behavior. Optics and Laser Technology 2020;121:105785. https://doi.org/10.1016/j.optlastec.2019.105785.
- [68] Shi Y, Zhang W, Cao J, Ehmann KF. Experimental study of water jet incremental micro-forming with supporting dies. Journal of Materials Processing Technology 2019;268:117–31. https://doi.org/10.1016/j.jmatprotec.2019.01.012.
- [69] Vollertsen F, Schulze Niehoff H, Hu Z. State of the art in micro forming. International Journal of Machine Tools and Manufacture 2006;46:1172–9. https://doi.org/10.1016/j.ijmachtools.2006.01.033.
- [70] Lai X, Peng L, Hu P, Lan S, Ni J. Material behavior modelling in micro/mesoscale forming process with considering size/scale effects. Computational Materials

 Science

 2008;43:1003–9. https://doi.org/10.1016/j.commatsci.2008.02.017.
- [71] Engel U, Eckstein R. Microforming From basic research to its realization. Journal of Materials Processing Technology 2002;125–126:35–44. https://doi.org/10.1016/S0924-0136(02)00415-6.
- [72] Hall EO. The deformation and ageing of mild steel: III Discussion of results. Proceedings of the Physical Society Section B 1951;64:747–53. https://doi.org/10.1088/0370-1301/64/9/303.
- [73] Armstrong RW. On size effects in polycrystal plasticity. Journal of the Mechanics and Physics of Solids 1961;9:196–9. https://doi.org/10.1016/0022-5096(61)90018-7.
- [74] Musa MA, Razali AR, Kasim NI. Grain and feature size effect on material behavior for micro-sheet- forming. Applied Mechanics and Materials 2014;680:77–80. https://doi.org/10.4028/www.scientific.net/AMM.680.77.
- [75] Xu J, Guo B, Shan D, Li M, Wang Z. Specimen dimension and grain size effects

- on deformation behavior in micro tensile of SUS304 stainless steel foil. Materials Transactions 2013;54:984–9. https://doi.org/10.2320/matertrans.M2013016.
- [76] Zhu J, Nunnally A, Gau JT, Xu S. A study of improving the formability of the commercial pure titanium foils. Journal of Engineering Materials and Technology, Transactions of the ASME 2020;142. https://doi.org/10.1115/1.4046368.
- [77] Mishra S, Yazar KU, Kar A, Lingam R, Reddy N V., Prakash O, et al. Texture and Microstructure Evolution During Single-Point Incremental Forming of Commercially Pure Titanium. Metallurgical and Materials Transactions A: Physical Metallurgy and Materials Science 2021;52:151–66. https://doi.org/10.1007/s11661-020-06000-y.
- [78] Chan WL, Fu MW. Studies of the interactive effect of specimen and grain sizes on the plastic deformation behavior in microforming. International Journal of Advanced Manufacturing Technology 2012;62:989–1000. https://doi.org/10.1007/s00170-011-3869-2.
- [79] Ben Hmida R, Thibaud S, Gilbin A, Richard F. Influence of the initial grain size in single point incremental forming process for thin sheets metal and microparts: Experimental investigations. Materials and Design 2013;45:155–65. https://doi.org/10.1016/j.matdes.2012.08.077.
- [80] Gau J, Zhang K, Wang Z. Utilizing a Meso Scale Limited Dome Test to Study the Effect of Strain Rate on the Formability of Commercial Pure Titanium Grade Two Foil 2018;2.
- [81] Gau JT, Gu H, Liu X, Huang KM, Lin BT. Forming micro channels on aluminum foils by using flexible die forming process. Journal of Manufacturing Processes 2015;19:102–11. https://doi.org/10.1016/j.jmapro.2015.04.006.
- [82] Wang C, Xue S, Chen G, Cui L, Zhang P. Investigation on formability of bipolar plates during flexible micro forming of Cu/Ni clad foils. Journal of Manufacturing Processes 2020;53:293–303. https://doi.org/10.1016/j.jmapro.2020.02.033.
- [83] Chang Z, Yang M, Chen J. Experimental investigations on deformation characteristics in microstructure level during incremental forming of AA5052 sheet. Journal of Materials Processing Technology 2021;291:117006. https://doi.org/10.1016/j.jmatprotec.2020.117006.
- [84] Lee RS, Chen CH, Gau JT. Effect of thickness to grain size ratio on drawability for micro deep drawing of AISI 304 stainless steel. 9th International Conference on Technology of Plasticity, ICTP 2008 2008:183–8.
- [85] Engel U. Tribology in microforming. Wear 2006;260:265–73.

- https://doi.org/10.1016/j.wear.2005.04.021.
- [86] Messner A, Engel U, Kals R, Vollertsen F. Size effect in the FE-simulation of micro-forming processes. Journal of Materials Processing Tech 1994;45:371–6. https://doi.org/10.1016/0924-0136(94)90368-9.
- [87] Vollertsen F. Size effects in micro forming. Key Engineering Materials 2011;473:3–12. https://doi.org/10.4028/www.scientific.net/KEM.473.3.
- [88] Diehl A, Engel U, Geiger M. Mechanical properties and bending behaviour of metal foils. Proceedings of the Institution of Mechanical Engineers, Part B: Journal of Engineering Manufacture 2008;222:83–91. https://doi.org/10.1243/09544054JEM838.
- [89] Wang C, Guo B, Shan D, Zhang M, Bai X. Tribological behaviors in microforming considering microscopically trapped lubricant at contact interface. International Journal of Advanced Manufacturing Technology 2014;71:2083–90. https://doi.org/10.1007/s00170-014-5657-2.
- [90] Wanheim T, Bay N, Petersen AS. A theoretically determined model for friction in metal working processes. Wear 1974;28:251–8. https://doi.org/10.1016/0043-1648(74)90165-3.
- [91] Sudarsan C, Panda SK. Evaluation of Coefficient of Friction and Investigation into the Effect of Friction and Lubrication on Formability of Ultra-thin Sheets. Journal of Materials Engineering and Performance 2023;32:7737–55. https://doi.org/10.1007/s11665-022-07689-1.
- [92] Weidel S, Engel U. Characterisation of the flattening behaviour of modelled asperities. Wear 2009;266:596–9. https://doi.org/10.1016/j.wear.2008.04.063.
- [93] Keeler SP. Chapter 4 Forming Limit Criteria Sheets, National Steel Research, Ecorse, Michigan. Advances in Deformation Processing 1965:127–8.
- [94] Goodwin GM. Application of strain analysis to sheet metal forming problems in the press shop. SAE Technical Papers 1968:380–7. https://doi.org/10.4271/680093.
- [95] Isik K, Silva MB, Tekkaya AE, Martins PAF. Formability limits by fracture in sheet metal forming. Journal of Materials Processing Technology 2014;214:1557–65. https://doi.org/10.1016/j.jmatprotec.2014.02.026.
- [96] Atkins AG. Fracture in forming. Journal of Materials Processing Technology 1996;56:609–18. https://doi.org/10.1016/0924-0136(95)01875-1.
- [97] Gatea S, Xu D, Ou H, McCartney G. Evaluation of formability and fracture of

- pure titanium in incremental sheet forming. International Journal of Advanced Manufacturing Technology 2018;95:625–41. https://doi.org/10.1007/s00170-017-1195-z.
- [98] Wu R, Hu Q, Li M, Cai S, Chen J. Evaluation of the forming limit of incremental sheet forming based on ductile damage. Journal of Materials Processing Technology 2021;287. https://doi.org/10.1016/j.jmatprotec.2019.116497.
- [99] Lou Y, Huh H, Lim S, Pack K. New ductile fracture criterion for prediction of fracture forming limit diagrams of sheet metals. International Journal of Solids and Structures 2012;49:3605–15. https://doi.org/10.1016/j.ijsolstr.2012.02.016.
- [100] Nirala HK, Agrawal A. Sheet Thinning Prediction and Calculation in Incremental Sheet Forming 2018:391–410. https://doi.org/10.1007/978-981-10-8767-7_15.
- [101] Shim MS, Park JJ. The formability of aluminum sheet in incremental forming. Journal of Materials Processing Technology 2001;113:654–8. https://doi.org/10.1016/S0924-0136(01)00679-3.
- [102] Sudarsan C, Banker KH, Hazra S, Bhagat R, Panda SK. Experimental investigations on forming limit diagram of ultra thin SS 304 steel: effect of circular grid size, sheet orientation, punch size and deformation speed. Advances in Materials and Processing Technologies 2019;5:25–38. https://doi.org/10.1080/2374068X.2018.1510679.
- [103] Mashalkar A, Kakandikar G, Nandedkar V. Micro-forming analysis of ultra-thin brass foil. Materials and Manufacturing Processes 2019;34:1509–15. https://doi.org/10.1080/10426914.2019.1655158.
- [104] Wang C, Wang H, Chen G, Zhu Q, Zhang G, Cui L, et al. Size effects affected uniaxial tensile properties and formability in rubber pad microforming process of pure nickel thin sheets. International Journal of Mechanical Sciences 2020;182. https://doi.org/10.1016/j.ijmecsci.2020.105757.
- [105] Petek A, Kuzman K, Kopač J. Deformations and forces analysis of single point incremental sheet metal forming. Archives of Materials Science and Engineering 2009;35:107–16.
- [106] Pérez-Santiago R, Bagudanch I, García-Romeu ML. Force modelling in single point incremental forming of variable wall angle components. Key Engineering Materials 2011;473:833–40. https://doi.org/10.4028/www.scientific.net/KEM.473.833.
- [107] Aerens R, Eyckens P, Van Bael A, Duflou JR. Force prediction for single point incremental forming deduced from experimental and FEM observations. International Journal of Advanced Manufacturing Technology 2010;46:969–82. https://doi.org/10.1007/s00170-009-2160-2.

- [108] Ambrogio G, Filice L, Micari F. A force measuring based strategy for failure prevention in incremental forming. Journal of Materials Processing Technology 2006;177:413–6. https://doi.org/10.1016/j.jmatprotec.2006.04.076.
- [109] Li Y, Daniel WJT, Liu Z, Lu H, Meehan PA. Deformation mechanics and efficient force prediction in single point incremental forming. Journal of Materials Processing Technology 2015;221:100–11. https://doi.org/10.1016/j.jmatprotec.2015.02.009.
- [110] Chang Z, Li M, Chen J. Analytical modeling and experimental validation of the forming force in several typical incremental sheet forming processes. International Journal of Machine Tools and Manufacture 2019;140:62–76. https://doi.org/10.1016/j.ijmachtools.2019.03.003.
- [111] Shrivastava P, Tandon P. Investigation of the effect of grain size on forming forces in Single Point Incremental Sheet Forming. Procedia Manufacturing 2015;2:41–5. https://doi.org/10.1016/j.promfg.2015.07.008.
- [112] Jeswiet J, Duflou JR, Szekeres A. Forces in single point and two point incremental Forming. Advanced Materials Research 2005;6–8:449–56. https://doi.org/10.4028/www.scientific.net/amr.6-8.449.
- [113] Nasulea D, Oancea G. Incremental deformation: A literature review. MATEC Web of Conferences 2017;121. https://doi.org/10.1051/matecconf/201712103017.
- [114] Rauch M, Hascoet J, Hamann J, Plenel Y. Computer-Aided Design Tool path programming optimization for incremental sheet forming applications 2009;41:877–85. https://doi.org/10.1016/j.cad.2009.06.006.
- [115] Lu B, Chen J, Ou H, Cao J. Feature-based tool path generation approach for incremental sheet forming process. Journal of Materials ProcessingTechnology 2013;213:1221–33.
- [116] Malhotra R, Reddy N V., Cao J. Automatic 3D Spiral Toolpath Generation for Single Point Incremental Forming. Journal of Manufacturing Science and Engineering 2010;132:061003. https://doi.org/10.1115/1.4002544.
- [117] Li Y, Chen X, Zhai W, Wang L, Li J, Guoqun Z. Effects of process parameters on thickness thinning and mechanical properties of the formed parts in incremental sheet forming. International Journal of Advanced Manufacturing Technology 2018;98:3071–80. https://doi.org/10.1007/s00170-018-2469-9.
- [118] Blaga A, Oleksik V. A study on the influence of the forming strategy on the main strains, thickness reduction, and forces in a single point incremental forming process. Advances in Materials Science and Engineering 2013;2013. https://doi.org/10.1155/2013/382635.

- [119] Rakesh L, Amit S, Reddy N V. Deflection Compensations for Tool Path to Enhance Accuracy during Double-Sided Incremental Forming. Journal of Manufacturing Science and Engineering, Transactions of the ASME 2016;138:1–11. https://doi.org/10.1115/1.4033956.
- [120] Singh A, Nirala HK, Agrawal A. Investigations on structural thinning in deformation machining stretching mode. AIP Conference Proceedings 2016;1769. https://doi.org/10.1063/1.4963470.
- [121] Boudhaouia S, Gahbiche MA, Giraud E, Ayed Y, Ben Salem W, Dal Santo P. Experimental and numerical study of single point incremental forming for a spiral toolpath strategy. Lecture Notes in Mechanical Engineering 2018;0:1007–15. https://doi.org/10.1007/978-3-319-66697-6 99.
- [122] Nirala HK, Agrawal A. Fractal Geometry Rooted Incremental Toolpath for Incremental Sheet Forming. Journal of Manufacturing Science and Engineering 2018;140:1–9. https://doi.org/10.1115/1.4037237.
- [123] Matsubara S. Incremental Backward Bulge Forming of a Sheet Metal with a Hemispherical Head Tool. Journal of the Japan Society for Technology of Plasticity 1994;35:1994.
- [124] Ambrogio G, Duflou J, Filice L, Aerens R. Some considerations on force trends in Incremental Forming of different materials 2007:193–8. https://doi.org/10.1063/1.2729510.
- [125] Kim TJ, Yang DY. Improvement of formability for the incremental sheet metal forming process. International Journal of Mechanical Sciences 2000;42:1271–86. https://doi.org/10.1016/S0020-7403(99)00047-8.
- [126] Dassault simulia Abaqus/CAE. Abaqus Analysis user manual, version 6.8. 2022 Damage Initiation for Ductile Metals 2018:2080.
- [127] Henrard C, Bouffioux C, Duchêne L, Duflou JR, Habraken AM. Validation of a New Finite Element for Incremental Forming Simulation Using a Dynamic Explicit Approach. Key Engineering Materials 2007;344:495–502. https://doi.org/10.4028/www.scientific.net/kem.344.495.
- [128] Henrard C. Numerical Simulations of the Single Point Incremental Forming Process 2008.
- [129] Bambach M, Hirt G, Ames J. Quantitative Validation of FEM Simulations for Incremental Sheet Forming Using Optical Deformation Measurement. Advanced Materials Research 2005;6–8:509–16. https://doi.org/10.4028/www.scientific.net/amr.6-8.509.
- [130] Nirala HK, Jain PK, Roy JJ, Samal MK, Tandon P. An approach to eliminate

- stepped features in multistage incremental sheet forming process: Experimental and FEA analysis. Journal of Mechanical Science and Technology 2017;31:599–604. https://doi.org/10.1007/s12206-017-0112-6.
- [131] Benallal A, Rene billardson, Issam Doghri. An integration algorithm and the corresponding consistent tangent operator for fully coupled elastoplastic and damage equations. COMMUNICATIONS IN APPLIED NUMERICAL METHODS 1988;4:731–40.
- [132] Hancock JW, Mackenzie AC. On the mechanisms of ductile failure in high-strength steels subjected to multi-axial stress-states. Journal of the Mechanics and Physics of Solids 1976;24:147–60. https://doi.org/10.1016/0022-5096(76)90024-7.
- [133] Gatea S, Ou H, Lu B, Mccartney G. Modelling of ductile fracture in single point incremental forming using a modified GTN model. Engineering Fracture Mechanics 2017;186:59–79. https://doi.org/10.1016/j.engfracmech.2017.09.021.
- [134] Lemaitre J. A continuous damage mechanics model for ductile fracture. Journal of Engineering Materials and Technology, Transactions of the ASME 1985;107:83–9. https://doi.org/10.1115/1.3225775.
- [135] Karimi Firouzjaei M, Moslemi Naeini H, Kasaei MM, Mirnia MJ, da Silva LF. Microscale modeling of the ductile fracture behavior of thin stainless steel sheets. Thin-Walled Structures 2024;196:111457. https://doi.org/10.1016/j.tws.2023.111457.
- [136] Ran JQ, Fu MW, Chan WL. The influence of size effect on the ductile fracture in micro-scaled plastic deformation. International Journal of Plasticity 2013;41:65–81. https://doi.org/10.1016/j.ijplas.2012.09.002.
- [137] Xu ZT, Peng LF, Fu MW, Lai XM. Size effect affected formability of sheet metals in micro/meso scale plastic deformation: Experiment and modeling. International Journal of Plasticity 2015;68:34–54. https://doi.org/10.1016/j.ijplas.2014.11.002.
- [138] Kim GY, Koç M, Ni J. Experimental and numerical investigations on microcoining of stainless steel 304. Journal of Manufacturing Science and Engineering, Transactions of the ASME 2008;130:0410171–6. https://doi.org/10.1115/1.2953235.
- [139] Mishra S, Yazar KU, More AM, Kumar L, Lingam R, Reddy N V., et al. Elucidating the deformation modes in incremental sheet forming process: Insights from crystallographic texture, microstructure and mechanical properties. Materials Science and Engineering A 2020;790:139311. https://doi.org/10.1016/j.msea.2020.139311.

- [140] Zhu J, Nunnally A, Gau J-T, Xu S. A Study of Improving the Formability of the Commercial Pure Titanium Foils. Journal of Engineering Materials and Technology 2020;142. https://doi.org/10.1115/1.4046368.
- [141] Nemat-Nasser S, Guo WG, Cheng JY. Mechanical properties and deformation mechanisms of a commercially pure titanium. Acta Materialia 1999;47:3705–20. https://doi.org/10.1016/S1359-6454(99)00203-7.
- [142] Pal M, Pandya V, Agrawal A. Study of Formability Limit Based on Ductile Damage Criteria of Incremental Sheet Forming of Titanium Grade 2 Sheet. Manufacturing Science and Engineering Conference, ASME; 2021, p. 1–7. https://doi.org/https://doi.org/10.1115/MSEC2021-64005.
- [143] Jing R, Liu CY, Ma MZ, Liu RP. Microstructural evolution and formation mechanism of FCC titanium during heat treatment processing. Journal of Alloys and Compounds 2013;552:202–7. https://doi.org/10.1016/j.jallcom.2012.10.083.
- [144] Xu J, Guo B, Wang C, Shan D. Blanking clearance and grain size effects on micro deformation behavior and fracture in micro-blanking of brass foil. International Journal of Machine Tools and Manufacture 2012;60:27–34. https://doi.org/10.1016/j.ijmachtools.2012.04.001.
- [145] Nirala CK, Saha P. Evaluation of µEDM-drilling and µEDM-dressing performances based on online monitoring of discharge gap conditions. International Journal of Advanced Manufacturing Technology 2016;85:1995–2012. https://doi.org/10.1007/s00170-015-7934-0.
- [146] Pal M, Kishore H, Agrawal A, Nirala CK. Fabrication of Precise Hemispherical End Tool for Micro Incremental Sheet Forming using Reverse-μEDM. Procedia CIRP 2022;107:1600–5. https://doi.org/10.1016/j.procir.2022.06.001.
- [147] Chan WL, Fu MW, Lu J, Liu JG. Modeling of grain size effect on micro deformation behavior in micro-forming of pure copper. Materials Science and Engineering A 2010;527:6638–48. https://doi.org/10.1016/j.msea.2010.07.009.
- [148] Ibrahim JS, Mathew RT, Prasad MJN V., Narasimhan K. Processing and Specimen Thickness to Grain Size (t/d) Ratio Effects on Tensile Behaviour and Microformability of Copper Foils. Metals and Materials International 2022. https://doi.org/10.1007/s12540-021-01145-w.
- [149] Zhu J, Lin Y, Liu S, Ma X, Wang G. Plasticity and size effects of micro-forming sheet processed by electropulsing. Materials and Manufacturing Processes 2020;35:1146–55. https://doi.org/10.1080/10426914.2020.1772482.
- [150] Petch JN. Cleavage Strength of Polycrystals. J Iron Steel Inst 1953;174:25–8.
- [151] Tan KJ, Mahmod S, Wahab MAA, Idris MI, Abdullah HZ. Effect of Heat

- Treatment on Surface Morphology of Titanium. Advanced Materials Research 2015;1125:445–9. https://doi.org/10.4028/www.scientific.net/amr.1125.445.
- [152] Wang G, Han J, Lin Y, Zheng W. Investigation on size effect of surface roughness and establishment of prediction model in micro-forming process. Materials Today Communications 2021;27:102279. https://doi.org/10.1016/j.mtcomm.2021.102279.
- [153] Dhal A, Panigrahi SK, Shunmugam MS. Insight into the microstructural evolution during cryo-severe plastic deformation and post-deformation annealing of aluminum and its alloys. Journal of Alloys and Compounds 2017;726:1205–19. https://doi.org/10.1016/j.jallcom.2017.08.062.
- [154] Wang T, Li B, Li Y, Li M, Nie Z. Evolution mechanism of dislocation boundary and characteristic micro-structure of commercial pure titanium during the projectile impact. Materials Science and Engineering A 2018;712:325–31. https://doi.org/10.1016/j.msea.2017.11.121.
- [155] Zhang R, Xu Z, Peng L, Lai X, Fu MW. Modelling of ultra-thin steel sheet in two-stage tensile deformation considering strain path change and grain size effect and application in multi-stage microforming. International Journal of Machine Tools and Manufacture 2021;164. https://doi.org/10.1016/j.ijmachtools.2021.103713.
- [156] Fu MW, Wang JL, Korsunsky AM. A review of geometrical and microstructural size effects in micro-scale deformation processing of metallic alloy components. International Journal of Machine Tools and Manufacture 2016;109:94–125. https://doi.org/10.1016/j.ijmachtools.2016.07.006.
- [157] Lederich RJ, Sastry SML, O'Neal JE, Rath BB. The Effect of Grain Size on Yield Stress and Work Hardening of Polycrystalline Titanium at 295 K and 575 K. Materials Science and Engineering 1978;33:183–8.
- [158] Jones RL, Conrad H. 'The effect of grain size on the strength of alpha-titanium at room temperature. Trans Am Inst Metall Eng 1969;245:779–89.
- [159] Stanford N, Carlson U, Barnett MR. Deformation twinning and the Hall-Petch relation in commercial purity Ti. Metallurgical and Materials Transactions A: Physical Metallurgy and Materials Science 2008;39 A:934–44. https://doi.org/10.1007/s11661-007-9442-9.
- [160] Guan B, Xin Y, Huang X, Liu C, Wu P, Liu Q. The mechanism for an orientation dependence of grain boundary strengthening in pure titanium. International Journal of Plasticity 2022;153:103276. https://doi.org/10.1016/j.ijplas.2022.103276.
- [161] Lasalmonie A, Strudel JL. Influence of grain size on the mechanical behaviour of

- some high strength materials. Journal of Materials Science 1986;21:1837–52. https://doi.org/10.1007/BF00547918.
- [162] Srinivasan N, Velmurugan R, Kumar R, Singh SK, Pant B. Deformation behavior of commercially pure (CP) titanium under equi-biaxial tension. Materials Science and Engineering A 2016;674:540–51. https://doi.org/10.1016/j.msea.2016.08.018.
- [163] Wang YN, Huang JC. Texture analysis in hexagonal materials. Materials Chemistry and Physics 2003;81:11–26. https://doi.org/10.1016/S0254-0584(03)00168-8.
- [164] Lin J, Zhuang W, Cao J, Wang S. Micro-mechanics modeling for micro-forming processes. First Edit. Elsevier Ltd.; 2010. https://doi.org/10.1016/B978-0-8155-1545-6.00023-5.
- [165] Furushima T, Tsunezaki H, Manabe KI, Alexsandrov S. Ductile fracture and free surface roughening behaviors of pure copper foils for micro/meso-scale forming. International Journal of Machine Tools and Manufacture 2014;76:34–48. https://doi.org/10.1016/j.ijmachtools.2013.10.001.
- [166] Peng L, Liu F, Ni J, Lai X. Size effects in thin sheet metal forming and its elastic-plastic constitutive model. Materials and Design 2007;28:1731–6. https://doi.org/10.1016/j.matdes.2006.02.011.
- [167] Nirala HK, Agrawal A. Fractal Geometry Rooted Incremental Toolpath for Incremental Sheet Forming. Journal of Manufacturing Science and Engineering, Transactions of the ASME 2018;140. https://doi.org/10.1115/1.4037237.
- [168] Schmid E, Boas IW. Plasticity of Crystals with Special Reference to Metals. Chapman and Hall Ltd, London 1968:1968.
- [169] Kishida K, Kim JG, Nagae T, Inui H. Experimental evaluation of critical resolved shear stress for the first-order pyramidal c+a slip in commercially pure Ti by micropillar compression method. Acta Materialia 2020;196:168–74. https://doi.org/10.1016/j.actamat.2020.06.043.
- [170] Lu HN, Wei DB, Jiang ZY, Liu XH, Manabe K. Modelling of size effects in microforming process with consideration of grained heterogeneity. Computational Materials Science 2013;77:44–52. https://doi.org/10.1016/j.commatsci.2013.03.033.
- [171] Ran JQ, Fu MW. A hybrid model for analysis of ductile fracture in micro-scaled plastic deformation of multiphase alloys. International Journal of Plasticity 2014;61:1–16. https://doi.org/10.1016/j.ijplas.2013.11.006.
- [172] Ingarao G, Ambrogio G, Gagliardi F, Di Lorenzo R. A sustainability point of view

- on sheet metal forming operations: Material wasting and energy consumption in incremental forming and stamping processes. Journal of Cleaner Production 2012;29–30:255–68. https://doi.org/10.1016/j.jclepro.2012.01.012.
- [173] Mang T, Bobzin K, T. B. Industrial Tribology: Tribosystems, Friction, Wear and Surface Engineering, Lubrication; Wiley-VCH: Weinheim, Germany. vol. 16. 1983. https://doi.org/10.1016/0301-679x(83)90075-0.
- [174] Ingarao G, Di Lorenzo R, Micari F. Sustainability issues in sheet metal forming processes: An overview. Journal of Cleaner Production 2011;19:337–47. https://doi.org/10.1016/j.jclepro.2010.10.005.
- [175] Hetzner H, Koch J, Tremmel S, Wartzack S, Merklein M. Improved sheet bulk metal forming processes by local adjustment of tribological properties. Journal of Manufacturing Science and Engineering 2011;133:1–11. https://doi.org/10.1115/1.4005313.
- [176] Schmid SR, Saha PK, Wang J, Schmitz T. Developments in Tribology of Manufacturing Processes. Journal of Manufacturing Science and Engineering, Transactions of the ASME 2020;142. https://doi.org/10.1115/1.4047723.
- [177] Lo S, Wilson WRD. A Theoretical Model of Micro-Pool Lubrication in Metal Forming. Journal of Tribology 1999;121:731–8.
- [178] Savan A, Pflüger E, Voumard P, Schröer A, Paul MS. Modern solid lubrication: Recent developments and applications of MoS2. Lubrication Science 2000;12:185–203. https://doi.org/10.1002/ls.3010120206.
- [179] Mushtaq S, Wani MF, Nadeem M, Najar KA, Mursaleen M. A study on friction and wear characteristics of Fe–Cu–Sn alloy with MoS2 as solid lubricant under dry conditions. Sadhana Academy Proceedings in Engineering Sciences 2019;44. https://doi.org/10.1007/s12046-019-1208-8.
- [180] Donnet C, Martin JM, Le Mogne T, Belin M. The origin of super-low friction coefficient of MoS2 coatings in various environments. Tribology Series 1994;27:277–84. https://doi.org/10.1016/S0167-8922(08)70317-1.
- [181] Meng F, Han H, Ma Z, Tang B. Effects of Aviation Lubrication on Tribological Performances of Graphene/MoS2 Composite Coating. Journal of Tribology 2021;143:1–12. https://doi.org/10.1115/1.4047895.
- [182] Fan G, Sun F, Meng X, Gao L, Tong G. Electric hot incremental forming of Ti-6Al-4V titanium sheet. International Journal of Advanced Manufacturing Technology 2010;49:941–7. https://doi.org/10.1007/s00170-009-2472-2.
- [183] Zhang Q, Xiao F, Guo H, Li C, Gao L, Guo X, et al. Warm negative incremental forming of magnesium alloy AZ31 Sheet: New lubricating method. Journal of

- Materials Processing Technology 2010;210:323–9. https://doi.org/10.1016/j.jmatprotec.2009.09.018.
- [184] Hussain, G GL. Tool and lubrication of negative incremental forming of cp titanium. Journal of Materials Processing TechProcessing Technology 2008;203:193–201.
- [185] Jawale K, Duarte JF, Reis A, Silva MB. Microstructural investigation and lubrication study for single point incremental forming of copper. International Journal of Solids and Structures 2018;151:145–51. https://doi.org/10.1016/j.ijsolstr.2017.09.018.
- [186] Brunette DM, Tengvall P, Textor M, Thomsen P. Titanium in Medicine: Material Science, Surface Science, Engineering, Biological Responses and Medical Applications, Springer. 2001.
- [187] Pal M, Agrawal A, Nirala CK. Enhancing formability in Micro-Incremental sheet forming by a novel stacking method of ultra-thin sheets. Manufacturing Letters 2024;40:159–63. https://doi.org/10.1016/j.mfglet.2024.05.002.
- [188] Skjoedt M, Silva MB, Bay N, Martins PAF, Lenau T. Single point incremental forming using a dummy sheet. International Conference on New Forming Technology 2007;2:267–76.
- [189] Chang Z, Chen J. Investigations on the deformation mechanism of a novel three-sheet incremental forming. Journal of Materials Processing Technology 2020;281:116619. https://doi.org/10.1016/j.jmatprotec.2020.116619.
- [190] Mastud SA, Garg M, Singh R, Joshi SS. Recent developments in the reverse micro-electrical discharge machining in the fabrication of arrayed micro-features. Proceedings of the Institution of Mechanical Engineers, Part C: Journal of Mechanical Engineering Science 2012;226:367–84. https://doi.org/10.1177/0954406211424672.
- [191] Nirala CK, Saha P. A New Approach of Tool Wear Monitoring and Compensation in RμEDM Process. Materials and Manufacturing Processes 2016;31:483–94. https://doi.org/10.1080/10426914.2015.1058950.
- [192] Kishore H, Nadda R, Nirala CK, Agrawal A. Modelling and simulation based surface characterization of reverse-µEDM fabricated micro pin-fins. Procedia CIRP 2019;81:1230–5. https://doi.org/10.1016/j.procir.2019.03.299.
- [193] Kishore H, Nirala CK, Agrawal A. Feasibility demonstration of µEDM for fabrication of arrayed micro pin-fins of complex cross-sections. Manufacturing Letters 2020;23:14–8. https://doi.org/10.1016/j.mfglet.2019.11.005.
- [194] Singh AK, Patowari PK, Deshpande N V. Experimental Analysis of Reverse

- Micro-EDM for Machining Microtool. Materials and Manufacturing Processes 2016;31:530–40. https://doi.org/10.1080/10426914.2015.1070426.
- [195] Roy T, Datta D, Balasubramaniam R. Numerical modelling, simulation and fabrication of 3-D hemi-spherical convex micro features using Reverse Micro EDM. Journal of Manufacturing Processes 2018;32:344–56. https://doi.org/10.1016/j.jmapro.2018.02.018.
- [196] Roy T, Datta D, Balasubramaniam R. Reverse micro EDMed 3D hemispherical protruded micro feature: Microstructural and mechanical characterization. Materials Research Express 2019;6. https://doi.org/10.1088/2053-1591/aaf490.
- [197] Kishore H, Nirala CK, Agrawal A, Kuriachen B. Assessment of process parameters and performance enhancement through a novel suction flushing technology in RµEDM. Materials and Manufacturing Processes 2021;36:1476–88. https://doi.org/10.1080/10426914.2021.1948051.